# Fabrication and study of multidimensional scaffolds for cellular and tissue engineering

Xiaolong Tu

# THÈSE DE DOCTORAT

de l'Université de recherche Paris Sciences et Lettres
PSL Research University

**École Normale Supérieure de Paris**

Fabrication and study of multidimensional scaffolds for cell and tissue engineering

# Fabrication et étude de scaffolds multidimensionnels pour l'ingénierie cellulaire et tissulaire

**Ecole doctorale n°388**

CHIMIE PHYSIQUE ET CHIMIE ANALYTIQUE DE PARIS CENTRE

**Spécialité** Chimie Physique et Chimie Analytique

**COMPOSITION DU JURY :**

M. PALLANDRE Antoine
Professeur Université Paris-Sacaly, Rapporteur

M. THERY Manuel
Directeur de recherche CEA, Rapporteur

Mme. VILLARD Catherine
Directrice de recherche CNRS, Examinateur

Mme. HAGHIRI-GOSNET Anne-Marie
Directrice de recherche CNRS, Examinateur

M. CHEN Yong
Directeur de recherche CNRS, Directeur de thèse

**Soutenue par Xiaolong TU**
**le 13 Octobre, 2017**

Dirigée par **Yong CHEN**

ENS ÉCOLE NORMALE SUPÉRIEURE | PSL RESEARCH UNIVERSITY PARIS

# Acknowledgement

Time flies! My PhD study in École normale supérieure de Paris is coming to an end, which is and will be forever the extraordinary experience for me. In retrospect of my past life and my PhD study here, I cherish great gratitude towards the school and people who guide, help and encourage me to complete my PhD thesis work.

First of all, I would like to present my gratitude to École normale supérieure de Paris providing me best working conditions and excellent research environment to work on my thesis.

Then I would like to express my great gratitude towards my supervisor Prof. Yong CHEN for his professional guidance and suggestion. With his help, I have acquired critical thinking and logical scientific methods which are highly beneficial for my PhD work. Besides, his suggestion helps me explore several important fields in the cross-disciplinary areas related to micro-engineering, cell biology, and biomedical applications. All of the suggestion he made means a lot to me, and will surely facilitate my future academic career.

Next, I am also grateful to the colleagues and friends in France for their kindly help, support and encouragement. They are: Dr. Jian Shi, Dr. Li Wang, Dr. Jacques Fattaccioli, Dr. Sandrine Quignard, Dr. Diana Molino, Dr. Yohan Farouz, Dr. Kalthoum Ben M'barek, Dr. Li Zhou, Francesco Paolo Ulloa Severino, Jin Wei, Bin Wang, Olivier Mesdjian, Xiaoqing Liu, Chenge Li, Lihui Hu and Yu Liu.

I would also like to give my gratitude to Mr. Stéphane Emery, Mr. Auguste Filippi, Mme Anne Halloppe, Mr. Stéphane Paties-Gorizza, Mme Katy Seloi, Mme Marie Chayla in ENS and Mme Soobrayen Koonavadee in UPMC, who are always so kind to arrange official affairs management.

Then I would like to present my great gratitude towards my family. I am especially grateful to my wife XinxinYang for her understanding and encouragement for my PhD study. I am also grateful to my parents and parents-in-law for their understanding and support for my study abroad.

Finally thank again for all the people mentioned for their selfless help and guidance.

Xiaolong Tu

06/07/2017

# Table of Contents

# Outline

Tissue engineering has drawn increasing attention and shows great potential in treatment of clinical diseases such as diseases in nervous system and cardiovascular system. Different from conventional methods, the recent approaches are based on *in vitro* regeneration of stem cell derived tissues for more efficient cell-based assays and implantation treatment. In tissue engineering, functional scaffolds play key roles in sustaining culture of stem cells, directing efficient differentiation of the stem cells into targeted tissues and guiding tissue organization in multidimensions. Therefore, the key point lies in fabricating optimal tissue scaffolds for improved cell culture and enhanced tissue formation.

The main purpose of this work is to propose solutions to the current problems encountered in stem cell based tissue engineering.

The stem cell based tissue engineering has proved to be reliable in the development of regenerative medicine. Unlike the previous clinical methods often limited due to the lack of cell source and organ donor, the stem cell technology allows producing large amounts of targeting cells with identical properties. In this work, neural progenitor cells (NPCs) and human induced pluripotent stem cells (hiPSCs) are used. NPCs are capable of dividing a limited number of times and differentiating into a restricted repertoire of neuronal and glial cell types, which are potentially applicable in the treatment of neural degenerative diseases like Alzheimer's disease. HiPSCs are embryonic-like stem cells, which can be obtained by reprogramming somatic cells (Yamanaka, 2006). Since hiPSCs can also be generated from patients, easily expanded and derived to other types of somatic cells, allowing perform more precise clinical tests with reduced immune rejection after implantation. So far, the studies on stem cells are mostly based on conventional culture techniques, which have been proven not suitable due to spontaneous differentiation and risks of genetic instability as well as tumorigenecity. Therefore there is a clear need of new culture conditions compatible to both *in vitro* and *in vivo* assays.

In this work, we developed functional scaffolds for improved culture and

differentiation of stem cells. Nature does nothing useless. The best strategy is therefore to emulate the nature or the *in vivo* microenvironment of targeted tissues. Cells are sensitive to their living surroundings including extracellular matrix, soluble factors, cells and their 3D organizations. In particular, the extracellular matrix provides mechanical supports and membrane mediated biochemical signaling, thus playing an essential role in controlling cell behaviors such as cell adhesion, migration, proliferation and differentiation. The functional scaffolds we are looking for have to recapitulate as much as the detail of the natural material composition and the natural organization of the ECM *in vivo*. Previously, different techniques, including 3D printing, freeze drying, electrospinning, microlithography, and self-assembly, have been used in tissue engineering of different purposes. We will show how these techniques can be used to improve our scaffold design and manufacturing. We will also demonstrate the improved performance of these scaffolds in cell culture and tissue engineering, including cell adhesion, proliferation, nutrients uptake and differentiation.

Accordingly, this thesis is organized as follow:

In chapter one, we first introduce the basic concepts of cell and extracellular microenvironment. Then we focus on two types of stem cells, i.e. neural progenitor cells and induced pluripotent stem cells. Next we describe the state-of-the-art developments of tissue engineering scaffolds from materials choice, fabrication methods to tissue engineering applications. Finally, we outline the objectives of the thesis work.

In chapter two, we present the technological development of this thesis work. First we introduce the UV lithography and soft lithography which are frequently used in our work for substrates preparation. Then we describe the electrospinning technique for nanofiber fabrication. Afterwards, we present 3D printing technique with a focus on photopolymerization method. Further, we talk about the freeze drying technique for porous scaffold fabrication. Finally, we discuss the self-assembly of polymer scaffolds and parylene C deposition technique.

In chapter three, we present a study of improved culture and differentiation of neural progenitor cells by using 3D printed PEGDA/porous gelatin scaffold. We first describe the fabrication methods of culture scaffold. As expected, the printed PEGDA shows regular 3D grids with strong mechanical strength and sponge-like gelatin porous

structures with good swellability and biodegradability. Cell culture has been studied, showing that NIH 3T3 cells exhibit high cell attachment, viability, proliferation and migration on the scaffold. The scaffold also provides supportive culture and neuron differentiation of NPCs. Interestingly, the porous structure of gelatin also provides structural cues for conduction of neural impulse. This combination strategy in scaffold fabrication is also advantageous in terms of easy processing, scaling-up, and translating from one type of scaffolds to another.

In chapter four, we present a study on self-assembly porous PCL patch to improve cell performance and supportive cardiac differentiation. First we present the fabrication of porous PCL film by self-assembly. The as-fabricated porous PCL patch possesses highly uniform pore with good shape integrity and are easy to handle for routine characterization and cell culture applications. The high porosity of the patch has been proved to significantly improve cell performance on the porous PCL patch including cell adhesion and proliferation as well as high efficient cell processing of gene transfection. Then we reveal that the porous PCL patch shows improved culture and promoted cardiac differentiation of hiPSCs with more robust contraction behavior than glass slide substrate in terms of contraction strength and uniformity. Finally we show that such kind porous PCL patch also shows controlled biodegradation with cells cultured on it, which shows great potential in tissue engineering applications.

In chapter five, we present a study on electrospun single layer gelatin nanofiber patch supported by elastic PDMS frame for improved culture and cardiac differentiation of hiPSCs. First we describe the fabrication of porous elastic PDMS honeycomb frame and single layer electrospun gelatin nanofiber with uniform nanofiber, high porosity and controllable pore size. Then we present the improved hiPSCs culture on the patch. We have demonstrates that cells show high viability and promoted proliferation on the patch. By varying the vitronectin coating, formation of monolayer and EB hiPSCs can be easily obtained, with high proliferation and sustained stem cell pluripotency. Next we present promoted cardiac differentiation of hiPSCs on the patch than on glass slide in terms of contraction strength and uniformity. Further we test the functionality of generated cardiac tissue with calcium imaging, electrical stimulation and drug test, which shows reasonable response compared with normal cardiac tissues. Finally we present the effects of PDMS frame with engineered elasticity on guiding cardiac tissue

contraction.

In chapter six, we present a summary of the thesis work and a perspective for the work focusing on fabrication methods development, biodegradable and smart materials, and integration of tissue engineering scaffolds with microfluidics for organ-on-a-chip research.

In appendix A, we present a study of cell performance on parylene C substrates with different patterns. We first describe the fabrication of parylene C substrates with different patterns (pillar and stripe) by putting forward a new thin layer transfer techniques. Then we present the results of cell adhesion and spreading on the above patterned substrates and flat parylene C films. Our results show that the as-deposited parylene C on a flat substrate does not support cell adhesion due to its hydrophobic surface while air plasma treated parylene C is readily useful for cell adhesion and spreading studies. Parylene C pillars without air plasma treatment can improve the adhesion but have little effect on cell spreading. Finally we show the contact guidance effects of parylene C stripes with different pitch sizes on cell alignment growth by cell orientation, nuclear deformation and cell elongation. As expected, parylene C strips have a strong effect of contact guidance. Thus, we demonstrate an easy fabrication of parylene C micro-patterns as well as their usefulness for cell behavior studies, which should be beneficial to improve the performance of implantable medical devices.

In Appendix B, we present a study on the fabrication of biodegradable porous gelatin patch. First we describe the fabrication of porous gelatin patch including gelatin honeycomb frame and aligned gelatin nanofibers. The electrospun nanofibers show high alignment even after crosslinking. Then we present the application of the gelatin nanofibers for delivery of vascular endothelial growth factor (VEGF) including loading and controlled release. The amount of heparin loaded on crosslinked gelatin nanofibers can be largely increased with chitosan/EDAC/NHS method and thus increases the amount of VEGF loaded on the patch. The VEGF loaded exhibits controlled and sustainable release under cell culture conditions.

# Chapter 1

# Introduction

In this chapter, we first introduce the basic concepts of cell and cellular microenvironment. Then, we focus on two types of stem cells, i.e. neural progenitor cells and induced pluripotent stem cells. Next, we describe the state-of-the-art developments of tissue engineering scaffolds, including issues of materials choice, fabrication methods and tissue engineering applications. Finally, we outline the objectives of the thesis work.

# 1.1 Cell and cellular environment

## 1.1.1 Cell

The human body is a complex entirety with distinct organ systems working together to maintain homeostasis, keeping the body in a stable state with safe levels of substances like sugar and oxygen and body signs like temperature and blood pressure. Typically these organ systems are defined as circulatory system, nervous system, digestive system, muscular/skeletal system, respiratory system, immune system, endocrine system, renal system and reproductive system. These systems ensure the physiologically conditions of the body by maintaining blood flow, movement, energy supply, temperature, acid balance, waste remove and protection. Circulatory system (**Fig. 1.1**), for example, comprises the heart, blood and blood vessels. The heart propels the circulation of blood to transfer oxygen, fuel, nutrients, waste products, immune cells and signaling molecules from one part of the body to another via blood vessel with the cooperation of respiratory system, digestive system, renal system, immune system and etc. The heart, blood and blood vessel are composed of different types of cells including cardiomyocytes, blood cells and endothelial cells. Actually, cells are the basic structures and functional units of the human body.

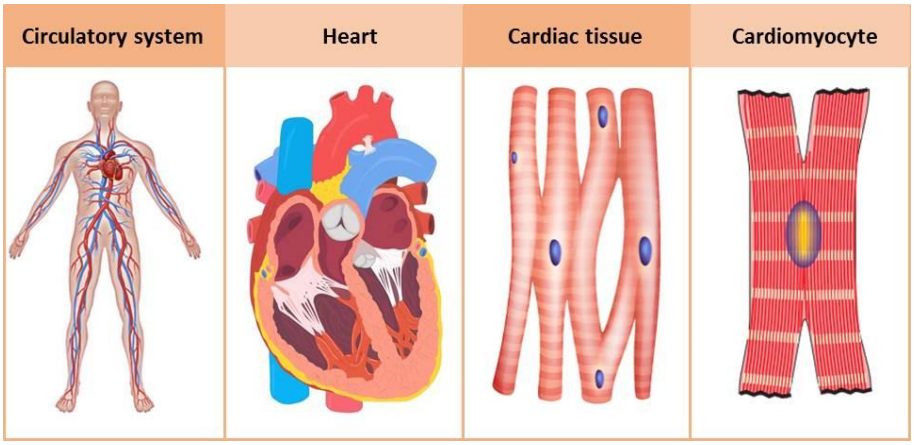


**Fig. 1.1** The human body in different levels: system, organ, tissue and cell [1].

As a basic unit of living things, cell is the building block of complex life. The inner structure of an individual cell is also complex and sophisticated designed by nature, as is shown in **Fig. 1.2** of a typical animal cell. Despite the complicated inner structure, cell behavior is highly ordered and well regulated in the metabolism of substance and energy and responding to extracellular signaling. Every subcellular structure has its unique functions necessary for the cell:

(1) Each cell has a dynamic membrane made of double-layer self-assembly lipids. For plant cells, there is a cell wall outside the lipid membrane. The cell membrane surrounds the cytoplasm within a cell, which isolates the cell from outer environment, provides specific routes for the exchange of chemicals like ions, fuels and signaling molecules and maintains the membrane electrical potential.

(2) Cells keep their hereditary information within an internal compartment called the nucleus, which is wrapped by a double layer of membrane called nuclear envelope. The hereditary information is stored in DNA in the form of chromatin or chromosome. The main function of nucleus is to regulate gene expression and DNA replication during cell cycle.

(3) The cell skeleton including microtubules, actin filaments and intermediate filaments plays an important role in many cellular behaviors like adhesion, migration, dividing and differentiation. The cell skeleton is made of assembly of specific proteins which can dynamically polymerize and depolymerize in specific cell behavior. Cell skeleton also acts as a track for motor proteins to carry vesicles into or out of the cell.

(4) The effects of nuclear exerting on cell behavior are mediated by the expression of functional proteins encoded in DNA base sequence. DNA can deliver its information to message RNA (mRNA) by a process call transcription. Ribosomes located in cytoplasm are the main platforms for the translation of mRNA into proteins.

(5) Almost all the processes in cells need energy. The mitochondrion performs most cellular oxidations and produces the bulk of the animal cell's ATP, the energy currency of cell. The mitochondrion contains a large variety of enzymes that convert carbohydrates and fatty acids to $H_2O$ and $CO_2$ through the citric acid cycle, which produces large amounts of energy stored in ATP. The energy can be released by hydrolysis of ATP.

(6) In multicellular organism, cells must communicate with each other. Cells both release and receive signals. Reception of the signals depends on receptor proteins, usually at the cell surface, which bind the signal molecule. The binding activates the receptor, which in turn activates one or more intracellular signaling pathways. The intracellular signaling proteins process the signal and distribute it to the appropriate intracellular targets. These targets implement the appropriate change of cell behavior.

(7) The only way to make a new cell is to duplicate a cell that already exists. A cell reproduces by performing an orderly sequence of events in which it duplicates its contents and then divides in two, known as the cell cycle. This process includes several complicated steps like chromosome duplication and segregation, other subcellular components duplication and cell splitting.

(8) Cell death also plays a crucially important role in development. In a healthy adult human, although billions of cells die in the bone marrow and intestine every hour, our tissues do not shrink because, cell division exactly balances the cell death. These normal cell deaths are suicides in which cells activate an intracellular death program and kill themselves, known as programmed cell death. However, cells may die accidentally in response to an acute insult, such as trauma or a lack of blood supply, usually called cell necrosis.

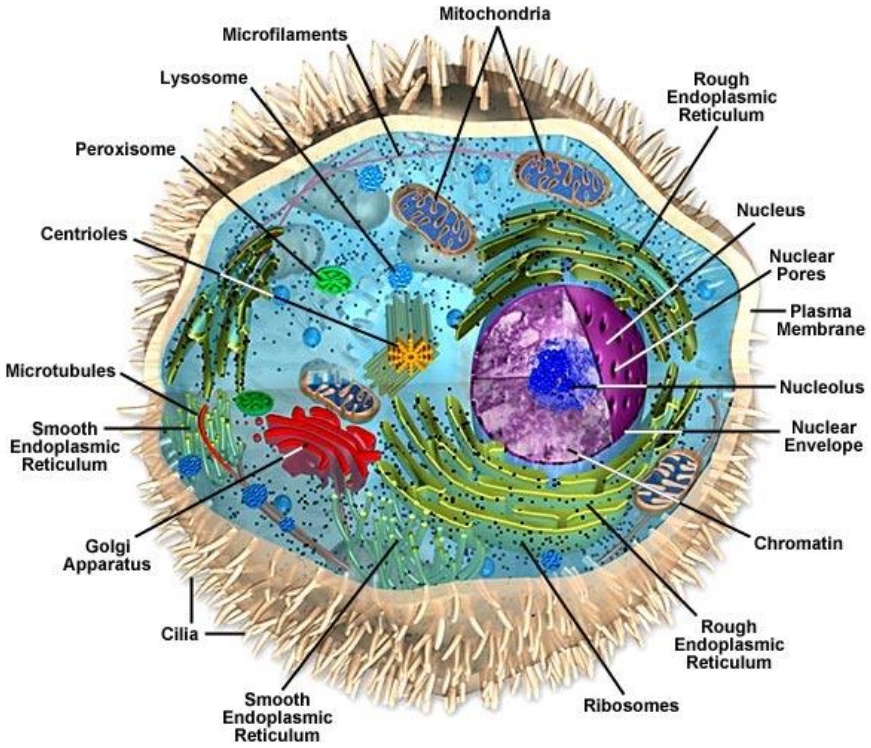


**Fig. 1.2** Scheme of the intracellular structure of an animal cell [2].

(9) Cells make their own living environments by regulatory production, organization and degradation of extracellular matrix (ECM) which, in turn, exerts powerful influence on cell behavior mainly through transmembrane proteins that act as matrix receptors. Clarification of cell matrix interaction is beneficial to understand the individual cell behavior in a cellular society. So next we will introduce in detail the extracellular matrix and its interaction with cells in **section 1.1.2**.

## 1.1.2 Cell microenvironment

In multicellular organisms, cells are not isolated but communicate each other directly or mediated by extracellular matrix. Here we will introduce the *in vivo* cell environment.

### 1.1.2.1 Cell-cell interaction

Of all the interactions between cells in a multicellular organism, the most fundamental are those that hold the cells together. Cells cling to each other via direct cell-cell junction. Cell-cell junction can be divided into three categories: occluding

junction (also called tight junction in animals), anchoring junction and communication junction (also called gap junction in animals), as is shown in **Fig. 1.3** [3]. Occluding junctions in endothelial cells in guts seal gaps between cells and prevent the leakage of nutrients back to gut lumen. Anchoring junction includes adherent junction that connects actin filament bundle in one cell with that in the next cell and desmosome junction which connects intermediate filaments in one cell to those in the next cell. Anchoring junctions transmit stresses and are tethered to cytoskeletal filaments inside the cell. Gap junction, which is made up of six transmembrane connexin subunits, is the main site for cell-cell signaling [4]. It allows inorganic ions and other small water-soluble molecules to pass directly from the cytoplasm of one cell to the cytoplasm of the other, thereby coupling the cells both electrically and metabolically. Cadherin mediates $Ca^{2+}$-dependent cell-cell adhesion and coordinates the actin-based motility of adjacent cells [5]. The making and breaking of the adhesion govern the way cells move within the organism, guiding them as the body grows, develops, and repairs itself.

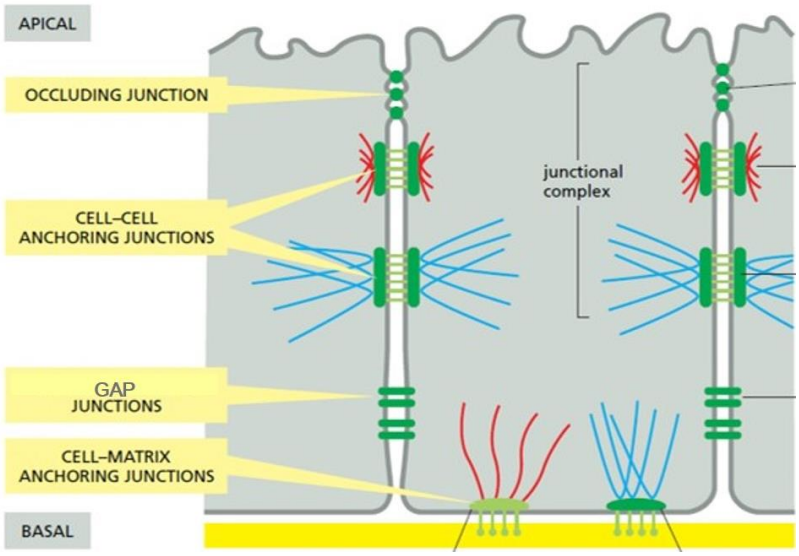


**Fig. 1.3** A summary of the various cell junctions found in a vertebrate epithelial cell [6].

### 1.1.2.2 Extracellular matrix and basal lamina

Tissues are not made up solely of cells. A part of their volume—sometimes a major part—is extracellular space occupied by an intricate network of macromolecules constituting the extracellular matrix (ECM), as is shown in **Fig. 1.4**. This matrix is composed of various proteins and polysaccharides that are secreted locally and

assembled into an organized meshwork in close association with the surfaces of the cells that produced them. ECM provides the structural and biochemical support to cells and regulates cell behaviors like adhesion, migration, proliferation and differentiation [7-10].

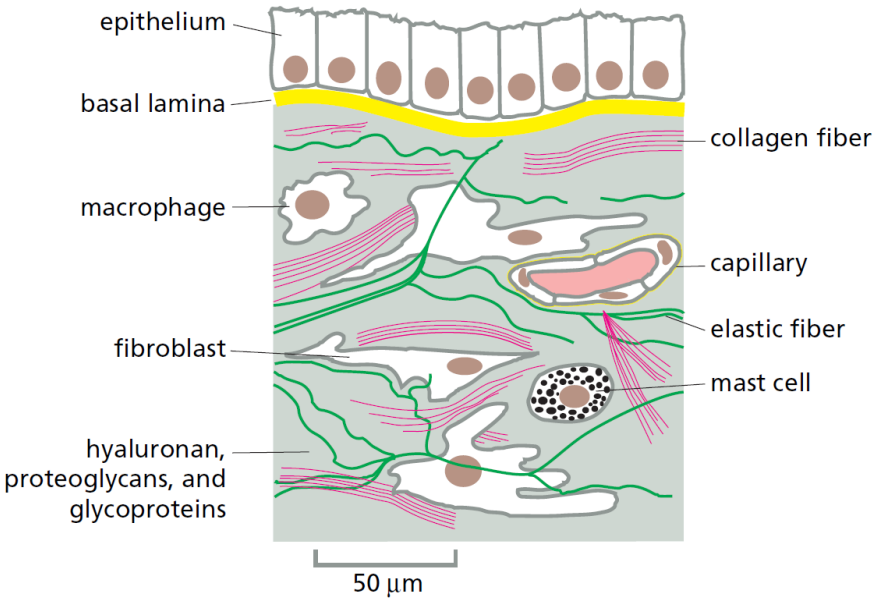


**Fig. 1.4** A scheme of ECM in connective tissue [11].

The most plentiful forms of ECM are found in bulky connective tissues such as bone, tendon, and the dermal layer of the skin. In most connective tissues, the matrix macromolecules are secreted largely by cells called fibroblasts. ECM is constructed by two main classes of macromolecules: (1) glycosaminoglycan polysaccharide chains, usually covalently linked to protein in the form of proteoglycans, and (2) fibrous proteins such as collagen and elastin.

**Tab. 1.1** Members of collagen family and their properties [12].

| | TYPE | POLYMERIZED FORM | TISSUE DISTRIBUTION |
|---|---|---|---|
| Fibril-forming (fibrillar) | I | fibril | bone, skin, tendons, ligaments, cornea, internal organs (accounts for 90% of body collagen) |
| | II | fibril | cartilage, invertebral disc, notochord, vitreous humor of the eye |
| | III | fibril | skin, blood vessels, internal organs |
| | V | fibril (with type I) | as for type I |
| | XI | fibril (with type II) | as for type II |
| Fibril-associated | IX | lateral association with type II fibrils | cartilage |
| Network-forming | IV | sheetlike network | basal lamina |
| | VII | anchoring fibrils | beneath stratified squamous epithelia |
| Transmembrane | XVII | non-fibrillar | hemidesmosomes |
| Proteoglycan core protein | XVIII | non-fibrillar | basal lamina |

The proteoglycan molecules typically form a highly hydrated, gel-like "ground substance" in which the fibrous proteins are embedded. The polysaccharide gel resists compressive forces on the matrix while permitting the rapid diffusion of nutrients, metabolites, and hormones between the blood and the tissue cells [13]. The collagen fibers are the major proteins in ECM, which strengthen and help organize the matrix [14, 15]. **Tab. 1.1** summarizes the members of collagen family and their distribution in tissues. Other fibrous proteins, such as the rubberlike elastin (**Fig. 1.5**), render ECM with resilience [16]. Fibronectin is an extracellular protein that helps cells attach to the matrix by bonding to integrin through an RGD peptide sequence [17]. The ECM components and their roles are summarized in **Tab. 1.2**.

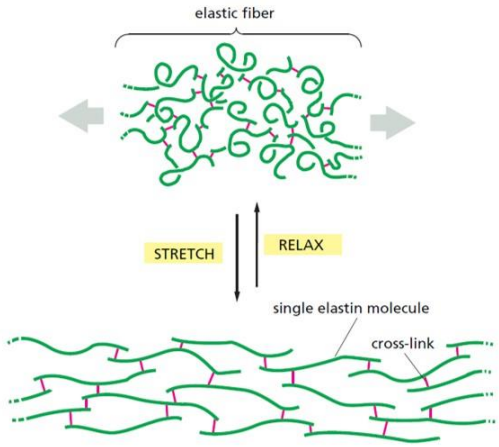


**Fig. 1.5** Scheme of stretching and relaxing of elastin network [18].

**Tab. 1.2** ECM components and their roles [19].

| Component | Function | Location |
|---|---|---|
| **Collagens** | Tissue scaffolding, tensile strength<br>Cell-ECM interactions<br>Cell-cell interactions<br>Fibroblast activation | Ubiquitous |
| **Proteoglycans** | Collagen embedding<br>Tissue resistance to compressive forces<br>Transport of nutrients<br>Fibroblast and chondrocyte proliferation<br>Endothelial and epithelial cell differentiation | Ubiquitous |
| **Hyaluronic acid** | Transport of metabolites and nutrients<br>Tissue resistance to compressive forces<br>Cell migration<br>Cell proliferation | Ubiquitous |
| **Laminins** | Intracellular signalling<br>Cell differentiation<br>Cell shape/movement | Basement membranes |
| **Fibronectin** | Cell attachment to ECM<br>Cell migration<br>Cell proliferation | Ubiquitous |
| **Growth factors** | Cellular signalling | Ubiquitous |

The ability of cells to degrade and destroy extracellular matrix is as important as their ability to make it and bind to it. Rapid matrix degradation is required in processes such as tissue repair. Even in the seemingly static extracellular matrix of adult animals there is a slow, continuous turnover with matrix macromolecules being degraded and resynthesized [20].

Under the epithelium layer and upon ECM lies a thin tough sheet of matrix molecules called basal lamina which is an essential underpinning of all epithelia and has a critical role in the architecture of the body. The basal lamina separates epithelia from the underlying or surrounding connective tissue and forms the mechanical connection between them [21]. More than roles in simple structuring and filtering, basal lamina is able to determine cell polarity, influence cell metabolism, organize the proteins in adjacent plasma membranes, promote cell survival, proliferation, or differentiation, and serve as highways for cell migration [22-26]. Although the precise composition of the mature basal lamina varies from tissue to tissue and even from region to region in the same lamina, it typically contains the glycoproteins laminin, type IV collagen, and nidogen, along with the proteoglycan perlecan [27], shown in **Fig. 1.5**. It also holds in its meshes, or is closely associated with, various other molecules including collagen XVIII and fibronectin, fibrous proteins important in the adhesion of connective-tissue cells to matrix. The laminin is thought to be the primary organizer of

the sheet structure, and early in development, basal lamina consist mainly of laminin molecules [28]. Type IV collagen is a second essential component of mature basal lamina, which renders the basal lamina tensile strength [29]. The components nidogen and perlecan are thought to serve as linkers to connect the laminin and type IV collagen networks once the laminin is in place. When cells are damaged or killed, basal lamina often survive and can help guide tissue regeneration.

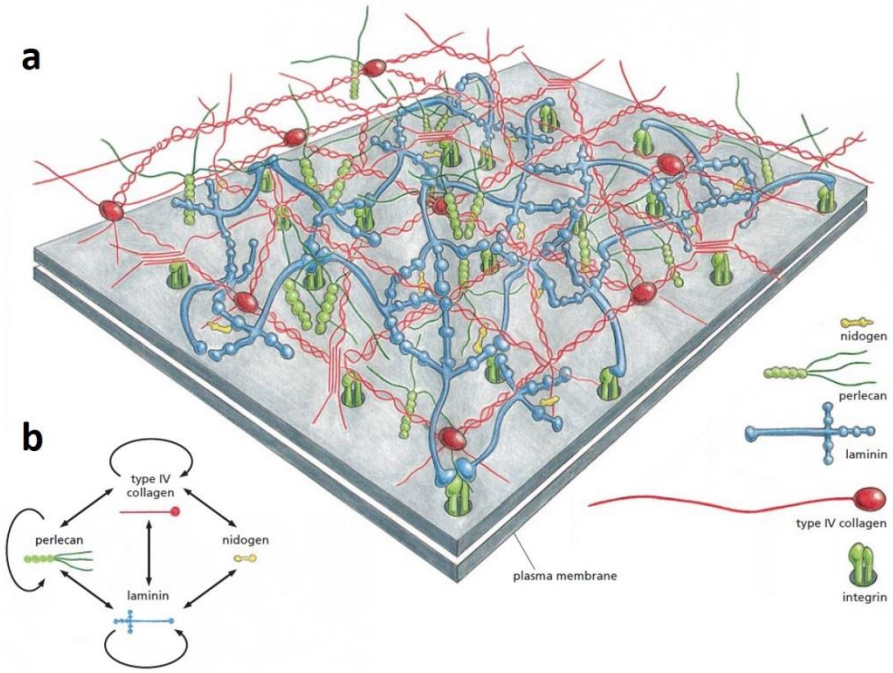


**Fig. 1.5** A schematic model of molecular interaction of a basal lamina. (a) The basal lamina is formed by specific interactions (b) between the proteins laminin, type IV collagen, and nidogen, and the proteoglycan perlecan [30].

### 1.1.2.3 Cell-matrix interaction

Cells make extracellular matrix, organize it, and degrade it. The matrix in its turn exerts powerful influences on the cells. The influences are exerted chiefly through transmembrane cell adhesion proteins that act as matrix receptors. The principal receptors on animal cells for binding most extracellular matrix proteins are the integrins which are transmembrane heterodimers linking to the cytoskeleton, as is shown in **Fig. 1.6** [31-33]. The head of the integrin molecule attaches directly to an extracellular protein such as fibronectin; the intracellular tail of the integrin binds to talin, which in

turn binds to filamentous actin. The binding of a matrix component to an integrin can send a message into the interior of the cell, and conditions in the cell interior can send a signal outward to control binding of the integrin to matrix. Tension applied to an integrin can cause it to tighten its grip on intracellular and extracellular structures, and loss of tension can loosen its hold, so that molecular signaling complexes fall apart on either side of the membrane. In this way, integrins can serve not only to transmit mechanical and molecular signals, but also to convert the one type of signal into the other [34-36]. Integrin defects are responsible for many different genetic diseases such as leucocyte adhesion deficiency and Glanzmann's disease [37].

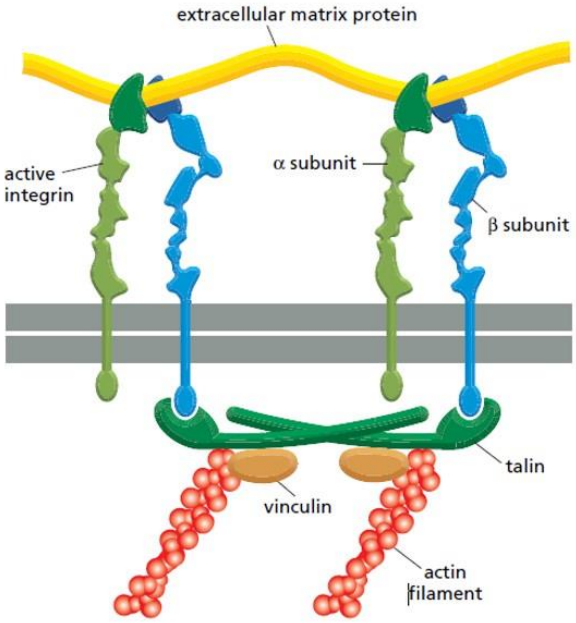


**Fig. 1.6** A scheme of cell surface integrin bonding with ECM protein [38].

Besides the ECM proteins, polysaccharides in ECM also play important roles in supporting cells, including hyaluronic acid, chondroitin sulfate and dermatan sulfate, heparin sulfate, and keratan sulfate [39, 40]. They are strongly hydrated and form gels even at very low concentrations to fill most of the extracellular space. Their high density of negative charges (**Fig. 1.7**) attracts a cloud of cations, especially $Na^+$ that are important in osmosis, causing large amounts of water to be trapped into the matrix [41]. This creates a swelling pressure that enables the matrix to withstand compressive forces. Hyaluronic acid synthesized locally from the basal side of an epithelium can deform

the epithelium by creating a cell-free space beneath it, into which cells subsequently migrate [42]. These polysaccharides also have an important role in chemical signaling between cells. They bind various secreted signal molecules, such as certain protein growth factors—controlling their diffusion through the matrix, their range of action, and their lifetime. For example, the heparan sulfate chains bind to fibroblast growth factors (FGFs), which stimulate a variety of cell types to proliferate [43-45]. In inflammatory responses, heparan sulfate immobilize secreted chemotactic attractants called chemokines on the endothelial surface of a blood vessel at an inflammatory site [46]. This allows the chemokines to remain there for a prolonged period, stimulating white blood cells to leave the bloodstream and migrate into the inflamed tissue.

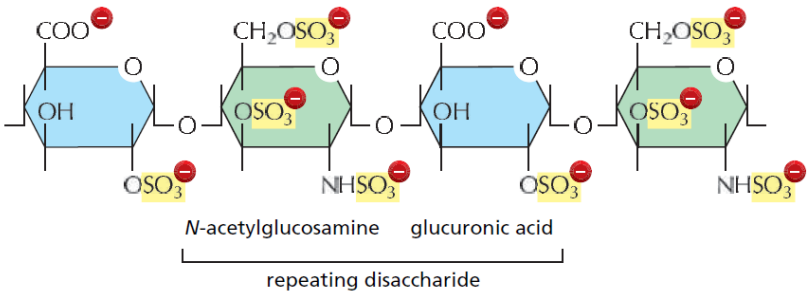


**Fig. 1.7** The repeating disaccharide sequence of a heparan sulfate glycosaminoglycan chain [47].

## 1.1.3 Cell culture

Cells can be isolated from human body and cultured directly in *in vitro* substrates different from their natural environment (**Fig. 1.8**). A cell line can be obtained by maintaining a population of cells which contain the same genetic makeup from a single cell [48]. The success in developing a cell line contributes to a continuous and renewable cell supply for repeatable researches. This *in vitro* cell culture technique is adopted and advanced by biological labs, pharmaceutical companies and hospitals for fundamental studies [49-51]. Now standards for cell culture has been developed and applied globally including cell lines, cell medium and culture protocol.

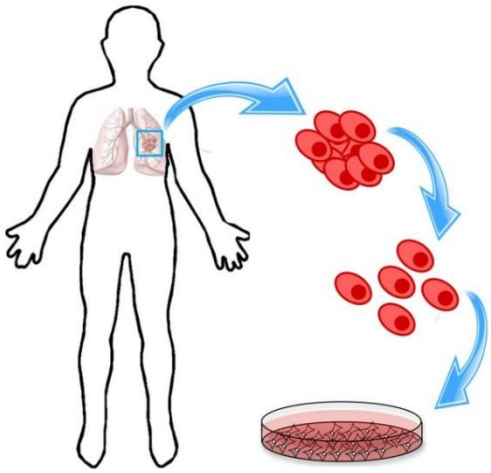

**Fig. 1.8** An illustration of cell extraction and *in vitro* culture [52].

Typically, mammalian cells are cultivated at an optimal condition of 37 ℃ and 5% $CO_2$. Aside from temperature and $CO_2$ level, the key factor is the cell growth medium. Recipes for growth media can vary in pH, glucose concentration, growth factors, and the presence of other nutrients.

In many cases cells are cultured in an adherent condition. After seeding, cells can cling to, deform and migrate on the bottom surface of culture dishes, flasks, multi-well plates and etc. After reaching a confluence of monolayer cell sheet, cell growth will be suppressed due to a phenomenon called contact inhibition [53]. In other cases, cells can be cultured in suspension such as cells in the bloodstream. Some cell lines have been modified to be able to survive in suspension cultures so they can be grown to a higher density than that adherent conditions would allow.

## 1.2 Stem cells and induced pluripotent stem cells

### 1.2.1 Stem cells

Stem cells are undifferentiated cells that are characterized by the ability to renew themselves through mitotic cell division and differentiating into a diverse range of specialized cell types (**Fig. 1.8**). They are found in all of us, from the early stages of human development to the end of life. They are vital to the development, growth, maintenance, and repair of our brains, bones, muscles, nerves, blood, skin, and other organs [54-56].

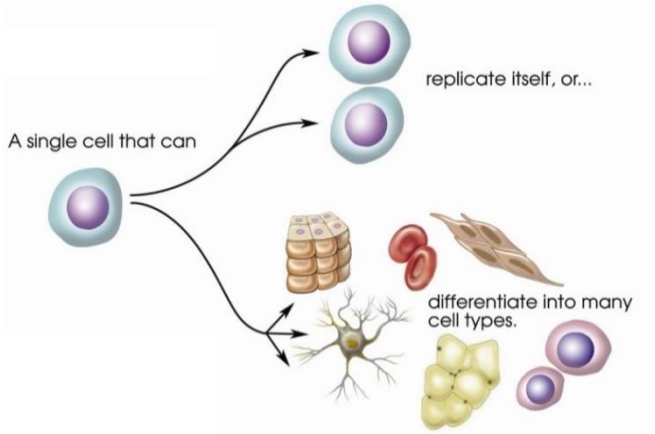


**Fig. 1.8** A scheme of stem cell that can renew itself and differentiate into many cell types [57].

Stem cells are classified into two major sub-types, based on the range of specialized cells they can generate: tissue stem cells and pluripotent stem cells [58]. Tissue stem cells are found throughout the body functioning to maintain the organ or tissue where they reside throughout the lifespan [59]. Under normal physiological conditions, each type of tissue stem cell only generates cells of the organ or tissue system to which it belongs: the blood stem cell generates blood, the skin stem cell generates skin, and so on. An exception is the mesenchymal stem cell, which can generate bone, cartilage, and muscle [55]. Pluripotent stem cells have the potential to generate any type of cell found in the body. Pluripotent stem cells are generated in the laboratory by capturing or recreating cell types that exist only transiently during embryonic development, and have not been identified in the adult body [60].

Embryonic stem cells (ESCs), the first type of pluripotent stem cells to be discovered, are derived from early-stage, pre-implantation embryos [61]. However, ESCs research is controversial because producing ESCs requires destroying embryos, generally human embryos, which has provoked debates regarding the ethics and regulation of the research and resulting therapies [62]. Some of the surplus human embryos available from *in vitro* fertilization clinics may have a high rate of genetic errors and therefore would be unsuitable for ESCs research. The number of ESCs lines approved for research usage is very limited. Additionally, in most cases available ESCs lines are generically foreign to any particular patient. Once for implantation purposes, immune rejection can occur because recipient's body does not recognize the exogenous

cells or requires lifelong therapy with immunosuppressive medication [63].

### 1.2.2 Neural progenitor cells

Neural progenitor cells (NPCs), which are located in the embryonic forebrain, are cells that are capable of dividing a limited number of times and have the capacity to differentiate into a restricted repertoire of neuronal and glial cell types, as is shown in **Fig. 1.9** [64]. NPCs are similar to neural stem cells which are from hippocampal area with a difference that neural stem cells can replicate indefinitely. NPCs have been used as a potential transplanted cell in the treatment of neural degenerative diseases like Alzheimer's disease [65, 66]. Transplanted NPCs can promote central nervous system (CNS) regeneration due to their therapeutic plasticity. On one hand, the differentiation plasticity of NPCs might lead to the replacement of damage cells; on the other hand, NPCs secrete neuroprotective molecules to promote endogenous regeneration [67].

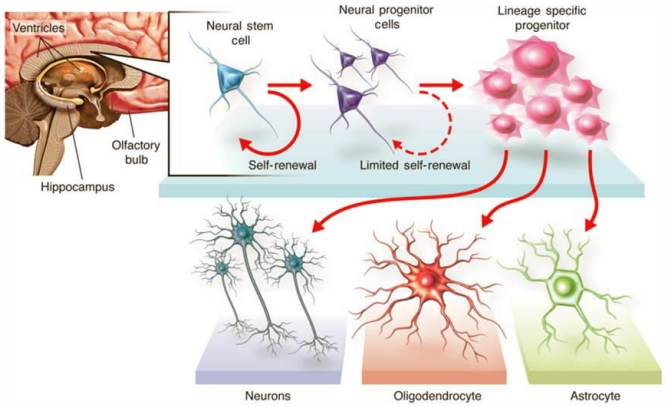


**Fig. 1.9** A scheme of origin of neural progenitor cells and their differentiated cells [68].

### 1.2.3 Induced pluripotent stem cells

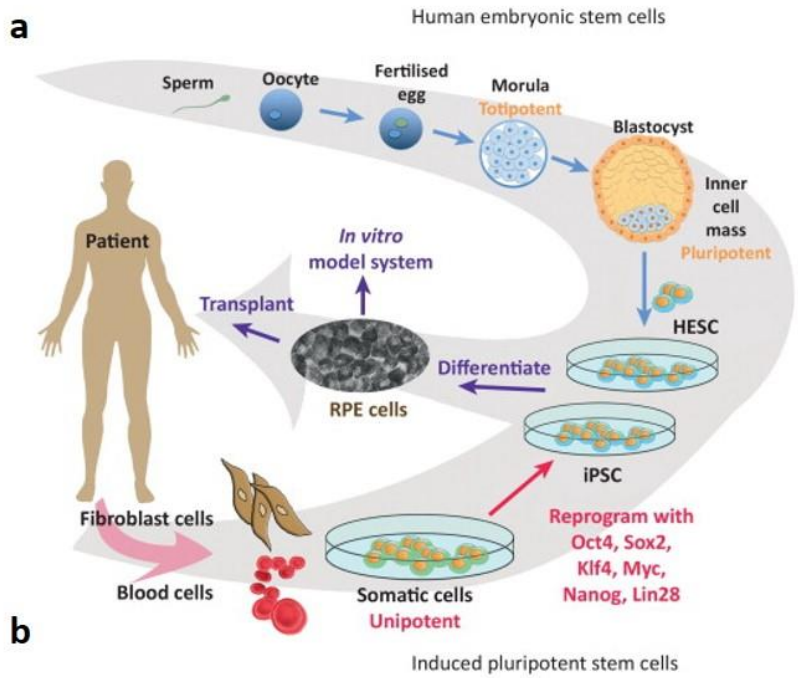


**Fig. 1.10** The origins, *in vitro* culture and tissue engineering applications of (a) human embryonic stem cells and (b) human induced pluripotent stem cells [69].

In 2006, Takahashi and Yamanaka opened a completely new venue in stem cell research by showing that the forced expression of only four transcription factors (Oct4, Sox2, Klf4, and c-Myc) was sufficient to convert human fibroblast cells into embryonic stem cell (ESCs)-like cells, which were named human induced pluripotent stem cells (hiPSCs) (**Fig. 1.10**) [70]. In recent years induced pluripotent stem cells have drawn increasing attention as a substitute of ESCs [71-73]. HiPSCs are able to differentiated into ectodermal, mesodermal and endodermal cells, which are similar to natural pluripotent stem cells such as embryonic stem cells in many aspects including the expression of certain stem cell genes and proteins, doubling time, chromatin methylation, embryonic body formation, viable chimera formation, potency and differentiability, but the full extent of their relation to natural pluripotent stem cells is still being assessed [74].

Compared with human ESCs in tissue engineering applications, hiPSCs have superior advantages, which can be generated from patient's somatic cells directly and can avoid the immune rejection risk. HiPSCs provide an alternative patient-specific strategy to get information of various diseases, to carry out *in vitro* drug screening, to

evaluate potential therapeutics and to explore cell-replacement therapy [75-77].

Concerns also rise in the studies of hiPSCs. One focuses on the proliferation of hiPSCs, i.e., hiPSCs have to proliferate for many times without losing their pluripotency, purity and quality. In conventional culture conditions, hiPSCs are of poor purity and often show chromosomal abnormalities and tumorigenic risks. By adding feeder cells, using Matrigel coating or using Xeno-free conditions, the quality of hiPSCs could be largely improved but not enough for clinical applications [78-80]. These studies mainly highlight the use of ECM protein in culture of hiPSCs while ignoring other factors related to extracellular microenvironments, i.e., 3D architect, mechanical and biochemical characters of substrates. The other focuses on the controlled differentiation of iPSCs. HiPSCs have been successfully re-differentiated into various cell lines including cardiovascular tissues, neurons and hepatocyte cells [81-83]. However, adult cells such as cardiac and neurons have different morphology and different physiochemical and biochemical functions which impose different organization and different mechanic stiffness. So the problem lies in how to efficiently derive hiPSCs into well-defined cell lineages with high yield and high quality.

Recently years the application of functional scaffolds for improved hiPSCs culture and directed differentiation into various cell lineages has drawn increasing attention. Guided by nature, this strategy relies largely on the materials manipulation to mimic *in vivo* ECM. The engineered scaffolds could largely promote hiPSCs culture and provide necessary structural and functional guidance for specific tissue generation in vitro, which will be discussed in detail in **section 1.3**.

## 1.3 Bioscaffolds for tissue engineering

The conventional methods for cell culture are based on plastic tissue culture dishes and flasks and glass slides. When cells are cultured in such substrates, their *in vivo* physiological conditions are lost due to the lack of surrounding organization of extracellular matrix. Cells are forced to adhere to a two-dimensional support where both underneath diffusion and cell-cell communication are less effective. Also, the rigid surface, inert character and high mechanical strength of the substrates are highly different from the *in vivo* compartments. Since cells are sensitive to culture

environments which in turn pose strong effects on cell behavior, the large disparity of the *in vitro* and *in vivo* culture environments will unavoidably lead to inconsistency of cell behavior and states. So studies based on the *in vitro* cell culture are not convincing enough. The problem arises when this change of cell culture environments become critical in the case of pluripotent stem cells like human ESCs and hiPSCs. So far, the most studies of hiPSCs, including hiPSCs production, renewal and differentiation have been based on conventional cell culture methods, which faces a problem of stem cell quality control and the risk of genetic instability, tumorigenecity, etc [84-86].

We put forward the great potential of stem cells derived tissues for regenerative medicine. For this purpose, functional scaffold fabrication with 3D structure topography is need. Therefore, we introduce the following notions of materials and methods that are used for fabricating culture scaffolds. Of all the topics in this section, the most central and primary one is biomaterial.

## 1.3.1 Biomaterials

Biomaterial is the substance engineered to interact with biological systems for a medical purpose. At very beginning, biomaterials based studies focus on their simple interaction with the body. In the past decades, increasing attention has been paid to using biomaterials to influence biological processes for tissue regeneration purpose [87]. Basically, currently used biomaterials can be divided into three main groups: inorganic materials such as metals, ceramics and minerals, natural polymers including proteins and polysaccharides and synthetic polymers.

### 1.3.1.1 Inorganic materials

Human body is almost composed of organic materials except for some hard tissues like bone and teeth which are mainly inorganic materials. Metals and ceramics have been widely used as substitutes for replacement of orthopedic or broken bone or teeth [88-91]. Ceramic scaffold hydroxyapatite (HA) (**Fig. 1.11a,b**), the major component of inorganic materials in bone, has been widespread applied for bone regeneration. Its special properties such as high mechanic stiffness, low elasticity, a hard brittle surface,

as well as the outstanding biocompatibility, make it excellent in bone regeneration field [92]. Besides, the interaction of osteogenic cells with the ceramic scaffolds can enhance the proliferation and differentiation of osteoblasts, and will probably improve bone regeneration. Additionally, some metals like Ti and Ti (**Fig. 1.11c,d**) alloy have also been extensively applied for implants, such as artificial bones, dentures, etc [93].

However, due to the low cell permeation, low cell interaction, non-biodegradation and the difficulty in material processing, the application of metals and ceramics is still very limited in tissue engineering. As a consequence, currently, polymer biomaterials have drawn increasing attention and are enjoying rapid development, including natural polymers and synthetic polymers.

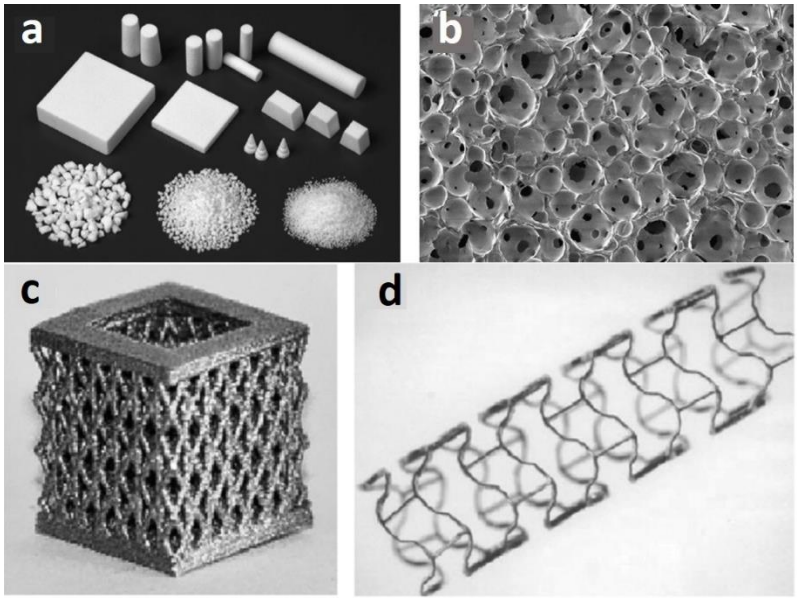


**Fig. 1.11** (a) Macroscopic images of HA scaffolds in different shapes and (b) SEM image of the microstructures of HA [94]. (c) NiTi scaffold for pseudoelastic applications and (d) Biodegradable Mg stent after expansion [93].

### 1.3.1.2 Natural polymers materials

The natural origin polymers are widely applied in tissue engineering [95, 96]. According to their chemical composition, there are two main groups of natural polymers, polysaccharides and proteins. Some polysaccharides are from plants, like alginate, agarose, cellulose and starch, and some are from animals like chitosan and chitin. The most frequently used proteins are collagen and its derivative gelatin, which

are the major components in natural ECM.

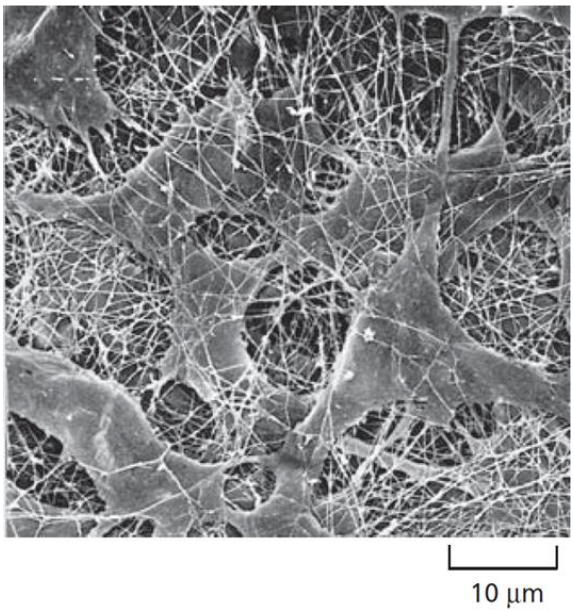


**Fig. 1.12** SEM image of fibroblasts surrounded by ECM proteins composed largely of collagen fibrils in connective tissue [97].

Natural polymers have several advantages over inorganic materials. Naturally polymers are usually marked with high biocompatibility and high cell attachment because they are directly from living things themselves. **Fig. 1.12** shows fibroblasts surrounded by fibrous ECM proteins they produced in connective tissue. Besides, due to high solubility in solvents and easy chemical functionalization, processing of natural polymers is relatively easy, from macroscale to nanoscale, with various shapes like fibers, films and 3D bulk scaffolds [98-100]. Another prominent quality is the biodegradability under physiological conditions, which is a brilliant merit for implants in tissue engineering.

Considering the importance of ECM for cell culture, collagen, the major component in ECM, receives extensively attention and has been proved a potential material for many clinical applications in the past decade, such as injectable collagen for the augmentation of tissue defects, hemostasis, burn and wound dressings and nerve regeneration [101, 102]. However, collagen is facing some potential problems like antigenic and immunogenic response that can be provoked during its *in vivo* application [103]. Gelatin, the product of partial hydrolysis of collagen, has been reported with a

lower immunogenicity *in vivo* [104]. Various gelatin scaffolds have been increasingly used in tissue engineering including nanofibers, 3D printed microstructures and lyophilized porous scaffolds (**Fig. 1.13**). So gelatin is the natural biomaterial we chose in this work. We will discuss in detail in **Chapter 3 and 5**.

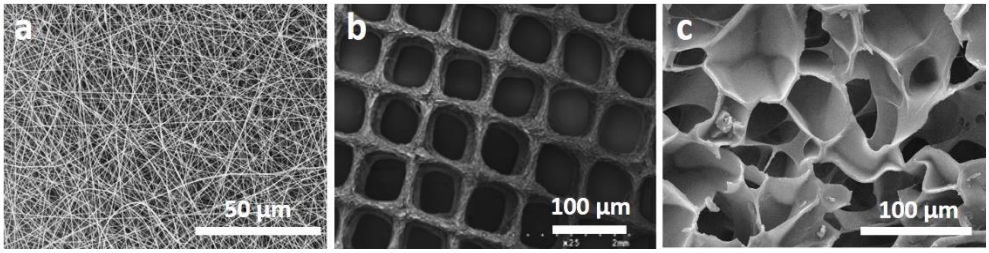


**Fig. 1.13** SEM images of gelatin scaffolds. (a) Electrospun nanofibers, (b) 3D printed microlattice [105] and (c) lyophilized porous scaffolds.

However, natural polymers are still suffering several disadvantages. Due to the different resources in different regions, there are some quality variations from batch to batch. The potential impurities may cause some unexpected immune reactions *in vivo*. Additionally, the poor mechanical strength results in difficult substrate handling and severe deformation during the *in vitro* and *in vivo* tests. From this point of view, we aim to fabricating porous gelatin substrates with easy handling and enough mechanical strength for cell culture and neuron differentiation, which we will discuss in details in **Chapter 3**.

#### 1.3.1.3 Synthetic polymers

Synthetic polymers represent the largest group of biodegradable polymers. They exhibit predictable and reproducible mechanical and physical properties such as tensile strength, elastic modulus and degradation rate [106]. The most commonly used synthetic polymers in tissue engineering include the linear polyesters, poly-lactic acid (PLA), poly-glycolic acid (PGA) poly lactic-co-glycolide (PLGA) copolymers, and polycaprolactone (PCL) [107].

PLGA, approved by American Food and Drug Administration (FDA) used in a host of therapeutic devices, is the most frequently used synthetic polymers in tissue engineering due to its excellent biocompatibility and predictable degradation rate.

PLGA has shown great potential in bone tissue engineering (**Fig. 1.14a**), artificial vessel construction and bioactive molecules delivery [108, 109]. PCL, also approved by FDA, is a versatile synthetic polymer. PCL been used intensely and are commonly studied materials for biomedical applications in bone and cartilage repair (**Fig. 1.14b**), as surgical suture as well as for drug delivery systems, especially those with longer working lifetimes [110, 111]. Although similar in physical and chemical properties, PCL possesses more stable qualities than PLGA due to its identical chemical composition and is much cheaper than PLGA, which shows great potential in commercial clinical applications. The processing of PCL, however, is more difficult than PLGA in size and shape control, for example, the control of size and density of electrospun PCL nanofibers (**Fig. 1.14c,d**) [112, 113]. In this thesis work we developed a novel method to fabricate porous PCL patch with easy processing, which we will discuss in detail in **Chapter 4**.

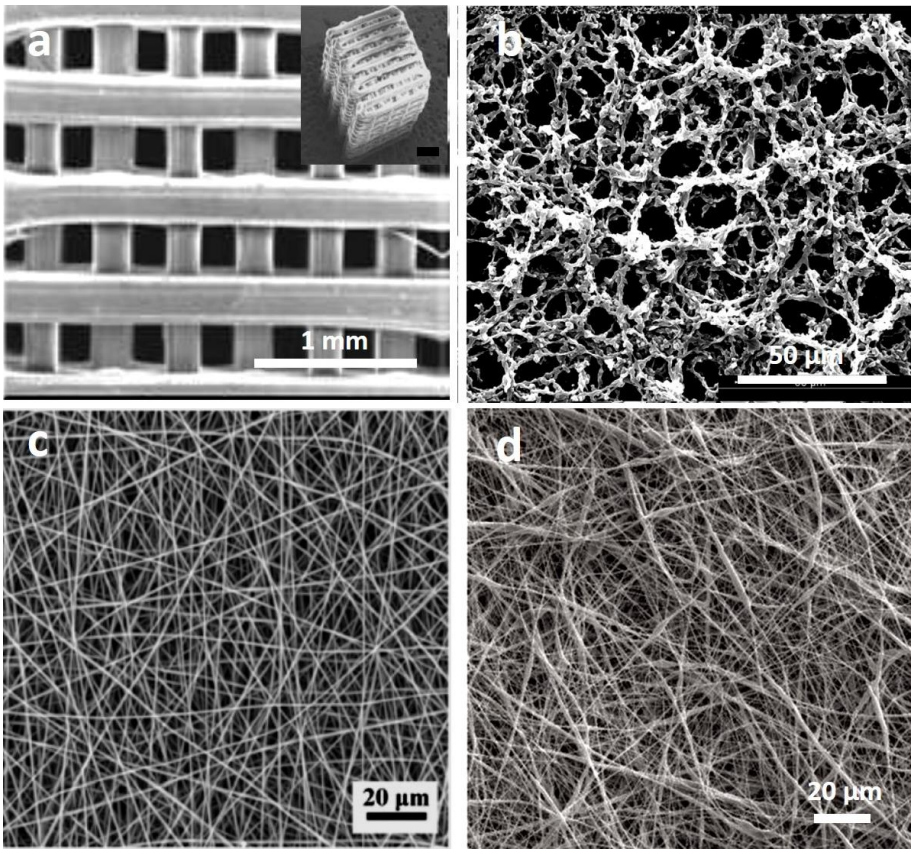


**Fig. 1.14** SEM images of (a) 3D PLGA bone scaffold by direct deposition [109], (b) self-assembly of porous PCL scaffold [111], and electrospun nanofibers of (c) PLGA [113] and PCL [112].

Another versatile synthetic polymer is Polydimethylsiloxane (PDMS). The mechanical strength of PDMS can be flexibly adjusted by changing the concentration of cross-linker component. Originally in liquid state, PDMS can be easily processed using microfabrication methods. Due to the adjustable elasticity, excellent biocompatibility, low toxicity and negligible immune reaction, PDMS has been widely used in clinical application as an implant substitute for bone, cartilage, ear, skin, etc. [114]. Taking advantages of all the merits above, we will discuss the application of PDMS in hiPSCs derived cardiac differentiation in **Chapter 5**, In medical implant field stands another synthetic polymer, parylene C, which has long been widely used as implant coating material due to its high biocompatibility and low liquid and gas permeation [115, 116]. Parylene C can be deposited uniformly on various kinds of substrates, such as metals, glass, plastics and wood, with little defects. In **Appendix A**, we will discuss the interaction of parylene C substrates and cells cultured on them, which has seldom been studied before.

However, the largest obstacle standing in front of synthetic polymers for tissue engineering application is their hydrophobic surface. One strategy used to improve the hydrophilicity is mix PCL with hydrophilic polymers like chitosan to make composite substrate. Due to the different wettability of these two kinds of polymers, this method has limits in solvent option and processing conditions.

## 1.3.2 Scaffolds requirements and fabrication methods

### 1.3.2.1 Limited cell culture substrates

In order to improve the cell performance in *in vitro* culture, various kinds of substrates are developed during the past decades. Matrigel or recombinant proteins such as laminin and fibronectin are commonly used to generate a gel layer on the surface of substrate to promote cell adhesion [117, 118]. This method is facile and flexible on numerous kinds of substrates, but fails to mimic the well-ordered organization of the extracellular matrix components. To obtain a closer mimic of ECM, ECM components collagen, gelatin, hyaluronic acid, etc. along with various biopolymers such as chitosan, alginate, PCL, PLGA, etc. have been used in substrates preparation with appropriate

physical and chemical qualities [119]. In addition, various kinds of methods such as surface patterning, plasma etching and functional materials doping have been successfully employed for improved cell culture [120, 121]. In parallel, suspension culture of cells like pluripotent stem cells using bioreactors has also been studied [122]. These methods can efficiently increase the yields but unavoidably introduce undesired shear forces and uncontrollable exogenous contact of materials. None of them, however, fully take into account the specificity of the cellular microenvironment in term of three dimensional protein organization and permeability cells and nutrients.

#### 1.3.2.2 Requirements for scaffolds

During the past decades, tissue engineering has emerged in the development of functional scaffolds which can reconstruct *in vivo* cellular microenvironment in order to restore, maintain, or improve function of tissues or organs. By mimicking the complex mechanical, chemical and biological characteristics of *in vivo* cellular microenvironment, tissue engineering is highly multidisciplinary, drawing on experts from clinical medicine, mechanical engineering, materials science, genetics, and related disciplines from both engineering and the life sciences. Tissue engineering uses porous 3D scaffolds to provide the appropriate environment for the regeneration of tissues and organs. These scaffolds usually act as a support for biomolecules decoration and cell loading and eventually for tissue formation, as is shown in **Fig. 1.15**. In many cases, mechanical, biophysical or chemical stimuli are integrated within the scaffolds for specific cell manipulation. These cell-seeded scaffolds are either cultured *in vitro* for the formation of tissues and then implanted into an injured site, or are implanted directly into the injured site where regeneration of tissues or organs is induced using the body's own systems.

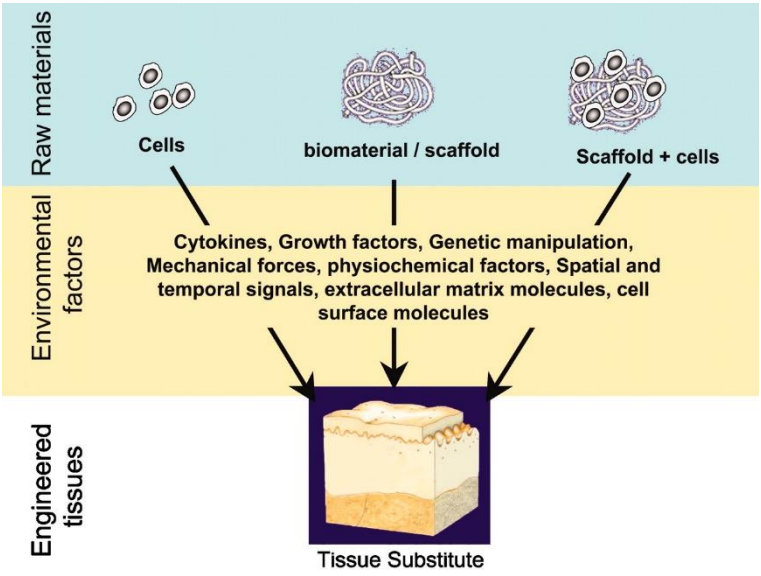


**Fig. 1.15** Tissue engineering approaches classified into three strategies: (i) cells alone, (ii) cells with scaffolds, and (iii) scaffolds alone, which can be enhanced by *in vitro* microenvironmental factors before application as a tissue substitute [123].

In tissue engineering, scaffold design plays an important role in manipulating cells behavior and guiding tissue formation. The optimal scaffold should mimic the ECM of the target tissue in its native condition. Although the disparity of tissues and organs in different site of body makes it difficult for exact mimic composition, organization and multiple functions of the ECM in native tissues, a number of key considerations and requirements are significant when designing or determining the feasibility of a scaffold for a specific application in tissue engineering:

### a) Biocompatibility

Biocompatible is the first criterion of any scaffold for tissue engineering. Cells must adhere to, spread, and migrate on the scaffold and also can proliferate and deposit new ECM on it. The scaffold must produce a negligible toxicity and immune reaction to the body after implantation.

The currently used biomaterials are mainly polymers from both natural and artificial sources. In natural polymers, biomaterials from animal sources show greater promise than those from plant sources. Collagen and glycosaminoglycan polysaccharides are major components in animal ECM which are produced and organized by cells and provide important supports for cell adhesion, migration, proliferation and differentiation. Gelatin, a collagen derivative protein, exhibits less

immune rejection than collagen in implants, which shows greater potential in application *in vivo*. Chitosan, another important animal source polysaccharide, shows great support for cell culture and provides enough mechanical strength in biomaterials composites. Plant source polymers including cellulose, alginate and agarose hardly exert toxicity on cells. However, these polymers provide little support for cells adhesion. Cells seldom attach on such polymers but interact each other and self-organize. In synthetic polymers, polyesters like PLGA and PCL, show little toxicity to cells and provide great support for cell adhesion, migration and proliferation. Their metabolic products are friendly to cells, too. PDMS, another widely used polymer, is nontoxic to cells and provides good support for cell culture. PDMS is nondegradable and often used as permanent implants for elastic tissues.

Although the multiple choices of biocompatible materials, for a specific application, the final decision should be made after taking into account other considerations such as cell adhesion, mechanical strength and biodegradation.

**b) Proper degradation**

The objective of tissue engineering is to allow the body own cells, over time, to eventually replace the implanted scaffold. The scaffold must therefore be biodegradable so as to allow cells to produce their own extracellular matrix. The by-products of this degradation should also be non-toxic and able to exit the body without interference with other organs.

**c) Suitable mechanical strength**

Ideally, the scaffold should have mechanical properties consistent with the targeted site. Sufficient mechanical strength allows stability of 3D porous structure and effective diffusion of nutrients and metabolic wastes. It also guarantees surgical handling during implantation, which is especially important in cardiovascular and orthopedic applications [124, 125].

**d) Scaffold architecture**

The architecture of scaffolds used for tissue engineering is of critical importance. Scaffolds should have an interconnected pore structure and high porosity to ensure cellular penetration and adequate diffusion of nutrients to cells within the construct and to the extra-cellular matrix formed by these cells. Furthermore, a porous interconnected structure is required to allow diffusion of waste products out of the scaffold, and the

products of scaffold degradation should be able to exit the body without interference with other organs and surrounding tissues.

**e) Easy modification**

The surface properties of the scaffold, to a large extent, determine the success of scaffolds in tissue engineering in terms of the response elicited from the surrounding biological environment. To achieve this, scaffolds should be easily modified to render specific properties on scaffolds, for example, wettability, surface charges and signal molecules, by methods including physical adsorption, radiation mediated modifications, grafting, and protein modifications [126]. It has been proved that modified scaffolds can lead to accelerated and functional tissue regeneration [127].

**f) Easy processing**

For clinical and commercial application, scaffold fabrication should be cost effective and possible to scale-up from research laboratory to industry [128]. The scaffolds should also be easy stored and easy handling by the clinician for during the implantation operation without the requirement for extra surgical procedures.

#### 1.3.2.3 Methods to make scaffolds

Guided by the key criterions discussed above, various methods have been developed to engineer biomaterials into desirable complex architectures for specific usage in tissue engineering.

**a) Solvent casting and particulate leaching**

Solvent casting is a very simple, easy and inexpensive method by dissolving a polymer in a volatile solvent, casting it on a substrate and evaporating the solvent [129]. This method often causes inadequate solvent evaporation and poor porosity. In order to obtain porous structure, particulate leaching is always associated by adding porogen such as salts, sugars and wax into polymer solution and dissolving the porogen after solvent evaporation (**Fig. 1.16**) [130]. This combined method is simple to control of the pore size and the porosity by selecting the particle size and the amount of the added salt particles. However, the distribution of the salt particles is often not uniform in contact within the polymer solution. So the degree of pore interconnection is not well controlled.

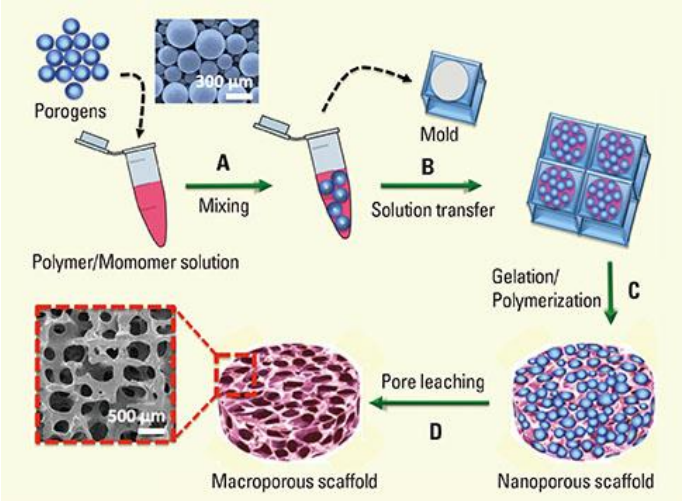


**Fig. 1.16** Illustration of the fabrication steps of macroporous hydrogel scaffolds using solvent casting and particulate leaching [130].

### b) Phase separation

The general strategy of phase separation method in scaffold fabrication is to dissolve biomaterials in one solvent and then to extract the solvent into another solvent or solids, resulting in the isolated biomaterials structure [131]. This method has been used to fabricate porous scaffolds. However, the distribution and size of pores are not uniform and difficult to control, which limits its use in fabricating tissue engineering scaffolds.

### c) 3D printing

3D printing is a newly emerging fast prototyping method, which exhibits great potentials in fabricating scaffolds with precise parameters (size, geometry, inner porosity and connection, orientation, etc.) [132]. 3D printer works according to an instruction file created by a 3D modeling program (**Fig. 1.17**). The design of an object is sliced into thousands of horizontal layers and then sent to the 3D printer to direct the printing process. 3D printing offers the promise of a simple, efficient and low-cost scaffolds fabrication. However, 3D printing is still facing two main challenges currently in scaffold fabrication. One is the limitation of printable biomaterials such as acrylate based polymer like PEGDA and GELMA and alginate based polymers followed by $Ca^{2+}$ gelation [133]. The other one is limited printing resolution for biomaterials, which is much larger than cellular size. The detailed 3D printing technique will be discussed in

**Chapter 2**.

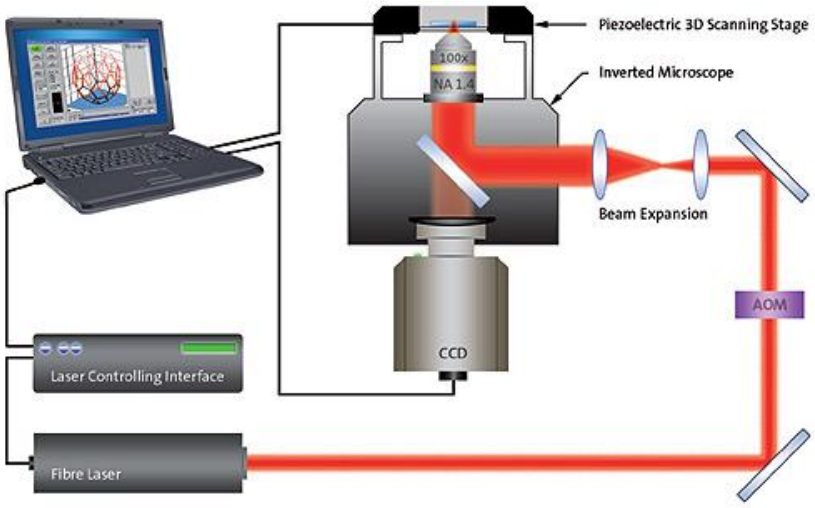


**Fig. 1.17** A schematic setup of 3D printer [134].

### d) Freeze drying

Freeze drying or lyophilization is a process in which water is frozen, followed by its removal from the sample and formation of biomaterials structure. This method has also been widely used to efficiently produce porous polymer scaffold for tissue engineering, which is especially suitable for making porous protein or thermoplastic scaffold, like collagen, PLGA and PCL, which otherwise will be denatured or deformed by heating drying [135]. This method can make scaffold with high porosity, which is highly advantageous in *in vivo* implant test due to sufficient capacity for vascularization. However, for most polymers, high porosity usually follows with weak mechanical strength. A balance between mechanical properties and porous architecture sufficient to allow cell infiltration is key to the success for porous scaffolds. The detailed description will be shown in **Chapter 2**.

### e) Electrospinning

Increasing attentions have been paid to the fabrication of nanofibers substrates which can mimic native ECM structure at nanoscale. Electrospinning holds high potential due to the easy operation, low cost and well-control of nanofiber morphology and chemical compositions (**Fig. 1.18**) [136]. The electrospinning is highly sensitive to environmental conditions such as temperature and humidity, which leads to disparity

from batch to batch. Besides, the electrospun nanofibers from biomaterials have weak mechanical strength, which makes it difficult for handling in further applications. We will introduce electrospinning technique in **Chapter 2**.

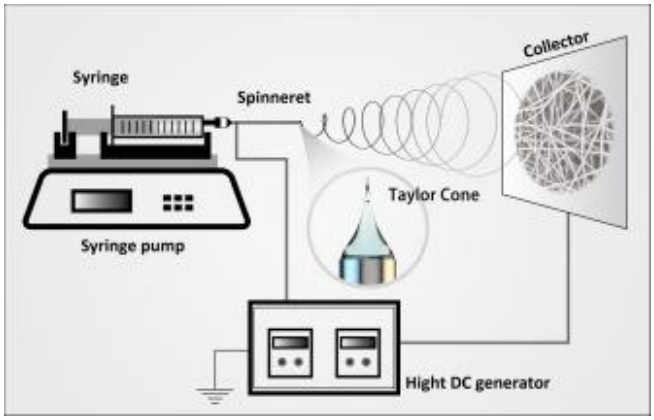


**Fig. 1.18** A scheme of electrospinning setup [137].

### f) Self-organization

Self-organization is a versatile way to make functional scaffolds in tissue engineering. Taking advantages of molecular interaction, this method uses pre-existing components to form organized structures or patterns as a consequence of specific, local interactions among the components themselves. The individual building blocks, designed to fabricate the polymeric architectures, include not only macromolecules such as polypeptides and DNA, but also a variety of synthetic monomeric species, including polyesters, dendrimers, and organic–inorganic compounds [138]. We will introduce self-organization technique in **Chapter 2**.

### g) Microfabrication

Microfabrication is a collection of technologies utilized in making microdevices, including photolithography and various soft lithography methods [139]. Photolithography is a technology using UV irradiation to transfer geometric shapes on a mask to a smooth surface. The generated patterns are further transferred to various other substrates by soft lithography methods such as PDMS replicating, micro-contact printing and hot embossing. This method allows free design of mask and fast fabrication process with precise control of geometry and size of patterns. However, this method has limited capacity to produce 3D structure due to the low spincoating thickness and

straight UV light pathway. For scaffold fabrication, the available biomaterials are limited. Detailed description will be presented in **Chapter 2**.

#### 1.3.2.4 Methods integration

The methods discussed above are currently the prevailing ways in the fabrication of tissue engineering scaffolds. They exhibit indeed some outstanding merits for improved cell culture and specific behavior such as adhesion, migration, proliferation and differentiation. However, their individual drawbacks still counts in the decision of method selection. **Tab. 1.3** summarizes the advantages and disadvantages of scaffolds fabrication methods discussed above.

**Tab. 1.3** Advantages and disadvantages of scaffold fabrication methods.

| Methods | Advantages | disadvantages |
|---|---|---|
| Solvent casting and particulate leaching | Easy processing, good pore size control | Limited solvent choice, poor pore interconnection |
| Phase separation | Good structure control | Limited solvent choice, complex processing |
| 3D printing | Free model design, simple and fast processing, precise structure control, green production, robust mechanical strength | Limited materials choice, low printing resolution |
| Freeze drying | Easy and fast processing, various materials choice, high porosity structure, biological sample friendly | Limited solvent choice, poor mechanical strength, large pore size range |
| Electrospinning | Fast processing, various materials choice, good fiber size control | Sensitive to electrospinning parameters, vulnerable to surrounding, poor fiber density control, poor repeated performance |
| Self-assembly | Easy processing, good structure control, | Limited solvent choice, sensitive to processing parameters, complex materials design |
| Microfabrication | Easy model design, fast processing, precise structure control, controllable mechanical strength | Limited 3D structure production, limited materials choice |

In decision making of scaffolds fabrication methods, the final choice is usually made after weighing their advantages and disadvantages according to the specific requirements of expected scaffold.

However, considering the fact shown in **Tab. 1.3** that the disadvantages of one method might be covered by the advantages of another, a combination of these two methods in scaffold fabrication can not only utilize their advantages but also bypass

their disadvantages. For example, freeze drying usually makes scaffolds from various materials with good biocompatibility but weak mechanical strength while 3D printing with good mechanical strength but usually poor biocompatibility due to limited materials choice. The combination of freeze drying and 3D printing can makes scaffolds with robust mechanical strength and good biocompatibility. In this work, we use this combination strategy for our scaffolds fabrication.

### 1.3.3 Key factors of scaffold affecting cell performance

The ability to predict and control the interactions of cells with scaffolds materials underlies the rational design of biocompatible implants and tissue engineered bio-hybrid organs. The following factors of scaffolds are of great significance to affect cell performance in tissue engineering and thus deserve careful clarification.

#### 1.3.3.1 Surface wettability

Surface wettability of scaffolds plays an important role in cell adhesion after cell seeding. Hydrophobic surface can severely change the structure of ECM proteins deposited on it. The denatured ECM proteins will lost their bioactivity and fail to provide enough structure motifs for integrin bonding during cell adhesion, resulting in few cell adhesion with minimal spreading [140]. Enhanced cell adhesion and spreading on hydrophilic surface relatively to hydrophobic one has been proved by much research due to the enhanced deposition of bioactive ECM proteins on scaffold surface [141]. Highly hydrophilic surface, however, will weaken cell adhesion because of low attachment of ECM proteins on the surface [142]. During implantation of scaffolds, the surface wettability also receives much attention due to its exposure to numerous proteins present in blood, interstitial fluid, and damaged extracellular matrix, resulting in the formation of a complex layer of adsorbed proteins at the material surface.

#### 1.3.3.2 Surface charge

Usually surface charge works together with surface wettability to influence cell performance. Positively charged surfaces, for example, modified with quaternary amine,

have been proved to largely enhance cell adhesion and cell spreading with or without serum on hydrophilic surfaces or even on hydrophobic surfaces in the presence of serum [141]. The enhancement of cell performance on positively charged surfaces can be explained as follows: (1) cell surface is negatively charged, which will interact with positively charged surface of scaffolds in the form of electrostatic attraction; (2) positively charged surface will promote the deposition of negatively charged ECM proteins and thus cell adhesion and spreading. Negatively charged surfaces, however, shows much lower promotion for cell adhesion and spreading than positively charged surfaces [141]. The negatively charged surface electrostatically may inhibit interactions with cell surface negatively charged proteoglycans or prevent adsorption of adhesive ECM proteins.

#### 1.3.3.3 Surface topography

Topography features have an important role in regulating cell adhesion, migration, proliferation, and differentiation on the substrates [143, 144]. Understanding the underlying mechanism of cell responses to scaffold surface with specific topography is a key to successful reconstruction of tissues with optimal structures and functions. The most famous phenomenon might be the contact guidance of cells: namely, cell alignment on an anisotropic surface [145]. Usually, the contact guidance leads cells to elongate along groove or ridge structures [146]. Cell viability and proliferation can also be regulated by surface topographical features [147]. As a basic cellular event, cell migration is also significantly sensitive to the topographic cues called topotaxis. Study shows that the migration speed of NIH 3T3 fibroblasts depended strongly on the width of ridges [148]. The topography features can also strongly affect stem cell differentiation. A significant upregulation of neuronal markers has been proved in human MSCs derived neural differentiation on the patterned surface of smaller gratings compared to the surfaces unpatterned and of larger gratings [149]. On ridge/groove pattern arrays with specific size alone hESCs could effectively and rapidly differentiate into a neuronal lineage without any differentiation-inducing agents [150].

#### 1.3.3.4 Stiffness

In human body, stiffness varies from tissue to tissue. Tissue cells feel and respond

to the stiffness of their substrate. In order to obtain good mimic of *in vitro* environment, it is essential to fabricate scaffolds with similar stiffness of targeted sites. Studies have revealed that the stiffness of scaffolds pose significant effect on cell performance, for example, cell spreading, migration and differentiation [151, 152]. Cells like NIH 3T3 fibroblasts prefer to adhere and spread on hard substrate than soft one [153]. This difference of cell adhesion and spreading on the region of varied stiffness leads to a preferred migration along a stiffness gradient, named durotaxis. Besides, the lineage commitment of human MSCs from bone marrow was significantly regulated by the stiffness [154]. On soft matrices that mechanically mimic the brain, a large number of stem cells committed to the neurogenic phenotype; by contrast, MSCs on moderately stiff matrices that mimic muscle experienced a myogenic commitment, and rigid matrices that mimic collagenous bone proved osteogenic.

#### 1.3.3.5 3D architecture

The architecture of scaffolds can directly regulate cell behavior in a similar way that ECM does to influence the integrin–ligand interaction between cells and surrounding matrix, in which the porosity, pore size and interconnectivity of 3D porous architecture play important roles [155]. Porous structure allows cells to grow and migrate in 3D space within scaffold as they do *in vivo*. Suitable pore size and good interconnectivity can allow efficient diffusion of nutrients and removal of metabolic wastes, thus promoting cell proliferation in 3D space (**Tab. 1.4**). So realization of pore microstructure is a prerequisite for increasing cell growth into the 3D scaffold and enhancing new tissue integration with the host. The porous scaffolds can also promote the structure reconstruction and function realization of tissues. In neural tissue engineering, the successful formation of neuron network for signal transmitting relies largely on the suitable pore size and interconnectivity. Angiogenesis is the growth of new blood vessels from existing vasculature, which is essential to supply oxygen and nutrients to developing tissues, and to facilitate wound healing. Study shows that the minimum pore size necessary for the regeneration of a blood vessel is approximately 30 to 40 μm to enable the exchange of metabolic components and to facilitate endothelial cell entrance [156, 157]. Larger pore sizes of approximately 160 to 270 μm facilitated angiogenesis throughout scaffold by using multilayered agent-based model

simulation [158].

**Tab. 1.4** Pore sizes and porosity required for different cellular activities [159].

| *Function* | *Cell type used*/in vivo *tests* | *Scaffold material* | *Pore size (μm)* | *Porosity (%)* |
|---|---|---|---|---|
| Angiogenesis | Multilayered agent-based model simulation/*in vivo* rat implantation | Porous PEG | 160–270 | — |
| Adipogenesis | Murine embryonic stem cells | PCL | 6–70 | 88 |
| | Rat BMCs | Silk gland fibroin from nonmulberry | 90–110 | 97 |
| | Mice ASCs | Porcine type 1 collagen | 70–110 | — |
| Cell infiltration | Dermal fibroblasts | Synthetic human elastin | 11 | 34.4 |
| | Primary rat osteoblasts | PHP | 100 | — |
| Chondrogenesis | Human ASCs | PCL | 370–400 | 95 |
| | Porcine chondrocytes | Chitosan | 70–120 | 80 |
| | Rabbit MSCs | PLGA-GCH | 200 | 74 |
| | Rabbit MSCs | PLGA | 200–500 | — |
| | Porcine chondrocytes | PCL | 750 | 30 |
| | Porcine BMSCs | PCL | 860 | 59 |
| Hepatogenesis | Human ASCs | PLGA | 120–200 | — |
| | Rat bone marrow stem cells | c-PLGA | 150–350 | 94 |
| Osteogenesis | *In vivo* rat implantation | Hydroxyapatite-BMPs | 300–400 | — |
| | hMSCs | Coralline hydroxyapatite | 200 | 75 |
| | *In vivo* mice implantation | β-tricalcium phosphate | 2–100 | 75 |
| | *In vivo* mice implantation | Natural coral | 150–200 | 35 |
| | RBMSCs | Sintered titanium | 250 | 86 |
| | Fetal bovine osteoblasts | PCL | 350 | 65 |
| Proliferation | hMSCs | Coralline hydroxyapatite | 500 | 88 |
| | Human trophoblast ED27 | PET | 30 | 84.9 |
| | Rat MSCs | PET | >12 | 96.7 |
| | Human foreskin fibroblasts | Silk fibroin | 200–250 | 86 |
| | Human foreskin fibroblasts | Silk fibroin | 100–150 | 91 |
| | Rat chondrocytes | Type A gelatin | 250–500 | — |
| | MC3T3-E1 cells | CG | 325 | 99 |
| | Primary rat osteoblasts | PHP | 40 | — |
| Skin regeneration | Guinea pig dermal and epidermal cells | CG | 20–125 | — |
| Smooth muscle cell differentitation | Dog BMSCs | PLGA | 50–200 | — |

## 1.3.4 Scaffolds for tissue engineering applications

During the past decades, scaffolds have shown superior advantages in tissue engineering field for improved cell culture and functional tissues reconstruction *in vitro* and implantation over traditional 2D method that lacks 3D structural support and growth guidance. Various kinds of functional tissues have been successfully generated with the help of functional scaffolds, including neurons, cardiac tissues, skeletal muscle, bone and cartilage, skin tissue, blood vessel, etc. Among all these applications, neuron and cardiac tissues generation has received intensively attention. A number of scaffold systems have been applied for functional tissue generations, in order to providing reliable results for alternative treatment for clinical neural and cardiovascular diseases that are difficult with conventional methods. Here we introduce the use of scaffolds in neural and cardiac tissue engineering.

### 1.3.4.1 Neural tissue engineering

The nervous system is divided into two subsections: the central nervous system

(CNS) and the peripheral nervous system (PNS). The CNS consists of the brain and the spinal cord, while the PNS consists of nerves that originate from the brain and spinal cord and innervate the rest of the body. Damages in nervous system have long been a tough and challenging topic facing neurologists [160, 161]. Patients with neural diseases experience functional difficulties, which result in conditions such as, headache, loss of feeling and memory, weak muscle strength and lack of coordination. Current treatment for neural diseases still suffers unavoidable difficulties such as lack of donor neurons, immune refuse reaction and poor function recovery after treatment.

The need for neural tissue engineering arises from the difficulty of the nerve cells and neural tissues to regenerate on their own after neural damage has occurred. The PNS has some, but limited, regeneration of neural cells. Adult stem cell neurogenesis in the CNS has been found to occur in the hippocampus and spinal cord. As a novel and promising alternative method, neural tissue engineering, by growing neural tissues *in vitro* from neural stem or progenitor cells in 3D scaffolds, exhibits great potential for treatment of neural system damages in clinical field [162, 163].

Various scaffolds with specific functioning have been fabricated and applied for *in vitro* nerves and neural tissues generation and *in vivo* implantation studies [164, 165]. Li et al reported a highly porous 3D graphene foam used for neuron generation from neural stem cells (NSC) *in vitro* [166]. This 3D graphene foam is high conductive which they believe can introduce internal stimuli to neural stem cells. Results show that the 3D graphene foams can not only support NSC growth, but also keep cell at an active proliferation state with upregulation of Ki67 expression than that on 2D graphene films. Phenotypic analysis indicated that 3D graphene foam can enhance the NSC differentiation towards astrocytes and especially neurons. Tang et al reported a monolayer porous gelatin nanofiber patch as a close mimic of ECM for enhanced culture and neuronal differentiation form human iPSCs [167]. Besides the monolayer iPSCs colonies, they can also generate uniform embryonic bodies form iPSCs with patch method. They found that patch method has superior advantages over dish method in both human iPSCs culture and neuronal differentiation. Xu et al reported a porous collagen scaffold tethered with a collagen-binding epidermal growth factor receptor (EGFR) antibody for effective retention of NSC in the scaffold and subsequent efficient neuron differentiation [168]. The implantation of this functional scaffold with

exogenous NSCs in rat SCI model can capture and retain NSCs at the injury sites, and promote the neuronal differentiation of the retained NSCs into functional neurons, and finally dedicate to improving motor function of SCI rats.

#### 1.3.4.2 Cardiac tissue engineering

Heart disease is the leading cause of death and disability, accounting for approximately 25% of all human mortality [169]. Heart disease is usually marked by difficulties in heart pumping efficiency caused by various diseases including ischemic heart disease, hypertensive heart disease, valvular heart disease, and primary myocardial disease. The injury of the heart is permanent because, after a massive cell loss or destruction, the cardiac tissue itself lacks intrinsic regenerative capability to replace the lost or destroyed cells.

Present strategies for treatment for heart diseases mainly focus on pharmacological therapy, interventional therapy and heart transplantation. Pharmacological therapy focuses on reduction of work load and protection from the toxic humoral factors which are over-activated in heart diseases [170]. Interventional therapy, such as surgery or implantation of pacing devices to control electrical/mechanical asynchrony, are now receiving more widespread application, in particular for patients with marked symptoms and marked limitation in activity [171, 172]. However, both drug and interventional therapies cannot adequately control disease progression to the end stage. Heart implantation always suffers limited donor source and strict type matching.

The need of cardiac tissue engineering, using functional scaffolds with stem cells to generate cardiac tissues *in vitro* for disease treatment, increases due to the lack of organ donor source and complicated immune suppressive treatments. Scientists and surgeons are continually making efforts in engineered cardiac tissue for treatment of the injured heart.

Inspired and prompted by the urgent need in clinical field, various cardiac tissue targeted scaffolds have been made and tested for efficacy and efficiency of cardiac tissue generation *in vitro* [173, 174]. By imitating the process of heart development, Kerscher et al reported a hydrogel scaffold for single human pluripotent cell encapsulation and differentiation into cardiomyocytes [175]. The method can generate cardiomyocytes with high production yield and similar calcium handling properties to

that in 2D monolayer model. The generated cardiac tissues become progressively anisotropic without external electromechanical stimuli and developed ultrastructural features characteristic of mature cardiac tissues with different geometries and sizes. Their results demonstrate the feasibility of 3D scaffolds in cardiac tissue generation as a biomimetic model of heart development. Functional patches are receiving increasing attention in heart diseases treatment due to supportive cardiac tissue generation and easy clinical administration. Tang et al reported a hierarchical patch made of nanoscale porous gelatin fiber monolayer supported by microscale PEGDA honeycomb frame for the formation iPSCs embryonic bodies (EBs) and cardiac tissue differentiation [176]. This patch system can allow efficient nutrient diffusion, enhanced cell-cell communication and formation of uniform EBs form iPSCs. They have demonstrated that cardiac differentiation on the patch can achieve higher production yield and much more homogeneous cardiac contraction, compared with 2D glass substrate. Chachques et al reported a clinical study about the feasibility and safety of implantation of 3D porous collagen scaffold loaded with bone marrow cells (BMCs) for treatment of infarcted ventricle in patients [177]. They have demonstrated that the BMCs-loaded collagen scaffold increases the thickness of the infarct scar with viable tissue and helps to normalize cardiac wall stress in injured regions, thus limiting ventricular remodeling and improving diastolic function.

## 1.4 Research objectives

The objective of this work is to develop a method of engineering multi-dimensional scaffolds for cell culture and tissue generation. More specifically, we are interested in fabricating functional scaffolds by mimicking *in vivo* ECM microenvironment and applying them for advanced cell culture and improved stem cell derived tissue engineering studies. Particularly, we focus on the application of our scaffolds in *in vitro* tissue (neurons and cardiomyocytes) reconstruction from stem cells (neural progenitors and human induced pluripotent stem cells).

To achieve desired tissue formation, the key point is to prepare ECM mimic scaffolds for high quality and high efficiency processing, including stem cell proliferation and differentiation as well as stem cell derived tissue formation and

manipulation. Therefore, we first developed a new type of scaffolds by considering the both the requests of enhanced cell performance and versatility for *in vitro* and *in vivo* processing. We applied a 3D printing technique to produce the designed frame in PEGDA and then filled the free-space of the frame with a porous gelatin gel. After freezing and drying, a hybrid 3D scaffold made of gelatin porous structures and PEDGA backbone was obtained. We hope that the PEGDA/porous gelatin scaffold can provide a 3D permeable environment for cells like *in vivo* conditions, which should be also convenient in manipulation in down streaming processing. Due to the importance of neuron cells in clinical disease therapy, we expected to build *in vitro* 3D neuron tissue within and guided by the 3D porous network of the scaffold. The feasibility and efficacy of the scaffold will be evaluated by testing the cell viability, proliferation and differentiation.

To more easily integrate into a microfluidic device, we also designed a 2D scaffold in form of a thin layer of honeycomb frame of PEGDA and self-assembled porous structure of PCL. Unlike conventional 2D cell culture, the substrate for cell adhesion is a thin layer biodegradable polymer with high porosity for 3D diffusion of nutrients and removal of metabolic wastes. Particularly, with much less material for cell contact, much more cell surface is exposed to extracellular fluids, which, we believe, provides more accesses for cells to take nutrients and soluble factors. The improved cellular uptake will promote cell proliferation and cell processing like gene transfection. Taking advantages of this scaffold, we believe culture and cardiac differentiation of human induced pluripotent stem cells will be improved as well as the functioning of generated cardiac tissues, like cardiac production yield and contraction strength and homogeneity. In particular, PCL is approved by FDA as a safety biodegradable material in medicine, we wish to test the *in vivo* biodegradation and apply the generated cardiac tissue for implantation test.

Natural cardiac tissue is marked by a series of unique characteristics like aligned muscle fiber, homogeneous contraction and specific contraction frequency. A closer mimic of microenvironment of heart is of great importance to generate a more similar cardiac tissue in vitro. We wish to fabricate a functional scaffold that can facilitate cardiac differentiation from human induced pluripotent stem cells and guide organized formation and contraction of cardiac tissue. We wish the scaffold can provide a similar

3D structural support, stiffness and orientation guidance. We choose PDMS as a functional material for scaffold production due to its excellent biocompatibility, flexible processing and adjustable stiffness. In order to mimic the fibrous structure of ECM proteins, we apply a thin layer of porous gelatin fiber. We wish the combination of flexible and elastic PDMS frame and porous gelatin nanofiber can work together to provide not only structure support and cell performance promotion in cell culture but also cardiac induction and functioning guidance. The generated cardiac tissue is expected to be integrated with microfluidic chip for efficient *in vitro* and *in vivo* cell based assays.

# Reference


1. http://www.livebinders.com/play/play?id=1936470; https://www.dreamstime.com/royalty-free-stock-photography-human-heart-anatomy-image10452637; http://www.scientistcindy.com/muscle-tissue.html; https://en.wikipedia.org/wiki/Cardiac_muscle_cell
2. https://micro.magnet.fsu.edu/cells/animals/animalmodel.html
3. E.D. Hay, *Cell biology of extracellular matrix*. 2013: Springer Science & Business Media.
4. N.M. Kumar and N.B. Gilula, *The gap junction communication channel.* Cell, 1996. **84**(3): p. 381-388.
5. M. Takeichi, *Cadherin cell adhesion receptors as a morphogenetic regulator.* Science, 1991. **251**(5000): p. 1451-1455.
6. B. Alberts, A. Johnson, J. Lewis, M. Raff, K. Roberts, P. Walter, *Molecular Biology of the Cell*: *5th edition*. Garland Science, Taylor & Francis Group, 2007: p. 1134.
7. J. Labat-Robert, M. Bihari-Varga, and L. Robert, *Extracellular matrix.* FEBS letters, 1990. **268**(2): p. 386-393.
8. J.E. Scott, *Extracellular matrix, supramolecular organisation and shape.* Journal of anatomy, 1995. **187**(Pt 2): p. 259.
9. G.S. Schultz, G. Ladwig, and A. Wysocki, *Extracellular matrix: review of its roles in acute and chronic wounds.* World wide wounds, 2005. **2005**: p. 1-18.
10. L.A. Liotta, *Tumor invasion and metastases—role of the extracellular matrix: Rhoads Memorial Award lecture.* Cancer research, 1986. **46**(1): p. 1-7.
11. B. Alberts, A. Johnson, J. Lewis, M. Raff, K. Roberts, P. Walter, *Molecular Biology of the Cell*: *5th edition*. Garland Science, Taylor & Francis Group, 2007: p. 1178.
12. B. Alberts, A. Johnson, J. Lewis, M. Raff, K. Roberts, P. Walter, *Molecular Biology of the Cell*: *5th edition*. Garland Science, Taylor & Francis Group, 2007: p. 1186.
13. A.J. Grodzinsky, *Electromechanical and physicochemical properties of connective tissue.* Critical reviews in biomedical engineering, 1983. **9**(2): p. 133-199.
14. R.J. Peach, D. Hollenbaugh, I. Stamenkovic, and A. Aruffo, *Identification of hyaluronic acid binding sites in the extracellular domain of CD44.* The Journal

of cell biology, 1993. **122**(1): p. 257-264.

15. G.A. Di Lullo, S.M. Sweeney, J. Körkkö, L. Ala-Kokko, and J.D. San Antonio, *Mapping the ligand-binding sites and disease-associated mutations on the most abundant protein in the human, type I collagen.* Journal of Biological Chemistry, 2002. **277**(6): p. 4223-4231.
16. L.B. Sandberg, N.T. Soskel, and J.G. Leslie, *Elastin structure, biosynthesis, and relation to disease states.* New England Journal of Medicine, 1981. **304**(10): p. 566-579.
17. T.A. Petrie, J.R. Capadona, C.D. Reyes, and A.J. García, *Integrin specificity and enhanced cellular activities associated with surfaces presenting a recombinant fibronectin fragment compared to RGD supports.* Biomaterials, 2006. **27**(31): p. 5459-5470.
18. B. Alberts, A. Johnson, J. Lewis, M. Raff, K. Roberts, P. Walter, *Molecular Biology of the Cell*: *5th edition*. Garland Science, Taylor & Francis Group, 2007: p. 1191.
19. F. Ungaro, M. Biondi, L. Indolfi, G. De Rosa, M. La Rotonda, F. Quaglia, and P. Netti, *Bioactivated polymer scaffolds for tissue engineering.* Topics in Tissue engineering, 2005. **2**.
20. C.M. Alexander and Z. Werb, *Extracellular matrix degradation*, in *Cell biology of extracellular matrix*. 1991, Springer. p. 255-302.
21. M.A. Ruegg, K.W. Tsim, S.E. Horton, S. Kröger, G. Escher, E.M. Gensch, and U. McMahan, *The agrin gene codes for a family of basal lamina proteins that differ in function and distribution.* Neuron, 1992. **8**(4): p. 691-699.
22. R. Montesano, L. Orci, and P. Vassalli, *In vitro rapid organization of endothelial cells into capillary-like networks is promoted by collagen matrices.* The Journal of cell biology, 1983. **97**(5): p. 1648-1652.
23. R. Vracko and E.P. Benditt, *Capillary basal lamina thickening: Its relationship to endothelial cell death and replacement.* The Journal of cell biology, 1970. **47**(1): p. 281.
24. A.J. Barber and E. Lieth, *Agrin accumulates in the brain microvascular basal lamina during development of the blood‐brain barrier.* Developmental dynamics, 1997. **208**(1): p. 62-74.
25. W. Halfter, R. Chiquet-Ehrismann, and R. Tucker, *The effect of tenascin and embryonic basal lamina on the behavior and morphology of neural crest cells in vitro.* Developmental biology, 1989. **132**(1): p. 14-25.

26. S.M. Hughes and H.M. Blau, *Migration of myoblasts across basal lamina during skeletal muscle development.* Nature, 1990. **345**(6273): p. 350-353.
27. W. Halfter, S. Dong, B. Schurer, A. Osanger, W. Schneider, M. Ruegg, and G. Cole, *Composition, synthesis, and assembly of the embryonic chick retinal basal lamina.* Developmental biology, 2000. **220**(2): p. 111-128.
28. B.P. Hierck, S. Thorsteinsdóttir, C.M. Niessen, E. Freund, L.V. Iperen, A. Feyen, F. Hogervorst, R.E. Poelmann, C.L. Mummery, and A. Sonnenberg, *Variants of the α6 β1 Laminin Receptor in Early Murine Development: Distribution, Molecular Cloning and Chromosomal Localization of the Mouse Integrin α6 Subunit.* Cell adhesion and communication, 1993. **1**(1): p. 33-53.
29. E. Pöschl, U. Schlötzer-Schrehardt, B. Brachvogel, K. Saito, Y. Ninomiya, and U. Mayer, *Collagen IV is essential for basement membrane stability but dispensable for initiation of its assembly during early development.* Development, 2004. **131**(7): p. 1619-1628.
30. B. Alberts, A. Johnson, J. Lewis, M. Raff, K. Roberts, P. Walter, *Molecular Biology of the Cell*: *5th edition*. Garland Science, Taylor & Francis Group, 2007: p. 1167.
31. F.G. Giancotti and E. Ruoslahti, *Integrin signaling.* Science, 1999. **285**(5430): p. 1028-1033.
32. J.D. Humphries, A. Byron, and M.J. Humphries, *Integrin ligands at a glance.* Journal of cell science, 2006. **119**(19): p. 3901-3903.
33. R.O. Hynes, *Integrins: versatility, modulation, and signaling in cell adhesion.* Cell, 1992. **69**(1): p. 11-25.
34. C.K. Miranti and J.S. Brugge, *Sensing the environment: a historical perspective on integrin signal transduction.* Nature cell biology, 2002. **4**(4): p. E83-E90.
35. M.A. Schwartz, M.D. Schaller, and M.H. Ginsberg, *Integrins: emerging paradigms of signal transduction.* Annual review of cell and developmental biology, 1995. **11**(1): p. 549-599.
36. C.H. Damsky and Z. Werb, *Signal transduction by integrin receptors for extracellular matrix: cooperative processing of extracellular information.* Current opinion in cell biology, 1992. **4**(5): p. 772-781.
37. K.M. Hodivala-Dilke, K.P. McHugh, D.A. Tsakiris, H. Rayburn, D. Crowley, M. Ullman-Culleré, F.P. Ross, B.S. Coller, S. Teitelbaum, and R.O. Hynes, *β3-integrin–deficient mice are a model for Glanzmann thrombasthenia showing placental defects and reduced survival.* Journal of Clinical Investigation, 1999.

**103**(2): p. 229.

38. B. Alberts, A. Johnson, J. Lewis, M. Raff, K. Roberts, P. Walter, *Molecular Biology of the Cell*: *5th edition*. Garland Science, Taylor & Francis Group, 2007: p. 1170.
39. U. Lindahl and M. Hook, *Glycosaminoglycans and their binding to biological macromolecules.* Annual review of biochemistry, 1978. **47**(1): p. 385-417.
40. L.A. Culp, B.J. Rollins, J. Buniel, and S. Hitri, *Two functionally distinct pools of glycosaminoglycan in the substrate adhesion site of murine cells.* The Journal of cell biology, 1978. **79**(3): p. 788-801.
41. J.-H. Oh, Y.K. Kim, J.-Y. Jung, J.-e. Shin, K.H. Kim, K.H. Cho, H.C. Eun, and J.H. Chung, *Intrinsic aging-and photoaging-dependent level changes of glycosaminoglycans and their correlation with water content in human skin.* Journal of dermatological science, 2011. **62**(3): p. 192-201.
42. D. Zhu and L.Y. Bourguignon, *Interaction between CD44 and the repeat domain of ankyrin promotes hyaluronic acid‐mediated ovarian tumor cell migration.* Journal of cellular physiology, 2000. **183**(2): p. 182-195.
43. W.H. Burgess and T. Maciag, *The heparin-binding (fibroblast) growth factor family of proteins.* Annual review of biochemistry, 1989. **58**(1): p. 575-602.
44. A. Passaniti, R. Taylor, R. Pili, Y. Guo, P. Long, J. Haney, R. Pauly, D. Grant, and G. Martin, *A simple, quantitative method for assessing angiogenesis and antiangiogenic agents using reconstituted basement membrane, heparin, and fibroblast growth factor.* Laboratory investigation; a journal of technical methods and pathology, 1992. **67**(4): p. 519-528.
45. S. Faham, R. Hileman, J. Fromm, R. Linhardt, and D. Rees, *Heparin structure and interactions with basic fibroblast growth factor.* SCIENCE-NEW YORK THEN WASHINGTON-, 1996: p. 1116-1119.
46. S.D. Wolpe, G. Davatelis, B. Sherry, B. Beutler, D.G. Hesse, H.T. Nguyen, L.L. Moldawer, C.F. Nathan, S.F. Lowry, and A. Cerami, *Macrophages secrete a novel heparin-binding protein with inflammatory and neutrophil chemokinetic properties.* Journal of Experimental Medicine, 1988. **167**(2): p. 570-581.
47. B. Alberts, A. Johnson, J. Lewis, M. Raff, K. Roberts, P. Walter, *Molecular Biology of the Cell*: *5th edition*. Garland Science, Taylor & Francis Group, 2007: p. 1179.
48. K. Xu, H. Ma, T.J. McCown, I.M. Verma, and T. Kafri, *Generation of a stable cell line producing high-titer self-inactivating lentiviral vectors.* Molecular

therapy, 2001. **3**(1): p. 97-104.

49. A. Abbott, *Cell culture: biology's new dimension.* Nature, 2003. **424**(6951): p. 870-872.
50. R.U. Agu, M. Jorissen, T. Willems, G. Van den Mooter, R. Kinget, and P. Augustijns, *Effects of pharmaceutical compounds on ciliary beating in human nasal epithelial cells: a comparative study of cell culture models.* Pharmaceutical research, 1999. **16**(9): p. 1380-1385.
51. C. Payan, J. Cottin, C. Lemarie, and C. Ramont, *Inactivation of hepatitis B virus in plasma by hospital in-use chemical disinfectants assessed by a modified HepG2 cell culture.* Journal of Hospital Infection, 2001. **47**(4): p. 282-287.
52. http://www.signalsblog.ca/cell-lines-patient-samples-and-cultures-oh-my/.
53. R.W. Holley and J.A. Kiernan, *" Contact inhibition" of cell division in 3T3 cells.* Proceedings of the National Academy of Sciences, 1968. **60**(1): p. 300-304.
54. D.L. Clarke, C.B. Johansson, J. Wilbertz, B. Veress, E. Nilsson, H. Karlström, U. Lendahl, and J. Frisen, *Generalized potential of adult neural stem cells.* Science, 2000. **288**(5471): p. 1660-1663.
55. M.F. Pittenger, A.M. Mackay, S.C. Beck, R.K. Jaiswal, R. Douglas, J.D. Mosca, M.A. Moorman, D.W. Simonetti, S. Craig, and D.R. Marshak, *Multilineage potential of adult human mesenchymal stem cells.* science, 1999. **284**(5411): p. 143-147.
56. Y. Jiang, B.N. Jahagirdar, R.L. Reinhardt, R.E. Schwartz, C.D. Keene, X.R. Ortiz-Gonzalez, M. Reyes, T. Lenvik, T. Lund, and M. Blackstad, *Pluripotency of mesenchymal stem cells derived from adult marrow.* Nature, 2002. **418**(6893): p. 41-49.
57. http://www.nationalmssociety.org/Research/Research-News-Progress/Stem-Cells-in-MS.
58. A. Smith, *A glossary for stem-cell biology.* Nature, 2006. **441**(7097): p. 1060-1060.
59. L. Conti, S.M. Pollard, T. Gorba, E. Reitano, M. Toselli, G. Biella, Y. Sun, S. Sanzone, Q.-L. Ying, and E. Cattaneo, *Niche-independent symmetrical self-renewal of a mammalian tissue stem cell.* PLoS biology, 2005. **3**(9): p. e283.
60. A.M. Wobus and K.R. Boheler, *Embryonic stem cells: prospects for developmental biology and cell therapy.* Physiological reviews, 2005. **85**(2): p. 635-678.
61. J.A.T. JI-E, S.S. Shapiro, M.A. Waknitz, J.J. Swiergiel, V.S. Marshall, and J.M.

Jones, *Blastocysts Embryonic Stem Cell Lines Derived from Human.* Science, 1998. **282**(5391): p. 1145-7.

62. S. Holland, K. Lebacqz, and L. Zoloth, *The human embryonic stem cell debate: Science, ethics, and public policy*. Vol. 3. 2001: MIT Press.
63. R.-J. Swijnenburg, S. Schrepfer, F. Cao, J.I. Pearl, X. Xie, A.J. Connolly, R.C. Robbins, and J.C. Wu, *In vivo imaging of embryonic stem cells reveals patterns of survival and immune rejection following transplantation.* Stem cells and development, 2008. **17**(6): p. 1023-1029.
64. R. McKay, *Stem cells in the central nervous system.* Science, 1997. **276**(5309): p. 66-71.
65. M. Blurton-Jones, M. Kitazawa, H. Martinez-Coria, N.A. Castello, F.-J. Müller, J.F. Loring, T.R. Yamasaki, W.W. Poon, K.N. Green, and F.M. LaFerla, *Neural stem cells improve cognition via BDNF in a transgenic model of Alzheimer disease.* Proceedings of the National Academy of Sciences, 2009. **106**(32): p. 13594-13599.
66. F. Rossi and E. Cattaneo, *Neural stem cell therapy for neurological diseases: dreams and reality.* Nature Reviews Neuroscience, 2002. **3**(5): p. 401-409.
67. V. Rafuse, P. Soundararajan, C. Leopold, and H. Robertson, *Neuroprotective properties of cultured neural progenitor cells are associated with the production of sonic hedgehog.* Neuroscience, 2005. **131**(4): p. 899-916.
68. http://www.sci-research.uzh.ch/en/research/ClinicalTrials/StemCells.html.
69. http://stemcelloverview.weebly.com/classes-of-stem-cells.html.
70. K. Takahashi and S. Yamanaka, *Induction of pluripotent stem cells from mouse embryonic and adult fibroblast cultures by defined factors.* cell, 2006. **126**(4): p. 663-676.
71. J. Yu, M.A. Vodyanik, K. Smuga-Otto, J. Antosiewicz-Bourget, J.L. Frane, S. Tian, J. Nie, G.A. Jonsdottir, V. Ruotti, and R. Stewart, *Induced pluripotent stem cell lines derived from human somatic cells.* science, 2007. **318**(5858): p. 1917-1920.
72. J.T. Dimos, K.T. Rodolfa, K.K. Niakan, L.M. Weisenthal, H. Mitsumoto, W. Chung, G.F. Croft, G. Saphier, R. Leibel, and R. Goland, *Induced pluripotent stem cells generated from patients with ALS can be differentiated into motor neurons.* science, 2008. **321**(5893): p. 1218-1221.
73. H. Okano, M. Nakamura, K. Yoshida, Y. Okada, O. Tsuji, S. Nori, E. Ikeda, S. Yamanaka, and K. Miura, *Steps toward safe cell therapy using induced*

*pluripotent stem cells.* Circulation research, 2013. **112**(3): p. 523-533.

74. N. Montserrat, E. Nivet, I. Sancho-Martinez, T. Hishida, S. Kumar, L. Miquel, C. Cortina, Y. Hishida, Y. Xia, and C.R. Esteban, *Reprogramming of human fibroblasts to pluripotency with lineage specifiers.* Cell stem cell, 2013. **13**(3): p. 341-350.
75. G.Q. Daley, *Customized human embryonic stem cells.* Nature biotechnology, 2005. **23**(7): p. 826-828.
76. S. Yamanaka, *Induced pluripotent stem cells: past, present, and future.* Cell stem cell, 2012. **10**(6): p. 678-684.
77. H. Inoue, N. Nagata, H. Kurokawa, and S. Yamanaka, *iPS cells: a game changer for future medicine.* The EMBO journal, 2014. **33**(5): p. 409-417.
78. K. Takahashi, K. Tanabe, M. Ohnuki, M. Narita, T. Ichisaka, K. Tomoda, and S. Yamanaka, *Induction of pluripotent stem cells from adult human fibroblasts by defined factors.* cell, 2007. **131**(5): p. 861-872.
79. C.S. Hughes, L.M. Postovit, and G.A. Lajoie, *Matrigel: a complex protein mixture required for optimal growth of cell culture.* Proteomics, 2010. **10**(9): p. 1886-1890.
80. A. Higuchi, Q.-D. Ling, S.S. Kumar, M. Munusamy, A.A. Alarfajj, A. Umezawa, and G.-J. Wu, *Design of polymeric materials for culturing human pluripotent stem cells: Progress toward feeder-free and xeno-free culturing.* Progress in Polymer Science, 2014. **39**(7): p. 1348-1374.
81. T.J. Kamp and G.E. Lyons, *On the road to iPS cell cardiovascular applications*. 2009, Am Heart Assoc.
82. S.M. Chambers, C.A. Fasano, E.P. Papapetrou, M. Tomishima, M. Sadelain, and L. Studer, *Highly efficient neural conversion of human ES and iPS cells by dual inhibition of SMAD signaling.* Nature biotechnology, 2009. **27**(3): p. 275-280.
83. M. Iwamuro, T. Komaki, Y. Kubota, M. Seita, H. Kawamoto, T. Yuasa, J.M. Shahid, R.A. Hassan, W.A. Hassan, and S. Nakaji, *Hepatic differentiation of mouse iPS cells in vitro.* Cell Transplantation, 2010. **19**(6-7): p. 841-847.
84. Y. Liang, H. Zhang, Q.-S. Feng, M.-B. Cai, W. Deng, D. Qin, J.-P. Yun, G.S.W. Tsao, T. Kang, and M.A. Esteban, *The propensity for tumorigenesis in human induced pluripotent stem cells is related with genomic instability.* Chinese journal of cancer, 2013. **32**(4): p. 205.
85. K. Okita and S. Yamanaka, *Induced pluripotent stem cells: opportunities and challenges.* Philosophical Transactions of the Royal Society of London B:

Biological Sciences, 2011. **366**(1575): p. 2198-2207.

86. A.S. Lee, C. Tang, M.S. Rao, I.L. Weissman, and J.C. Wu, *Tumorigenicity as a clinical hurdle for pluripotent stem cell therapies.* Nature medicine, 2013. **19**(8): p. 998-1004.
87. F.J. O'brien, *Biomaterials & scaffolds for tissue engineering.* Materials today, 2011. **14**(3): p. 88-95.
88. T. Albrektsson and B. Albrektsson, *Osseointegration of bone implants: A review of an alternative mode of fixation.* Acta Orthopaedica Scandinavica, 1987. **58**(5): p. 567-577.
89. A. Bansiddhi, T. Sargeant, S. Stupp, and D. Dunand, *Porous NiTi for bone implants: a review.* Acta biomaterialia, 2008. **4**(4): p. 773-782.
90. S. Samavedi, A.R. Whittington, and A.S. Goldstein, *Calcium phosphate ceramics in bone tissue engineering: a review of properties and their influence on cell behavior.* Acta biomaterialia, 2013. **9**(9): p. 8037-8045.
91. I. Denry and J.A. Holloway, *Ceramics for dental applications: a review.* Materials, 2010. **3**(1): p. 351-368.
92. C.H. Hämmerle, R.E. Jung, and A. Feloutzis, *A systematic review of the survival of implants in bone sites augmented with barrier membranes (guided bone regeneration) in partially edentulous patients.* Journal of clinical periodontology, 2002. **29**(s3): p. 226-231.
93. X. Wang, S. Xu, S. Zhou, W. Xu, M. Leary, P. Choong, M. Qian, M. Brandt, and Y.M. Xie, *Topological design and additive manufacturing of porous metals for bone scaffolds and orthopaedic implants: a review.* Biomaterials, 2016. **83**: p. 127-141.
94. H. Yoshikawa, N. Tamai, T. Murase, and A. Myoui, *Interconnected porous hydroxyapatite ceramics for bone tissue engineering.* Journal of the Royal Society Interface, 2009: p. rsif. 2008.0425. focus.
95. P.B. Malafaya, G.A. Silva, and R.L. Reis, *Natural–origin polymers as carriers and scaffolds for biomolecules and cell delivery in tissue engineering applications.* Advanced drug delivery reviews, 2007. **59**(4): p. 207-233.
96. J.M. Dang and K.W. Leong, *Natural polymers for gene delivery and tissue engineering.* Advanced drug delivery reviews, 2006. **58**(4): p. 487-499.
97. T. Nishida, K. Yasumoto, T. Otori, and J. Desaki, *The network structure of corneal fibroblasts in the rat as revealed by scanning electron microscopy.* Investigative ophthalmology & visual science, 1988. **29**(12): p. 1887-1890.

98. C.S. Ki, D.H. Baek, K.D. Gang, K.H. Lee, I.C. Um, and Y.H. Park, *Characterization of gelatin nanofiber prepared from gelatin–formic acid solution.* Polymer, 2005. **46**(14): p. 5094-5102.
99. A. TANAKA, T. NAGATE, and H. MATSUDA, *Acceleration of wound healing by gelatin film dressings with epidermal growth factor.* Journal of Veterinary Medical Science, 2005. **67**(9): p. 909-913.
100. X. Wu, Y. Liu, X. Li, P. Wen, Y. Zhang, Y. Long, X. Wang, Y. Guo, F. Xing, and J. Gao, *Preparation of aligned porous gelatin scaffolds by unidirectional freeze-drying method.* Acta biomaterialia, 2010. **6**(3): p. 1167-1177.
101. J. Glowacki and S. Mizuno, *Collagen scaffolds for tissue engineering.* Biopolymers, 2008. **89**(5): p. 338-344.
102. L. Cen, W. Liu, L. Cui, W. Zhang, and Y. Cao, *Collagen tissue engineering: development of novel biomaterials and applications.* Pediatric research, 2008. **63**(5): p. 492-496.
103. A. Lynn, I. Yannas, and W. Bonfield, *Antigenicity and immunogenicity of collagen.* Journal of Biomedical Materials Research Part B: Applied Biomaterials, 2004. **71**(2): p. 343-354.
104. M. Gómez-Guillén, M. Pérez-Mateos, J. Gómez-Estaca, E. López-Caballero, B. Giménez, and P. Montero, *Fish gelatin: a renewable material for developing active biodegradable films.* Trends in Food Science & Technology, 2009. **20**(1): p. 3-16.
105. J. Huang, H. Fu, Z. Wang, Q. Meng, S. Liu, H. Wang, X. Zheng, J. Dai, and Z. Zhang, *BMSCs-laden gelatin/sodium alginate/carboxymethyl chitosan hydrogel for 3D bioprinting.* RSC Advances, 2016. **6**(110): p. 108423-108430.
106. A. Asti and L. Gioglio, *Natural and synthetic biodegradable polymers: different scaffolds for cell expansion and tissue formation.* The International journal of artificial organs, 2014. **37**(3): p. 187-205.
107. A. Vats, N. Tolley, J. Polak, and J. Gough, *Scaffolds and biomaterials for tissue engineering: a review of clinical applications.* Clinical Otolaryngology, 2003. **28**(3): p. 165-172.
108. J.-M. Lü, X. Wang, C. Marin-Muller, H. Wang, P.H. Lin, Q. Yao, and C. Chen, *Current advances in research and clinical applications of PLGA-based nanotechnology.* Expert review of molecular diagnostics, 2009. **9**(4): p. 325-341.
109. J.Y. Kim, E.K. Park, S.-Y. Kim, J.-W. Shin, and D.-W. Cho, *Fabrication of a SFF-based three-dimensional scaffold using a precision deposition system in*

*tissue engineering.* Journal of Micromechanics and Microengineering, 2008. **18**(5): p. 055027.

110. H. Kweon, M.K. Yoo, I.K. Park, T.H. Kim, H.C. Lee, H.-S. Lee, J.-S. Oh, T. Akaike, and C.-S. Cho, *A novel degradable polycaprolactone networks for tissue engineering.* Biomaterials, 2003. **24**(5): p. 801-808.
111. L. Huang, S. Zhang, L. He, C. Zhang, Y. Chen, and X. Luo, *Self-assembled porous film with interconnected 3-dimensional structure from 6sPCL-PMPC copolymer.* RSC Advances, 2016. **6**(6): p. 4826-4834.
112. G. Xu, Y. Tan, T. Xu, D. Yin, M. Wang, M. Shen, X. Chen, X. Shi, and X. Zhu, *Hyaluronic acid-functionalized electrospun PLGA nanofibers embedded in a microfluidic chip for cancer cell capture and culture.* Biomaterials Science, 2017. **5**(4): p. 752-761.
113. N. Abbasi, S. Soudi, N. Hayati-Roodbari, M. Dodel, and M. Soleimani, *The effects of plasma treated electrospun nanofibrous poly (ε-caprolactone) scaffolds with different orientations on mouse embryonic stem cell proliferation.* Cell Journal (Yakhteh), 2014. **16**(3): p. 245.
114. S. Li, P. Glynne-Jones, O.G. Andriotis, K.Y. Ching, U.S. Jonnalagadda, R.O. Oreffo, M. Hill, and R.S. Tare, *Application of an acoustofluidic perfusion bioreactor for cartilage tissue engineering.* Lab on a chip, 2014. **14**(23): p. 4475-4485.
115. E. Schmidt, J. McIntosh, and M. Bak, *Long-term implants of Parylene-C coated microelectrodes.* Medical and Biological Engineering and Computing, 1988. **26**(1): p. 96-101.
116. P.-J. Chen, D.C. Rodger, S. Saati, M.S. Humayun, and Y.-C. Tai, *Microfabricated implantable parylene-based wireless passive intraocular pressure sensors.* Journal of Microelectromechanical Systems, 2008. **17**(6): p. 1342-1351.
117. K. Chaw, M. Manimaran, F. Tay, and S. Swaminathan, *Matrigel coated polydimethylsiloxane based microfluidic devices for studying metastatic and non-metastatic cancer cell invasion and migration.* Biomedical microdevices, 2007. **9**(4): p. 597-602.
118. J.W. Dean III, K.C. Culbertson, and A.M. D'Angelo, *Fibronectin and laminin enhance gingival cell attachment to dental implant surfaces in vitro.* International Journal of Oral & Maxillofacial Implants, 1995. **10**(6).
119. L.E. Freed, G. Vunjak-Novakovic, R.J. Biron, D.B. Eagles, D.C. Lesnoy, S.K.

Barlow, and R. Langer, *Biodegradable polymer scaffolds for tissue engineering.* Nature Biotechnology, 1994. **12**(7): p. 689-693.

120. Q. Cheng, S. Li, and K. Komvopoulos, *Plasma-assisted surface chemical patterning for single-cell culture.* Biomaterials, 2009. **30**(25): p. 4203-4210.
121. K. Rezwan, Q. Chen, J. Blaker, and A.R. Boccaccini, *Biodegradable and bioactive porous polymer/inorganic composite scaffolds for bone tissue engineering.* Biomaterials, 2006. **27**(18): p. 3413-3431.
122. C.Y. Sargent, G.Y. Berguig, and T.C. McDevitt, *Cardiomyogenic differentiation of embryoid bodies is promoted by rotary orbital suspension culture.* Tissue Engineering Part A, 2009. **15**(2): p. 331-342.
123. A. Khademhosseini, R. Langer, J. Borenstein, and J.P. Vacanti, *Microscale technologies for tissue engineering and biology.* Proceedings of the National Academy of Sciences of the United States of America, 2006. **103**(8): p. 2480-2487.
124. D.W. Hutmacher, *Scaffolds in tissue engineering bone and cartilage.* Biomaterials, 2000. **21**(24): p. 2529-2543.
125. S. Mitragotri and J. Lahann, *Physical approaches to biomaterial design.* Nature materials, 2009. **8**(1): p. 15-23.
126. T. Desmet, R. Morent, N.D. Geyter, C. Leys, E. Schacht, and P. Dubruel, *Nonthermal plasma technology as a versatile strategy for polymeric biomaterials surface modification: a review.* Biomacromolecules, 2009. **10**(9): p. 2351-2378.
127. D.S. Katti, R. Vasita, and K. Shanmugam, *Improved biomaterials for tissue engineering applications: surface modification of polymers.* Current topics in medicinal chemistry, 2008. **8**(4): p. 341-353.
128. T.C. Lee and P. Niederer, *Basic engineering for medics and biologists: An ESEM primer*. Vol. 152. 2010: IOS Press.
129. B.K. Kuila and A.K. Nandi, *Physical, mechanical, and conductivity properties of poly (3-hexylthiophene)− montmorillonite clay nanocomposites produced by the solvent casting method.* Macromolecules, 2004. **37**(23): p. 8577-8584.
130. S.A. Bencherif, T.M. Braschler, and P. Renaud, *Advances in the design of macroporous polymer scaffolds for potential applications in dentistry.* Journal of periodontal & implant science, 2013. **43**(6): p. 251-261.
131. X. Liu and P.X. Ma, *Phase separation, pore structure, and properties of nanofibrous gelatin scaffolds.* Biomaterials, 2009. **30**(25): p. 4094-4103.

132. B. Marolia, *3D Printing and Its Applications.* Contemporary Literary Review India, 2016. **3**(3): p. 70-73.
133. K. Markstedt, A. Mantas, I. Tournier, H.c. Martínez Ávila, D. Hägg, and P. Gatenholm, *3D bioprinting human chondrocytes with nanocellulose–alginate bioink for cartilage tissue engineering applications.* Biomacromolecules, 2015. **16**(5): p. 1489-1496.
134. http://www.3ders.org/articles/20130209-microscale-printing-of-a-spaceship-on-worlds-fastest-3d-printer.html.
135. D. von Heimburg, S. Zachariah, H. Kühling, I. Heschel, H. Schoof, B. Hafemann, and N. Pallua, *Human preadipocytes seeded on freeze-dried collagen scaffolds investigated in vitro and in vivo.* Biomaterials, 2001. **22**(5): p. 429-438.
136. D.I. Braghirolli, D. Steffens, and P. Pranke, *Electrospinning for regenerative medicine: a review of the main topics.* Drug discovery today, 2014. **19**(6): p. 743-753.
137. http://www.scielo.br/scielo.php?script=sci_arttext&pid=S1516-14392011000300006.
138. S. Zhang, *Fabrication of novel biomaterials through molecular self-assembly.* Nature biotechnology, 2003. **21**(10): p. 1171-1178.
139. J.T. Borenstein, E.J. Weinberg, B.K. Orrick, C. Sundback, M.R. Kaazempur-Mofrad, and J.P. Vacanti, *Microfabrication of three-dimensional engineered scaffolds.* Tissue engineering, 2007. **13**(8): p. 1837-1844.
140. E. Delivopoulos, M.M. Ouberai, P.D. Coffey, M.J. Swann, K.M. Shakesheff, and M.E. Welland, *Serum protein layers on parylene-C and silicon oxide: Effect on cell adhesion.* Colloids and Surfaces B: Biointerfaces, 2015. **126**: p. 169-177.
141. K. Webb, V. Hlady, and P.A. Tresco, *Relative importance of surface wettability and charged functional groups on NIH 3T3 fibroblast attachment, spreading, and cytoskeletal organization.* Journal of biomedical materials research, 1998. **41**(3): p. 422.
142. L. Bacakova, E. Filova, M. Parizek, T. Ruml, and V. Svorcik, *Modulation of cell adhesion, proliferation and differentiation on materials designed for body implants.* Biotechnology advances, 2011. **29**(6): p. 739-767.
143. C.J. Bettinger, R. Langer, and J.T. Borenstein, *Engineering substrate topography at the micro‐and nanoscale to control cell function.* Angewandte Chemie International Edition, 2009. **48**(30): p. 5406-5415.

144. B. Chehroudi and D. Brunette, *Effects of surface topography on cell behavior.* Encyclopedic handbook of biomaterials and bioengineering, 1995: p. 813-842.
145. P. Weiss, *Experiments on cell and axon orientation in vitro: the role of colloidal exudates in tissue organization.* Journal of Experimental Zoology Part A: Ecological Genetics and Physiology, 1945. **100**(3): p. 353-386.
146. R. Flemming, C. Murphy, G. Abrams, S. Goodman, and P. Nealey, *Effects of synthetic micro-and nano-structured surfaces on cell behavior.* Biomaterials, 1999. **20**(6): p. 573-588.
147. A.M. Green, J.A. Jansen, J. Van der Waerden, and A.F. Von Recum, *Fibroblast response to microtextured silicone surfaces: texture orientation into or out of the surface.* Journal of Biomedical Materials Research Part A, 1994. **28**(5): p. 647-653.
148. D.-H. Kim, K. Han, K. Gupta, K.W. Kwon, K.-Y. Suh, and A. Levchenko, *Mechanosensitivity of fibroblast cell shape and movement to anisotropic substratum topography gradients.* Biomaterials, 2009. **30**(29): p. 5433-5444.
149. E.K. Yim, S.W. Pang, and K.W. Leong, *Synthetic nanostructures inducing differentiation of human mesenchymal stem cells into neuronal lineage.* Experimental cell research, 2007. **313**(9): p. 1820-1829.
150. M.R. Lee, K.W. Kwon, H. Jung, H.N. Kim, K.Y. Suh, K. Kim, and K.-S. Kim, *Direct differentiation of human embryonic stem cells into selective neurons on nanoscale ridge/groove pattern arrays.* Biomaterials, 2010. **31**(15): p. 4360-4366.
151. R.G. Wells, *The role of matrix stiffness in regulating cell behavior.* Hepatology, 2008. **47**(4): p. 1394-1400.
152. N.D. Leipzig and M.S. Shoichet, *The effect of substrate stiffness on adult neural stem cell behavior.* Biomaterials, 2009. **30**(36): p. 6867-6878.
153. R.J. Pelham and Y.-l. Wang, *Cell locomotion and focal adhesions are regulated by substrate flexibility.* Proceedings of the National Academy of Sciences, 1997. **94**(25): p. 13661-13665.
154. A.J. Engler, S. Sen, H.L. Sweeney, and D.E. Discher, *Matrix elasticity directs stem cell lineage specification.* Cell, 2006. **126**(4): p. 677-689.
155. S.J. Hollister, *Porous scaffold design for tissue engineering.* Nature materials, 2005. **4**(7): p. 518-524.
156. L.R. Madden, D.J. Mortisen, E.M. Sussman, S.K. Dupras, J.A. Fugate, J.L. Cuy, K.D. Hauch, M.A. Laflamme, C.E. Murry, and B.D. Ratner, *Proangiogenic*

*scaffolds as functional templates for cardiac tissue engineering.* Proceedings of the National Academy of Sciences, 2010. **107**(34): p. 15211-15216.

157. O. Oliviero, M. Ventre, and P. Netti, *Functional porous hydrogels to study angiogenesis under the effect of controlled release of vascular endothelial growth factor.* Acta biomaterialia, 2012. **8**(9): p. 3294-3301.
158. A. Artel, H. Mehdizadeh, Y.-C. Chiu, E.M. Brey, and A. Cinar, *An agent-based model for the investigation of neovascularization within porous scaffolds.* Tissue Engineering Part A, 2011. **17**(17-18): p. 2133-2141.
159. Q.L. Loh and C. Choong, *Three-dimensional scaffolds for tissue engineering applications: role of porosity and pore size.* Tissue Engineering Part B: Reviews, 2013. **19**(6): p. 485-502.
160. R.M. Park, P.A. Schulte, J.D. Bowman, J.T. Walker, S.C. Bondy, M.G. Yost, J.A. Touchstone, and M. Dosemeci, *Potential occupational risks for neurodegenerative diseases.* American journal of industrial medicine, 2005. **48**(1): p. 63-77.
161. K.J. Barnham, C.L. Masters, and A.I. Bush, *Neurodegenerative diseases and oxidative stress.* Nature reviews Drug discovery, 2004. **3**(3): p. 205-214.
162. C.E. Schmidt and J.B. Leach, *Neural tissue engineering: strategies for repair and regeneration.* Annual review of biomedical engineering, 2003. **5**(1): p. 293-347.
163. C. Patrick, *Neural tissue engineering.* Annals of Biomedical Engineering, 1997. **25**(1): p. S-41.
164. B. Dhandayuthapani, Y. Yoshida, T. Maekawa, and D.S. Kumar, *Polymeric scaffolds in tissue engineering application: a review.* International Journal of Polymer Science, 2011. **2011**.
165. M. Martina and D.W. Hutmacher, *Biodegradable polymers applied in tissue engineering research: a review.* Polymer International, 2007. **56**(2): p. 145-157.
166. N. Li, Q. Zhang, S. Gao, Q. Song, R. Huang, L. Wang, L. Liu, J. Dai, M. Tang, and G. Cheng, *Three-dimensional graphene foam as a biocompatible and conductive scaffold for neural stem cells.* Scientific reports, 2013. **3**: p. 1604.
167. Y. Tang, L. Liu, J. Li, L. Yu, F.P.U. Severino, L. Wang, J. Shi, X. Tu, V. Torre, and Y. Chen, *Effective motor neuron differentiation of hiPSCs on a patch made of crosslinked monolayer gelatin nanofibers.* Journal of Materials Chemistry B, 2016. **4**(19): p. 3305-3312.
168. B. Xu, Y. Zhao, Z. Xiao, B. Wang, H. Liang, X. Li, Y. Fang, S. Han, X. Li, and

C. Fan, *A Dual Functional Scaffold Tethered with EGFR Antibody Promotes Neural Stem Cell Retention and Neuronal Differentiation for Spinal Cord Injury Repair.* Advanced Healthcare Materials, 2017. **6**(9).

169. R. Lozano, M. Naghavi, K. Foreman, S. Lim, K. Shibuya, V. Aboyans, J. Abraham, T. Adair, R. Aggarwal, and S.Y. Ahn, *Global and regional mortality from 235 causes of death for 20 age groups in 1990 and 2010: a systematic analysis for the Global Burden of Disease Study 2010.* The Lancet, 2013. **380**(9859): p. 2095-2128.
170. J. Young and R. Mills, *Clinical Management of Heart Failure. Professional Communications*. 2001, Inc.
171. F.Y. Chen and L.H. Cohn, *The surgical treatment of heart failure. A new frontier: nontransplant surgical alternatives in heart failure.* Cardiology in review, 2002. **10**(6): p. 326-333.
172. C. Martinez, A. Tzur, H. Hrachian, J. Zebede, and G.A. Lamas, *Pacemakers and defibrillators: recent and ongoing studies that impact the elderly.* The American journal of geriatric cardiology, 2006. **15**(2): p. 82-87.
173. H. Jawad, N. Ali, A. Lyon, Q. Chen, S. Harding, and A. Boccaccini, *Myocardial tissue engineering: a review.* Journal of tissue engineering and regenerative medicine, 2007. **1**(5): p. 327-342.
174. M. Radisic, H. Park, F. Chen, J.E. Salazar-Lazzaro, Y. Wang, R. Dennis, R. Langer, L.E. Freed, and G. Vunjak-Novakovic, *Biomimetic approach to cardiac tissue engineering: oxygen carriers and channeled scaffolds.* Tissue engineering, 2006. **12**(8): p. 2077-2091.
175. P. Kerscher, I.C. Turnbull, A.J. Hodge, J. Kim, D. Seliktar, C.J. Easley, K.D. Costa, and E.A. Lipke, *Direct hydrogel encapsulation of pluripotent stem cells enables ontomimetic differentiation and growth of engineered human heart tissues.* Biomaterials, 2016. **83**: p. 383-395.
176. Y. Tang, L. Liu, J. Li, L. Yu, L. Wang, J. Shi, and Y. Chen, *Induction and differentiation of human induced pluripotent stem cells into functional cardiomyocytes on a compartmented monolayer of gelatin nanofibers.* Nanoscale, 2016. **8**(30): p. 14530-14540.
177. J.C. Chachques, J.C. Trainini, N. Lago, M. Cortes-Morichetti, O. Schussler, and A. Carpentier, *Myocardial assistance by grafting a new bioartificial upgraded myocardium (MAGNUM trial): clinical feasibility study.* The Annals of thoracic surgery, 2008. **85**(3): p. 901-908.

# Chapter 2

# Fabrication methods

In this chapter, we present the technological development of this thesis work. Firstly, we introduce the UV lithography and soft lithography which are most frequently used. Then we describe the electrospinning technique for nanofibers fabrication. Afterwards, we describe the 3D printing technique with a focus on photopolymerization method. Further, we present the freeze drying technique for the porous scaffold fabrication. Finally, we discuss the self-organization of polymers.

## 2.1 UV lithography

UV lithography is a technology to transfer geometric patterns on a mask to a smooth surface (Silica wafer, glass, metal sheet and etc.) with a UV light, which has been used for many years in the manufacturing of integrated circuits, MEMS devices, etc. [1-3]. A major advantage of UV lithography is that it can transfer many features of complex patterns of a mask on a substrate simultaneously and on a large number of substrates repeatedly at high production rate.

A typical UV lithography includes mask preparation, substrate cleaning, photoresist spin-coating, UV exposure and developing.

### 2.1.1 Mask preparation

A photomask is a device that allows light to pass through a predetermined area to project an image on a surface. There are two kinds of masks for UV lithography: optical mask and transparent mask. Optical mask is a glass plate with ~ 100 nm thick chromium patterns on it, which is made by micro pattern generator with a high resolution (~1 μm). Transparent mask is a plastic transparent film with black ink patterns, which is produced by a printer with a relative low resolution (>20 μm).

In this work, all the masks are designed with software L-Edit (Tanner research, USA) and produced by micro pattern generator μPG 101 (Heidelberg Instruments), as shown in **Fig. 2.1**. This pattern generator works with a focused laser beam and a high precision X-Y stage (**Fig. 2.2**).


**Fig. 2.1** μPG 101 micropattern generator (Heidelberg Instruments) [4]

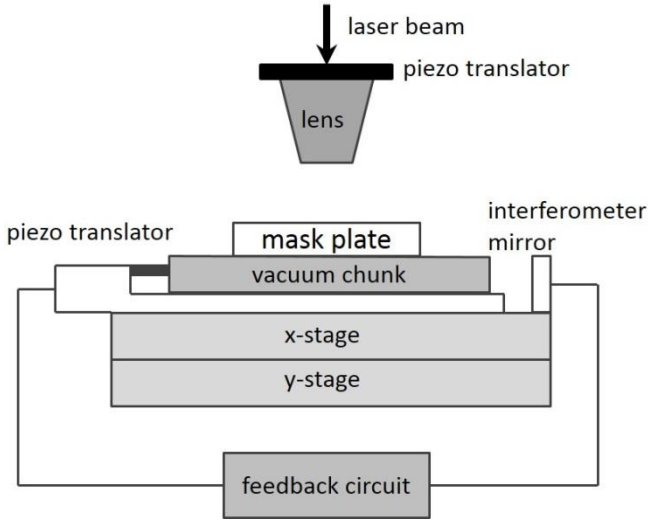


**Fig. 2.2** Working principle of μPG 101 micropattern generator

Typically, the designed pattern is loaded into μPG 101 and a glass plate with 100 nm thick of chromium layer and 1 μm thick of AZ 1518 positive photoresist (Nanofilm, CIPEC Company) is placed on the X-Y stage. After setting the desired laser power, the writing time is estimated according the pattern size and the laser power. The designed pattern can then be exposed with the laser beam and X-Y stage displacement. A minimum feature size of 1 μm with an accuracy of 0.1 μm can be reached. After laser exposure, the chromium plate is developed in AZ-726 MIF developer (Micro Chemicals) for 30 s with gentle shaking, followed by DI water rinsing to remove the residual developer. Then, the chromium plate is treated with a chrome etching solution (Chrome-Etch 3144) for ~ 60 s to remove the exposed area of the chromium layer,

followed by DI water rinsing. Finally, the remained AZ 1518 photoresist is removed in acetone by sonication for 5 min.

### 2.1.2 Substrate cleaning

The substrates frequently used in this work are Si wafers and glass slides. Their clean process is as follows:

For Si wafer:

- Piranha clean: mixture of $H_2SO_4$:$H_2O_2$ (3:1), 10~20 min
- DI water rinse: 15 min, 5 min for each
- Air flow dry: $N_2$ gun
- Hotplate baking: 200℃ for 5 min

The Piranha clean is highly oxidative which can remove metals and organic contamination on the Si wafer. DI water is used to remove all chemicals on the Si wafer. $N_2$ air flow and hotplate baking can totally remove the residual DI water on the Si wafer.

For glass substrate:

- Acetone + Ultra-sonication: 5 min
- Isopropanol + Ultra-sonication: 5 min
- Oxygen plasma: 5 min
- Hotplate baking: 200℃ for 5 min

Acetone can remove organic contamination on glass substrate. Isopropanol and oxygen plasma are used to remove all chemicals on glass substrate.

### 2.1.3 Photoresist processing

Photoresist is an ultraviolet (UV) light sensitive material spin coated on a substrate, which is usually composed of UV sensitive materials, UV initiator and solvents [5]. The photoresists responds to the UV light by changing the solubility of the exposed area in a developing solution, based on which photoresists are divided into two groups: positive and negative, as is shown in **Fig. 2.3**. A positive resist will result in an exact

copy of what is on the photomask, while a negative resist will result in the inversed pattern.

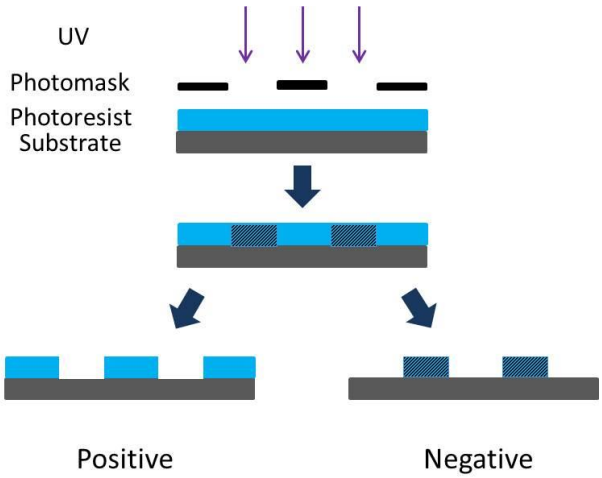


**Fig. 2.3** Illustration of two types of photolithography

In this work, negative photoresists (SU-8 series) are frequently used for cell culture patch fabrication. The SU-8 photoresists are main negative photoresists containing epoxy based molecules which will cross link under UV exposure. They are viscous polymers that can be spread by spin coating to a thickness ranging from 1μm to 300μm. The cross-linked SU8 resist is highly resistant to acids, bases and organic solvents and has excellent thermal and mechanical stability.

The frequently used SU-8 series photoresists are SU-8 3005, SU-8 3010 and SU-8 3050 in this thesis work, which can achieve thicknesses of 5, 10 and 50 μm according to the manufacturer's guide (3000 rpm spin speed). The exposed photoresist is developed in SU-8 developer and rinsed with isopropanol.

## 2.2 Soft lithography

Soft lithography refers to a class of non-photolithographic methods replying on self-assembly and cast molding [6, 7], providing a convenient and cost-effective alternative to the conventional lithography methods for fabricating micro- and nanostructures. In soft lithography, an elastomeric stamp with patterned relief structures on its surface is used to generate patterns and structures with feature sizes ranging from 30 nm to 100 μm. In this work, the most frequently used material for soft lithography

is Polydimethylsiloxanes (PDMS), which has been proven to be an efficient and economic method for micro- and nanofabrication [8-12]. Other elastomers such as polyurethanes, polyimides, and cross-linked Novolac$^{TM}$ resins can also be used in soft lithography [13].

PDMS has a unique combination of properties resulting from the inorganic siloxane backbone and organic methyl groups attached to silicon. Thus, PDMS elastomers have many outstanding properties as follows. (a) They have very low glass transition temperature and hence are fluids at room temperature, enabling them to be easily casted with molds of different geometries, and solids after curing (b) The solidified PDMS elastomer have low interfacial free energy ($21.6 \times 10^{-3}$ J m$^{-2}$) and good chemical stability [14], exhibiting great repugnance to conjugate with most polymers or molecules patterned on them. (c) PDMS elastomer is gas permeable but not swelling in humidity. (d) It also has good thermal stability (up to 186℃ in air) and optical transparency (down to 300 nm). (e) The PDMS elastomer is durable as a stamp or a stencil, which can be used for many times without noticeable decrease in performance. (f) The surface of PDMS can be easily activated by plasma or chemicals for molecules and polymers functionalization, rendering PDMS with multi-functions.

PDMS pre-polymers are commercially available in large quantities. In my thesis work, all PDMS are RTV 615, which is composed of part A (**Fig. 2.4a**) and part B (**Fig. 2.4b**) (curing agent). In general, the A/B ratio can be adjusted from 5:1 to 20:1 (w/w). After complete mixing, casting and curing, PDMS replica of different stiffness (varying from hard to soft) can be obtained. Typically, PDMS pre-polymer is cured in an oven of 80 ℃ for 2 h. **Fig. 2.4c** shows the scheme of PDMS crosslinking.

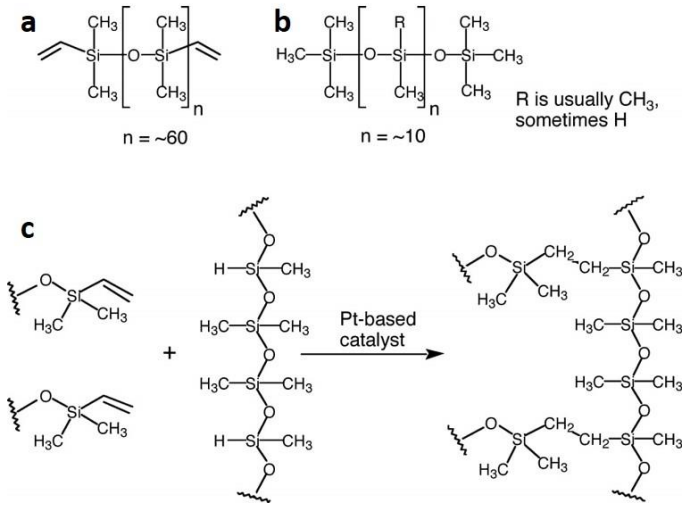


**Fig. 2.4** Scheme of PDMS crosslinking [15]

The PDMS stamp for molecular printing or subsequent cast is obtained from a master usually fabricated by photolithography. Alternatively, it can also be obtained from a master prepared by electron beam or focused ion beam lithography as well as 3D printing. In most cases, to facilitate the mold release, it is necessary to modify the surface of the master with a release agent named Trimethylchlorosilane (TMCS). This can be done by simply putting the master into TMCS vapor for 15 min based on a silanization reaction shown in **Fig. 2.5**.

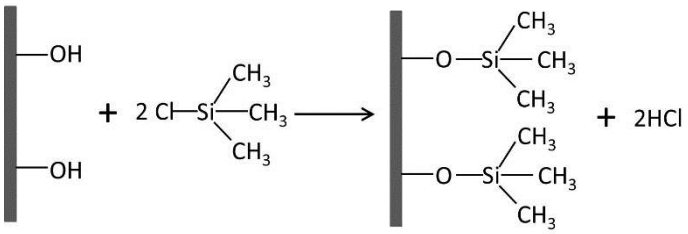


**Fig. 2.5** Effect of TMCS deposition on the surface of a mold.

A typical PDMS soft lithography process is described below. Briefly, PDMS part A and B are weighed with desirable ratio and mixed completely by stirring, which may produce many air bubbles. PDMS pre-polymers with bubbles are transferred to a vacuum chamber to degas the PDMS. The bubbles rise, float on the surface of PDMS pre-polymers and burst under low vacuum. Then, the PDMS pre-polymers are poured into the master slowly and degassed again on a horizontal platform until the PDMS

surface is flat. The PDMS pre-polymers with the master are placed in an 80 ℃ oven. After 2 h, solid PDMS can be taken out of the oven and peeled off from the master after cooling down to the room temperature, resulting in a PDMS stamp ready to use.

## 2.3 Electrospinning

### 2.3.1 Principle and parameters

Electrospinning provides a simple and fast way to generate ultrathin nanofibers layers from a variety of materials [16-18]. The basic setup for electrospinning includes a high voltage supply, a syringe with metallic needle and a conductive collector, as is shown in **Fig. 2.6**. In electrospinning, high viscous polymer solution is pumped out of syringe needle and deformed by surface charges. The deformed polymer solution is then continuously stretched to generate a solid fiber due to the electrostatic repulsions between the surface charges and evaporation of the solvents. The electrostatic force between solution extrusion tip and the collector will direct the solid fibers to deposit on the collector.

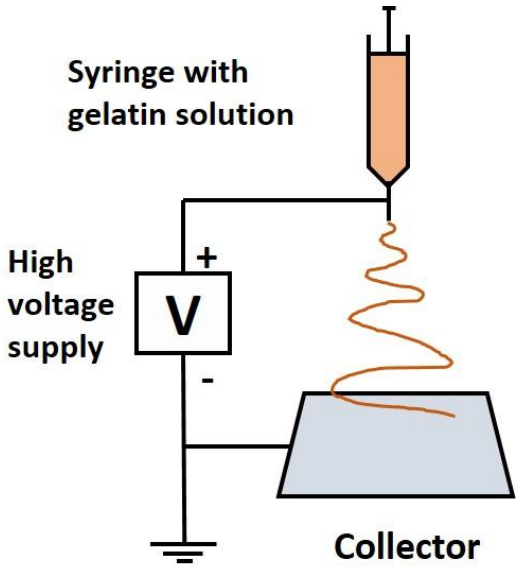


**Fig. 2.6** A scheme of electrospinning setup.

Electrospinning is highly sensitive to the processing parameters and conditions

[17]. The following factors play important roles in the process of electrospinning: voltage, flow rate, distance between needle and collector, polymer concentration and solution viscosity, solvents choice and temperature and humidity.

**a) Voltage**

High voltage is essential to polarize solution, form Taylor cone, and stretch polymer solution. Ultrafine nanofibers can be achieved at a critical voltage. An increase of applied voltage beyond the critical value will result in the formation of beads or beaded nanofibers, which is attributed to the decrease in the size of Taylor cone and increase the jet velocity [19, 20]. Furthermore, the increase of voltage also leads to the increase of nanofibers diameter [21].

**b) Flow rate**

The flow rate of polymeric solution through the needle tip affects the morphology of electrospun nanofibers. By applying the critical flow rate of a polymeric solution uniform beadless nanofibers can be fabricated. Increasing the flow rate above the critical value can cause the increase of nanofibers diameter and sometimes the formation of beads. Besides, at an elevated flow rate, ribbon-like defects and unspun droplets have also been reported [22, 23].

**c) Distance between needle and collector**

The distance between the needle tip and the collector plays an essential role in determining the morphology of electrospun nanofibers [24]. The distance determines the deposition time, evaporation rate and electrical stretching. By varying the distance, the nanofibers morphology can be easily adjusted. If the distance is kept small, large-diameter nanofibers can be made [25].

**d) Polymer concentration**

The electrospinning process depends on the uniaxial stretching of a charged jet, which is strongly affected by the concentration of polymer solution. If the concentration of polymer is low, the applied electric field and surface tension pull the elongated polymer chains to break into fragments before reaching the collector. An increase in the concentration of polymer will lead to an increase in the viscosity, which then increase chain entanglement among polymer chains. These chain entanglements overcome surface tension and finally reach the collector to form uniform beadless electrospun nanofibers. Further increase of concentration far beyond the critical point will spoil the

flow of the solution through the needle tip because the polymer solution will dry quickly and block the needle tip.

**e) Solvent selection**

The selection of solvent is one of the key factors for the formation of ultrafine and beadles electrospun nanofibers. Polymer should be totally soluble in the solvent. Besides, solvent should have a moderate boiling point. Generally, moderately volatile solvents are preferred, which encourage solvents evaporation from the nanofibers during their flight from needle tip to collector. Highly volatile solvents will lead to fast dry of polymer at the needle tip, while less volatile solvents will prevent drying of nanofibers during their flight, causing beaded nanofibers. Solvents also play important roles in producing highly porous nanofibers by using mixing solvents.

**f) Environmental factors**

Environmental factors like relative humidity and temperature also affect the diameter and morphology of electrospun nanofibers. Environmental humidity can affect the solidification process of charged jet and thus will change the nanofibers diameter. Researchers observed that the diameter of the nanofibers decreased from 667 nm to 161 nm (PVA) and 252 nm to 75 nm (PEO) with increase in humidity from 4% to 60% [26]. Temperature affects the average diameter of electrospun nanofibers via two aspects. One is that temperature increase can facilitate evaporation rate of solvent. The other is that it can also decrease the viscosity of the solution. The increase in the solvent evaporation and the decrease in the solution viscosity work simultaneously, both leading to the decrease in the mean fiber diameter.

## 2.3.2 Materials

Various biodegradable natural and synthetic polymers can be easily electrospun to form nanoscale fibers [27]. In order to improve performance of nanofibers in tissue engineering, the fabricated nanofibers can be functionalized based on the following strategies. Electrospinning process can be engineered to produce porous or hollow nanofibers [28, 29]. The nanofibers can be modified to change wettability and surface charge [30]. They can also be chemically modified with specific bioactive ligands to

improve cell adhesion, spreading, proliferation and differentiation by mimicking the ECM morphology and functions [31].

### 2.3.3 Applications

A large number of studies have revealed that cellular behavior like attachment, proliferation and differentiation can be modulated by engineering parameters of nanofibers like surface charge and wettability, chemical composition, morphology, diameter and alignment [32]. Studies also show that the porosity of the fiber mat plays an important in controlling cell behavior like attachment, migration, spreading and proliferation [33, 34]. Porous nanofiber mat allows more efficient diffusion of nutrients as well as metabolic wastes. Besides, the high porosity surface provides the minimum extra contact for culturing cells. The mechanical property of nanofiber is also important due to the different appetite of cells to substrate stiffness.

Nanofibers are used in tissue engineering as biocompatible substrates loading targeted cells to repair damaged tissues including sciatic nerve, heart, tendon and blood vessel [19, 35, 36]. Li et al [35] reported that fibrous scaffolds not only showed an impact on the cell-to-cell interaction but also increased the interaction between cells and matrix. Electrospun nanofiber scaffolds exhibited an excellent cell growing capability. Wong et al [37] revealed that PCL electrospun nanofiber scaffolds enhanced the MC3T3-E1 pre-osteoblasts cell adhesion and proliferation as well as assisted in the differentiation of the cells. Li et al [38] demonstrated that silk fibroin blended with bone morphogenetic protein 2 and hydroxyapatite nanoparticles has exhibited excellent bone tissue regeneration.

### 2.3.4 Limitations

There are still some limitations, however, in the use of electrospun nanofiber scaffolds in tissue engineering. One hurdle is the infiltration of cells inside the fibrous scaffolds because of the small intra-fiber pore size. Another hurdle is the poor

mechanical strength of the nanofiber mat. The nanofibers mats are generally fragile and lack enough mechanical strength for *in vitro* and *in vivo* cell based assays. Previous solution to this issue is to increase the thickness of the nanofibers mat, which causes low porosity and limited diffusion of nutrients and metabolic wastes. In this work, we developed a new method by integrating PMDS backbone with monolayer nanofibers to overcome the above obstacles. The third hurdle is that the electrospinning method lacks repeated performance and varies from batch to batch, which is vulnerable to electrospinning parameters and environmental factors. In this work, we developed a self-organization method to fabricate porous PCL film with facile processing steps.

## 2.4 3D printing

3D printing is a collection of manufacturing techniques defined as the process of adding materials layer upon layer to produce objects from 3D model data [39]. 3D printing is a rapidly developing manufacturing technology, which is applicable to the fabrication of 3D objects of different scales using different materials.

### 2.4.1 Advantages

The advantages of 3D printing include design freedom, faster product development cycles, low setup costs for production, local production and on-demand manufacturing. 3D printing offers the promise of a simple, efficient and low-cost supply chain, with no need for mass production in factories, or for global logistics of both raw materials and products. 3D printing offers the promise of manufacturing with less waste and less energy. People can print metals, ceramics, food, plastics and even living organic cells. With 3D printing, people can create, design and manufacture whatever we want, wherever we want, which, I believe, will create a revolution in manufacturing.

### 2.4.2 Printing technologies

3D printing is a computer-controlled production technique that builds a product

layer by layer. Although there are different techniques available, three basic requirements are needed: model design, 3D printing technology and material used. 3D printer works according to an instruction file created by a 3D modeling program called a Computer Aided Design file. Such a file can be designed from scratch, from an existing file or it can be created by a 3D scanner. The design of an object is sliced into thousands of horizontal layers and then sent to the 3D printer to direct the printing process.

Currently there are several technologies that cover the term 3D printing, including: extrusion, direct energy deposition, solidification of powder, sheet lamination and photopolymerization.

**a) Extrusion**

A molten material - plastic, clay, cements silicone, ink, or even chocolate or cheese - is extruded and becomes solid after it emerges from the printer head. Designs are built up layer by layer until the final product is complete. One of examples based on extrusion principle is Fused Deposition Modeling shown in **Fig. 2.7a** [40, 41]. Briefly, thermoplastic material is extruded from the printer head. The molten material is printed layer by layer, on top of the previous layer and fuses when the material hardens, almost instantly after leaving the printing head. Every time a layer is fully printed, the printer platform is lowered a fraction until the product is finished. This is one of the cheapest 3D printing methods and most often used in 3D printers at home. At present the most common materials used are ABS (common plastic, oil based plastic) and PLA (polylactic acid, a bio-based plastic) [41].

**b) Direct energy deposition**

Direct energy deposition is a process that uses molten metal wire or powder to form an object layer by layer, using a high energy power source such as an electron beam, a plasma welding torch or a laser. This 3D printing technology is specifically used to produce metal objects. One of techniques using direct energy deposition principle is electron beam direct manufacturing shown in **Fig. 2.7b**. Briefly, an electron beam gun provides the energy source for melting metal. Using electromagnetic coils, this electron beam can be both precisely focused or deflected. A computer controls the electron beam and the movable table, to build up the object layer by layer. The process is conducted in a high-vacuum environment, preventing contaminations, which can

produce very large objects rather quickly.

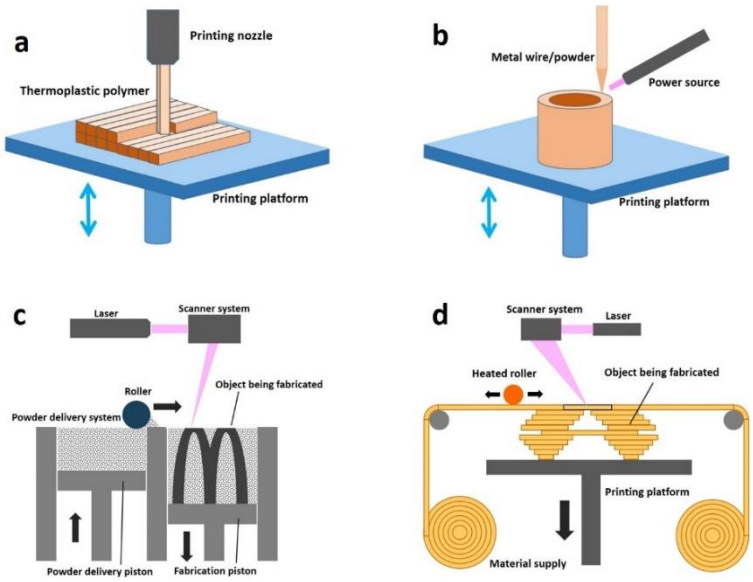


**Fig. 2.7** Schema of 3D printing technologies [42]

### c) Solidification of powder

Powder-based 3D print techniques are based on fusing or hardening (sintering) of powders. The most important solidification of powder techniques are selective laser sintering (SLS) shown in **Fig. 2.7c** [41, 43]. Briefly, powder of a thermoplastic polymer, metal or ceramic is hardened (sintered) with a $CO_2$ laser. The platform lowers and another layer of powder is applied and sintered. This process is repeated until the object is finished. The un-sintered powder functions as a support structure for the product. This powder can be re-used for the next printing, so there is no residual waste. Resolution restraints are caused by the minimum size of the powder particles of around 100 μm. Powdered materials such as polystyrene, ceramics, glass, nylon, and metals can be used in SLS [41].

### d) Sheet lamination

This 3D printing technique builds objects by trimming sheets of material and binding them together layer by layer, as is shown in **Fig. 2.7d**. Laminated Object Manufacturing (LOM) is one of these sheet lamination techniques. Layers of adhesive-coated paper, plastic, or metal laminates are successively glued together and cut to shape with a knife or laser cutter.

### e) Photopolymerization

Photo-polymerization-based 3D printing techniques are based on layer by layer hardening of liquid photo-curable resins by UV-light. The most important photo-polymerization techniques are Stereo-Lithography (SLA) and the PolyJet process. As shown in **Fig. 2.8**, a stereolithography system (SLA) contains a vat or container filled with a liquid photopolymerizable resin. The platform lowers and a sweeper evenly distributes a layer of the photopolymerizable resin. The resin is hardened with UV-lasers. This process is repeated until the object is created.

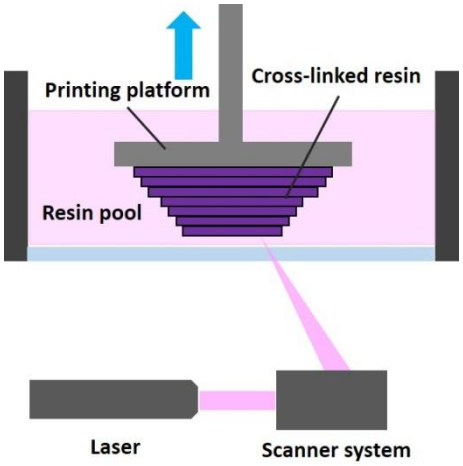


**Fig. 2.8** Scheme of layer-by-layer scanning photopolymerization

In this thesis work, the 3D printer (ProJet 1200, 3D System, Inc., USA) we used, shown in **Fig. 2.9** is based on this principle. The photopolymerizable resin used for the printer is polyethylene glycol diacrylates (PEGDA). **Fig. 2.10** shows a schematic network of cross-linked PEGDA resin.

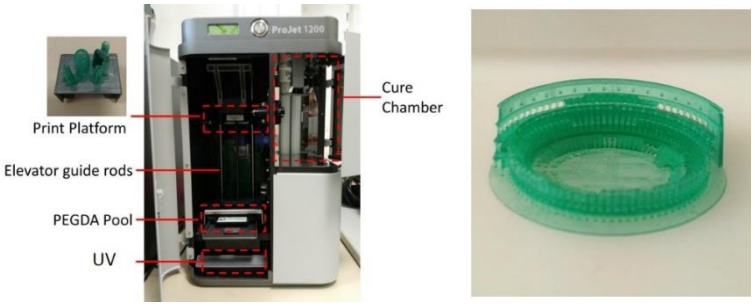


**Fig. 2.9** 3D Printer (ProJet 1200) used in this work and a 3D printed feature.

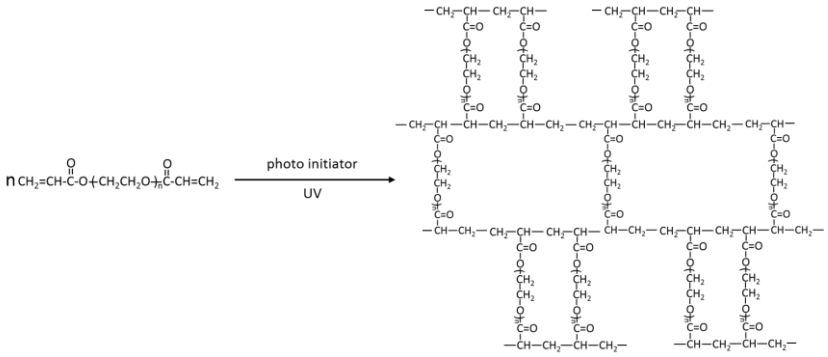


**Fig. 2.10** Scheme of PEGDA cross-linking reaction

## 2.4.3 Materials

In principle, all kind of materials can be used for manufacturing with 3D printing techniques; from sand to metals, ceramics, food, living cells and plastics. In relation to 3D printing a whole range of (bio) plastics is under development combined with (bio) additives to create special properties. The main characteristics of interest are melting temperatures, melting viscosity and coagulation time of materials.

## 2.4.4 Applications

3D printing technique has been proved a powerful tool for tissue engineering by enabling 3D cell culture with complex 3D biomimetic architectures [44-46]. There are two main strategies for current 3D printing in tissue engineering. One strategy is printing 3D scaffold and then loading cells on it. Miao et al [47] reported a smart scaffold by 3D printing novel photo-curable soybean oil epoxidized acrylate, which is highly biocompatible and supported well the growth of multi-potent human bone marrow mesenchymal stem cells. Interestingly, the scaffold also has a temperature dependent shape memory and can fully recover at human body temperature. Leukers et al [48] fabricated a hydroxyapatite scaffold with complex internal structures and high resolution for bone tissue engineering. They found the dynamic cultivation method led to a stronger population compared to the static cultivation method. The cells

proliferated deep into the structure forming close contact to hydroxyapatite granules. The other is printing scaffold and cells simultaneously, or 3D bioprinting. Markstedt et al [49] reported a 3D bioprinting of nanocellulose-alginate scaffold loaded with human chondrocytes which show high viability after 7-day culture. Huang et al [50] reported a 3D bioprinting method using a mixture solution of gelatin/sodium alginate/carboxymethyl chitosan loaded with bone mesenchymal stem cells. The scaffold shows excellent mechanical properties, antibacterial activity, slow degradation rate, and high biocompatibility. However, in some 3D bioprinting systems, cells show high repugnance to spread and proliferate.

### 2.4.5 Limitations

Although great progress has been achieved in developing powerful 3D printed systems, there are still significant technological challenges for the successful development of functional tissue or organ substitutes. Resolution needs to be improved to the subcellular level to better control the physical guidance provided by microstructure and distribution of functional biomolecules such as growth factors and peptide ligands. Additionally, the compatibility of the 3D printer needs to be extended to embrace a wider range of biomaterials. Further improvements to the printing capability and speed are in great need for large scale tissue production for clinical uses.

## 2.5 Freeze drying

Freeze drying or lyophilization is a process in which water is frozen, followed by its removal from the sample, initially by sublimation (primary drying) and then by desorption (secondary drying) [51, 52]. It is a drying process applicable to manufacture of certain pharmaceutical and biological products that are thermolabile or otherwise unstable in aqueous solutions for prolonged storage periods, but that are stable in dry state [53]. It can also be used in food industry to make dry food [54, 55].

This method has also been widely used to efficiently produce porous polymer scaffold for tissue engineering [56, 57]. By adjusting polymer concentration and using different solvents, freeze drying can produce scaffold with different morphologies.

After removal of frozen solvents, the space originally occupied by solvents will become pores in the prepared scaffold. The pore size depends on the growth rate of ice crystal during the freeze drying process. This method can make scaffold with porosity over 90%. By keeping in low temperature, polymer in frozen state will not re-dissolves and possesses enough mechanical strength to prevent pore collapse during drying. This method is especially suitable for making porous protein or thermoplastic scaffold, like collagen, PLGA and PCL, which otherwise will be denatured or deformed by heating drying.

## 2.5.1 Principle

The main principle involved in freeze drying is a phenomenon called sublimation, that is, water passes directly from solid state (ice) to the vapor state without passing through the liquid state. Sublimation of water can take place at pressures and temperature below triple point i.e. 4.579 Torr and 0.0099℃ shown in **Fig. 2.11**. The material to be dried is first frozen and then subjected under a high vacuum to heat (by conduction or radiation or by both) so that frozen liquid sublimes leaving only solid, dried components in the original liquid. The concentration gradient of water vapor between the drying front and condenser is the driving force for removal of water during lyophilization.

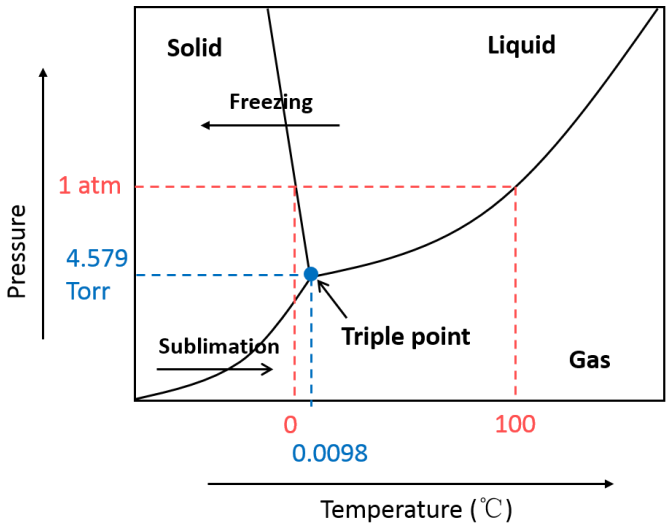


**Fig. 2.11** Phase diagram of water.

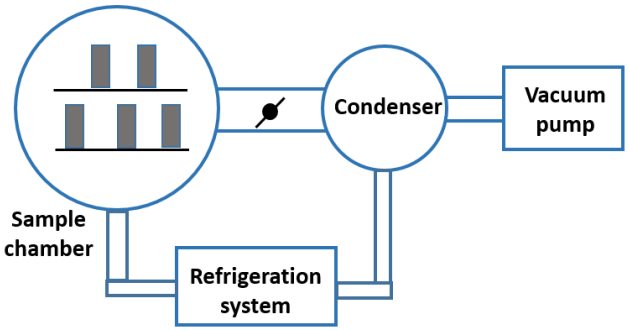


**Fig. 2.12** A scheme of freezing dryer.

Based on the working principle above, the typical freezing dryer is composed of the following key parts: sample chamber, condenser, vacuum pump and refrigeration system, as is shown in **Fig. 2.12**. Sample chamber contains one or several shelves to hold samples, usually glasswares or trays. The condenser is a cold trap to condense vapor by a process of deposition (vapor to solid) coming from the drying product onto a cold surface within the system. Refrigeration system helps to cool down and freeze sample as well as to cool the condensing process for better drying. A vacuum pump is used to evacuate the sample chamber and condenser to the working pressure.

The fundamental processing steps include:

a) Freezing: The sample is frozen, usually in -80℃ refrigerator or liquid nitrogen, which provides a necessary condition for low temperature drying.

b) Sample loading: After freezing, the sample is placed under vacuum, which enables the frozen solvent in the product to vaporize without passing through the liquid phase.

c) Cool-down: It is applied to frozen product to accelerate sublimation.

d) Condensation: Low temperature condenser plates remove the vaporized solvent from the vacuum chamber by converting it back to a solid. This completes the separation process.

e) Sample unload: release the vacuum, stop vacuum pump and take out of the sample.

### 2.5.2 Applications

Freeze drying has been widely used to produce highly porous natural and synthetic scaffolds for tissue engineering. Shen et al [58] reported a porous methylcellulose-based scaffold produced by cross-linking and freeze drying. Results shows scaffolds at different cross-linking density show different porosity, mechanical strength and degradability. Differentiation experiments revealed that hMSCs cultured on scaffolds displayed high level of osteogenic differentiation marker expression, alkaline phosphatase activity and osteocalcin secretion. Li et al [59] reported a highly porous collagen scaffold functionalized with cetuximab, an EGFR antibody. Therapeutic test in rat SCI model showed that the after neural progenitor cells loading, the scaffold caused a wide range of positive effects, including enhanced neuronal differentiation, promoted axonal regeneration and synapse formation, and improved functional recovery.

## 2.6 Self-organization of polymer scaffolds

Self-organization is a process in which a disordered system of pre-existing components forms an organized structure or pattern as a consequence of specific, local interactions among the components themselves [60, 61]. The components can be small molecular, polymers and particles. Polymer self-organization, which uses non-covalent interactions to direct the self-organization of mono-units, has become a topic of increasing interest in recent years [61-63]. The individual building blocks, designed to fabricate the polymeric architectures, include not only macromolecules but also a variety of synthetic monomeric species [64-67].

The crucial driving force for self-organization is based on multiple intermolecular interactions such as hydrogen bonding, p–p stacking, metal–ligand coordination, hydrophobic interactions and host–guest interactions. The reversible and tunable nature of such noncovalent interactions endows these supramolecular assemblies with the important properties of reversibility and stimuli-responsiveness. In turn, this allows for relatively large physical or chemical changes in response to a weak stimulating signal in the environment (e.g., pH, temperature, light, redox agents, enzymes, ions, gases,

mechanical force, electric and magnetic fields). Based on polymer self-organization, many interesting one-, two- and three dimensional morphologies, such as spherical micelles, cylinders, rods and vesicles, have been constructed, as is shown in **Fig. 2.13**.

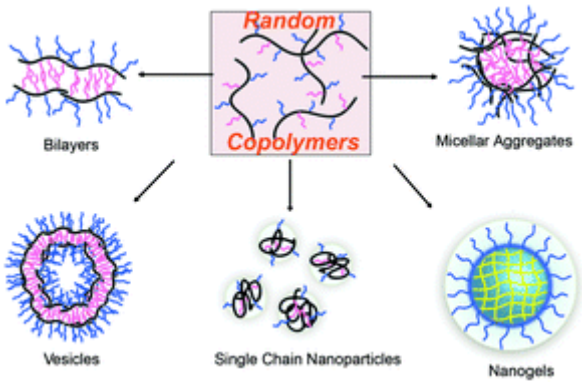


**Fig. 2.13** Scheme of self-organization of copolymers into different constructs [68].

Biodegradable polyesters such as poly-lactide (PLA), poly ε- caprolactone (PCL), and poly (lactide-co-glycolide) (PLGA) have also been widely used in self-organization system for controlled drug delivery. They can be degraded by hydrolytic or enzymatic degradation under physiological conditions. A biodegradable poly-(3-caprolactone-co-phosphoester) random copolymer, [poly (CL-co-OPEA)], was synthesized and conjugated with liver-targeting galactosamine (Gal) to prepare the amphiphilic copolyesters poly (CL-co-OPEA-Gal) [69]. The copolymer has been shown to exhibit low toxicity, where the cell viabilities are still higher than 80% at concentrations up to 200 mg/mL. The hydrophobic core was able to encapsulate the anticancer drug DOX, which could be released in an acidic environment (pH 5.0) due to the acid accelerated hydrolytic degradation of polyphosphoester. Cell uptake experiments show that Gal greatly improved the specific cell binding and cellular uptake. Huang et al [70] reported a Self-assembled porous film with interconnected 3-dimensional structure from 6sPCL-PMPC copolymer just by evaporating solvent of THF and methanol. With this convenient method, the porous films of 6sPCL-PMPC with average pore size around 16±6 mm and porosity 50% are easily fabricated. They found that the morphology of the films is sensitive to temperature, ratio of THF to methanol and even trace amount of water. Since biodegradable porous films have been widely used in tissue engineering

as scaffold, this handy procedure may significantly facilitate the scaffold fabrication.

## 2.7 Parylene C deposition

### 2.7.1 Introduction of parylene C

Parylene is the generic name for members of a unique polymer series shown in **Fig. 2.14**. The basic member of the series, called parylene N, is poly-para-xylylene, a completely linear, highly crystalline material. The second commercially available member of the series is parylene C which is produced from the same monomer modified only by the substitution of a chlorine atom for one of the aromatic hydrogen atoms. The third commercially available member of the series is parylene D which is produced from the same monomer modified by the substitution of the chlorine atoms for two of the aromatic hydrogen atoms. Parylene D is similar in properties to parylene C with the ability to withstand higher use temperatures.

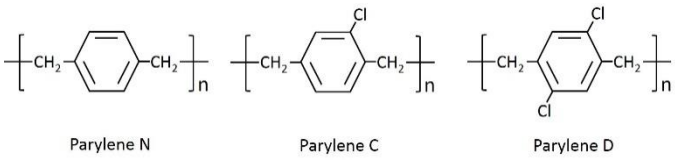


**Fig. 2.14** Chemical structures of parylene N, C and D.

Among these polymers, parylene C has a useful combination of electrical and physical properties plus a very low permeability to moisture and other corrosive gases. Along with its ability to provide a true pinhole free conformal insulation, parylene C is the material of choice for coating critical assemblies. Parylene C can be deposited on various substrates like glass, Si wafer, metal, ceramic, polymer and wood. It is also biostable and biocompatible, which has wide applications in medical devices and implants [71, 72].

Parylene C can be deposited efficiently and easily via a chemical vapor deposition (CVD) process developed by Gorham [73]. In this CVD process, the dimer precursor di-para-xylylene is first vaporized and then undergoes vacuum pyrolysis at

temperatures 690℃ to yield the reactive monomers. The monomers adsorb to the substrate surface and spontaneously polymerize at room temperature to form linear, high molecular weight and transparent Parylene films.

## 2.7.2 Principle

In my work, parylene C deposition is done by a Labcoater Parylene Deposition System (Model 2010E, SCS LTD., UK). The parylene deposition system consists of a series of connected vacuum chambers that sequentially produce Parylene vapor, pyrolize it, deposit it as a polymer, and then capture its effluent. The vaporizer chamber is a horizontal tube at the bottom of the equipment behind the front cover. It has a hinged door held in place by a simple latch. This is where an Aluminum foil boat with the parylene dimer pellets is loaded into the system. The pyrolysis furnace is a vertical tube connected to the back of the horizontal vaporizer, and is the place that the dimer vapor is broken into monomers in preparation for deposition on the substrates in the deposition chamber. The exhaust is pumped into a trap by a mechanical oil pump. **Fig. 2.15** depicts the parylene C chemistry and deposition process.

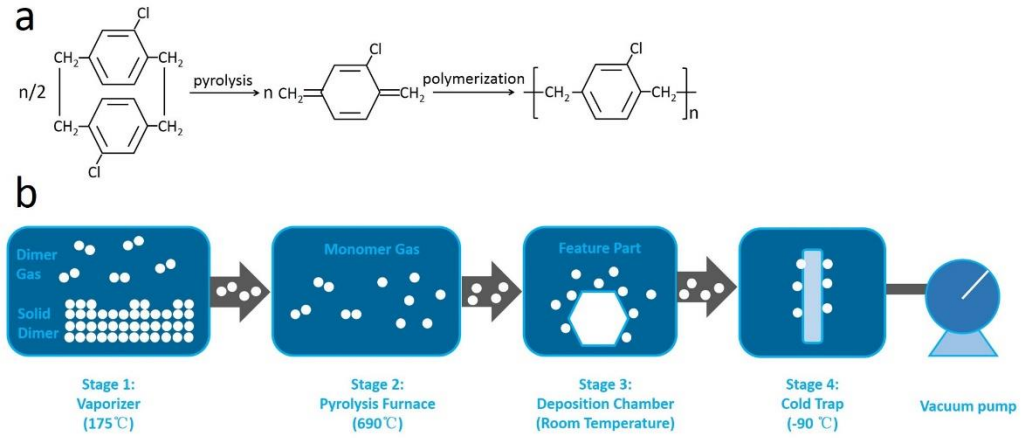


**Fig. 2.15** Parylene C chemistry and deposition process.

## 2.7.3 Working process

A typical parylene C deposition process includes the following steps: material

preparation, system power up, sample loading, dimer loading, parylene C deposition, unload substrate, cleaning and system power off.

(1) Material preparation:

a) Make a boat out of Aluminum foil with the size less than 3.5×6 inches for parylene C dimer.

b) Weigh parylene C dimer according to the film thickness required with a balance (1.65g/micron according to manufacturer's guide).

(2) System power up:

a) Release the red emergency button, as is shown in **Fig. 2.16**.

b) Press the white power button.

c) Turn cold finger chiller ON and wait 45 min before starting deposition.

d) Turn 1st left rotary switch (Furnace control) from DISABLE to ENABLE.

e) Press green "PROCESS START/STOP" button.

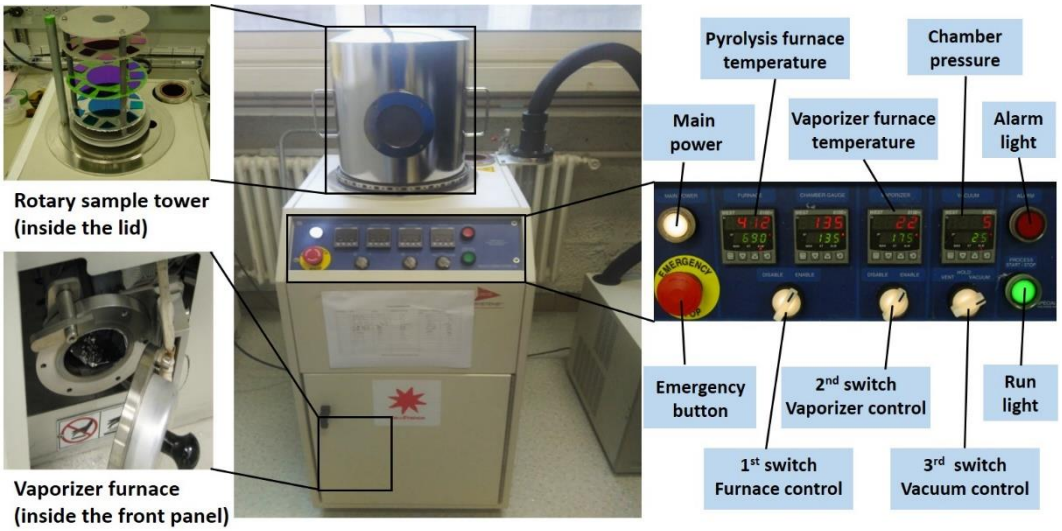


**Fig. 2.16** Photograph of parylene C deposition system used in this work.

(3) Sample loading:

a) Remove the lid from the top of the deposition chamber and put it on a stable surface upside down.

b) Load samples on rotary sample tower. Make sure that samples are uniformly separated by at least 1 cm distance.

c) Put back the lid and take care that no parylene C is trapped between the O-ring

and its sealing surface.

(4) Dimer loading:

a) Open the vaporizer furnace door and carefully put the Aluminum boat. Spread the dimer with a spatula into 1-2 layers thick.

b) Close and latch the vaporizer door.

(5) Parylene C deposition:

a) Check parameters of furnace and vaporizer (vaporizer set to 175℃, pyrolysis heater set to 690℃, vacuum set to 20 Torr).

b) Turn 2nd rotary switch (vaporizer) from DISABLE to ENABLE.

c) Turn 3rd rotary switch from VENT to VACUUM. Vacuum in the deposition chamber will go down to 10 Torr and Parylene C begins to deposit automatically.

d) The run is complete when the green "PROCESS START/STOP" button is blinking.

(6) Unload samples:

a) Turn the 3rd rotary switch from VACUUM to HOLD and wait 10s.

b) Turn the 3rd rotary switch from HOLD to VENT and wait until the pressure gauge stops increasing its readout (~950 Torr).

c) Turn cold finger chiller OFF.

d) Turn 2nd rotary switch from ENABLE to DISABLE.

e) Open the lid and take out of the samples and put back the lid.

f) Unload Aluminum boat when the temperature in the vaporizer chamber is below 60℃.

(7) Clean and system power off:

a) Take out the cold chiller.

b) Scrape off the thick Parylene deposit with a knife blade.

c) Clean the remaining deposits with a soft scrub pad.

d) Rinse the cold chiller with 2% Micro90 in DI water.

e) Wipe lightly with a lint free cloth and leave it slightly moist.

f) Disable all control switches on the panel.

g) Press red emergency button and the system will be shut down.

## 2.7.4 Substrates for Parylene C coating

Parylene C can be deposited on various substrates including glass, Si wafer, elastomer, plastic, metal and paper. Optimal adhesion of parylene C to above substrate has been achieved with A-174 silane fuming prior to Parylene deposition. Parylene C can be copolymerized with methacrylate group of A-174 silane shown in **Fig. 2.17**.

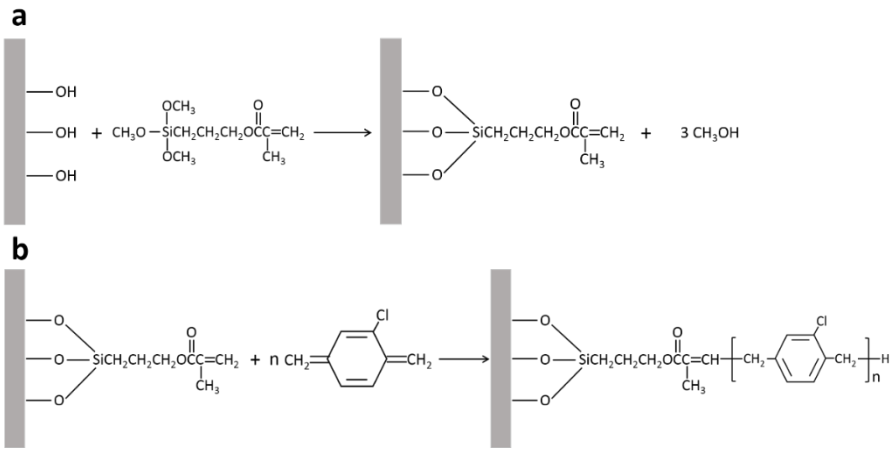


**Fig. 2.17** A-174 coating for parylene C deposition.

In some cases, for example in my work, low attachment of parylene C to PDMS stencil is needed in order to facilitate PDMS stencil release after parylene C deposition. I developed a method by coating PEG on PDMS stencil, which can effectively prevent parylene C attachment to PDMS stencil, as is shown in **Fig. 2.18**.

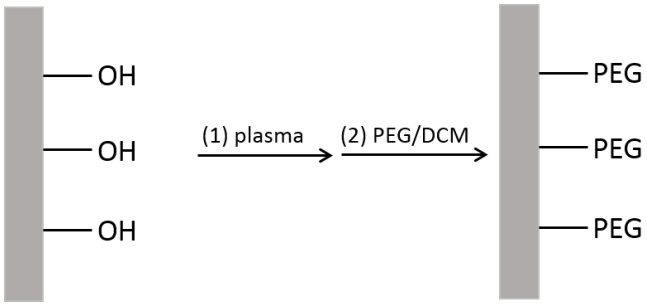


**Fig. 2.18** Scheme of PEG coating on PDMS stencil

### 2.7.5 Applications

Parylene coatings have slowly found their place in the medical devices because of their excellent safety. Parylene becomes a suitable material for all the fabrication devices, like medical devices and implants. Parylene C is used as coatings for bladder volume sensor [74]. The test was performed on different materials and inflammatory cells were observed in the area close to the sensor. By H&E staining, the Parylene coating was deposited on the implant and it was observed that there was mild neovascularization close to the implant. Also, the formation of the new blood vessels was not observed in the later stages which makes Parylene a suitable coating material for the implant. In orthopaedic implants, the most commonly used materials are stainless steel and titanium alloy. It has been proved that the critical load for initial cracks has increased by 3-5 times and the total metal ions release has decreased by 3 times for Parylene C [75]. In dental implants, the neodymium iron boron magnets coated with Parylene C were used intra orally [76]. The Parylene C coating material stands strong in all the surface characteristics and biological properties that suit the body environment, while it falls back in the fatigue wear testing.

Although Parylene C has been used as coatings for medical field, the interaction of cells *in vivo* and Parylene C coating has not been clarified yet. Current studies mainly focus on the use of Parylene C as peel-off stencils for deposition of biomolecular patterns [77]. Only a few studies investigated cell behavior on plasma treated Parylene C [78]. Since Parylene C is used in human body, it is necessary to study the cell behavior to Parylene C coatings.

# Reference


1. A. Pimpin, W. Srituravanich, P. Praserthdam, E. Editor, E. Intakan, E. Office, and Y. Zhao, *Review on micro-and nanolithography techniques and their applications.* Engineering Journal, 2011. **16**(1).
2. H. Miyajima and M. Mehregany, *High-aspect-ratio photolithography for MEMS applications.* Journal of microelectromechanical systems, 1995. **4**(4): p. 220-229.
3. J.B. Lee, K.-H. Choi, and K. Yoo, *Innovative SU-8 lithography techniques and their applications.* Micromachines, 2014. **6**(1): p. 1-18.
4. https://www.johnmorrisgroup.com/AU/Vacuum/Product/126923/%CE%BCP G-101-Tabletop-Micro-Pattern-Generator
5. M.J. Madou, *Fundamentals of microfabrication: the science of miniaturization*. 2002: CRC press.
6. Y. Xia and G.M. Whitesides, *Soft lithography.* Annual review of materials science, 1998. **28**(1): p. 153-184.
7. J.A. Rogers and R.G. Nuzzo, *Recent progress in soft lithography.* Materials today, 2005. **8**(2): p. 50-56.
8. F. Bessueille, M. Pla-Roca, C.A. Mills, E. Martinez, J. Samitier, and A. Errachid, *Submerged microcontact printing (SμCP): An unconventional printing technique of thiols using high aspect ratio, elastomeric stamps.* Langmuir, 2005. **21**(26): p. 12060-12063.
9. V.B. Sadhu, A. Perl, M. P éter, D.I. Rozkiewicz, G. Engbers, B.J. Ravoo, D.N. Reinhoudt, and J. Huskens, *Surface modification of elastomeric stamps for microcontact printing of polar inks.* Langmuir, 2007. **23**(12): p. 6850-6855.
10. S.J. Kang, B. Kim, K.S. Kim, Y. Zhao, Z. Chen, G.H. Lee, J. Hone, P. Kim, and C. Nuckolls, *Inking Elastomeric Stamps with Micro‐Patterned, Single Layer Graphene to Create High‐Performance OFETs.* Advanced Materials, 2011. **23**(31): p. 3531-3535.
11. A. Plecis and Y. Chen, *Fabrication of microfluidic devices based on glass–PDMS–glass technology.* Microelectronic Engineering, 2007. **84**(5): p. 1265-1269.
12. H.l.n. Lalo and C. Vieu, *Nanoscale Patterns of Dendrimers Obtained by Soft Lithography Using Elastomeric Stamps Spontaneously Structured by Plasma Treatment.* Langmuir, 2009. **25**(13): p. 7752-7758.

13. A. Kumar and G.M. Whitesides, *Features of gold having micrometer to centimeter dimensions can be formed through a combination of stamping with an elastomeric stamp and an alkanethiol "ink"followed by chemical etching.* Applied Physics Letters, 1993. **63**(14): p. 2002-2004.
14. C. Martos, F. Rubio, J. Rubio, and J. Oteo, *Surface energy of silica-TEOS-PDMS ormosils.* Journal of sol-gel science and technology, 2001. **20**(2): p. 197-210.
15. A. Esteves, J. Brokken-Zijp, J. Lavèn, H. Huinink, N. Reuvers, M. Van, and G. De With, *Influence of cross-linker concentration on the cross-linking of PDMS and the network structures formed.* Polymer, 2009. **50**(16): p. 3955-3966.
16. D. Li and Y. Xia, *Electrospinning of nanofibers: reinventing the wheel?* Advanced materials, 2004. **16**(14): p. 1151-1170.
17. A. Haider, S. Haider, and I.-K. Kang, *A comprehensive review summarizing the effect of electrospinning parameters and potential applications of nanofibers in biomedical and biotechnology.* Arabian Journal of Chemistry, 2015.
18. Z.-M. Huang, Y.-Z. Zhang, M. Kotaki, and S. Ramakrishna, *A review on polymer nanofibers by electrospinning and their applications in nanocomposites.* Composites science and technology, 2003. **63**(15): p. 2223-2253.
19. T.J. Sill and H.A. von Recum, *Electrospinning: applications in drug delivery and tissue engineering.* Biomaterials, 2008. **29**(13): p. 1989-2006.
20. J.M. Deitzel, J. Kleinmeyer, D. Harris, and N.B. Tan, *The effect of processing variables on the morphology of electrospun nanofibers and textiles.* Polymer, 2001. **42**(1): p. 261-272.
21. P.K. Baumgarten, *Electrostatic spinning of acrylic microfibers.* Journal of colloid and interface science, 1971. **36**(1): p. 71-79.
22. S. Megelski, J.S. Stephens, D.B. Chase, and J.F. Rabolt, *Micro-and nanostructured surface morphology on electrospun polymer fibers.* Macromolecules, 2002. **35**(22): p. 8456-8466.
23. S. Zargham, S. Bazgir, A. Tavakoli, A.S. Rashidi, and R. Damerchely, *The effect of flow rate on morphology and deposition area of electrospun nylon 6 nanofiber.* Journal of Engineered Fibers and Fabrics, 2012. **7**(4): p. 42-49.
24. K. Matabola and R. Moutloali, *The influence of electrospinning parameters on the morphology and diameter of poly (vinyledene fluoride) nanofibers-effect of sodium chloride.* Journal of Materials Science, 2013. **48**(16): p. 5475-5482.

25. X. Wang, S.-H. Lee, C. Drew, K.J. Senecal, J. Kumar, and L.A. Samuelson. *Highly sensitive optical sensors using electrospun polymeric nanofibrous membranes*. in *Materials Research Society Symposium Proceedings*. 2002. Warrendale, Pa.; Materials Research Society; 1999.

26. J. Pelipenko, J. Kristl, B. Janković, S. Baumgartner, and P. Kocbek, *The impact of relative humidity during electrospinning on the morphology and mechanical properties of nanofibers.* International journal of pharmaceutics, 2013. **456**(1): p. 125-134.

27. M. Zafar, S. Najeeb, Z. Khurshid, M. Vazirzadeh, S. Zohaib, B. Najeeb, and F. Sefat, *Potential of electrospun nanofibers for biomedical and dental applications.* Materials, 2016. **9**(2): p. 73.

28. S. Nair, E. Hsiao, and S.H. Kim, *Melt-welding and improved electrical conductivity of nonwoven porous nanofiber mats of poly (3, 4-ethylenedioxythiophene) grown on electrospun polystyrene fiber template.* Chemistry of Materials, 2008. **21**(1): p. 115-121.

29. I.G. Loscertales, A. Barrero, M. Márquez, R. Spretz, R. Velarde-Ortiz, and G. Larsen, *Electrically forced coaxial nanojets for one-step hollow nanofiber design.* Journal of the American Chemical Society, 2004. **126**(17): p. 5376-5377.

30. K. Park, Y.M. Ju, J.S. Son, K.-D. Ahn, and D.K. Han, *Surface modification of biodegradable electrospun nanofiber scaffolds and their interaction with fibroblasts.* Journal of Biomaterials Science, Polymer Edition, 2007. **18**(4): p. 369-382.

31. S. Sahoo, L.T. Ang, J.C.H. Goh, and S.L. Toh, *Growth factor delivery through electrospun nanofibers in scaffolds for tissue engineering applications.* Journal of biomedical materials research Part A, 2010. **93**(4): p. 1539-1550.

32. A.J. Hassiba, M.E. El Zowalaty, G.K. Nasrallah, T.J. Webster, A.S. Luyt, A.M. Abdullah, and A.A. Elzatahry, *Review of recent research on biomedical applications of electrospun polymer nanofibers for improved wound healing.* Nanomedicine, 2016. **11**(6): p. 715-737.

33. N. Annabi, J.W. Nichol, X. Zhong, C. Ji, S. Koshy, A. Khademhosseini, and F. Dehghani, *Controlling the porosity and microarchitecture of hydrogels for tissue engineering.* Tissue Engineering Part B: Reviews, 2010. **16**(4): p. 371-383.

34. Q.P. Pham, U. Sharma, and A.G. Mikos, *Electrospinning of polymeric*

*nanofibers for tissue engineering applications: a review.* Tissue engineering, 2006. **12**(5): p. 1197-1211.

35. W.J. Li, C.T. Laurencin, E.J. Caterson, R.S. Tuan, and F.K. Ko, *Electrospun nanofibrous structure: a novel scaffold for tissue engineering.* Journal of biomedical materials research, 2002. **60**(4): p. 613-621.
36. W.-J. Li, R. Tuli, C. Okafor, A. Derfoul, K.G. Danielson, D.J. Hall, and R.S. Tuan, *A three-dimensional nanofibrous scaffold for cartilage tissue engineering using human mesenchymal stem cells.* Biomaterials, 2005. **26**(6): p. 599-609.
37. H.M. Wong, P.K. Chu, F.K. Leung, K.M. Cheung, K.D. Luk, and K.W. Yeung, *Engineered polycaprolactone–magnesium hybrid biodegradable porous scaffold for bone tissue engineering.* Progress in Natural Science: Materials International, 2014. **24**(5): p. 561-567.
38. C. Li, C. Vepari, H.-J. Jin, H.J. Kim, and D.L. Kaplan, *Electrospun silk-BMP-2 scaffolds for bone tissue engineering.* Biomaterials, 2006. **27**(16): p. 3115-3124.
39. B. Marolia, *3D Printing and Its Applications.* Contemporary Literary Review India, 2016. **3**(3): p. 70-73.
40. N. Ludmila and K. Ivan, *Basic and advanced materials for fused deposition modeling rapid prototyping technology.* Manufacturing and Industrial Engineering, 2012. **11**(1): p. 1338-6549.
41. P. Chennakesava and Y.S. Narayan. *Fused Deposition Modeling-Insights*. in *Proceedings of the International Conference on Advances in Design and Manufacturing ICAD&M*. 2014.
42. http://neyasystems.com/tailoring-mechanical-designs-for-3d-printing/; http://www.lboro.ac.uk/research/amrg/about/the7categoriesofadditivemanufacturing/directedenergydeposition/; https://en.wikipedia.org/wiki/Selective_laser_sintering; http://www.lboro.ac.uk/research/amrg/about/the7categoriesofadditivemanufacturing/sheetlamination/.
43. J.-P. Kruth, P. Mercelis, J. Van Vaerenbergh, L. Froyen, and M. Rombouts, *Binding mechanisms in selective laser sintering and selective laser melting.* Rapid prototyping journal, 2005. **11**(1): p. 26-36.
44. S. Bose, S. Vahabzadeh, and A. Bandyopadhyay, *Bone tissue engineering using 3D printing.* Materials Today, 2013. **16**(12): p. 496-504.

45. P. Bajaj, R.M. Schweller, A. Khademhosseini, J.L. West, and R. Bashir, *3D biofabrication strategies for tissue engineering and regenerative medicine.* Annual review of biomedical engineering, 2014. **16**: p. 247-276.
46. S.S. Rehmani and F.Y. Bhora, *Current state of 3D printing in tissue engineering*. 2017, Future Medicine.
47. W.Z. Shida Miao, N.J. Castro, M. Nowicki, X. Zhou, H. Cui, J.P. Fisher, and L.G. Zhang, *4D printing smart biomedical scaffolds with novel soybean oil epoxidized acrylate.* Scientific reports, 2016. **6**.
48. B. Leukers, H. Gülkan, S.H. Irsen, S. Milz, C. Tille, M. Schieker, and H. Seitz, *Hydroxyapatite scaffolds for bone tissue engineering made by 3D printing.* Journal of Materials Science: Materials in Medicine, 2005. **16**(12): p. 1121-1124.
49. K. Markstedt, A. Mantas, I. Tournier, H.c. Martínez Ávila, D. Hägg, and P. Gatenholm, *3D bioprinting human chondrocytes with nanocellulose–alginate bioink for cartilage tissue engineering applications.* Biomacromolecules, 2015. **16**(5): p. 1489-1496.
50. J. Huang, H. Fu, Z. Wang, Q. Meng, S. Liu, H. Wang, X. Zheng, J. Dai, and Z. Zhang, *BMSCs-laden gelatin/sodium alginate/carboxymethyl chitosan hydrogel for 3D bioprinting.* RSC Advances, 2016. **6**(110): p. 108423-108430.
51. S. Shukla, *Freeze drying process: A review.* International Journal of Pharmaceutical Sciences and Research, 2011. **2**(12): p. 3061.
52. G. Nireesha, L. Divya, C. Sowmya, N. Venkateshan, M.N. Babu, and V. Lavakumar, *Lyophilization/freeze drying—an review.* International journal of novel trends in pharmaceutical sciences, 2013. **3**(4): p. 87-98.
53. C.J. Lowe, I.M. Reucroft, M.C. Grota, and D.I. Shreiber, *Production of highly aligned collagen scaffolds by freeze-drying of self-assembled, fibrillar collagen gels.* ACS biomaterials science & engineering, 2016. **2**(4): p. 643-651.
54. V. Sagar and P.S. Kumar, *Recent advances in drying and dehydration of fruits and vegetables: a review.* Journal of food science and technology, 2010. **47**(1): p. 15-26.
55. A. Ciurzyńska and A. Lenart, *Freeze-drying-application in food processing and biotechnology-a review.* Polish Journal of Food and Nutrition Sciences, 2011. **61**(3): p. 165-171.
56. D.W. Hutmacher, *Scaffolds in tissue engineering bone and cartilage.* Biomaterials, 2000. **21**(24): p. 2529-2543.

57. T. Freyman, I. Yannas, and L. Gibson, *Cellular materials as porous scaffolds for tissue engineering.* Progress in Materials Science, 2001. **46**(3): p. 273-282.
58. H. Shen, Y. Ma, Y. Luo, X. Liu, Z. Zhang, and J. Dai, *Directed osteogenic differentiation of mesenchymal stem cell in three-dimensional biodegradable methylcellulose-based scaffolds.* Colloids and Surfaces B: Biointerfaces, 2015. **135**: p. 332-338.
59. X. Li, Z. Xiao, J. Han, L. Chen, H. Xiao, F. Ma, X. Hou, X. Li, J. Sun, and W. Ding, *Promotion of neuronal differentiation of neural progenitor cells by using EGFR antibody functionalized collagen scaffolds for spinal cord injury repair.* Biomaterials, 2013. **34**(21): p. 5107-5116.
60. D. Lombardo, M.A. Kiselev, S. Magazù, and P. Calandra, *Amphiphiles self-assembly: basic concepts and future perspectives of supramolecular approaches.* Advances in Condensed Matter Physics, 2015. **2015**.
61. P. Kaner, P. Bengani-Lutz, I. Sadeghi, and A. Asatekin, *Responsive filtration membranes by polymer self-assembly.* Technology, 2016: p. 1-12.
62. L. Wang, J. Lin, and X. Zhang, *Hierarchical microstructures self-assembled from polymer systems.* Polymer, 2013. **54**(14): p. 3427-3442.
63. J.E. Raynor, J.R. Capadona, D.M. Collard, T.A. Petrie, and A.J. García, *Polymer brushes and self-assembled monolayers: versatile platforms to control cell adhesion to biomaterials (Review).* Biointerphases, 2009. **4**(2): p. FA3-FA16.
64. H.A. Klok and S. Lecommandoux, *Supramolecular materials via block copolymer self‐assembly.* Advanced Materials, 2001. **13**(16): p. 1217-1229.
65. Y. Lin, A. Böker, J. He, K. Sill, H. Xiang, C. Abetz, X. Li, J. Wang, T. Emrick, and S. Long, *Self-directed self-assembly of nanoparticle/copolymer mixtures.* Nature, 2005. **434**(7029): p. 55-59.
66. S. Zhang, D.M. Marini, W. Hwang, and S. Santoso, *Design of nanostructured biological materials through self-assembly of peptides and proteins.* Current opinion in chemical biology, 2002. **6**(6): p. 865-871.
67. R.P. Andres, J.D. Bielfeld, J.I. Henderson, and D.B. Janes, *Self-assembly of a two-dimensional superlattice of molecularly linked metal clusters.* Science, 1996. **273**(5282): p. 1690.
68. L. Li, K. Raghupathi, C. Song, P. Prasad, and S. Thayumanavan, *Self-assembly of random copolymers.* Chemical Communications, 2014. **50**(88): p. 13417-13432.

69. Y. Tao, J. He, M. Zhang, Y. Hao, J. Liu, and P. Ni, *Galactosylated biodegradable poly (ε-caprolactone-co-phosphoester) random copolymer nanoparticles for potent hepatoma-targeting delivery of doxorubicin.* Polymer Chemistry, 2014. **5**(10): p. 3443-3452.

70. L. Huang, S. Zhang, L. He, C. Zhang, Y. Chen, and X. Luo, *Self-assembled porous film with interconnected 3-dimensional structure from 6sPCL-PMPC copolymer.* RSC Advances, 2016. **6**(6): p. 4826-4834.

71. J.P. Seymour, Y.M. Elkasabi, H.-Y. Chen, J. Lahann, and D.R. Kipke, *The insulation performance of reactive parylene films in implantable electronic devices.* Biomaterials, 2009. **30**(31): p. 6158-6167.

72. S. Kuppusami and R.H. Oskouei, *Parylene coatings in medical devices and implants: a review.* Univ. J. Biomed. Eng, 2015. **3**: p. 9-14.

73. W.F. Gorham, *A New, General Synthetic Method for the Preparation of Linear Poly‐p‐xylylenes.* Journal of Polymer Science Part A‐1: Polymer Chemistry, 1966. **4**(12): p. 3027-3039.

74. D.S. Wuu, T.N. Chen, C.C. Wu, C.C. Chiang, Y.P. Chen, R.H. Horng, and F.S. Juang, *Transparent Barrier Coatings for Flexible Organic Light‐Emitting Diode Applications.* Chemical Vapor Deposition, 2006. **12**(4): p. 220-224.

75. M. Cieślik, M. Kot, W. Reczyński, K. Engvall, W. Rakowski, and A. Kotarba, *Parylene coatings on stainless steel 316L surface for medical applications—Mechanical and protective properties.* Materials Science and Engineering: C, 2012. **32**(1): p. 31-35.

76. J.H. Noar, A. Wahab, R.D. Evans, and A.G. Wojcik, *The durability of parylene coatings on neodymium-iron-boron magnets.* The European Journal of Orthodontics, 1999. **21**(6): p. 685-693.

77. B. Ilic and H. Craighead, *Topographical patterning of chemically sensitive biological materials using a polymer-based dry lift off.* Biomedical Microdevices, 2000. **2**(4): p. 317-322.

78. T.Y. Chang, V.G. Yadav, S. De Leo, A. Mohedas, B. Rajalingam, C.-L. Chen, S. Selvarasah, M.R. Dokmeci, and A. Khademhosseini, *Cell and protein compatibility of parylene-C surfaces.* Langmuir, 2007. **23**(23): p. 11718-11.

# Chapter 3

# Fabrication of hierarchic scaffolds by 3D printing and freeze-drying for cell culture and neuron differentiation

In this chapter, we present a study on fabrication of hierarchic scaffolds made of 3D printed PEGDA and porous gelatin matrix for cell culture and neuron differentiation. First, we describe the fabrication process of 3D printing of PEGDA lattices which can be served as backbone of the scaffolds. Then, we describe the fabrication of porous gelatin matrix which is embedded in the free-space of the PEGDA. Afterwards, we present the results of using the 200 µm thickness hierarchic scaffolds in cell culture studies including cell adhesion, proliferation and migration. Finally, we present the fabrication of scaffolds with thickness of 2.5 mm and its application for culture and differentiation of neural progenitor cells.

## 3.1 Introduction

3D printing is an emerging technique with high application potential in many fields such as automobile, aircraft, food and medical service [1-3]. In 3D printing, successive layers of material are patterned under the control of computer to make predicted objects of almost any shape or geometry. Among many others, 3D printing facilitates the scaffold fabrication that can be used in tissue engineering and regenerative medicine [4-6]. Technology limitations, however, still lie ahead for printing directly complex tissues and organs [7]. The present focus is thus on the fabrication of biocompatible 3D scaffolds with designed geometry and functions. To this regards, the efforts are directed to find printable biomaterials with high resolution and high functionality for improved cell culture and tissue and organ formation.

Biomaterials commonly used in tissue engineering are synthetic polymers [8]. For example, polyethylene glycol (PEG), which is nontoxic and non-immunogenic, has wide applications from industrial manufacturing to medicine [9, 10]. If PEG is end capped with acrylate groups, PEG diacrylate (PEGDA) is formed which can be used for 3D printing. The stiffness of cross-linked PEGDA is excellent [11, 12] but cells cannot adhere, remodel or proliferate in a PEG scaffold directly due to the inertial nature of PEG. Natural polymers such as collagen, gelatin, silk fibrin, chitosan, starch, alginate and hyaluronic can also be used for tissue engineering. Gelatin, which is a hydrolyzed product of collagen, is not only biocompatible but also biodegradable with low

immunogenicity [13]. Furthermore, gelatin can be obtained from a wide range of natural sources and easily manipulated or surface functionalized. Thus, gelatin has been extensively used in tissue engineering alone or associated with other materials [14-17]. Through lyophilizing or "freezing-drying" process, gelatin scaffold with controlled pore size can be made, which is suitable for cell attachment, proliferation and differentiation. Unfortunately, the mechanical strength of the gelatin scaffold is not sufficiently good and it is also not easy to produce gelatin scaffold with desired geometry and stiffness uniformity which limits its biomedical use [18].

In this work, we fabricate a hierarchic scaffold composed of a PEGDA frame by 3D printing and integrated porous gelatin microstructures by freezing-drying techniques to bypass the undesirable resolution of 3D printing and poor mechanical strength of pure gelatin scaffolds. The PEGDA frame is designed and printed by a 3D printer with regular shape and interconnected pores where sponge-like gelatin is filled to reduce pore size and increase the surface area for cell attachment. Our results show that the printed PEGDA frame is strong to against mechanical stress whereas the porous gelatin structures, supported by the PEGDA scaffold, have unchanged swellability and degradability after integration. Our results also show that the fabricated PEGDA/porous gelatin scaffold is excellent for attachment, proliferation and migration of fibroblast NIH 3T3 cells and differentiation of neural progenitor cells (NPCs) into neurons.

## 3.2 Fabrication of hierarchic scaffolds

The PEGDA/porous gelatin scaffold is fabricated by combination of 3D printing technique and freeze drying of protein. Briefly, a porous PEGDA frame was produced by 3D printing. Then the gelatin solution was used to fill the free space of PEGDA frame. Finally freeze drying was used to make porous gelatin in PEGDA frame. The detailed processes were described below:

### 3.2.1 3D printing of honeycomb lattice made of PEGDA

3D microstructures of PEGDA frame have been obtained using the 3D printer ProJet 1200 (3D SYSTEMS Company) and a green PEGDA solution from the same manufacturer. The printing principle of our printer is photopolymerization and the

PEGDA we used is UV curable in pure liquid form with its density, tensile strength and tensile modulus being 1.04g/mL, 30MPa and 1.7GPa, respectively. Briefly, a scaffold model was designed by software SolidWorks. At first, we designed a simple honeycomb frame with feature size, pitch size and thickness being 200, 1200 and 200 μm, respectively. We put great emphasis on the thickness of the scaffolds. So we started with small thickness of 200 μm which is within several times of cellular size and thus simplifies the cell culture study. The designed pattern was then loaded into the 3D printer. After parameter setting, the 3D printer can calculate the printing time according to the height of targeted scaffold. The fabricated 3D PEGDA frame together with printing platform was washed in isopropanol for 5 min, dried carefully with air flow and post-baked with UV light for 10 min. Then the 3D printing of PEGDA frame was finished and the PEGDA frame was carefully detached from the platform. **Fig. 3.1** shows the 3D printed PEGDA honeycomb frame.

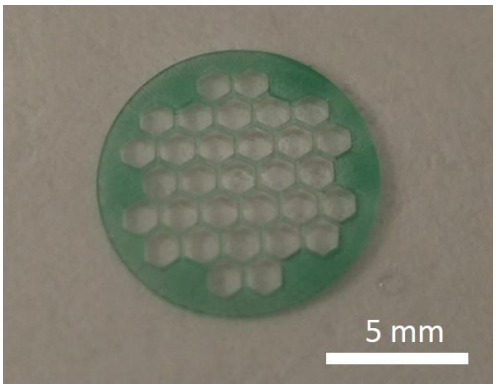


**Fig. 3.1** Photograph of 3D printed PEGDA honeycomb frame.

The 3D printed PEGDA honeycomb frame was sputtered a thin Au layer for SEM observation, as is shown in **Fig. 3.2a,b**. The feature size and pitch size of the fabricated PEGDA frame are 200 and 1200 μm, respectively. The thickness is estimated to be 200 μm, shown in **Fig. 3.2c**. The above results reveal the good fidelity of the 3D printer to design model.

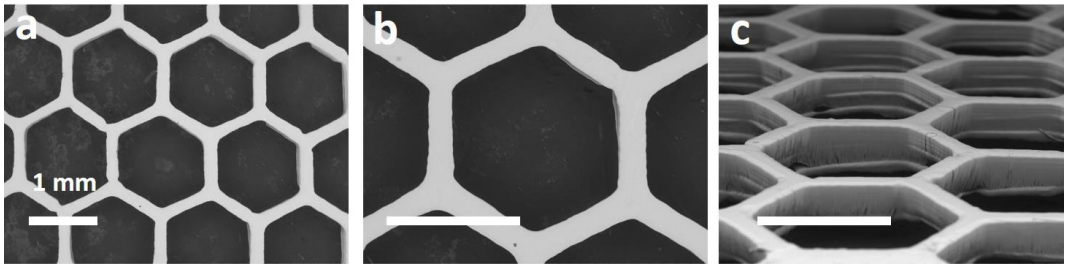


**Fig. 3.2** SEM images of 3D printed PEGDA honeycomb frame.

## 3.2.2 Freeze-drying of porous gelatin in PEGDA lattices

The printed 3D PEGDA frame is used as backbone to support the formation of gelatin porous structures inside. Freeze drying method is a convenient way to make highly porous 3D scaffold meanwhile can both keep activity of biomaterials and avoid deformation of 3D scaffold to great extent, which is widely used in tissue engineering [19, 20]. Without freeze drying, air drying, for example, will cause shrinkage, deformation and even denaturation of gelatin scaffold with much lower porosity. Briefly, 0.2 g of gelatin powder (from porcine skin, Sigma) was dissolved in 20 mL of deionized water containing 0.02g of citric acid under vigorous stirring at room temperature. The 3D PEGDA frame was treated with oxygen plasma to promote its hydrophilicity and then was immersed in the gelatin solution which was frozen at -20℃ overnight and dried in vacuum for 24h at room temperature. Afterwards the porous gelatin together with PEGDA frame was heated at 140℃ for 4h, in which porous gelatin can be cross-linked in the presence of citric acid. Finally, excessive gelatin was removed with a sharp knife, remaining a porous gelatin layer inside the hexagonal lattices with similar thickness of PEGDA frame, as is shown in **Fig. 3.3**.

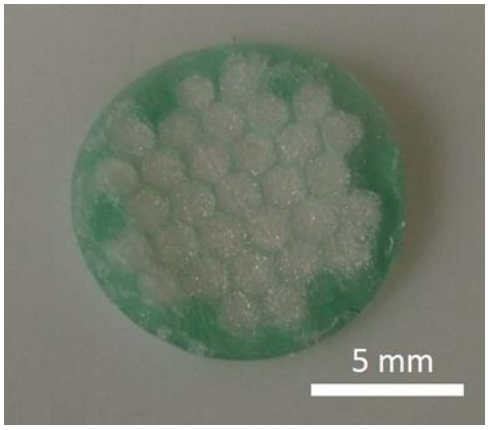


**Fig. 3.3** Photograph of a hierarchic scaffold made of 3D printed PEGDA frame and freeze-drying porous gelatin structures (not visible here).

The morphology of porous gelatin was characterized with SEM, as is shown in **Fig. 3.4**. The PEGDA/gelatin scaffold shows sponge-like gelatin microstructures which are embedded in the PEGDA frame. This sponge-like microstructure has high porosity due to the low content of gelatin, showing pore sizes in the range from 20 μm to 200 μm which are suitable for cell culture. The thickness of porous gelatin is consistent with that of PEGDA frame. This highly porous structure will facilitate diffusion of nutrients and metabolic products and provide excellent 3D microenvironment for cells.

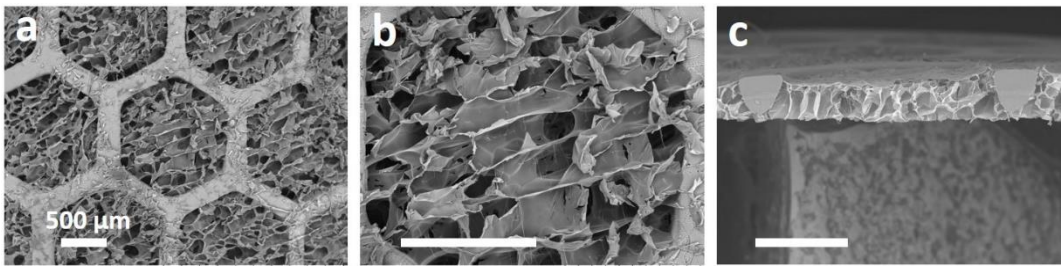


**Fig. 3.4** SEM images of 200 μm thickness hierarchic scaffold made of 3D printed PEGDA frame and freeze-drying porous gelatin structures.

The highly porous structure of scaffold holds great potential in water retaining, also called the swellability of PEGDA/gelatin scaffolds. The equilibrium swelling ratio ($Q_S$), which is a measure of swellability of hydrogel materials, is estimated by immersing the dried PEGDA/gelatin samples to swell in PBS at 37 ℃ for 7 days. $Q_S$ is defined according to the following equation:

$$Q_s = \frac{W_s - W_d}{W_d} \quad (3.1)$$

where Ws and Wd are the weights of the swollen sample and the dried sample, respectively [21].

The fabricated scaffold was immersed in PBS and weighed after 1, 3, 5 and 7 days. The resulted swellability is shown in **Fig. 3.5**. This scaffold can hold about 9 times of its dried weight within one day and tends to be saturated after 7 days, estimated to be 13 times of its dried weight. The high water-holding capacity is beneficial for tissue engineering, providing enough space for diffusion of nutrients and metabolism products as well as for cell growth, migration, interaction and differentiation.

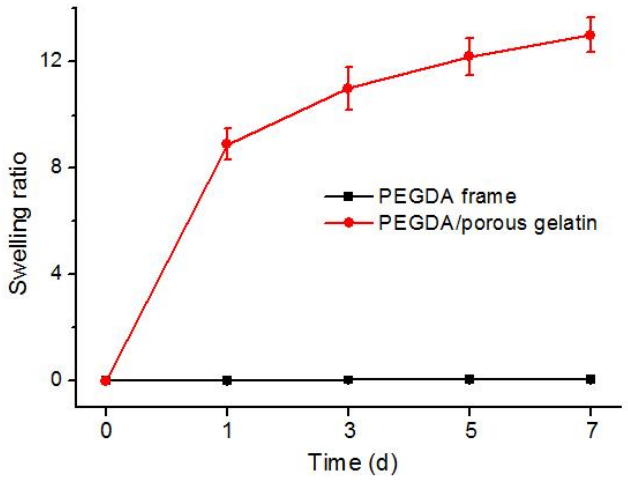


**Fig. 3.5** Equilibrium swelling ratio of PEGDA frame and PEGDA/gelatin scaffold in PBS at 37 ℃. Samples were weighed at 1st, 3rd, 5th and 7th days.

Degradability is another important factor to evaluate a scaffold. A proper degradation time of the scaffold will not only ensure enough time for tissue treatment but also avoid long time retention *in vivo*. To mimic the physiological condition *in vivo*, PEGDA/gelatin scaffold was immersed and incubated with PBS containing trypsin at 37℃ with 5% $CO_2$ in incubator. The degradation ratio of scaffold was measured for 30 days incubation. Samples, in triplicate, were incubated in physiological saline solution with 0.01% trypsin at 37℃, respectively. The samples were weighed after being frozen and lyophilized. The degradation ratio ($R_d$) of scaffold was calculated according to the following equation:

$$R_d = \frac{W_0 - W_{30}}{W_0} \quad (3.2)$$

where $W_0$ and $W_{30}$ represent the initial dried weight and the dried weight of the sample at day 30, respectively.

After 10, 20, and 30 days incubation, scaffolds were rinsed with PBS, lyophilized overnight and weighed, as shown in **Fig. 3.6**. The gelatin remained is about 45% of initial weight after 30 days. This degradation rate is comparable to that of gelatin nanofiber reported before [22].

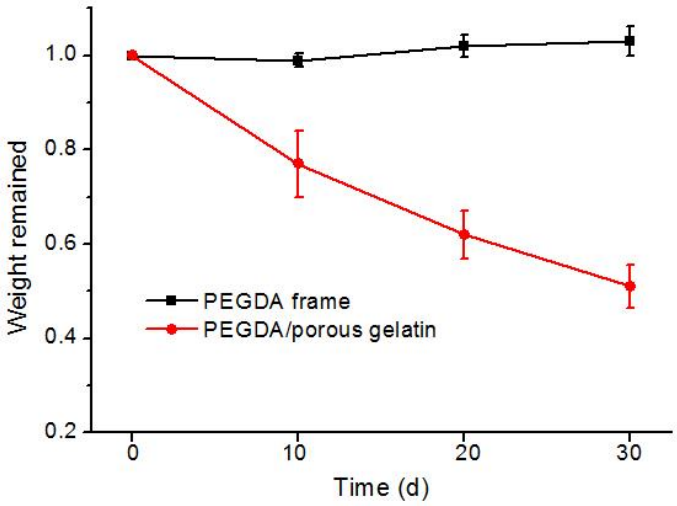


**Fig. 3.6** Biodegradability of PEGDA frame and PEGDA/gelatin scaffold in PBS at 37 ℃. Samples were weighed every 10 days.

## 3.3 Cell culture studies

Fibroblast NIH 3T3 cells were used in the cell culture test of PEGDA/porous gelatin scaffold. Before cell culture, the PEGDA/porous gelatin scaffold was sterilized in 70% ethanol solution for 30 min, washed with PBS three times to remove ethanol and coated with Matrigel to facilitate cell adhesion. NIH 3T3 cells were cultured in DMEM medium supplemented with 10% FBS. When cells reached 80% confluence, cells were dissociated, collected by centrifuge and seeded on scaffold at a density of $2 \times 10^4$ for each sample. The cell loading scaffolds were further cultured in an incubator.

Biocompatibility is a prerequisite for applications of PEGDA/gelatin scaffolds in

tissue engineering. We first studied the *in vitro* toxicity of PEGDA/gelatin scaffold by MTT assay after NIH 3T3 cells cultured on scaffold for 24h. MTT, a chemical reagent, can react with dehydrogenases, indicators of cell viability, in mitochondrion to form formazan. Cells with higher viability will produce more formazan. The resulted formazan can be quantified by microplate reader. Cell viability was calculated based on the absorbance intensity of formazan.

Briefly, 20 μL of 5mg/mL MTT solution was added into each well, followed by 4 h incubation. 200 μL of Dimethylsulfoxide (DMSO) was added to each well to replace culture medium. Cell viability was evaluated based on the absorbance of each well at 450 nm. To make NIH 3T3 cells adhere to the scaffold, PEGDA/gelatin scaffold was coated with a layer of Matrigel. The viability of NIH 3T3 cells was used to assess the cytotoxicity of scaffold toward cells cultured on it. For comparison, traditional tissue culture plate (TCP) was used as a control (100% cell viability) and pure gelatin scaffold was used as another control. The results were shown in **Fig. 3.7**. Compared with TCP and pure gelatin scaffold, PEGDA/gelatin scaffold shows negligible toxicity toward NIH 3T3 cells, indicating its good biocompatibility.

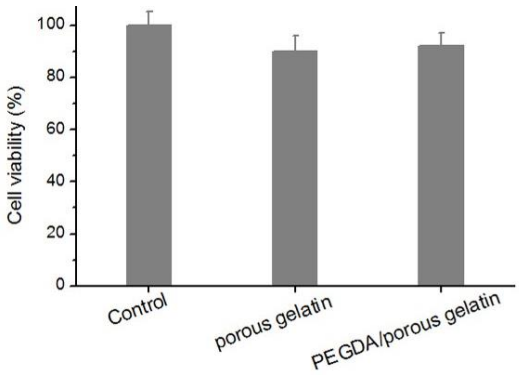


**Fig. 3.7** Cell viability of NPCs cultured on PEGDA/gelatin and pure gelatin scaffold after 24 h incubation. Cells on tissue culture plate were used as a control (100% cell viability)

The proliferation of NIH 3T3 cells on PEGDA/gelatin scaffold was then investigated, which is another factor to evaluate the biocompatibility of scaffold. Cells were seeded in the PEGDA/gelatin scaffold for 1, 2, and 3 d culture, respectively. The proliferation of cells was determined by MTT assay, as shown in **Fig. 3.8**. TCP was used as a control. Assuming the cell viability of the control is 100% at day 1, the cell

viability on PEGDA/gelatin scaffold are 80%, 150% and 220%, at day 1, 2 and 3, respectively. Compared with TCP, cells show much higher proliferation on PEGDA/porous scaffold than on TCP.

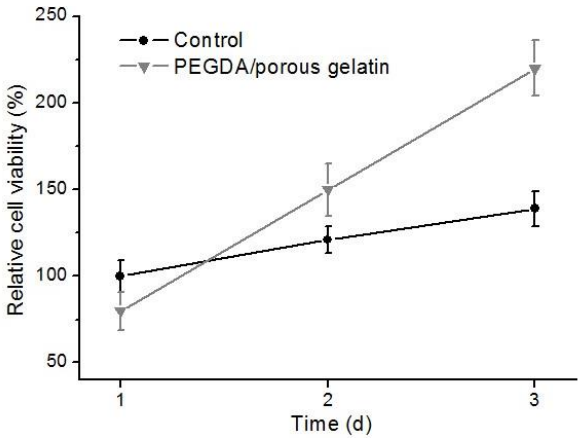


**Fig. 3.8** Cell viability of NPCs cultured on PEGDA/gelatin scaffold for 1, 2 and 3 days. Tissue culture plate was used as a control (cell viability after 1-day culture is set as 100%).

Ideal porous scaffolds should possess interconnected pores and allow efficient cell migration. Cell migration is measured by investigating the distribution of cells within the scaffolds in terms of the deepness. Briefly, we first seeded NIH 3T3 cells on the scaffold. After 1, 2 and 3 days incubation, cells were fixed with PFA, permeated with 0.5% Triton X 100 solution, blocked with 1% BSA solution and stained with dyes labelled Phalloidin for actin filament. The cell holding scaffolds were observed under confocal microscope with a Z-stack mode. The results were shown in **Fig. 3.9a-c**. After 1 day incubation, the permeation deepness of cells inside the scaffold was estimated to be 50 μm. After 2 and 3 days incubation, the permeation deepness increases to about 120 and 190 μm, respectively. This increase of permeation deepness is caused by the migration of cells inside the porous scaffolds. Besides the downward migration above, we also investigate whether cells could migrate upward in the scaffold. We seeded cells on the scaffold and turned the scaffold upside down when cell adhered to the scaffold 2h after seeding. After 1, 2 and 3 days incubation, the immunostaining results are shown in **Fig. 3.9d-f**. In day 1, 2, and 3 the migration heights of cells in scaffolds are about 50, 90 and 140 μm, respectively. The results reveal that the highly porous scaffold is highly supportive for cell migration. Besides, the gravity exerts limited effects on cell

migration, which can be seen from the difference between distances in downward and upward migration. The successful cell migration in scaffold also provides evidence for pore interconnectivity. We also investigate the deepness dependent distribution of cells inside the scaffolds, as is shown in **Fig. 3.10**. After 3 days culture, nearly all cells migrate inside the scaffold with the majority of cells in deepness of 70~150 μm.

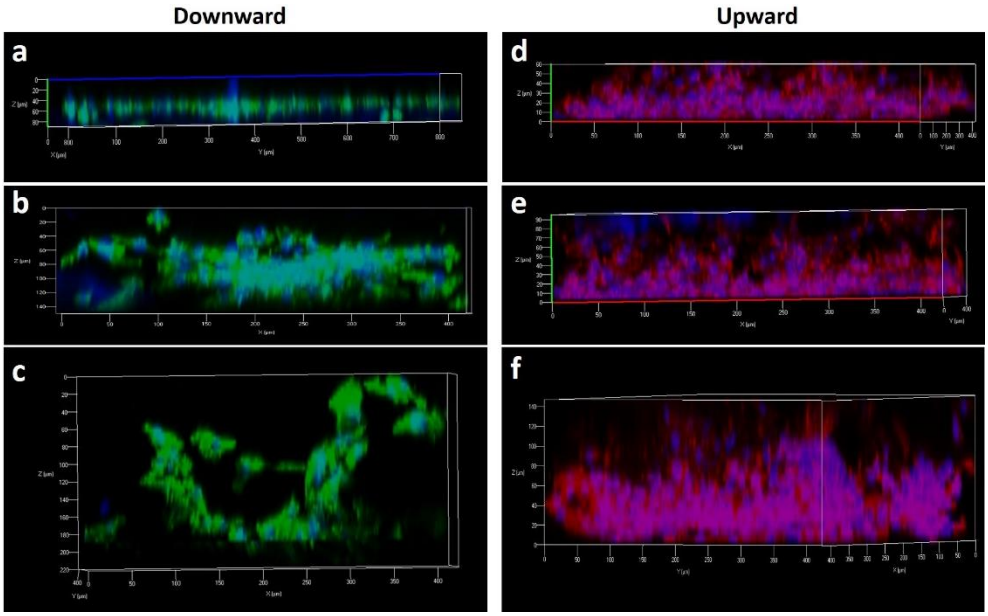


**Fig. 3.9** Fluorescent images of NIH 3T3 cells cultured in PEGDA/porous gelatin scaffold for (a) 1, (b) 2 and (c) 3 days.

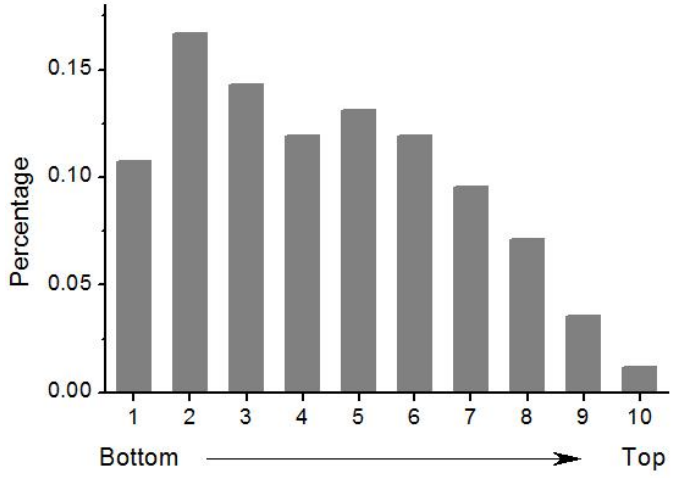


**Fig. 3.10** The deepness dependent distribution of NIH 3T3 cells inside the PEGDA/porous gelatin scaffold after 3 days culture.

# 3.4 3D printed PEGDA/porous gelatin scaffold for neuronal differentiation

## 3.4.1 Fabrication of 3D printed PEGDA/porous gelatin scaffold

Based on previous results of scaffolds with thickness of 200 μm, we have investigated the feasibility of scaffold fabrication and clarified the support of scaffolds for cell adhesion, proliferation and migration. Here we advance our study by increasing the thickness to make a 3D scaffolds. First we fabricated a 3D porous PEGDA scaffold by 3D printing. The model design started from a basic tripod unit with each angle being 60°. The final structure is a regular assembly of the basic unit by moving parallelly every tripod to make all the tripod intersection points form an equilateral triangle pattern. The 3D structure was produced in 8 min for a scaffold of $1 \times 0.5 \times 0.25$ $cm^3$ in size. Afterward, the scaffold was washed in isopropanol and post-baked with UV light. The fabricated PEGDA frame was shown in **Fig. 3.11a**. As expected, this lattice type scaffold is strong enough to keep its shape but somehow elastic against the external force (**Fig. 3.11b,c**).

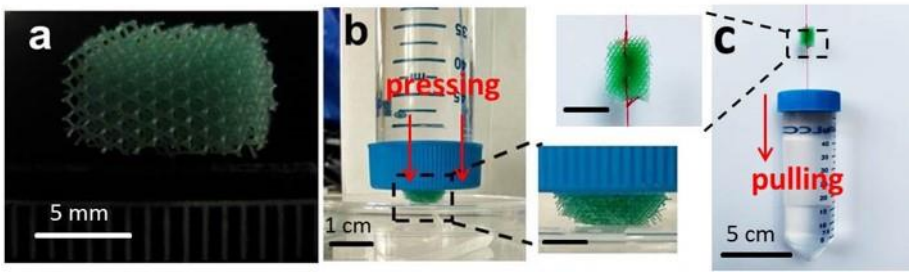


**Fig. 3.11** a) Photograph of a typical PEGDA scaffold produced by 3D printing; b) and c) Deformation effects of PEGDA by pressing and pulling. Briefly, a centrifuge tube containing 50 mL water (total weight 63 g) was used to: 1) press the PEGDA scaffold directly (Fig. 3.13b) and 2) pull the PEGDA scaffold by hanging with strings (Fig. 3.13c). The enlarged figures showed detailed shape of PEGDA scaffold when external forces applied, showing that the scaffolds exhibit negligible deformation (scale bar 5 mm).

**Fig. 3.12a** shows scanning electron microscope (SEM) image of the fabricated

scaffold lattice. The growth rings of the PEGDA layers can be now seen on the surface of grid, due to layer-by-layer crosslinking of the 3D printing procedure. However, such a scaffold is not suitable for cell culture because of the large pore size and the inert character of PEG. Similarly, for porous gelatin integration, PEGDA frame was immersed in gelatin solution, frozen at -20℃ overnight, dried in vacuum for 24h at room temperature and crosslinked. The cross section of the scaffold was characterized with SEM, shown in **Fig. 3.12b,c**. The PEGDA/gelatin scaffold shows sponge-like gelatin microstructures which are embedded in the PEGDA frame. This sponge-like microstructure has high porosity due to the low content of gelatin, showing pore sizes in the range from 20 μm to 100 μm which are suitable for cell culture. This highly porous structure will facilitate diffusion of nutrients and metabolic products and provide excellent 3D microenvironment for cells.

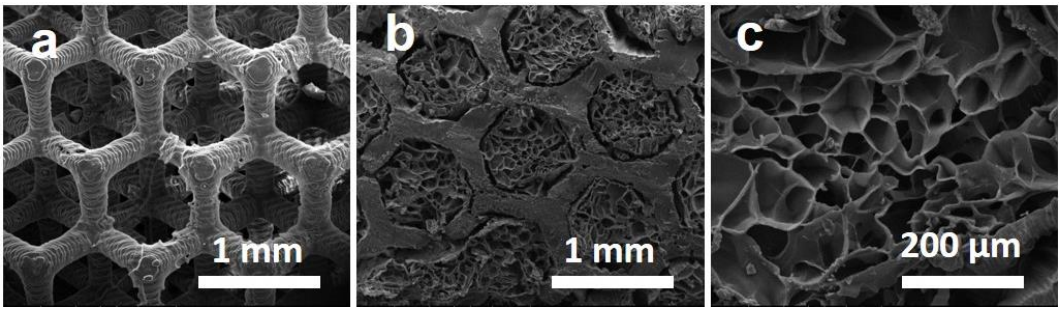


**Fig. 3.12** SEM image of a) printed 3D PEGDA backbone and b) and c) gelatin porous structure filled in the PEGDA frame.

The swellability of PEGDA/gelatin scaffolds is then investigated. The fabricated scaffold was immersed in PBS and weighed after 1, 3, and 7 days. The resulted swellability is shown in **Fig. 3.13a**. This scaffold can hold about 8 times of its dried weight within one day and tends to be saturated after 7 days, estimated to be 10 times of its dried weight. The high water-holding capacity is beneficial for tissue engineering, providing enough space for diffusion of nutrients and metabolism products as well as for cell growth, differentiation and interaction.

A proper degradation time of the scaffold will not only ensure enough time for tissue treatment but also avoid long time retention *in vivo*. To mimic the physiological condition *in vivo*, PEGDA/gelatin scaffold was immersed and incubated with PBS

containing trypsin at 37℃ with 5% $CO_2$ in incubator. After 10, 20, and 30 days incubation, scaffolds were rinsed with PBS, lyophilized overnight and weighed, as shown in **Fig. 3.13b**. The gelatin degraded, weighed about 45% of initial weight after 30 days. This degradation rate is comparable to that of gelatin nanofiber reported before. The degradation time is therefore enough for NPCs differentiation into neurons and gradually replaced by neurons.

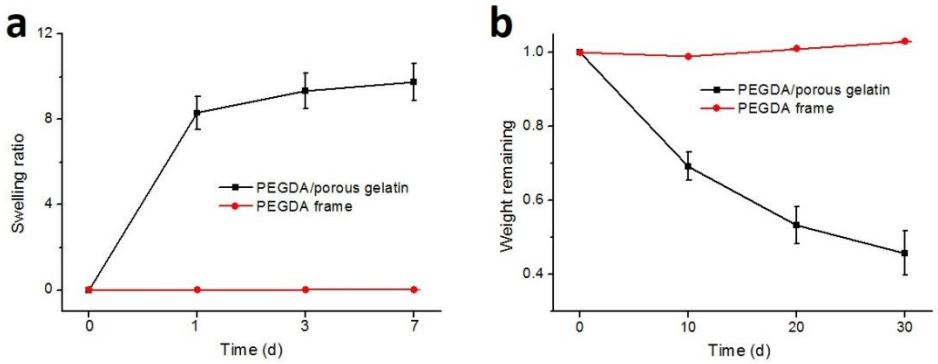


**Fig. 3.13** a) Equilibrium swelling ratio of PEGDA/gelatin scaffold in PBS at 37 ℃. Samples were weighed at 1st, 3rd and 7th day. b) Biodegradability of PEGDA/gelatin scaffold in PBS at 37 ℃. Samples were weighed every 10 days.

## 3.4.2 Culture and differentiation of neural progenitor cells

Neural progenitor cells (NPCs) were obtained from the frontal cortex of unborn mouse after 14-day pregnancy. The obtained NPCs were cultured in suspension and expanded in NeuroCult™ Basal Medium (Mouse) with 10% NeuroCult™ Proliferation Supplement (Mouse), 20 ng/mL Epidermal Growth Factor (EGF, human) and 10 ng/mL basic Fibroblast Growth Factor (bFGF, human) under 37 ℃ and 5% $CO_2$ in a humidified atmosphere incubator.

Before cell culture, the PEGDA/porous gelatin scaffold was sterilized in 70% ethanol solution for 30 min, washed with PBS three times to remove ethanol and coated with laminin to facilitate cell adhesion. The suspended NPCs were collected by centrifuge, dissociated and seeded on scaffolds at a density of 5×104 for each sample.

Biocompatibility is a prerequisite for applications of PEGDA/gelatin scaffolds in tissue engineering. We first studied the *in vitro* toxicity of PEGDA/gelatin scaffold by

WST assay after NPCs cultured on scaffold for 24h. To make NPCs adhere to the scaffold, PEGDA/gelatin scaffold was coated with a layer of Laminin (NPCs will adhere on the Laminin coated area). The viability of NPCs was used to assess the cytotoxicity of scaffold toward NPCs cultured on it. For comparison, traditional tissue culture plate (TCP) was used as a control (100% cell viability) and pure gelatin scaffold was used as another control. As shown in **Fig. 3.14a**, compared with TCP and pure gelatin scaffold, PEGDA/gelatin scaffold shows negligible toxicity toward NPCs, indicating its good biocompatibility.

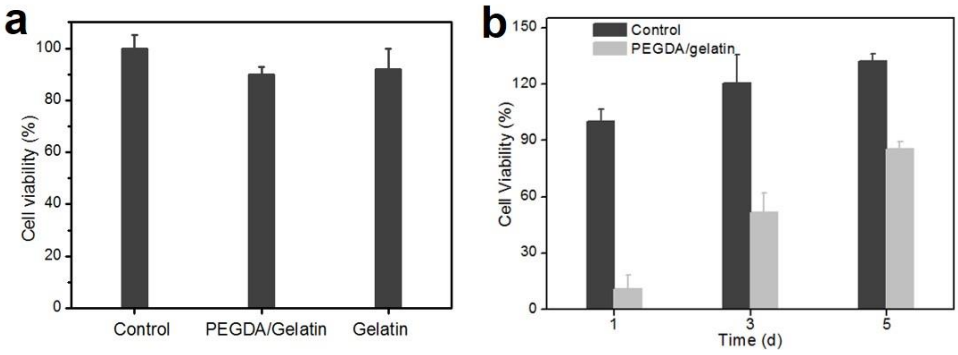


**Fig. 3.14** a) Cell viability of NPCs cultured on PEGDA/porous gelatin and porous gelatin scaffold after 24 h incubation. Cells on tissue culture plate were used as a control (100% cell viability). (b) Cell viability of NPCs cultured on PEGDA/gelatin scaffold for 1, 3 and 5 days. Tissue culture plate was used as a control (cell viability after 1-day culture is set as 100%).

The proliferation of NPCs on PEGDA/gelatin scaffold was then investigated, which is another factor to evaluate the biocompatibility of scaffold. NPCs were seeded in the PEGDA/gelatin scaffold for 1, 3, and 5 d culture, respectively. The proliferation of NPCs was determined by WST assay, as shown in **Fig. 3.14b**. Assuming the viability of NPCs of the control is 100% at day 1, the viability of the NPCs cultured on PEGDA/gelatin scaffold are 11%, 52% and 85%, at day 1, 3 and 5, respectively. Results show that cells show much higher proliferation on PEGDA/porous scaffold than on TCP.

After 5-day culture, CAM/PI based Live/Dead cell viability assay was used to assess live and dead NPCs cultured on the scaffolds. $5x10^4$ cells per well were seeded in Laminin coated PEGDA/gelatin scaffolds in 48-well plate. After 3 days of incubation,

20 ng/L CAM and 10 ng/L PI were added and incubated for 15 min. After being washed 3 times with PBS, the samples were detected by a Nikon Fluorescence Microscope. The fluorescence spots shown in **Fig. 3.15** have different brightness, suggesting that the NPCs were localized in different depths of the scaffold.

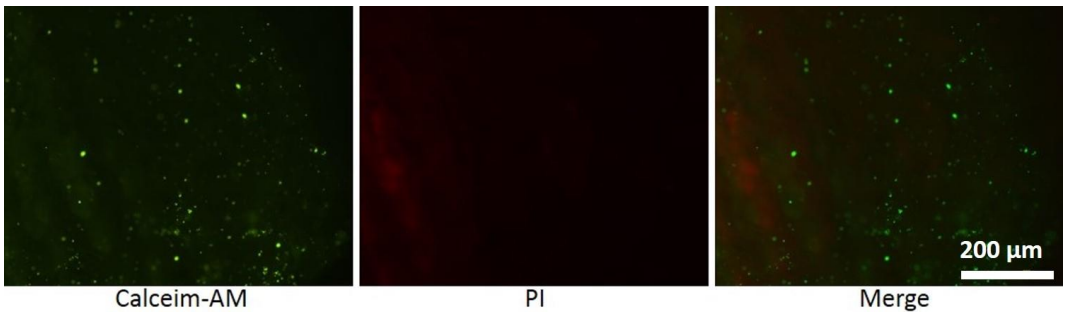


**Fig. 3.15** Fluorescence images of NPCs on PEGDA/porous gelatin scaffold after 5-day culture and Calcein-AM (green) and PI (red) staining.

We further studied the differentiation of NPCs on PEGDA/gelatin scaffold. Briefly, NPCs were seeded in PEGDA/gelatin scaffolds at a density of $2x10^5$ per well in 24-well plate. After 24h incubation, the culture medium was replaced by 1 mL neuron differentiating medium composed of Neurobasal Medium with 1% B27 and 1 mg/L L-Glutamic acid. After 3d incubation, another 200 μL of neuron differentiating medium was added into each well. After 5 d incubation, mature neurons can be obtained. After mature neurons were obtained, samples were washed with PBS (free of $Ca^{2+}$ and $Mg^{2+}$) three times, followed by 30 min fixation in 4% paraformaldehyde at 4℃. Samples were then permeated and blocked with commercially available solution for 1 h. After primary antibody incubation overnight at 4 ℃ followed by washing for 3 times with immunostaining wash buffer, samples were incubated with secondary antibody at room temperature for 2 h at 37℃. At last samples were incubation with DAPI for nuclei staining for 30 min. Fluorescence images were obtained by a Nikon A1 confocal laser scanning microscope.

**Fig. 3.16** shows the representative images of MAP-2 immunostained neurons after 7-day differentiation. As can be seen, each neuron has a spherical cell body with several thin cellular filaments extending for tens or hundreds of microns. These filaments tend to connect with each other (shown by white arrows) to form a large and probably 3D

neuron network. We suggest that the PEGDA backbone played a key role to prohibit swelling induced large deformation of embedded gelatin foam, which should not be the case of the gelatin foam without backbone. Such a hierarchic 3D architecture should be in favor of neural network formation and their impulsion activities, thereby providing an alternative choice of the scaffolds for repairing injured nervous systems.

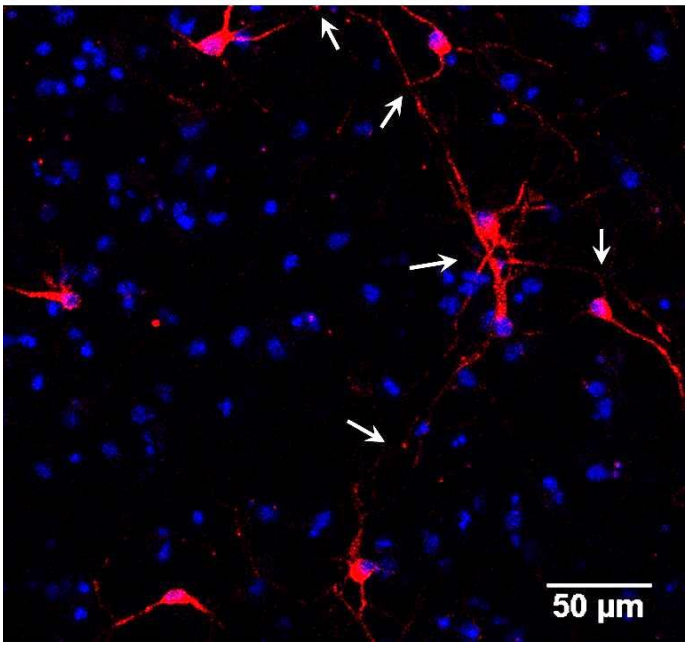


**Fig. 3.16** Fluorescent image of MAP-2 immunostained neurons (red) after 7-day differentiation, showing clearly spherical cell bodies and thin cellular filaments which are connected with each other (indicated by white arrows) to form a large network.

## 3.5 Conclusion

We have fabricated hierarchical scaffolds by 3D printing of PEGDA backbone and freeze-drying of gelatin gels. As expected, the printed PEGDA shows regular 3D grids with strong mechanical strength and sponge-like gelatin porous structures with good swellability and biodegradability. Cell tests demonstrated a high cell compatibility and viability and faster cell proliferation than that on culture dish. The highly porous scaffolds show high support for cell migration due to the interconnected pores. We also prove that the scaffolds can promote the culture and neuronal differentiation of neural progenitor cells, in which the porous gelatin structure is helpful for neuron network formation.

# Reference


[1] M. Sugavaneswaran and G. Arumaikkannu, "Modelling for randomly oriented multi material additive manufacturing component and its fabrication," *Materials & Design (1980-2015)*, vol. 54, pp. 779-785, 2014.

[2] B. Garrett, "3D printing: new economic paradigms and strategic shifts," *Global Policy*, vol. 5, pp. 70-75, 2014.

[3] N. De Beer, "Advances in three dimensional printing-state of the art and future perspectives," *Journal for New Generation Sciences*, vol. 4, pp. 21-49, 2006.

[4] S. V. Murphy and A. Atala, "3D bioprinting of tissues and organs," *Nature biotechnology*, vol. 32, pp. 773-785, 2014.

[5] C. C. Chang, E. D. Boland, S. K. Williams, and J. B. Hoying, "Direct‐write bioprinting three‐dimensional biohybrid systems for future regenerative therapies," *Journal of Biomedical Materials Research Part B: Applied Biomaterials*, vol. 98, pp. 160-170, 2011.

[6] Y. Xu and X. Wang, "Application of 3D biomimetic models in drug delivery and regenerative medicine," *Current pharmaceutical design*, vol. 21, pp. 1618-1626, 2015.

[7] H. N. Chia and B. M. Wu, "Recent advances in 3D printing of biomaterials," *Journal of biological engineering*, vol. 9, p. 4, 2015.

[8] B. Seal, T. Otero, and A. Panitch, "Polymeric biomaterials for tissue and organ regeneration," *Materials Science and Engineering: R: Reports*, vol. 34, pp. 147-230, 2001.

[9] F. M. Veronese and A. Mero, "The impact of PEGylation on biological therapies," *BioDrugs*, vol. 22, p. 315, 2008.

[10] K. Ueno, S. Nakamura, H. Shimotani, A. Ohtomo, N. Kimura, T. Nojima, *et al.*, "Electric-field-induced superconductivity in an insulator," *Nature materials*, vol. 7, pp. 855-858, 2008.

[11] V. Chan, J. H. Jeong, P. Bajaj, M. Collens, T. Saif, H. Kong, *et al.*, "Multi-material bio-fabrication of hydrogel cantilevers and actuators with stereolithography," *Lab on a Chip*, vol. 12, pp. 88-98, 2012.

[12] M. P. Cuchiara, A. C. Allen, T. M. Chen, J. S. Miller, and J. L. West, "Multilayer microfluidic PEGDA hydrogels," *Biomaterials*, vol. 31, pp. 5491-5497, 2010.

[13] J. B. Rose, S. Pacelli, A. J. E. Haj, H. S. Dua, A. Hopkinson, L. J. White, *et al.*, "Gelatin-based materials in ocular tissue engineering," *Materials*, vol. 7, pp.

3106-3135, 2014.

[14] Z. Guo, J. Xu, S. Ding, H. Li, C. Zhou, and L. Li, "*In vitro* evaluation of random and aligned polycaprolactone/gelatin fibers via electrospinning for bone tissue engineering," *Journal of Biomaterials Science, Polymer Edition,* vol. 26, pp. 989-1001, 2015.

[15] M. Norouzi, I. Shabani, H. H. Ahvaz, and M. Soleimani, "PLGA/gelatin hybrid nanofibrous scaffolds encapsulating EGF for skin regeneration," *Journal of Biomedical Materials Research Part A,* vol. 103, pp. 2225-2235, 2015.

[16] C.-H. Chuang, R.-Z. Lin, H.-W. Tien, Y.-C. Chu, Y.-C. Li, J. M. Melero-Martin, *et al.*, "Enzymatic regulation of functional vascular networks using gelatin hydrogels," *Acta biomaterialia,* vol. 19, pp. 85-99, 2015.

[17] Y. Liu and M. B. Chan-Park, "Hydrogel based on interpenetrating polymer networks of dextran and gelatin for vascular tissue engineering," *Biomaterials,* vol. 30, pp. 196-207, 2009.

[18] R. Dash, M. Foston, and A. J. Ragauskas, "Improving the mechanical and thermal properties of gelatin hydrogels cross-linked by cellulose nanowhiskers," *Carbohydrate polymers,* vol. 91, pp. 638-645, 2013.

[19] H. Shen, Y. Ma, Y. Luo, X. Liu, Z. Zhang, and J. Dai, "Directed osteogenic differentiation of mesenchymal stem cell in three-dimensional biodegradable methylcellulose-based scaffolds," *Colloids and Surfaces B: Biointerfaces,* vol. 135, pp. 332-338, 2015.

[20] X. Li, Z. Xiao, J. Han, L. Chen, H. Xiao, F. Ma, *et al.*, "Promotion of neuronal differentiation of neural progenitor cells by using EGFR antibody functionalized collagen scaffolds for spinal cord injury repair," *Biomaterials,* vol. 34, pp. 5107-5116, 2013.

[21] K. Chawla, T. B. Yu, S. W. Liao, and Z. Guan, "Biodegradable and biocompatible synthetic saccharide− peptide hydrogels for three-dimensional stem cell culture," *Biomacromolecules,* vol. 12, pp. 560-567, 2011.

[22] F. Gang and Y. XiaoPing, "Crosslinking and degradation of gelatin nanofiber membranes [J]," *Journal of Beijing University of Chemical Technology (Natural Science Edition),* vol. 6, p. 014, 2008.

# Chapter 4

# Fabrication of self-organized porous PCL membrane for improved cell culture and hiPSCs differentiation

In this chapter, we present a study to fabricate self-organized porous PCL membrane for improved cell culture and stem cell differentiation. First, we describe the fabrication of porous PCL membranes by self-organization in the free-space of a honeycomb micro-frame (patch). Then, we present the results of cell culture and genetic material transfection using the fabricated porous PCL patch. Next, we show how this culture patch can be used to support cardiac differentiation from human induced pluripotent stem cells (hiPSCs). Finally we report the results of biodegradation of the patch in case of fibroblast culture for several weeks.

## 4.1 Introduction

Extracellular matrix (ECM), a complicated organization of various biomolecules like proteins and polysaccharides, plays an important role in not only keeping cells on their places and binding cells together but also influencing their survival, development, shape, polarity, migration, and proliferation behavior [1-3]. The matrix contains various protein fibers interwoven in a hydrated gel composed of a network of polysaccharide chains, providing ECM with various unique properties such as high water containing, ease for cell anchoring, robust elasticity, and strong tensile strength [4]. *In vitro* engineering of advanced cell culture substrates that closely mimic the *in vivo* ECM has long been s a challenging issue [5].

A variety of substrates have been proposed to improve the *in vitro* cell culture. Matrigel or recombinant proteins such as laminin are commonly used to generate a gel layer on the flat surface of substrate to promote cell adhesion [6, 7]. These methods are versatile but not allow mimicking the organization of the extracellular matrix proteins. Surface patterning substrates made of natural and synthetic biopolymers such as collagen, alginate, PCL and PLGA are fabricated with appropriate surface stiffness for the control of cell performance [8, 9]. However, these substrates are lacking of 3D structure and effective diffusion of cells and nutrients. To improve the cell migration in 3D structure and facilitate effective nutrients diffusion, 3D porous scaffolds have drawn increasing attention [10, 11]. The high porosity is highly advantageous for 3D cell migration and nutrients diffusion. However, current methods are still limited to make

highly interconnected pore inside 3D scaffolds. Improving the porosity, a frequent method to make interconnected pores, usually accompanies with low mechanical strength and unexpected scaffold deformation.

Inspired by the fibrous protein structure in ECM, nanofiber substrates fabricated by electrospinning as a close mimic of ECM fibrous protein organization, have drawn increasing attention in the past decade [12-14]. However, nanofiber substrates are thin and fragile, so they are usually with a handling support such as glass slide and metal plates which are water impermeable and spoil the merits of nanofibers. To solve this problem, Tang et al in our laboratory proposed a new nanofibers substrate made of a monolayer of porous gelatin nanofibers on permeable PEGDA frame, which has promoted the growth and differentiation of hiPSCs into neurons and cardiomyocytes [15, 16]. This patch can be extended by considering alternative approaches for more homogenous porous density, more controllable biodegradability, etc.

Synthetic biodegradable polymers such as PCL and PLGA have exhibited growing potential in the fabrication of tissue engineering scaffolds, due to their high mechanical strength, easy processing and controllable biodegradation [17]. Both PLGA and PCL have been widely used as electrospun nanofibers alone or mixed with natural polymers like gelatin and chitosan for tissue engineering applications [18-21]. However, such nanofibers electrospinning process still faces limited solvent selection especially for electrospinning of mixed polymers. Besides, for synthetic polymer electrospinning, nanofibers formation is highly sensitive to surrounding environment parameters like temperature, humidity and air flow [22].

Self-organization of polymers is a novel method to fabricate substrates with specific ordered structures [23, 24]. Taking advantage of non-covalent interactions, self-organization starts from disordered system of pre-existing polymers to form an organized particles, film or 3D structure with easy processing steps. Several stimuli are often used to facilitate the formation of self-organization structures such as temperature, humidity, volatile solvents and air flow. However, self-organization still has some problems in polymer structure fabrication. It is difficult to handle with self-organization thin structure like films. Deformation is difficult to avoid during the formation of 3D structure.

In this work, we developed a method by self-organization of porous PCL structures

in the free-space of a PEGDA honeycomb frame. Here, PEGDA is mechanically stable on which a thin layer of porous PCL can be deposited by self-organization. PEGDA frame acts as not only an easy processing and handling support but also a structure controller for high integrity and uniform porosity. Oxygen plasma was used to improve cell adhesion of porous PCL patch. Cell tests demonstrated improved cell performance such as proliferation, cellular uptake of nutrients and gene transfection on such kind of substrate. We also investigated its application for culture and cardiac differentiation of hiPSCs. Finally we also studied the biodegradation of porous PCL patch.

## 4.2 Fabrication of the culture patch

The culture patch is made of porous PCL membrane. The patch frame is a honeycomb shaped and highly porous PEGDA grid with sufficient mechanic strength for easy handling. The porous PCL patch can be produced by solvent-driven fast self-organization while the honeycomb frame can be produced by soft-lithography, both relying batch processes for mass production. In the following, we will give the details of the fabrication process.

### 4.2.1 Fabrication of PEGDA honeycomb frame

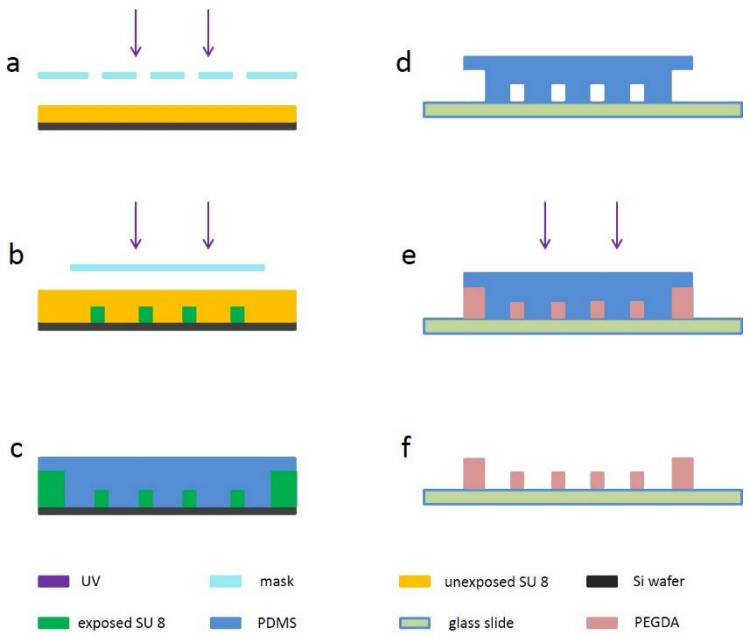


**Fig. 4.1** A schematic fabrication flowchart of PEGDA honeycomb frame including SU 8 photo lithography, PDMS soft lithography, PEGDA solution aspiration and UV crosslinking.

The fabrication procedure of PEGDA honeycomb frame is shown in **Fig. 4.1,** which includes two main steps:

### a) Preparation of PDMS mold

PDMS mold fabrication began with production of Cr mask of honeycomb arrays frame of 400 μm diameter and 50 μm width by micro pattern generator (μPG 101, Heidelberg Instruments) with 60% 40mW energy, followed with resist developing (AZ 726 MIF, 1 min) and 45s Cr etching. After rinsing and sonication removal of residual resist in acetone, a Cr mask with designed honeycomb pattern can be obtained.

For the photolithography process, negative resist SU8 3050 is used to generate the master mold by UV lithography. First, 50 μm of SU8 3050 resist layer was spin-coated on the mask at 500 rpm for 10s and then 3000 rpm for 30s. The resist was then prebaked following the sequence of 1 min at 65 ℃ and 20 min at 95 ℃. After cooling down to room temperature, the resist was exposed against the honeycomb Cr mask with UV light (365 nm wavelength and 12 mJ/s) for 20s, followed by a post-bake process (1 min at 65°C and 3 min at 95°C). Then another layer of 50 μm of SU8 3050 resist layer was spin-coated on exposed resist, prebaked, exposed against 9 mm diameter round shape

mask and post-baked. After cooling down to room temperature, the resist was then developed in SU8 developer for about 5 min with mild agitation. After rinsing with isopropanol, the resist was dried with nitrogen gun, resulting in SU8 master mold.

Next, SU8 3050 resist master was passivated by TMCS for anti-sticking surface treatment for 1-3 min. A PDMS solution was prepared using GE RTV 615 PDMS components A and B at a ratio of 10:1 and then poured on the top of the resist master. After degassing in vacuum for 15 min, PDMS was cast at 80 ℃ for 2 h, peeled off and punched into column shape PDMS mold (shown as **Fig. 4.2**).

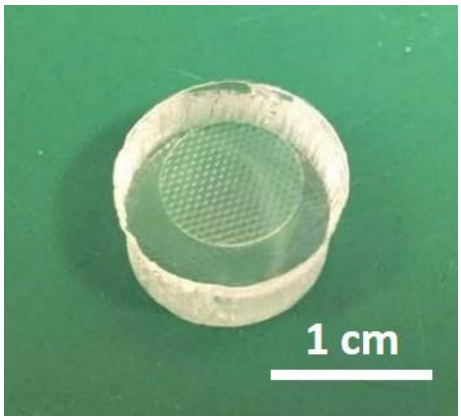


**Fig. 4.2** Photograph of PDMS mold for PEGDA honeycomb frame.

### b) Aspiration-assisted UV molding

PEGDA honeycomb frame is fabricated with PDMS aspiration-assisted molding technique. In brief, the PDMS mold was attached upside down on a clean glass slide. Then, the PDMS-glass assembly was transferred to a vacuum chamber for 15 min degasing. At the same time, a PEGDA pre-polymer solution containing 1 v/v% Irgacure 2959 as photo-initiator was prepared and used to fill the PDMS-glass cavity by degassing induced micro-aspiration. After the free space of PDMS-glass cavity was filled with PEGDA solution completely, the whole assembly was exposed with UV light (365 nm wavelength) at 12 mJ/s for 40s. Then the PEGDA network was solidified, peeled off from glass slide and rinsed with isopropanol for ready use, as is shown in **Fig. 4.3**.

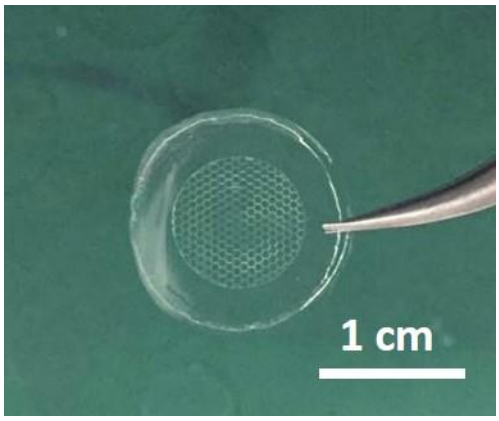


**Fig. 4.3** Photograph of a PEGDA honeycomb frame.

## 4.2.2 Self-organization of porous PCL membrane

Self-organization of porous PCL membrane is promoted by solvent evaporation in air flow. Briefly, PCL (MW 80k) was dissolved in Dichloromethane to prepare PCL solution. Then PEGDA honeycomb frame was fully immersed in PCL solution for 10 s with a tweezers and then taken out from the PCL solution. After removing immediately excessive PCL solution on PEGDA frame, the retained PCL solution on PEGDA frame was dried quickly with gentle air flow to produce porous PCL membrane on PEGDA frame. The porous PCL membrane was further dried in vacuum overnight, resulting in a dried porous PCL membrane as is shown in **Fig. 4.4**.

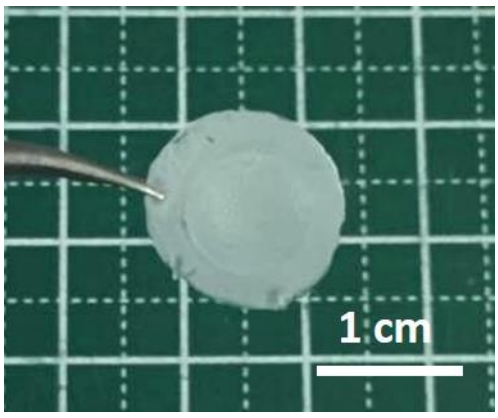


**Fig. 4.4** Photograph of porous PCL membrane on PEGDA honeycomb frame.

### 4.2.2.1 Morphology

To optimize the porosity and morphology of self-organization of PCL membranes,

PCL solution in DCM with different concentrations (10%, 5% and 2%) were prepared for patch fabrication. Samples made from different PCL concentrations were characterized with scanning electron microscope (SEM), as is shown in **Fig. 4.5**. PCL membranes not only fill the pores of honeycomb frame but also wrap the honeycomb grid. The surface of PCL membranes was filled with well packed self-organization pores. For sample from 10% PCL solution, pore size is not uniform and can be divided into two groups by size, large size pores (15~30 μm) and small size pore (2~5 μm). For sample from 5% PCL solution, pores are well organized with the size around 5 μm. For sample from 2% solution, pores are well organized while the size distribution (2~5 μm) is a little larger than 5% sample.

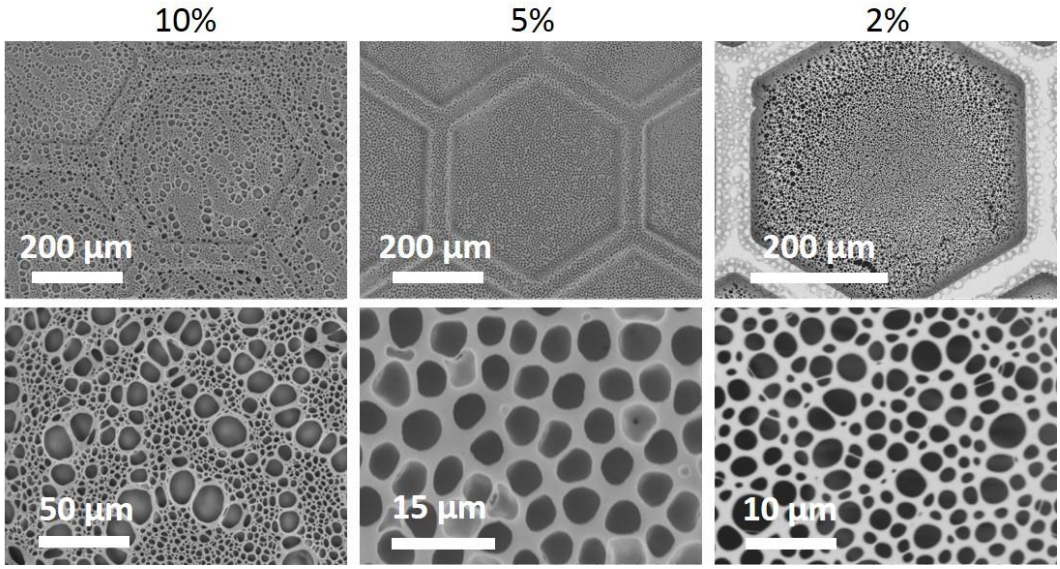


**Fig. 4.5** SEM images of 2D self-organized porous PCL membranes in PEGDA honeycomb frame made from PCL solution at different concentrations (10%, 5% and 2%).

### 4.2.2.2 Thickness

The porous PCL membranes were cut to characterize the cross-section structure and the thickness, as is shown in **Fig. 4.6**. For sample from 10% PCL solution, the membrane thickness is around 30 μm. There are pore structure on both sides of the patch while between them lies a solid PCL membrane. When PCL concentration was reduced to 5%, the thickness reduced significantly to around 6 μm. When the PCL concentration was further reduced to 2%, the thickness of PCL membrane can be further reduced to around 2 μm.

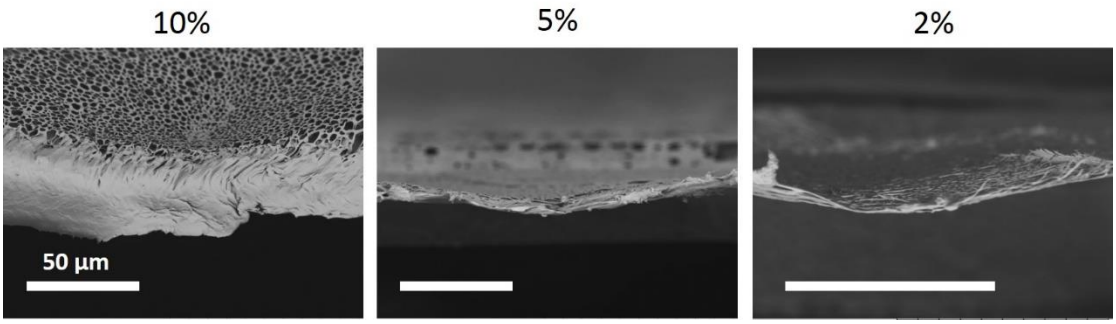


**Fig. 4.6** SEM images of cross section of the porous PCL membranes on PEGDA honeycomb frames made from PCL solution with different concentrations (10%, 5% and 2%).

### 4.2.2.3 Water permeation

The PCL membranes are further tested for permeability which is important in cell culture for the cell permeation and distribution of nutrients and metabolic wastes. The PCL membranes were treated with oxygen plasma on both sides to facilitate the hydrophilicity of the PCL membrane. By dropping a water droplet on the upside of the membrane, a dry paper was used to attach the other side of the membrane to see whether the paper will be wetted by water. Results are shown in **Tab. 4.1**. Without oxygen plasma treatment, all sample are water impermeable. After oxygen plasma treatment, membrane made from 2% PCL solution exhibits high water permeability while the other two samples still keep water impermeable.

**Tab. 4.1** Water permeation tests of different PCL membranes on PEGDA honeycomb frames with and without plasma treatment (+ means water permeable; - means water impermeable)

| sample | 2% | 5% | 10% |
|---|---|---|---|
| No treatment | - | - | - |
| Plasma treatment | + | - | - |

### 4.2.2.4 Porosity

Since high permeability of substrates plays an important role in mimicking *in vivo* microenvironment for improved cell culture application, we choose the PCL membrane made from 2% PCL solution for further study, which is also called porous PCL patch. **Fig. 4.7a** is a typical SEM image of porous PCL patch made from 2% PCL solution.

The pore size in each hexagonal lattice was collected and analyzed using ImageJ. **Fig. 4.7b** shows a typical pore size distribution. The pore size are in a range of 1-7 μm with an average pore size around 3.5 μm in diameter. The pore size is suitable for cell culture, permeation and nutrients distribution. We also investigated porosity disparity in each hexagonal lattice. **Fig. 4.7c** shows a porosity distribution in a lattice from one side to another. The porosity is the highest in the middle of the lattice, reaching 0.72. The porosity decreases from center to edge. The average porosity is measured by ImageJ to be 57%.

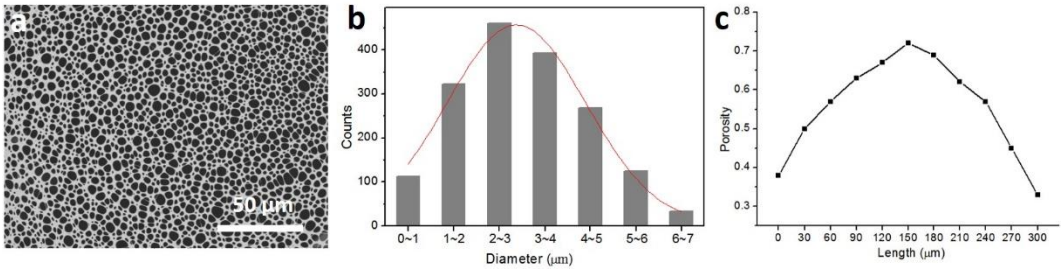


**Fig. 4.7** The porosity of porous PCL patch. (a) SEM image of a typical 2D porous PCL. (b) Pore size distribution profile. (c) Porosity distribution of 2D porous PCL in one hexagonal lattice. Data was collected from one side to another with the center at length of 150 μm.

## 4.3 Cell based assays

To demonstrate the feasibility and advantages of porous PCL patch for effective cell processing, we test the porous PCL patch for cell studies including cell proliferation and cellular uptake. We also study the feasibility of applying the patch for enhanced gene transfection.

### 4.4.1 Cell proliferation on 2D porous PCL patch

NIH-3T3 cells were prepared in Dulbecco's modified eagle medium (DMEM) supplemented with 10% fetal bovine serum (FBS) and 1% penicillin/streptomycin at 37 ℃ with 5% $CO_2$. When cells reach 80~90% confluence, they were dissociated with

Trypsin at 37 ℃ for 3 min. After centrifugation at 1000 rpm for 5 min, cells were collected. At the same time cells were counted with a commercial hemocytometer. After centrifuge and counting, cells were resuspended in a fresh medium for seeding at a specific density.

Before cell seeding, the porous PCL was treated with oxygen plasma to improve the surface hydrophicility of PCL. Then, the patch was sterilized in 70% ethanol for 30 min. After being rinsed with PBS, 50μl of culture medium containing $2\times10^4$ cells was added on the top of the PCL patch. After incubation at 37 ℃ for 1 h for cell adhesion, the porous PCL patch was transferred to 12-well plate and 1 ml fresh medium was added around it gently. It's worth mentioning that the porous PCL patch can be suspended inside the medium, which results into an "off-ground" culture for the cells. As control, we also seeded cells on tissue culture plate and flat PCL membrane.

We first evaluated the possible cytotoxicity of porous PCL patch exerts on cells culture on it. Cell viability was measured by MTT assay. Briefly, cells were seeded on 24-well plate, flat PCL membrane and porous PCL patch at a density of $5\times10^4$ per well. After 1, 2 and 3 days incubation, 20 μL of MTT solution (5mg/mL in PBS) was added into each well, followed by 4 h incubation. The incubation medium was replaced with 200 μL DMSO to dissolve resulted formazan. Cell proliferation was evaluated by cell viability based on the absorbance of each well at 490 nm. The results are shown in **Fig. 4.8**. After 1 day culture, the cell viability on three substrates are similar, indicating that the porous PCL patch together with flat PCL membrane pose negligible toxicity to NIH 3T3 cells. Compared with tissue culture plate, cells exhibit higher proliferation ability on PCL based substrates. Besides, porous PCL patch is better than impermeable PCL membrane. After 3 days culture, the number of cells on porous PCL patch is twice over that on tissue culture plate while the number on impermeable PCL membrane is about 1.5 times over that on tissue culture plate. The results reveal that porous PCL patch can obviously promote cell proliferation.

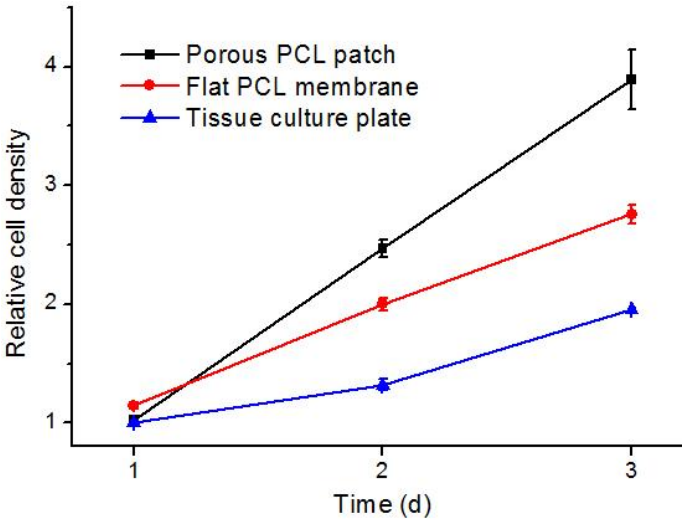


**Fig. 4.8** Viability of NIH 3T3 cells cultured on 2D porous PCL, flat PCL membrane and tissue culture plate for 1, 2, and 3 days culture.

Then we studied the cell morphology cultured on porous PCL patch, as is shown in **Fig. 4.9**.

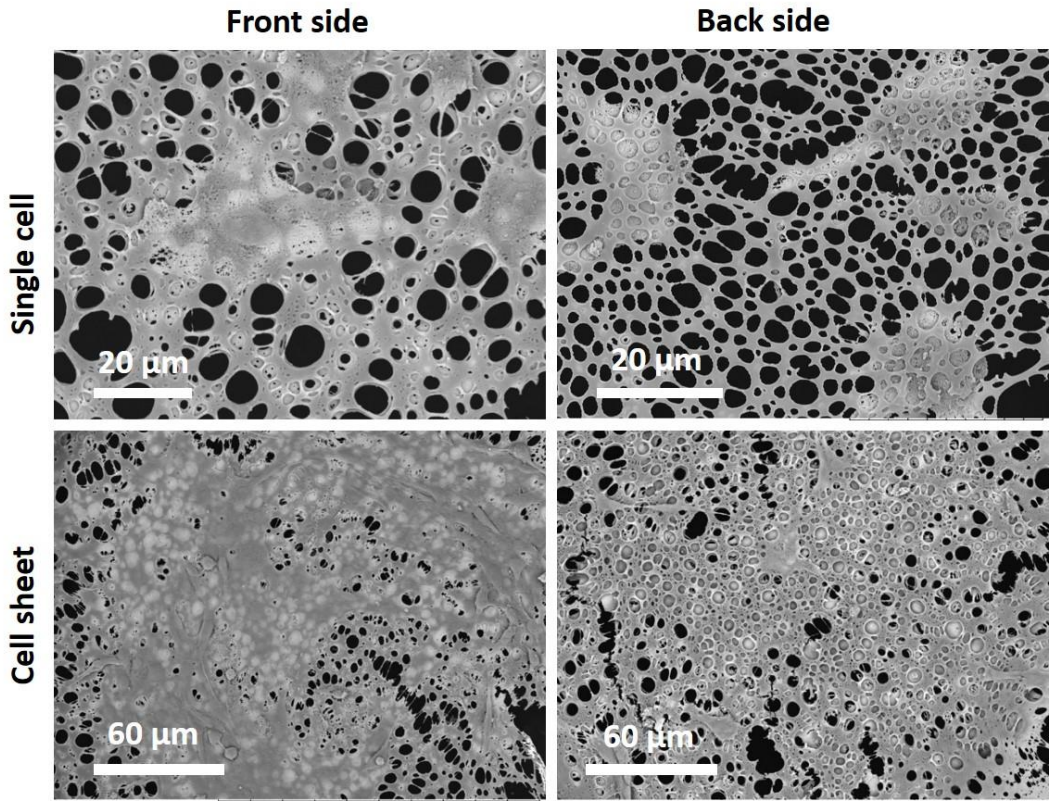


**Fig. 4.9** SEM images of NIH 3T3 cells cultured on 2D porous PCL in single cell and cell colony. Images are taken from both front side and back side.

After 1 and 3 days culture on porous PCL patch, cells were fixed and gradually dehydrated for SEM characterization. After 1 day culture, cells attach to the surface of porous PCL patch in isolated state. Cells exhibit high spreading ability and stretch several pseudopods outside cling on to the surface of porous PCL patch. From a bottom view, due to the high cell spreading, significant portion of cell surface was exposed the outside through the pores on porous PCL patch. After 3 days culture, cells proliferated and connected with each other to form a single layer cell sheet. Similarly, the cell sheet also has a large portion of surface exposed the outside through the pores on porous PCL patch. Compared with traditional cell culture methods on planar culture dishes, cells on porous PCL patch should have more access to culture medium, uptake more nutrients from medium and release easily the metabolic wastes.

### 4.4.2 Cellular uptake

The off-ground culture using a PCL patch allows cells obtaining nutrients from both sides of the patch, i.e., the cellular uptake occur on both front and back sides. In principle, the backside uptake is less efficient than that of front size due to limited permeability but it should be more efficient than that of conventional culture where the nutrient diffusion underneath the contact area of the cell should be much less efficient than that through the PCL membrane holes. To demonstrate the enhanced nutrients uptake by cells on porous PCL patch, we studied the cellular uptake on porous PCL patch by using a molecule PLL (MW 15k~30k) as a model. A fluorescent dye fluorescein isothiocyanate (FITC) is conjugated to PLL to track and quantify the PLL inside the cells. Briefly, NIH 3T3 cells were seeded on glass slide and porous PCL patch at a density of $2 \times 10^4$ per well. 50 μg/mL of PLL-FITC was added to each well for a series of incubation time (0.5, 1, 3, 6 and 12 h). After incubation, cells were further stained with Hochest 33342 for 30 min. All the samples were characterization by Zeiss confocal laser microscope at 37℃ and 5% $CO_2$.

The result is shown in Fig. For each substrate, the fluorescence intensity becomes stronger with the increase of incubation time. For each incubation time, intensity on

porous PCL patch is much stronger than that on glass substrate, as can be seen from the **Fig. 4.10**. Due to the positive charge of PLL, PLL-FITC accumulated in the cell nucleus and interacted with DNA.

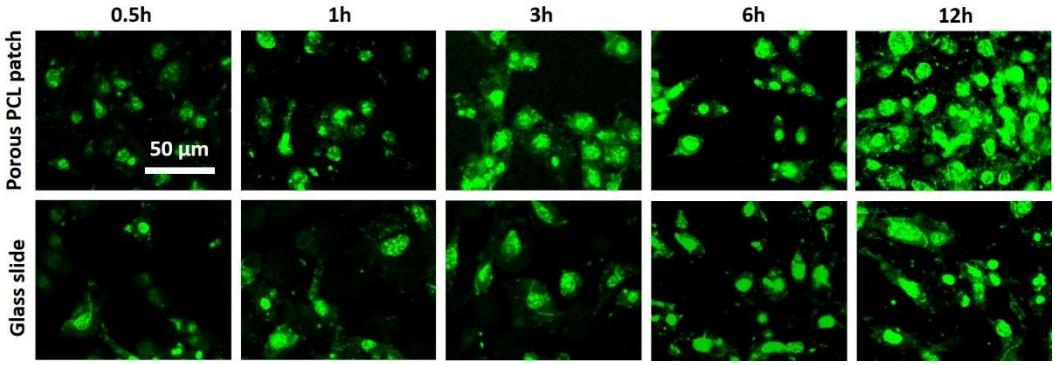


**Fig. 4.10** Fluorescence images of NIH 3T3 cells culture on 2D porous PCL and glass slide after incubation with PLL-FITC for 0.5, 1, 3, 6 and 12h.

As is shown in **Fig. 4.11**, statistical result shows that at each incubation time of 0.5, 1, 3, 6 and 12h, the average fluorescence intensities in single cell on porous PCL patch are 1.48, 1.34, 1.43, 1.67 and 1.89 times than those on glass slide, indicating that the porous PCL patch can facilitate cell uptake of molecules in culture medium. We also studied the percentage of cells uptaking PLL-FITC at each incubation time on the two substrates, as uptake efficiency. We measure the efficiency by calculating the rate of cells stained with FITC against total cells stained with DAPI. On glass slide, about 64% cells were stained after 0.5 h incubation. With the increase of incubation time (1, 3, 6 and 12h), the efficiencies reach 67%, 74%, 90% and 93%, respectively. While on porous PCL patch, the efficiency reaches as high as 90% after 0.5h incubation. After 3h incubation, the efficiency reaches 100% and keeps until 12h incubation. The results indicate that porous PCL patch possesses great potential for cellular uptake of nutrients with high efficiency.

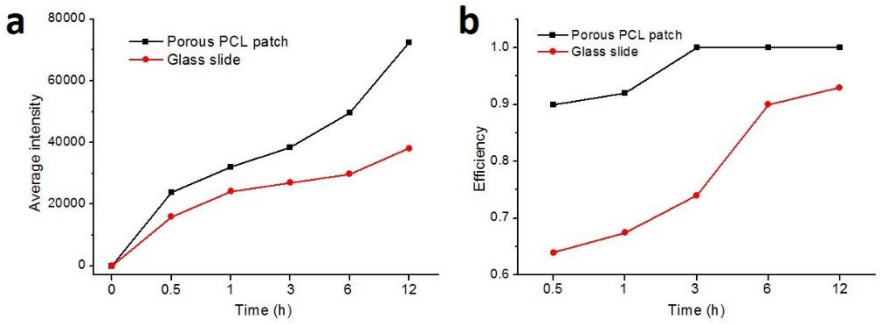


**Fig. 4.11** Uptake of PLL-FITC by NIH 3T3 cells with different incubation time. (a) The average fluorescence intensity of NIH 3T3 cells on 2D porous PCL and glass slide. (b) The efficiency of cellular uptake on 2D porous PCL and glass slide.

## 4.4.3 Gene transfection

Due to the high cellular uptake efficiency of the porous PCL patch, we further investigate the gene transfection into the cell using the same device. HEK 293T cells, normal human embryonic kidney cells, are often used to conduct the experiment due to their high efficiency in gene transfection. Positively charged liposomes are used as vectors to deliver plasmid DNA into cells. Briefly, HEK 293T cells were seeded on glass slide and porous PCL patch at a density of $2 \times 10^4$ per sample. For each well, 2 μg of Lipofectamine 2000 and 0.8 μg of plasmid DNA were added into DMEM without FBS at a final volume of 50 μL and reacted for 10 min before incubating with cells. Then the culture medium in each well was removed followed by PBS rinsing of cells. Liposome/DNA mixture was added to each well and fresh DMEM without FBS was added to a final volume of 500 μL. After 6 h incubation, the medium was replaced by fresh DMEM containing 10% FBS and 200 μg/mL of G418. Cells were further incubated for one or two days for the expression of fluorescent proteins encoded by the plasmid DNA. After cells were further stained with Hochest 33342 for 30 min, all the samples were characterization by Zeiss confocal laser microscope at 37℃ and 5% $CO_2$.

The results are shown in **Fig. 4.12**. On glass slide, only partial cells expressed the fluorescent proteins after 1 and 2 days culture, with a little higher fluorescence intensity in day 2 than that in day 1. However, on porous PCL patch, nearly all the cells expressed the fluorescent proteins, with much stronger fluorescence intensity than that on glass

slide in both day 1 and day 2.

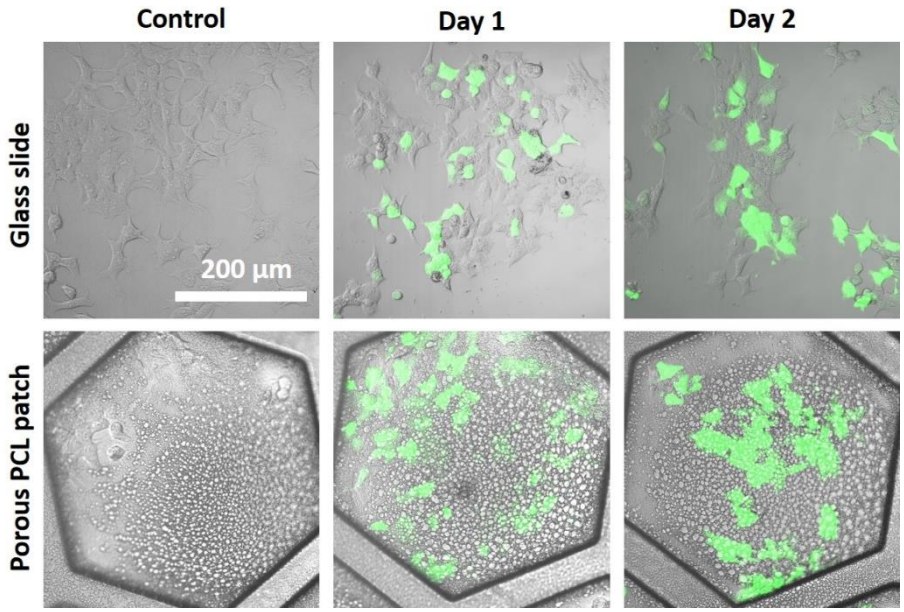


**Fig. 4.12** Fluorescence images of HEK 293T cells on glass and 2D porous PCL patch for 1 and 2 days incubation after gene transfection.

Then we measured the fluorescent intensity inside the cells 1 day after transfection. We compared the intensities on such two substrates by average intensity in single cell. As is shown in **Fig. 4.13**, statistical result shows that the intensity on porous PCL patch is about 1.8 times than that on glass slide 1 day after transfection. The intensities on both substrates further increase in day 2 compared to day 1. The intensity on porous PCL patch is about 2.1 times than that on glass slide at day 2. Additionally, we also studied the percentage of cells expressing fluorescent proteins, as the gene transfection efficiency. Results show that on glass slide the percentage of cells expressing fluorescent proteins is 39%, with a little increase to 46% in day 2. For porous PCL patch, the percentage is as high as 86% at day 1, which is about 2.2 times than that on glass slide. Similar to that on glass slide, a slight increase of intensity on porous PCL patch occur in day 2 to be 91%. The results indicate that porous PCL patch possesses great potential for highly efficient gene transfection compared to traditional methods on culture dishes.

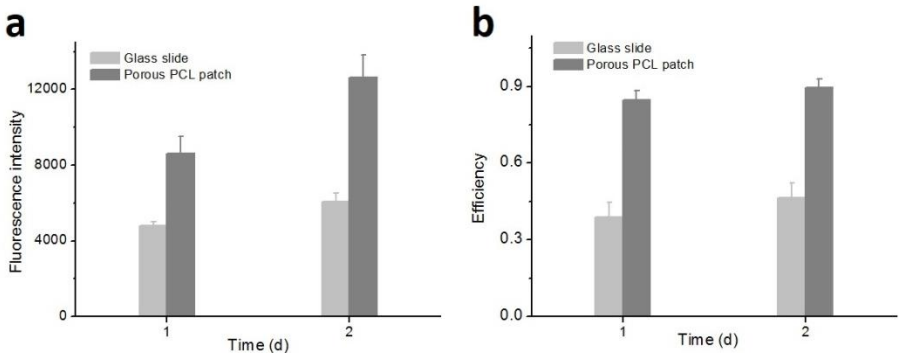


**Fig. 4.13** (a) Average fluorescence intensity of HEK 293T cells on porous PCL patch and glass slide with 1 and 2 days incubation after gene transfection. (b) The efficiency of gene transfection on 2D porous PCL and glass slide with 1 and 2 days incubation after gene transfection.

## 4.5 Cardiac differentiation of hiPSCs on 2D porous PCL

Due to the prominent promotion of porous PCL patch in cell performance, we applied the porous PCL patch for hiPSCs culture and differentiation into cardiomyocytes in order to seek the possibility to promote hiPSCs differentiation performance.

### 4.5.1 HiPSCs culture on 2D porous PCL

Before hiPSCs culture, porous PCL patch was sterilized in 70% ethanol solution for 30 min at room temperature. Then the sterilized porous PCL patch was rinsed with PBS to remove the residual ethanol and subsequently immersed into PBS solution containing diluted vitronectin for 1 h at room temperature for vitronectin coating on the surface of PCL. **Fig. 4.14** shows the relative fluorescence intensity porous PCL patch coated with FITC labeled vitronectin of 1 and 5 μg/mL in DPBS, indicating the successful vitronectin coating on the patch and the concentration-dependent coating amount of vitronectin.

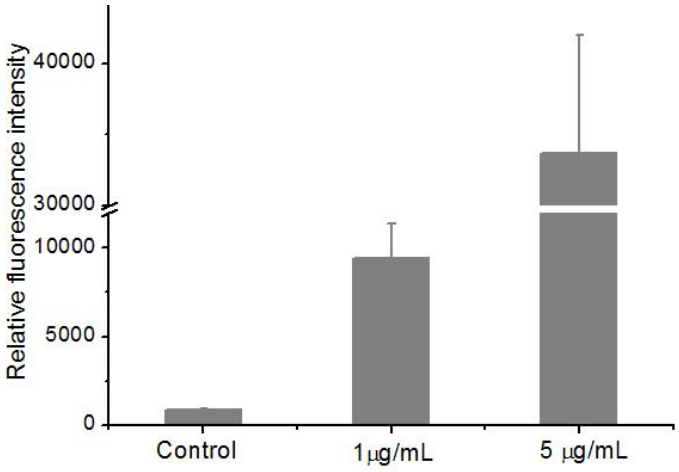


**Fig. 4.14** Relative fluorescence intensity of porous PCL patch coated with FITC labeled vitronectin of 1 and 5μg/mL in DPBS.

HiPSCs were dissociated in the culture dish by PBS solution containing 5 μM EDTA, aspirated into single cells and seeded on 5 μg/mL of vitronectin coated porous PCL patch in 50 μL E8 medium supplemented with 0.1% ROCK inhibitor. The coated vitronectin can facilitate hiPSCs adhesion on porous PCL patch. After incubation at 37 ℃ for 1 h for cell adhesion, the porous PCL patch was transferred to 12-well plate and 1 ml fresh medium was added around it gently. After 1 day incubation, hiPSCs formed monolayer cell sheet, as can be seen in **Fig. 4.15a**. If the concentration of vitronectin was reduced to 1 μg/mL, hiPSCs had lower tendency to form monolayer cell sheet, but they preferred to aggregate and form dome-like embryonic bodies (EB), as is shown in **Fig. 4.15b**. The reason for different hiPSCs morphologies can be explained by the effect of vitronectin which works by providing cell recognized adhesion sites for hiPSCs attachment. In high concentration vitronectin (5 μg/mL), patches can be coated with large amount of vitronectin, which provides enough adhesion sites for cell matrix interaction, thus hiPSCs tend to form monolayer on patches. However, in low concentration vitronectin (1 μg/mL), the amount of vitronectin coated on patches is far less enough for cell adhesion, thus hiPSCs tends to aggregate by cell-cell junctions to form EB with less cell matrix interaction.

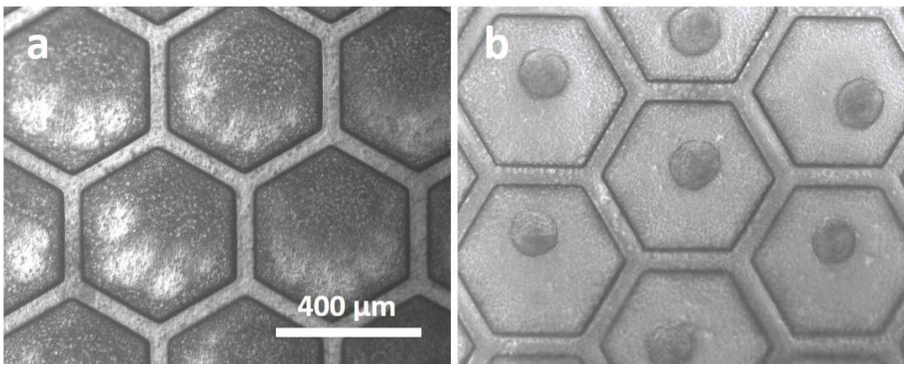


**Fig. 4.15** Microscope bright field images of (a) monolayer and (b) EB-like hiPSCs on 2D porous PCL with different vitronectin coating.

## 4.5.2 Pluripotency of hiPSCs

The first issue we investigate is whether hiPSCs on porous PCL patch can keep their pluripotency. To evaluate the pluripotency of hiPSCs monolayer and EBs generated on our porous PCL patch, pluripotent stem cell markers SOX2 and TRA-1-60 are used to stain the hiPSCs. Immunostaining was conducted as follows: cells were fixed with 4% PFA for 15 min, permeabilized with 0.5% Triton X-100 for 30 min, blocked with 1% BSA for 30 min. HiPSCs were stained with primary antibodies (anti-SOX2 in rat and anti-TRA-1-60 in mouse IgM), second antibodies (Alexa Fluor 594 goat anti-mouse IgM and Alexa Fluor 488 donkey anti-rat) and DAPI. All the samples were conducted for fluorescence imaging on a Zeiss 710 confocal microscope.

The Immunostaining results are shown in **Fig. 4.16**. The immunofluorescence showed a typical hiPSC-like staining pattern on both hiPSCs monolayer and EB, revealing that the expression of these markers was maintained. The results confirm that the formation of monolayer and EBs on porous PCL patch does not affect the pluripotency of hiPSCs.

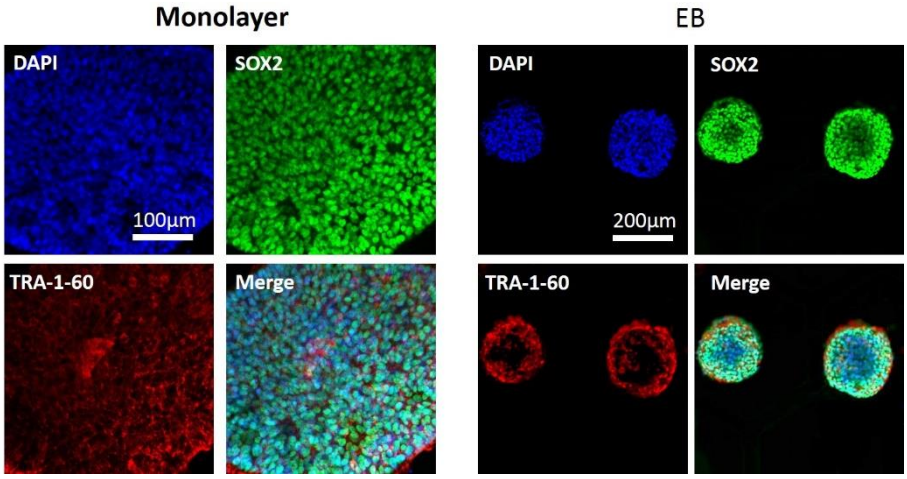


**Fig. 4.16** Immunofluorescence images of pluripotency stained hiPSCs in monolayer and EB on 2D porous PCL patch.

## 4.5.3 Proliferation of hiPSCs

The second issue we care about is the viability and proliferation of hiPSCs on porous PCL patch. After sterilization of porous PCL patch in 70% ethanol solution, 50 μL of E8 medium containing $1.5\times10^5$ cells was added on the top of the porous PCL patch. After incubation at 37 ℃ for 1 h for cell adhesion, the porous PCL patch was transferred to 12-well plate and 1 mL of fresh E8 medium was added around it gently. After 1, 2 and 3 days culture, 100 μL of 5mg/mL MTT solution was added to each well for cell viability assay, as is shown in **Fig. 4.17**.

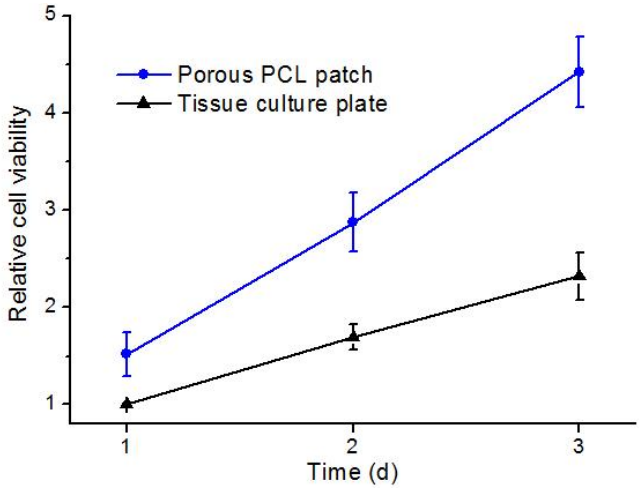


**Fig. 4.17** Viability of hiPSCs on 2D porous PCL patch and tissue culture plate for 1, 2 and 3 days

incubation.

Compared with tissue culture plate, at day 1 hiPSCs exhibit higher viability on porous PCL patch, revealing that porous PCL patch provides more support for cell adhesion. The proliferation rate on porous PCL patch is faster than that on tissue culture plate, as can be seen from the slopes of the curves. The viability at days 1, 2 and 3 is 1.5, 1.7 and 2.1 times, respectively, than that on tissue culture plate. The results show that porous PCL patch can obvious promote hiPSCs proliferation.

## 4.5.4 Cardiac differentiation from hiPSCs

### 4.5.4.1 Differentiation process

Once monolayer and EBs formed, cardiomyocytes differentiation was started since the next day, according to GiWi protocol developed by Lian et al, by modulating Wnt signaling with small molecules [25]. As shown in **Fig. 4.18a**, differentiation started by adding RPMI 1640/B27 without insulin medium containing 12 μM CHIR99021 into culture dish to replace E8 medium. After 24h of CHIR99021 treatment, the medium was changed with RPMI/B27 without insulin. 72 h after addition of CHIR99021, RPMI 1640/B27 without insulin medium containing 5 μM IWP2 was added to replace previous medium. At day 5 of differentiation, IWP2 was replaced by new RPMI/B27 without insulin medium. Then every 3 days, change medium with RPMI/B27 medium. Cell morphology during differentiation was recorded by an inverted microscope, as is shown in **Fig. 4.18b**. Since GSK3 inhibitor was added, many cells stated to migrate out from EBs or monolayer hiPSCs. In differentiation separated EBs begun to connect to each other to form a thick cell sheet. With the same protocol, hiPSCs cultured on glass slide were differentiated into cardiomyocytes at the same time as a control.

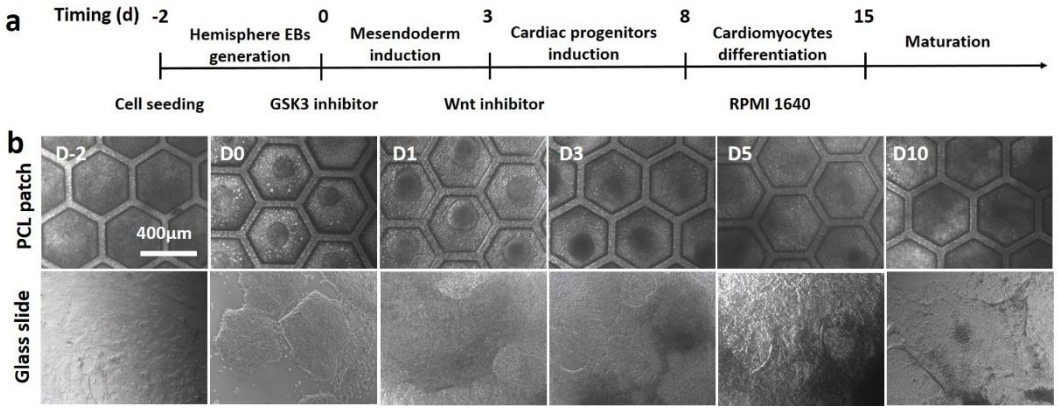


**Fig. 4.18** a) A schematic protocol for the differentiation of cardiomyocytes from hiPSCs generated hemisphere EBs; b) Bright-field images of the typical cell morphology on PCL patch and glass slide at day -2, day 0, day 1, day 3, day 5 and day 10.

After treated by GSK3 inhibitor and Wnt inhibitor successively, cell contraction on porous PCL patch and glass slide can be observed around Day 7 or Day 8. On cells on PCL patch, cell contraction occurs in large continuous area and shows high uniformity, while on glass slide contraction happens only in several separate small zones and exhibits obvious nonuniformity.

### 4.5.4.2 Immunostaining

To analyze the expression of cardiomyocytes related proteins, the differentiated cells on both porous PCL patch and glass slide at day 20 were immunostained with cardiomyocytes related antibodies. Immunostaining was conducted as follows: cells were fixed with 4% PFA for 15 min, permeabilized with 0.5% Triton X-100 for 30 min, blocked with 5% goat serum (cardiomyocytes) for 1h. Then cells were stained with primary antibodies (anti-α-actinin and anti-cardiac muscle myosin in mouse, and anti-TnnT2 and anti-Connexin 43 in rabbit), second antibodies (Alexa Fluor 488 goat anti-mouse and Alexa Fluor 633 goat anti-rabbit) and DAPI. All the samples were conducted for fluorescence imaging on a Zeiss 710 confocal microscope.

The immunofluorescence staining results are shown as **Fig. 4.19**. TnnT2, a highly cardiomyocytes-specific protein, is positive for the cells differentiated on porous PCL patch, while on glass slide, the expression of TnnT2 shows extremely low, which indicates a more mature cardiac cell state on porous PCL patch. Myosin is a cardiac

muscle-specific protein involved in active force generation. An increasing expression of Myosin on porous PCL patch is found compared to the cells on glass slide. Immunostaining of α-actinin and connexin43 is also achieved. Striated sarcomeres (α-actinin positive) can be observed for the differentiated cells on porous PCL patch while on 2D glass slide the expression of α-actinin is relatively low. Connexin43, active in gap junction, plays a significant role in the coordination of cells contraction, which shows more positive on porous PCL patch than that on glass slide.

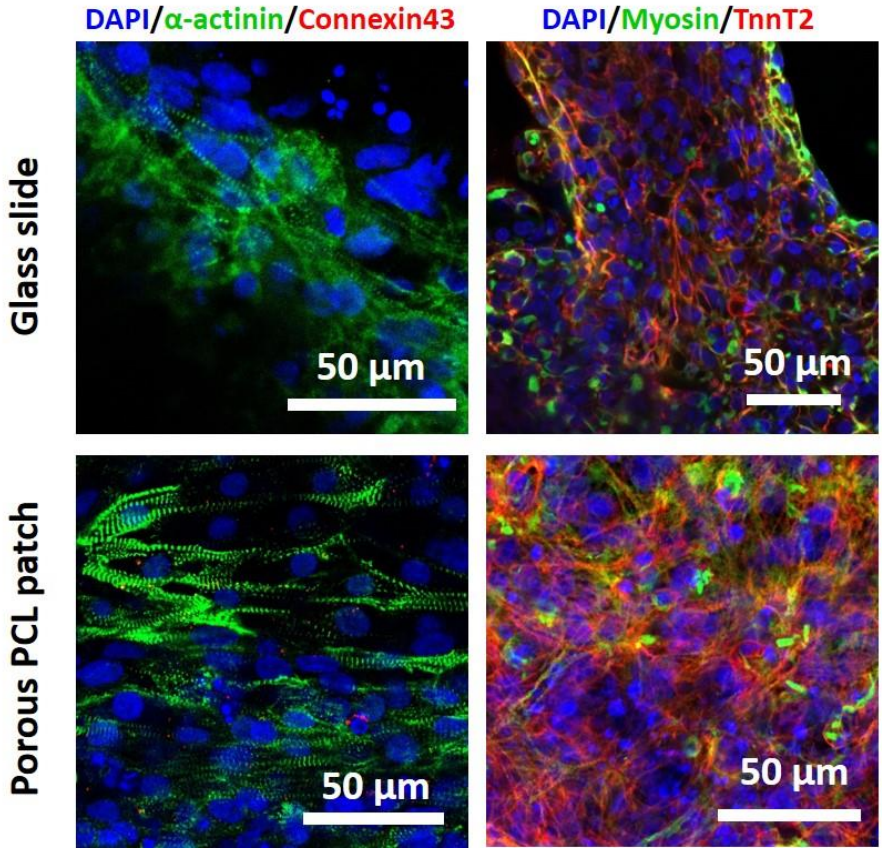


**Fig. 4.19** Immunofluorescence staining images of cardiomyocytes derived from hiPSCs on 2D porous PCL and glass slide.

### 4.5.4.3 Calcium imaging

Cardiac muscle contraction is initiated by the sudden rise of cytosolic $Ca^{2+}$ concentration. Briefly, when the incoming action potential activates a $Ca^{2+}$ channel in the plasma membrane, a $Ca^{2+}$ influx triggers the opening of $Ca^{2+}$-release channels in the sarcoplasmic reticulum. $Ca^{2+}$ flooding into the cytosol then initiates the contraction of cardiac muscle. The increase in $Ca^{2+}$ concentration is transient because the $Ca^{2+}$ is

rapidly pumped back into the sarcoplasmic reticulum by an abundant, ATP-dependent $Ca^{2+}$-pump in its membrane. Typically, the cytoplasmic $Ca^{2+}$ concentration is restored to resting levels, allowing the cardiac muscle to relax. The contraction force is dependent on the $Ca^{2+}$ concentration. So by measuring the fluctuation of $Ca^{2+}$ concentration in the cytosol, we can evaluate cardiac contraction performance such as contraction rate and strength. Briefly, Calcium imaging is conducted by using an intracellular $Ca^{2+}$ indicator fluo-4. Culture medium of cardiomyocytes was replaced by 500 μL Tyrode's salt solution containing 4 μg of fluo-4 and 10 μL of 10% F127. After 30 min incubation, incubation solution was replaced with 1mL of fresh Tyrode's salt solution for Calcium imaging on a Zeiss 710 confocal microscope. The results are shown in **Fig. 4.20**.

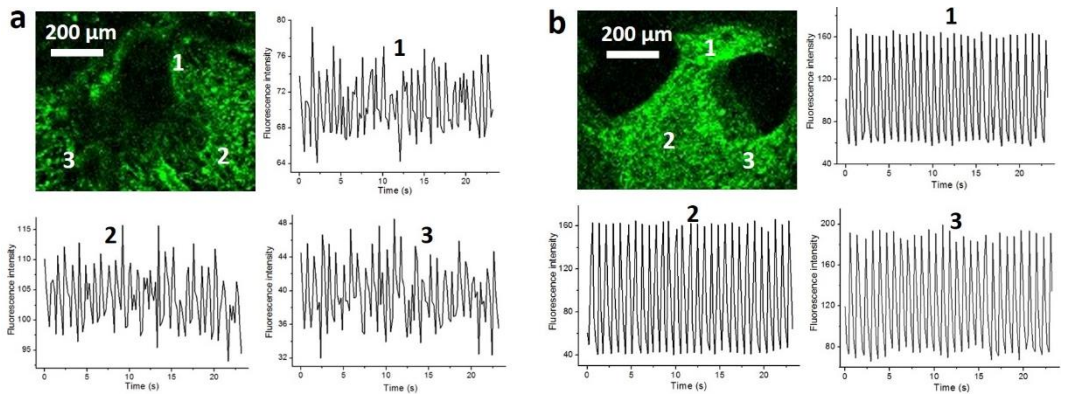


**Fig. 4.20** Calcium imaging of hiPSCs derived cardiomyocytes on a) glass slide and b) porous PCL patch. For each sample, three typical zone (shown as 1, 2 and 3) were selected for recording the fluorescence intensity during cardiac contraction.

**Fig. 4.20a** shows a typical fluorescence profile recorded during calcium imaging experiment of a cardiac tissue on glass slide. Different zones of a cardiac tissue were measured, shown as 1, 2 and 3. As can be seen from the results, the fluctuation of the fluorescence intensities in zone 1, 2 and 3 is notably irregular, indicating the large variation of $Ca^{2+}$ concentration in cytosol. All the three zones have different fluorescence intensity peaks (74, 76, and 79, respectively), indicating different contraction rate of the cardiac tissue. **Fig. 4.20b** shows a typical fluorescence profile recorded during calcium imaging experiment of a cardiac tissue on porous PCL patch.

In three typical zones recorded, the fluorescence intensities fluctuate regularly, revealing the regular change of cytosolic $Ca^{2+}$. Besides, the recorded fluorescence has a uniform sparking rate. The contraction rate is estimated to be 74 per minute, which is in the normal range (60-100/min). The above results demonstrate that compared with glass slide cardiomyocytes on porous PCL patch show higher contraction homogeneity and stronger contraction.

## 4.6 Biodegradation

In order to apply the porous PCL patch for *in vivo* study, a prerequisite is the controllable *in vivo* degradation. In our experiment, we cultured NIH 3T3 cells on porous PCL patch during the degradation test to mimic the *in vivo* microenvironments. We also made a control group of porous PCL patch without cells in culture medium. Briefly, before cell seeding, all porous PCL patches were treated with plasma, sterilized in 70% ethanol solution and washed with PBS to remove all ethanol on the patch. NIH 3T3 cells were seeded in 50 μL on the patch at a density of $5\times10^4$ per sample. After cells adhered to the patches, another 1 mL of fresh medium was added.

The degradation test was conducted for six weeks. The result was shown in **Fig. 4.21**. For the control group, degradation of porous PCL patch is very slow, nearly 5% PCL degrades after six weeks. However, for porous PCL patch with cells on it, degradation is faster, nearly 35% PCL degrades after six weeks, which is 7 times as much as that in control group. Our results show that cells should interact with the substrate and play key roles in the degradation of the substrate.

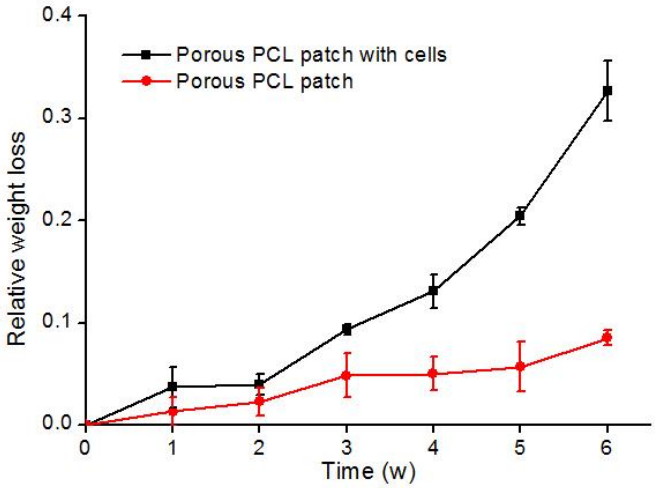


**Fig. 4.21** Relative weight loss of porous PCL patch after incubation with or without NIH 3T3 cells.

## 4.7 Conclusion

We have fabricated 2 μm thick porous PCL membrane supported by a PEGDA honeycomb micro-frame based on a confined 2D self-organization. The as-fabricated substrate possesses highly uniform pore with good shape integrity and are easy to handle for a variety cell based assays. On such a device, cells could be attached and spread while the high porosity of membrane allows cells more efficient nutrients uptake from the medium, which significantly improves the performance of cell-based assays such as proliferation and gene transfection. Results also revealed that the porous PCL patch improved the culture of hiPSCs and promoted the cardiac differentiation of hiPSCs in terms of contraction strength and uniformity. Finally, such culture devices made of porous PCL showed controlled biodegradation in a cellular environment, which is promising for cell-based tissue engineering applications.

# Reference


1. G.S. Schultz, G. Ladwig, and A. Wysocki, *Extracellular matrix: review of its roles in acute and chronic wounds.* World wide wounds, 2005. **2005**: p. 1-18.
2. E.D. Hay, *Cell biology of extracellular matrix*. 2013: Springer Science & Business Media.
3. J. Halper and M. Kjaer, *Basic components of connective tissues and extracellular matrix: elastin, fibrillin, fibulins, fibrinogen, fibronectin, laminin, tenascins and thrombospondins,* in *Progress in Heritable Soft Connective Tissue Diseases*. 2014, Springer. p. 31-47.
4. R.O. Hynes, *The extracellular matrix: not just pretty fibrils.* Science, 2009. **326**(5957): p. 1216-1219.
5. L.G. Griffith and G. Naughton, *Tissue engineering--current challenges and expanding opportunities.* Science, 2002. **295**(5557): p. 1009-1014.
6. K. Chaw, M. Manimaran, F. Tay, and S. Swaminathan, *Matrigel coated polydimethylsiloxane based microfluidic devices for studying metastatic and non-metastatic cancer cell invasion and migration.* Biomedical microdevices, 2007. **9**(4): p. 597-602.
7. M. Yoshikawa, N. Tsuji, Y. Shimomura, H. Hayashi, and H. Ohgushi. *Effects of laminin for osteogenesis in porous hydroxyapatite*. in *Macromolecular Symposia*. 2007. Wiley Online Library.
8. L.E. Freed, G. Vunjak-Novakovic, R.J. Biron, D.B. Eagles, D.C. Lesnoy, S.K. Barlow, and R. Langer, *Biodegradable polymer scaffolds for tissue engineering.* Nature Biotechnology, 1994. **12**(7): p. 689-693.
9. H.J. Levis, R.A. Brown, and J.T. Daniels, *Plastic compressed collagen as a biomimetic substrate for human limbal epithelial cell culture.* Biomaterials, 2010. **31**(30): p. 7726-7737.
10. S.J. Hollister, *Porous scaffold design for tissue engineering.* Nature materials, 2005. **4**(7): p. 518-524.
11. V. Karageorgiou and D. Kaplan, *Porosity of 3D biomaterial scaffolds and osteogenesis.* Biomaterials, 2005. **26**(27): p. 5474-5491.
12. W.J. Li, C.T. Laurencin, E.J. Caterson, R.S. Tuan, and F.K. Ko, *Electrospun nanofibrous structure: a novel scaffold for tissue engineering.* Journal of Biomedical Materials Research Part A, 2002. **60**(4): p. 613-621.
13. X. Wang, B. Ding, and B. Li, *Biomimetic electrospun nanofibrous structures*

*for tissue engineering.* Materials today, 2013. **16**(6): p. 229-241.

14. D. Sundaramurthi, U.M. Krishnan, and S. Sethuraman, *Electrospun nanofibers as scaffolds for skin tissue engineering.* Polymer Reviews, 2014. **54**(2): p. 348-376.
15. Y. Tang, L. Liu, J. Li, L. Yu, F.P.U. Severino, L. Wang, J. Shi, X. Tu, V. Torre, and Y. Chen, *Effective motor neuron differentiation of hiPSCs on a patch made of crosslinked monolayer gelatin nanofibers.* Journal of Materials Chemistry B, 2016. **4**(19): p. 3305-3312.
16. Y. Tang, L. Liu, J. Li, L. Yu, L. Wang, J. Shi, and Y. Chen, *Induction and differentiation of human induced pluripotent stem cells into functional cardiomyocytes on a compartmented monolayer of gelatin nanofibers.* Nanoscale, 2016. **8**(30): p. 14530-14540.
17. E.S. Place, J.H. George, C.K. Williams, and M.M. Stevens, *Synthetic polymer scaffolds for tissue engineering.* Chemical Society Reviews, 2009. **38**(4): p. 1139-1151.
18. J. Lipner, W. Liu, Y. Liu, J. Boyle, G. Genin, Y. Xia, and S. Thomopoulos, *The mechanics of PLGA nanofiber scaffolds with biomimetic gradients in mineral for tendon-to-bone repair.* Journal of the mechanical behavior of biomedical materials, 2014. **40**: p. 59-68.
19. S.-M. Jung, G.H. Yoon, H.C. Lee, and H.S. Shin, *Chitosan nanoparticle/PCL nanofiber composite for wound dressing and drug delivery.* Journal of Biomaterials Science, Polymer Edition, 2015. **26**(4): p. 252-263.
20. Y. Qian, H. Chen, Y. Xu, J. Yang, X. Zhou, F. Zhang, and N. Gu, *The preosteoblast response of electrospinning PLGA/PCL nanofibers: effects of biomimetic architecture and collagen I.* International journal of nanomedicine, 2016. **11**: p. 4157.
21. P. Sanaei-rad, T.-s.J. Kashi, E. Seyedjafari, and M. Soleimani, *Enhancement of stem cell differentiation to osteogenic lineage on hydroxyapatite-coated hybrid PLGA/gelatin nanofiber scaffolds.* Biologicals, 2016. **44**(6): p. 511-516.
22. A. Haider, S. Haider, and I.-K. Kang, *A comprehensive review summarizing the effect of electrospinning parameters and potential applications of nanofibers in biomedical and biotechnology.* Arabian Journal of Chemistry, 2015.
23. A. Satyam, P. Kumar, X. Fan, A. Gorelov, Y. Rochev, L. Joshi, H. Peinado, D. Lyden, B. Thomas, and B. Rodriguez, *Macromolecular crowding meets tissue engineering by self‐assembly: A paradigm shift in regenerative medicine.*

Advanced materials, 2014. **26**(19): p. 3024-3034.

24. R.J. Wade and J.A. Burdick, *Advances in nanofibrous scaffolds for biomedical applications: From electrospinning to self-assembly.* Nano Today, 2014. **9**(6): p. 722-742.

25. X. Lian, J. Zhang, S.M. Azarin, K. Zhu, L.B. Hazeltine, X. Bao, C. Hsiao, T.J. Kamp, and S.P. Palecek, *Directed cardiomyocyte differentiation from human pluripotent stem cells by modulating Wnt/β-catenin signaling under fully defined conditions.* Nature protocols, 2013. **8**(1): p. 162.

# Chapter 5

# Monolayer gelatin nanofibers on PDMS frame for cardiac differentiation

In this chapter, we present a fabrication method of monolayer gelatin nanofibers on an elastic frame of PDMS for improved culture and cardiac differentiation of human induced pluripotent stem cells (hiPSCs). This device is in form of culture patch and can be used for a variety of cell-based assays. First, we describe the fabrication of honeycomb frame made of PDMS by lithography methods and the deposition of monolayer electrospun gelatin nanofibers on the frame. Then, we present the improved hiPSCs culture on the patch. Next, we show how this culture patch device is used for enhanced cardiac differentiation of hiPSCs. Further, we test the functionality of generated cardiac tissue with calcium imaging, electrical stimulation and drug test. Finally we study the regulatory effect of elastic PDMS frame on cardiac contraction.

## 5.1 Introduction

Heart disease is the leading cause of death and disability, accounting for approximately 30% of all human mortality [1, 2]. Heart disease is a condition reflecting impairment of heart pumping efficiency caused by a variety of underlying diseases including ischemic heart disease, hypertensive heart disease, valvular heart disease, and primary myocardial disease. The injury of the heart is permanent because, after a massive cell loss or destruction, the cardiac tissue lacks significant intrinsic regenerative capability to replace the lost or destroyed cells [3].

Current treatments for heart diseases mainly focus on pharmacological therapy, interventional therapy and heart transplantation. Pharmacological therapy focuses on reduction of work load and protection from the toxic humoral factors which are over-activated in heart diseases [4]. Interventional therapy, such as surgery or implantation of pacing devices to control electrical/mechanical asynchrony, are now receiving more widespread application, in particular for patients with marked symptoms and marked limitation in activity [5, 6]. However, both drug and interventional therapies cannot adequately control disease progression to the end stage [7, 8]. Eventually, heart transplantation is an alternative treatment to end-stage heart failure. Owing to the lack of organ donor source and complicated immune suppressive treatments, however, scientists and surgeons are constantly pursuing new strategies for treatment of the injured heart [9, 10].

Early studies focused on an intriguing strategy: the application of cell transplantation. It was confirmed that diseased cardiac tissue could be restored by the transplantation of functional cardiomyocytes [11, 12]. Since then a number of research groups have conducted pioneering experiments confirming that cell implantation can improve cardiac contractile function [13-15]. However, obtaining enough cell population with minimal immune incompatibility is always a huge obstacle lying ahead of researchers. In order to get enough cells for implantation, a more ambitious strategy is to generate cardiac tissue ex vivo from stem cells differentiation, and transplant the cardiac tissue into targeted site for treatment applications [16-18]. Stem cells are undifferentiated cells that retain the ability to differentiate into multiple cell lineages. In principle, stem cells are the optimal cell source for tissue regeneration including cardiac tissue. Firstly, they can self-replicate throughout life so that an unlimited number of stem cells of similar properties can be produced in vitro. Secondly, the stem cells are clonogenic, which means each cell can generate a colony in which all the cells are derived from this single cell and thus have identical genetic constitution. Thirdly, they possess the capacity to differentiate into various specialized cell types. For these reasons, stem cell-based therapy for cardiac tissue regeneration has been under intensive research during the last decade. Of all, hiPSCs have drawn increasing attention due to their superior advantages that hiPSCs can be easily obtained from patient's somatic cell via a reprogramming process [19]. This patient's specific hiPSCs will allow for more precise drug test and hiPSCs derived tissue implantation with minimal immune rejection.

Previous work has mainly been conducted with hiPSCs cultured in petri dishes which are totally different from *in vivo* ECM [20]. Currently increasing attentions have been paid to a new tissue engineering strategy which cultivates stem cells on engineered scaffolds in order to achieve improved stem cell culture and cardiac differentiation performance [21, 22]. A number of research groups have done pioneering work in fabricating advanced scaffolds mimicking *in vivo* extracellular microenvironment and applying them for stem cells culture and cardiac differentiation, aiming to improving the performance of reconstructed cardiac tissue including cell alignment, mechanical stability, contractile and electrophysiological functionality [22]. Various kinds of scaffolds have been fabricated to facilitate cell performance, including nanofiber mat,

hydrogel, and micro-fabricated substrates [23, 24]. However, the above scaffolds are still not close mimic of *in vivo* ECM in aspects like substrate stiffness, organization mimic of ECM components, cell and nutrients permeation and intercellular communication.

To fabricate an ECM closely mimicking substrate for cardiac tissue engineering, Tang et al reported a monolayer porous gelatin nanofiber patch supported by PEGDA honeycomb frame which showed improved hiPSCs derived cardiac differentiation and functioning compared with glass substrate [25]. They revealed that gelatin nanofiber will degraded during cardiac differentiation and the generated cardiac tissue was supported by PEGDA frame. However, compared to human heart, PEGDA is too rigid for cardiac tissue. Because the mechanical strength of substrate is very important to cells, it is necessary to fabricate soft substrate mimicking *in vivo* cardiac ECM.

Polydimethylsiloxane (PDMS) is a flexible and elastic synthetic polymer. PDMS is made of Si-O backbone with numerous side methyl groups, which is chemically inert, biocompatible, biostable and highly gas permeable. Its elasticity can be easily modulated by adjusting the ratio of the two components during crosslinking. PDMS is very flexible and can be engineered into different structures, geometries and patterns in both 2D and 3D. PDMS has been widely used in biomedical field. PDMS shows high tolerance in ophthalmologic applications [26, 27]. Besides, it has been used in breast implants [28], and intraarticular implants [29]. PDMS also shows great potential in fabricating artificial smart skin.

In this work, we fabricate a porous PDMS honeycomb frame with tunable elasticity on which a porous monolayer gelatin nanofibers are electrospun for better cell culture application. With this method, we also make PDMS frames with various elastic properties. The elastic qualities of these PDMS frames are investigated. The as-fabricated gelatin nanofiber patch has been applied for hiPSCs culture and cardiac differentiation. We then conduct immunostaining, calcium imaging and drug test on generated cardiac tissues, which shows improved performance on gelatin nanofiber patch compared with control group on glass slide. Finally we find the elasticity guided PDMS deformation during cardiac contraction, which shows great potential in directing cardiac differentiation and cardiac tissue organization.

## 5.2 Fabrication of PDMS/gelatin nanofibers patch

The culture patch is made of monolayer gelatin nanofibers and PDMS micro-frame. The frame, fabricated by micro-fabrication, is a honeycomb shaped and highly porous PDMS grid with both sufficient mechanic strength for easy handling and enough elasticity for reversed deformation. The monolayer of gelatin nanofibers is randomly deposited on the PDMS frame by electrospinning with controlled pore sizes and porosity. In the following, we will give the details of the fabrication process.

### 5.2.1 Fabrication of PDMS honeycomb frame

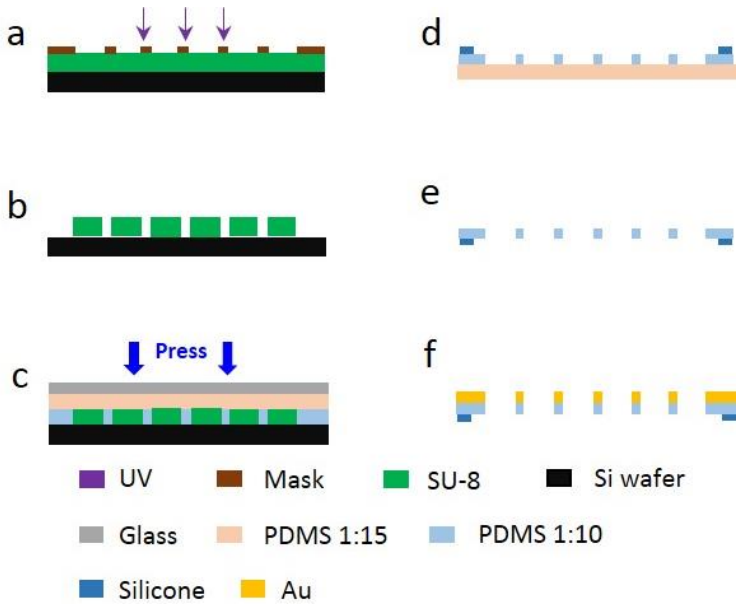


**Fig. 5.1** The schematic flowchart of PDMS honeycomb frame fabrication

The fabrication procedure of PDMS honeycomb frame is shown in **Fig. 5.1,** which includes three main steps:

#### a) SU-8 master fabrication

SU-8 master fabrication began with production of Cr mask of honeycomb arrays frame of 400 μm diameter and 100 μm width by micro pattern generator (μPG 101, Heidelberg Instruments) with 60% of 40 mW laser power, followed by photoresist developing in AZ 726 MIF for 1 min and 45s Cr etching. After rinsing and sonication

removal of residual resist in acetone, a Cr mask with designed honeycomb pattern can be obtained, as is shown in **Fig. 5.2**.

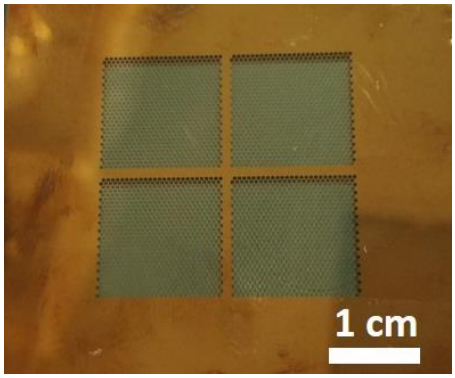


**Fig. 5.2** Photograph of honeycomb Cr mask made by micro pattern generator.

During the photolithography process, negative photoresist SU-8 3050 was used to generate the master mold by UV lithography. First, 50 μm thick SU-8 3050 photoresist layer was spin-coated on a clean Si wafer at speeds of 500 rpm for 10s and then 3000 rpm for 30s. The photoresist was then prebaked following the sequence of 1 min at 65 ℃ and 20 min at 95 ℃. After cooling down to room temperature, the photoresist was exposed against the honeycomb Cr mask with UV light (365 nm wavelength and 12 mJ/s) for 20s, followed by a post-bake process (1 min at 65 ℃ and 3 min at 95 ℃). After cooling down to room temperature, the photoresist was then developed in SU-8 developer for about 5 min with mild agitation. After rinsing with isopropanol, the photoresist was dried with nitrogen gun and baked at 170℃ for 15 min, resulting in SU-8 master mold, as is shown in **Fig. 5.3**.

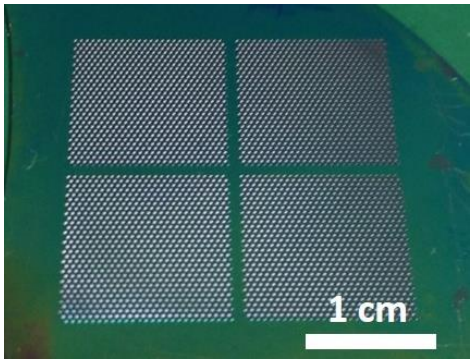


**Fig. 5.3** Photograph of SU-8 photoresist master with honeycomb pattern.

### b) Fabrication of PDMS thin-layer

Next, SU-8 3050 photoresist master was treated with oxygen plasma and passivated by 200 nm thick parylene C coating for anti-sticking surface treatment. At the same time, a 5 mm thick flat PDMS substrate (1:15) with the same size of SU-8 master was cured, treated with oxygen plasma and passivated by TMCS for anti-sticking surface treatment. A PDMS (1:10) solution was then poured on the top of the SU-8 master and transferred to vacuum chamber for 15 min degasing. Then the flat PDMS substrate was used to press against the SU-8 master. To achieve a uniform pressing, a clean square glass slide was attached on top of the flat PDMS substrate. With enough press force, SU-8 master can penetrate liquid PDMS (1:10). After 1 h pressing, the whole assembly was cured overnight at 80℃. After cooling down to room temperature, the flat PDMS substrate with the generated porous honeycomb PDMS thin layer was peeled off from the SU-8 master (shown in **Fig. 5.4**).

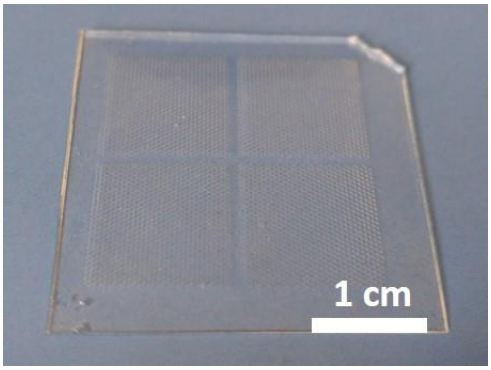


**Fig. 5.4** Photograph of porous honeycomb PDMS on flat PDMS substrate.

### c) Silicone ring mounting

The generated porous honeycomb PDMS thin layer is ready to be detached from flat PDMS substrate. Before peeling off from the flat PDMS, the porous honeycomb PDMS thin layer was mounted with a 500 μm thick silicone rubber ring with outer and inner diameters being 13 and 9 mm, respectively. Briefly, silicone rubber ring was designed by CAD, produced by a cutting machine and sonication cleansing in isopropanol before use. Then both the porous honeycomb PDMS thin layer and silicone rubber ring were treated with oxygen plasma for 3 min, immediately mounted together, and baked at 100℃ for 10 min for permanent bonding. After cooling down to room

temperature, the porous honeycomb PDMS thin layer mounted with a silicone rubber ring was peeled off from the flat PDMS substrate with a tweezers, resulting in the PDMS honeycomb frame (shown in **Fig. 5.5**).

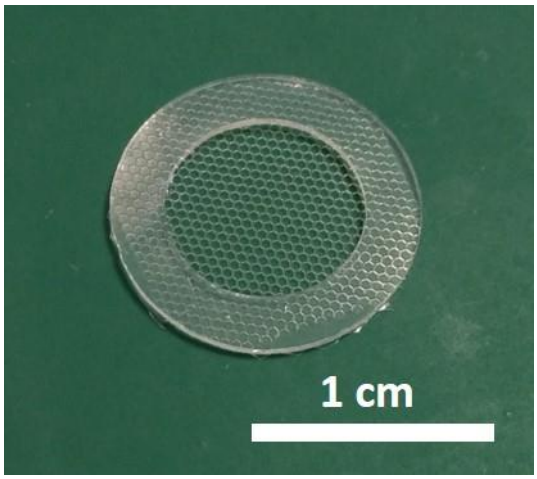


**Fig. 5.5** Photograph of silicone ring mounted PDMS honeycomb frame

The as-fabricated PDMS honeycomb frame was characterization with SEM. Before that, the surface of PDMS honeycomb frame was deposited with 10 nm thick Au by sputter coater (K675X, EMITECH, Germany) at 125 mA current. The results were shown in **Fig. 5.6a,b**. The fabricated PDMS honeycomb frame has a regular and uniform hexagonal lattice free of defects. The feature size and pitch size are 400 and 100 μm, respectively, which is consistent with our designed sizes. **Fig.5.6c** is an image obtained with a tilted sample holder, which shows the thickness of PDMS frame estimated to be 52 μm.

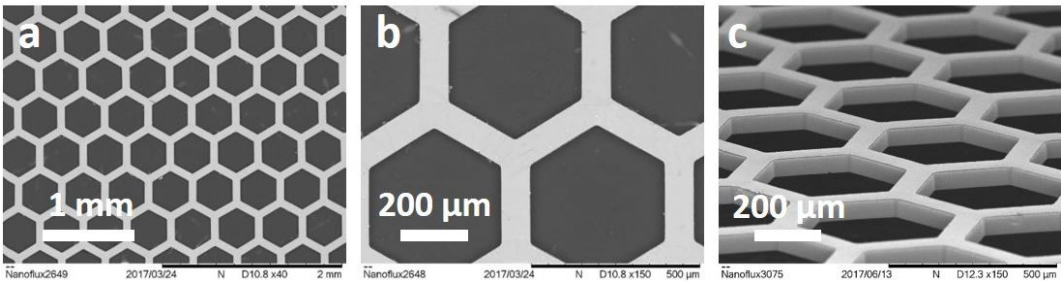


**Fig. 5.6** SEM images of PDMS honeycomb frame. (a) Low and (b) high magnification images of PDMS. (c) PDMS honeycomb frame on a tilted supporter.

In order to measure the exact thickness of PDMS honeycomb frame, we made a copy of PDMS honeycomb frame with PEGDA which was characterized by DekTaK Profilometer. The result is shown in **Fig. 5.7**. The thickness was about 49 μm. The result indicates that the thickness of PDMS honeycomb frame is consistent with that of SU-8 master.

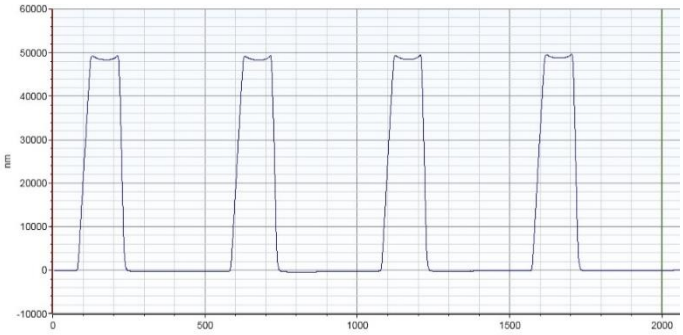


**Fig. 5.7** Thickness profile of PDMS honeycomb frame obtained by DekTak Profilometer.

With this size and thickness dependent method, we can also fabricate other porous PDMS frame with various parameters based on SU-8 3050 masters. **Fig. 8a-c** shows a honeycomb PDMS frame with feature size and pitch size being 400 and 50 μm, respectively. **Fig. 8d-f** shows a deformed shape of honeycomb PDMS frame, with two long sides 600 μm each, four short sides 300 μm each and two acute angles 60 °. The thickness of both of these two kinds of PDMS frames is well controlled by the SU-8 masters, which is about 52 μm determined by DekTak Profilometer, as is shown in **Fig. 5.9**.

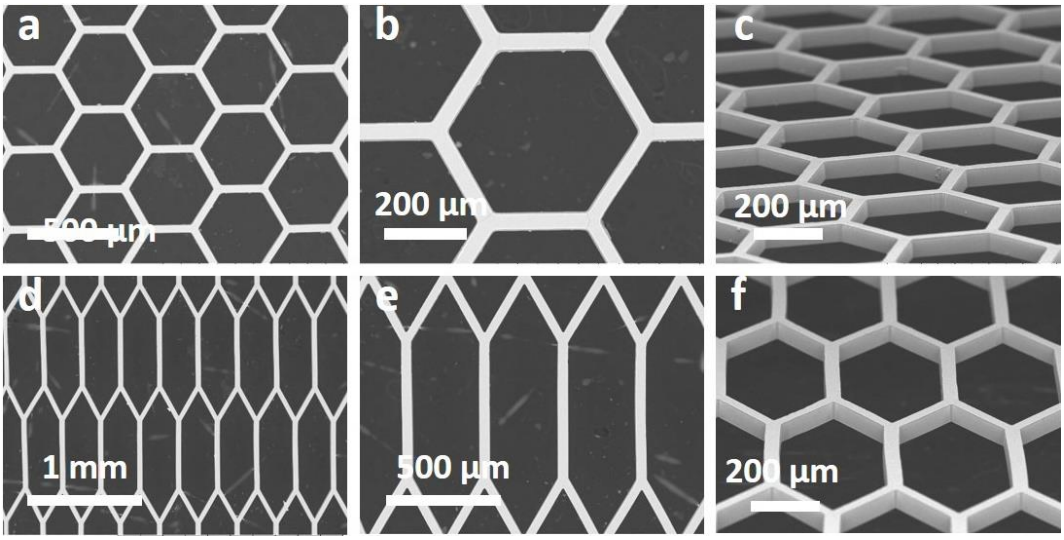


**Fig. 5.8** SEM images of two other PDMS frames. (a), (b) and (c) PDMS honeycomb frame with feature size 50 µm. (d), (e) and (f) PDMS deformed honeycomb frame.

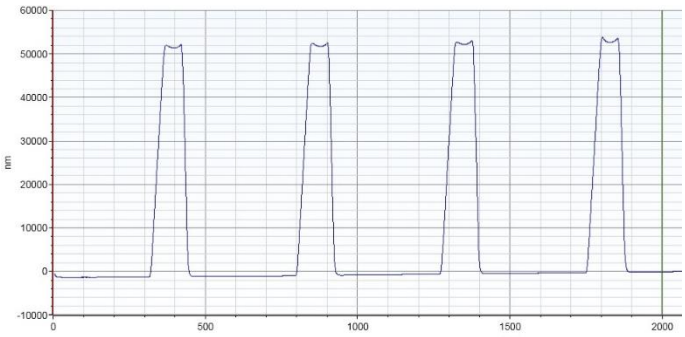


**Fig. 5.9** Thickness profile of PDMS honeycomb frame obtained by DekTak Profilometer.

Since PDMS is a flexible elastic material. Different PDMS frames should have different strain-stress performance. So we measure the strain-stress profiles of the three types of PDMS frames with mechanical testing instrument (Instron 5544). We also fabricated three different ratios (B: A) of PDMS for every designed frame. After obtaining the strain-stress data, we calculated the Young's Modulus of each tests. The results are shown in **Fig. 5.10**. The samples are measure in two different directions, direction **a** and direction **b**. For frames with the same pattern design and same pulling direction, Young's modulus decreases with the reduction in concentration of PDMS B component. For individual frame design with the same concentration of PDMS B component, Young's modulus is complicated at two pulling directions. Briefly, for honeycomb frame, Young's modulus at direction b is larger than that at direction a while,

for deformed honeycomb, Young's modulus at direction a is much larger than that at direction b. For situations that all other parameters are the same except the frame design, in direction a, Young's modulus of deformed PDMS frame is much larger than those of the other two kinds of frames while in direction b Young's modulus of deformed PDMS frame is much smaller than those of the other two frames.

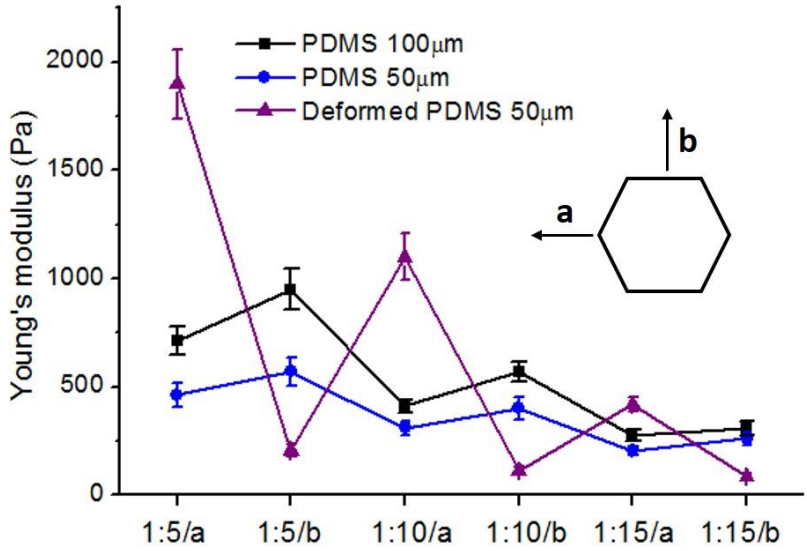


**Fig. 5.10** Young's modulus of three different PDMS frames made by different component ratios (1:5, 1:10 and 1:15). Directions a and b are shown in the inset.

### 5.2.2 Electrospinning of gelatin nanofibers

The fabricated PDMS honeycomb frame is used as a substrate for gelatin nanofibers deposition. To obtain more uniform nanofibers layer and enhance the attachment of gelatin nanofibers to PDMS frame, a 10 nm thick Au layer was sputtered on frame surface.

**Fig. 5.11** illustrates the typical electrospinning setup. To fabricate electrospun gelatin nanofibers, an Aluminum foil attached on a flat substrate was used as a collector. The fabricated PDMS honeycomb frame was fixed on the surface of the collector with gold layer exposed. First, the gelatin solution was prepared by adding 10% (wt) gelatin powder (G2625, Sigma-Aldrich, France) and 1% (wt) citric acid into a mixed solution of acetic acid, ethyl acetate and distilled water with a volume ratio of 21:14:10 and vigorous stirring at room temperature. Then a 1 mL syringe containing gelatin solution

was equipped on a syringe pump (KD Scientific, USA) with a 21 gauge hypodermic needle called spinneret. The spinneret was connected to the anode of high potential power supply (Heinzinger, Germany) with bias voltage of 10 kV and the cathode was connected to the grounded Aluminum foil collector. The feeding rate of syringe pump was fixed at 0.2 ml/h and the distance between spinneret tip and PDMS substrate was set at 10 cm. When high voltage is applied between spinneret tip and collector, gelatin nanofiber can be generated and deposited randomly on the collector.

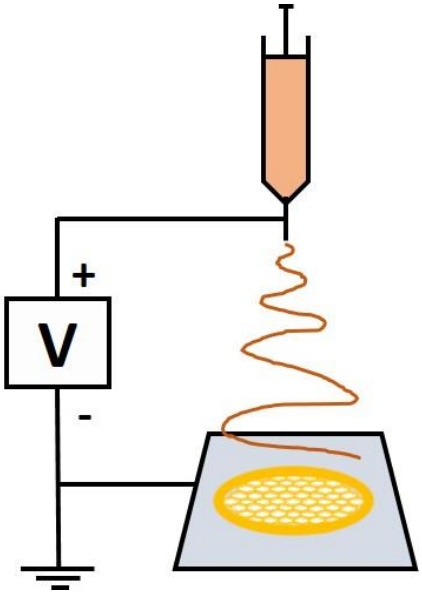


**Fig. 5.11** Schematic diagram of electrospinning setup.

Though various parameters affect the performance of electrospinning, electrospinning time is the overwhelming factor in determining the density of nanofibers in a specific trial under a stable environment. To optimize the porosity and pore size of gelatin nanofibers, different electrospinning time was tested based on the other constant parameters. The morphology of fibers observed by SEM was shown as **Fig. 5.12**. For both 2 min and 5 min of spinning time, monolayer nanofiber mat can be obtained. But when spinning time was 10 min or more, nanofiber mat becomes multilayers and there was almost no through hole among fibers. The size of pores and porosity of nanofiber mat were analyzed by ImageJ from SEM images. The porosities for 2 min and 5 min of spinning time were 95.4±0.8% and 61.6±1.9%, respectively. Both of them are permeable enough for a final suspension culture system. But for 10 min of electrospinning, the porosity was difficult to measure since the multi-layer and

small pores. As is shown in **Fig. 13**, the pores of gelatin nanofibers for 5 min spinning were mainly less than 6 μm, which is suitable for cell seeding and culture. For 2 min of spinning time, however, the most pores was over 10 μm, which was much larger than the size of cells, thus unsuitable for cell culture. So we choose 5 min of electrospinning time in further experiments.

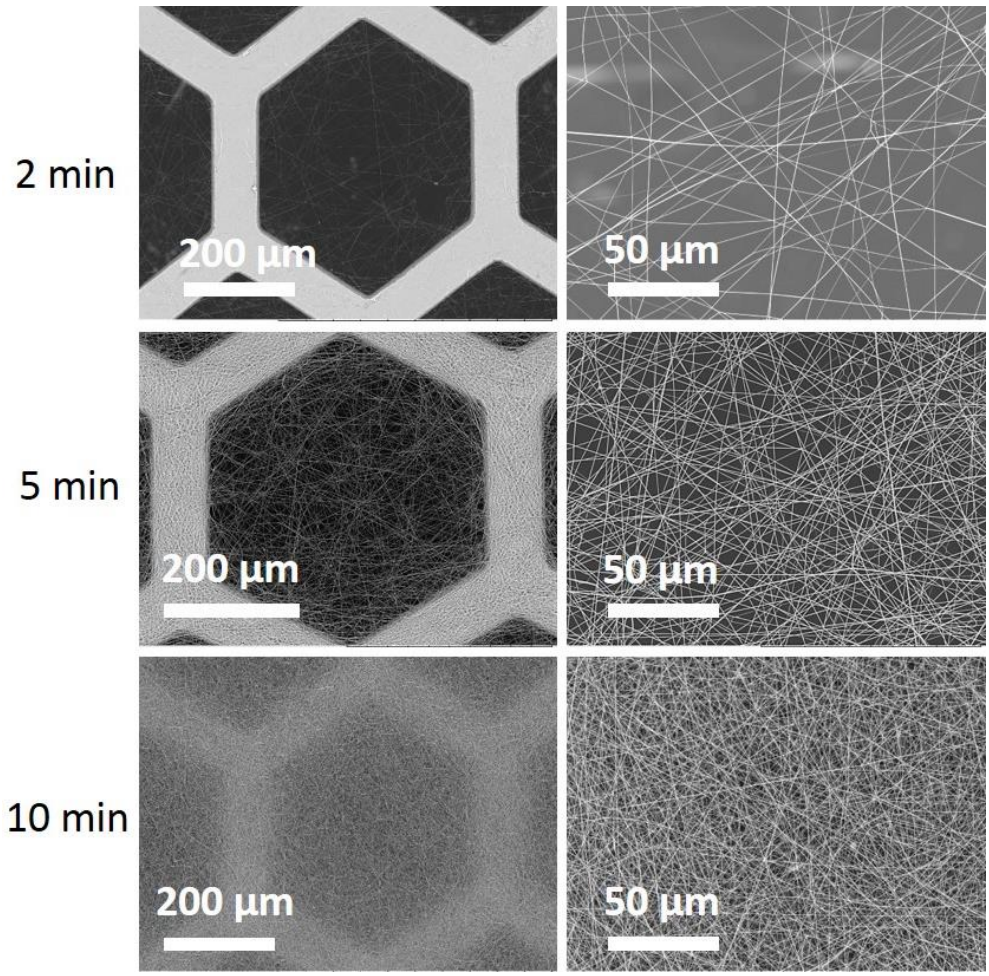


**Fig. 5.12** SEM images of gelatin nanofibers on PDMS honeycomb frame at different electrospinning time (2, 5 and 10 min).

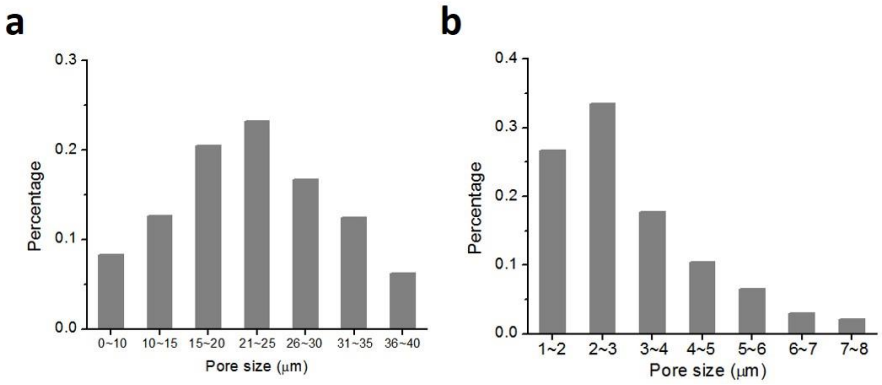


**Fig. 5.13** Diameter distribution of gelatin nanofibers on PDMS frame. (a) 2 min electrospinning time. (b) 5 min electrospinning time.

The electrospun nanofibers were dry in vacuum overnight and sputtered with a thin layer of gold for nanofiber diameter characterization by SEM. Diameter profile is shown in **Fig. 14**. The diameters of all nanofibers are in the range from 0.25~0.65 μm with a majority (~77%) in a narrow range from 0.35~0.5 μm.

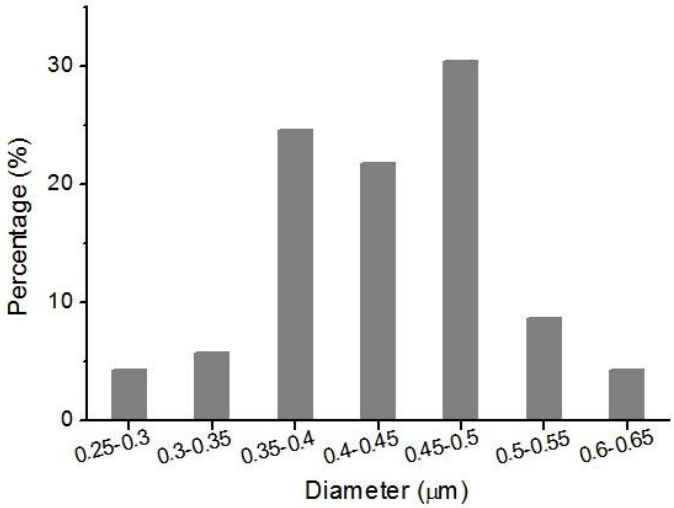


**Fig. 5.14** Diameter distribution of gelatin nanofibers after drying in vacuum.

After gelatin nanofibers were dried in vacuum overnight to evaporate the remaining solvent, the PDMS substrate with gelatin nanofibers was transferred to an oven for thermo-crosslinking of gelatin nanofibers at 140 ℃ for 4 h. Citric acid was used as a corsslinker between gelatin proteins via the formation amide bonds in high temperature. After crosslinking, samples were used without further treatment. **Fig. 15**

shows the final PDMS frame supported gelatin nanofibers network. Compared with gelatin nanofiber before thermo-crosslinking, there are nearly no changes in the morphology, pore size and diameter of nanofibers after thermo-crosslinking. Our results reveals that the morphology of gelatin nanofibers can be well kept during thermo-crosslinking process, much better than the EDC/NHS crosslinking methods which will destroy the original morphology of nanofibers.

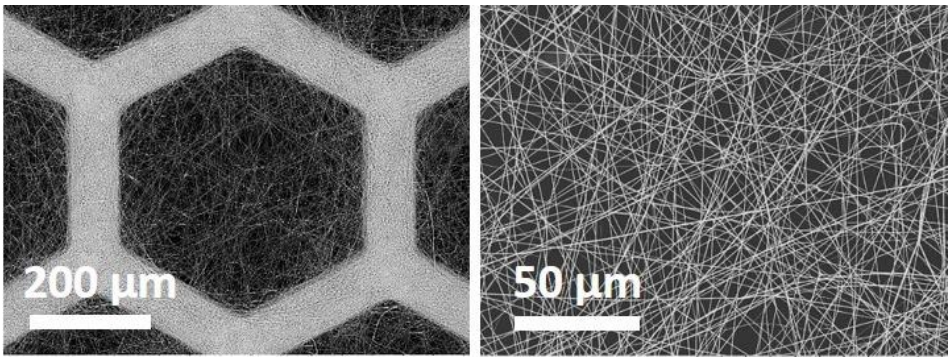


**Fig. 5.15** SEM images of gelatin nanofibers after thermo-crosslinking.

## 5.3 Cell based assays

### 5.3.1 Culture and seeding of hiPSCs

HiPSCs were cultured in a tissue culture plate (TCP) coated with 5 µg/mL of vitronectin (Life Technologies, France) in complete E8 medium under 37℃ in 5% $CO_2$ in a humidified incubator. The medium was refreshed every day until the cells reached to about 80% confluence. After treatment with DPBS solution containing 0.5 mM EDTA at 37℃ for 4 min, cells were then detached from TCP by gentle aspiration to form small colonies for passage or by repeated aspiration to generate single cells for counting and seeding on patches. To promote the adhesion of hiPSCs on gelatin fibers, the culture patches were coated with 1 or 5 µg/mL of vitronectin in DPBS, and then placed in a 12-well plate. $1.5\times10^5$ hiPSCs in 50 µL E8 medium containing 10 µM Y-27632 (ROCK inhibitor, Life technologies, France) were dropped carefully on the culture patch and then incubated under 37℃ in 5% $CO_2$ in a humidified incubator for 1 h for cell adhesion. Afterwards, a fresh 1 ml of E8 medium was gently added in each

well. **Fig. 5.16** shows the typical hiPSCs morphology on gelatin nanofiber patch 1 day after seeding. On patches treated with 5 μg/mL of vitronectin, hiPSCs tend to form monolayer cell colonies while, on patches treated with 1 μg/mL of vitronectin, hiPSCs tend to form EB. The reason for different hiPSCs morphologies has been explained in **Chapter 4**.

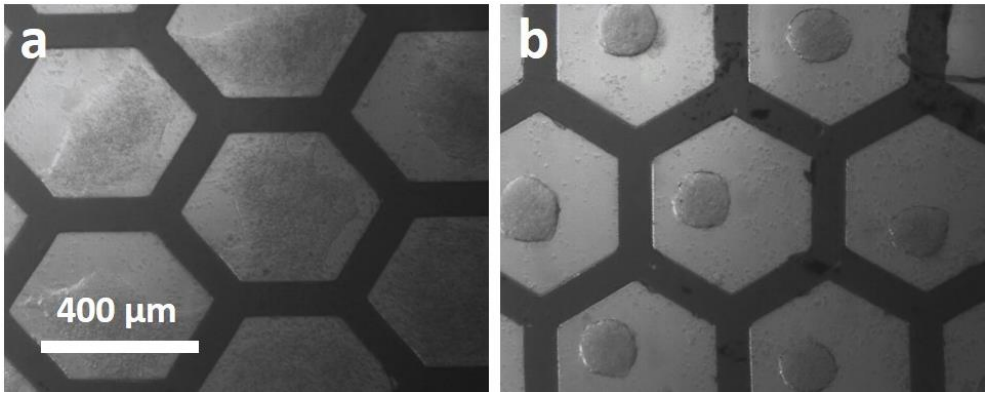


**Fig. 5.16** Bright field photographs of (a) monolayer and (b) EB of hiPSCs on PDMS/gelatin nanofiber patch.

## 5.3.2 Cell viability assay

Cell viability is an important criterion for cell culture patch. Indeed, cell culture patch should be biocompatible and provide necessary support or promotion for cell adhesion and proliferation. Thus we assessed the viability and proliferation of hiPSCs cultured on patches by MTT assay.

MTT assay is used for a quantified measurement of cell viability for 1, 2 and 3 days culture. MTT reacts with dehydrogenases, indicators of cell viability, in mitochondrion to form formazan which can be quantified by microplate reader. Cell viability is calculated based on the absorbance intensity of formazan in DMSO. Briefly, cells were seeded on 12-well plate and gelatin nanofibers patch at a density of $5 \times 10^4$ per well. After 1, 2 and 3 days incubation, 50 μL of MTT solution (5mg/mL in PBS) was added into each well, followed by further 4 h incubation. The incubation medium was replaced by 200 μL DMSO to dissolve resulted formazan. Cell proliferation is evaluated by cell viability based on the absorbance of each well at 490 nm. The results are shown in **Fig. 5.17**. Compared with tissue culture plate, hiPSCs exhibit higher

proliferation ability on PDMS/gelatin nanofiber patch. The total viability of cells after 1, 2 and 3 days culture are 1.12, 1.46 and 1.61 times of those on TCP, respectively. The results show that gelatin nanofibers patch can obviously promote cell proliferation.

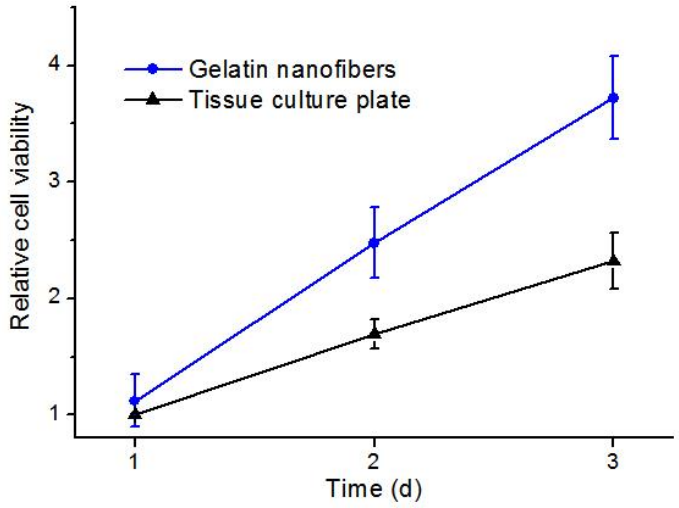


**Fig. 5.17** Relative cell viability of hiPSCs on tissue culture plate and PDMS/gelatin nanofibers patch.

### 5.3.3 Pluripotency of hiPSCs

To evaluate the stemness of hemisphere EBs generated on our PDMS supported gelatin nanofiber substrate, pluripotent stem cell markers SOX2 and TRA-1-60 were used to stain the hiPSCs. SOX2 is a transcription factor that is essential for maintaining self-renewal, or pluripotency of undifferentiated stem cells. TRA-1-60 (Podocalyxin) is a pluripotent stem cell-specific protein expressed on the surface of induced pluripotent stem cells.

HiPSCs were fixed with 4% PFA for 15 min, permeabilized with 0.5% Triton X-100 for 30 min, blocked with 1% BSA for 30 min. Then cells were stained with primary antibodies (anti-SOX2 in rat and anti-TRA-1-60 in mouse IgM) at 4℃ overnight, second antibodies (Alexa Fluor 594 goat anti-mouse IgM and Alexa Fluor 488 donkey anti-rat) at room temperature for 1 h and DAPI at room temperature for 30 min. Finally the cells were characterized under confocal microscope and the results are shown in **Fig. 5.18**. The immunofluorescence results showed a typical hiPSC-like staining pattern on both hiPSCs monolayer and EB, revealing that the expression of these markers was

maintained. The results confirm that the formation of monolayer and EBs on gelatin nanofiber patch does not affect the pluripotency of hiPSCs.

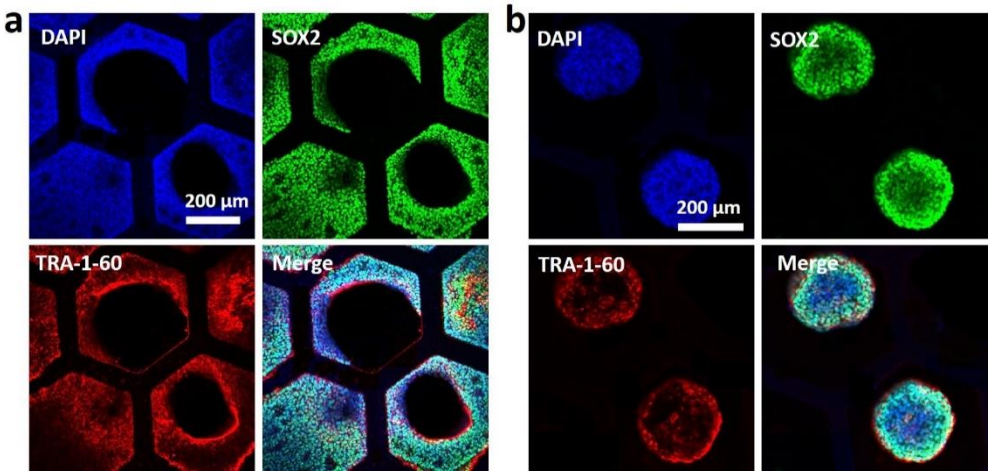


**Fig. 5.18** Fluorescence images of hiPSCs in monolayer and EB for pluripotency staining

## 5.3.4 Cardiac differentiation

Cardiomyocytes differentiation was conducted according to GiWi protocol developed by Lian et al, by modulating Wnt signaling with small molecules [30]. As shown in **Fig. 5.19a**, differentiation started by replacement of E8 medium with RPMI 1640 medium containing B27 minus insulin and 12 µM CHIR99021. After 24h treatment of CHIR99021 with cells, the medium was replaced with RPMI 1640 medium with B27 minus insulin. 72 h after addition of CHIR99021, RPMI 1640 medium containing B27 minus insulin and 5 µM IWP2 was added to replace previous medium. At day 5 of differentiation, the medium was replaced by new RPMI 1640 medium containing B27 minus insulin. Then every 3 days, RPMI 1640 medium containing B27 medium was added to replace previous medium. With the same protocol, hiPSCs cultured on glass slide were differentiated into cardiomyocytes at the same time as a control. Cell morphology during differentiation was recorded by an inverted microscope, shown in **Fig. 5.19b**.

Cell contraction is observed usually at day 7 or day 8 after differentiation. On PDMS/gelatin nanofiber patch, cell contraction occurs in large continuous area and

shows high uniformity, while on glass slide contraction happens only in several separate small zones and exhibits obvious nonuniformity.

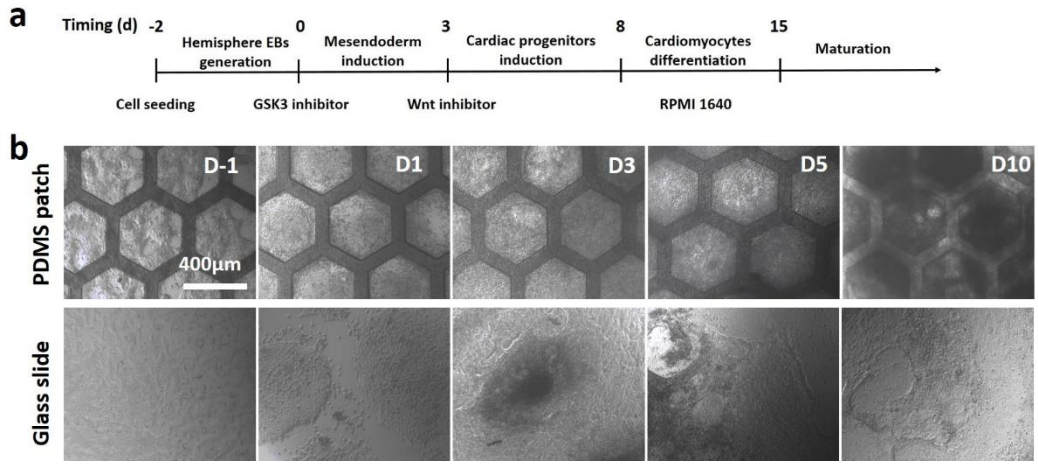


**Fig. 5.19** (a) A schematic protocol for the differentiation of cardiomyocytes from hiPSCs; (b) Bright-field images of the typical morphology at day -2, day 0, day 1, day 3, day 5 and day 10.

## 5.3.5 Immunostaining

Cells were further cultured for maturation in RPMI 1640 medium containing B27. To assess the expression of cardiomyocytes related proteins, the differentiated cells on both porous gelatin nanofiber patch and glass slide at day 20 were stained with cardiomyocytes related antibodies.

Briefly, cells were fixed with 4% PFA for 15 min, permeabilized with 0.5% Triton X-100 for 30 min, blocked with 5% goat serum for 1h. Then cells were stained with primary antibodies (anti-α-actinin and anti-cardiac muscle myosin in mouse, and anti-TnnT2 and anti-Connexin 43 in rabbit) at 4℃ overnight, second antibodies (Alexa Fluor 488 goat anti-mouse and Alexa Fluor 633 goat anti-rabbit) at room temperature for 1 h and DAPI at room temperature for 30 min.

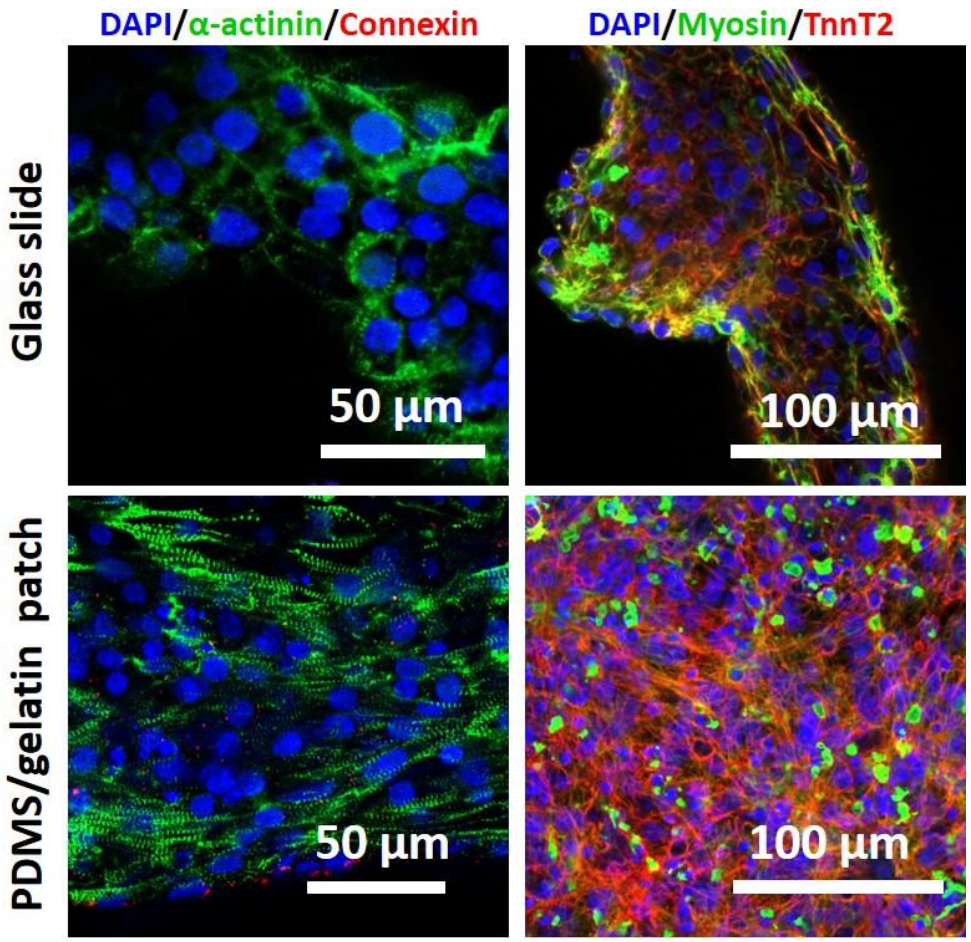


**Fig. 5.20** Immunofluorescence staining images of cardiomyocytes derived from hiPSCs on PDMS/gelatin nanofiber patch and glass slide.

All the samples were characterized under a Zeiss 710 confocal microscope. The results are shown as **Fig. 5.20**. TnnT2, a highly cardiomyocytes-specific protein, is positive for the cells differentiated on gelatin nanofiber patch, while on glass slide, the expression of TnnT2 shows extremely low, which indicates a more mature cardiac cell state gelatin nanofiber patch. Cardiac myosin is a cardiac muscle-specific protein involved in active force generation. An increasing expression of Myosin on PDMS/gelatin nanofiber patch is found compared to that on glass slide. Immunostaining of α-actinin and connexin43 is also achieved. Striated sarcomeres (α-actinin positive) can be observed for the differentiated cells on both gelatin nanofiber patch and glass slide. Connexin43, for staining gap junction, plays a significant role in the coordination of cells contraction, which shows more positive on PDMS/gelatin nanofiber patch.

## 5.3.6 Calcium imaging

Cardiac muscle contraction occurs at day 7 or day 8 after differentiation and become stable after 20 days. Cardiac muscle contraction is initiated by the sudden rise of cytosolic $Ca^{2+}$ concentration which also dominates the contraction frequency and strength of cardiac tissue. So by measuring the fluctuation profile of $Ca^{2+}$ concentration in the cytosol, we can assess cardiac contraction performance. **Fig. 5.21** is typical fluorescence intensity profile recorded from cardiac tissues on glass slide and PDMS/gelatin nanofiber patch. Different zones of a cardiac tissue were measured, shown as 1, 2 and 3. As can be seen from the results (**Fig. 5.21a**), the fluctuation of the fluorescence intensities in zone 1, 2 and 3 is notably irregular, indicating the large variation of $Ca^{2+}$ concentration in cytosol. Besides, the contraction frequency varies obviously among the three zones. **Fig. 5.21b** shows a typical fluorescence profile recorded during calcium imaging experiment of a cardiac tissue on PDMS/gelatin nanofiber patch. In three typical zones recorded, the fluorescence intensities fluctuate regularly, revealing the regular change of cytosolic $Ca^{2+}$ and thus the contraction strength. Besides, the recorded fluorescence has a uniform sparking rate estimated to be 87 per minute, which is in the normal range (60-100/min) of human heart beating rate. This cardiac beating rate on PDMS/gelatin nanofiber patch is faster than that on porous PCL patch, indicating the possibility of scaffolds in affecting cardiac tissue contraction quality.

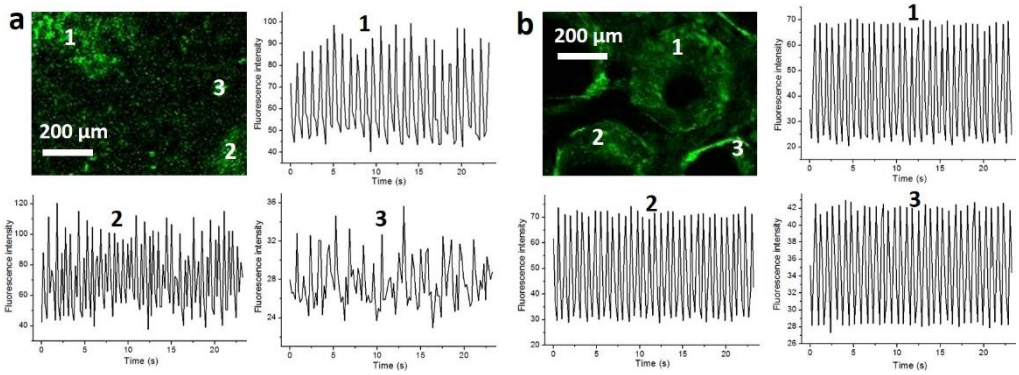


**Fig. 5.21** Calcium imaging of hiPSCs derived cardiomyocytes on a) glass slide and b) PDMS/gelatin nanofiber patch. For each sample, three typical zone (shown as 1, 2 and 3) were

selected for recording the fluorescence intensity during cardiac contraction.

### 5.3.7 Electric stimulation

Electrophysiological functionality is an important characteristic of engineered cardiac constructs. Electrical field stimulation has proposed to improve cell differentiation, alignment and functional properties, and is considered crucial for the generation of synchronously contracting cardiac cells. On the molecular level, electrical stimulation has induced a rise in myosin heavy chain levels, which correlates with the contractile velocity of cardiac muscle, and increased the production of gap junction protein connexin-43.

In order to conduct the electrical stimulation on hiPSCs derived cardiomyocytes, we make a simple stimulation chamber which can well match our gelatin nanofiber patch. An electrochemical workstation is used as electrical stimulus source. The illustration of overall experimental setup is shown in **Fig. 5.22a**. The cardiac patch is placed in culture dish of 35 mm in diameter. Two platinum filaments are used as electrodes shown in orange. The information of electrical impulse is shown in **Fig. 5.22b**. We applied a series of 1 Hz electrical impulse in the range from -10 ~ 10 V on the cardiomyocytes and recorded their contractile information by Calcium imaging. Results are shown in **Fig. 5.22c**. Cardiac contraction rate keeps stable except for stimulus of -1 and -2 V with obvious increases. Then we focused on stimulus of -1 V for further test. Voltage is set with -1V and frequency is 2 Hz. As can be seen in **Fig. 5.22d**, an increase in stimulus frequency significantly accelerates cardiac contraction. However, the cardiac contraction rate is not stable but gradually changes. As can be seen from **Fig. 5.22e,f**, under 0.5 Hz stimulation cardiomyocytes contraction rate is consistent with stimulation frequency at the beginning and gradually returns to its normal rate.

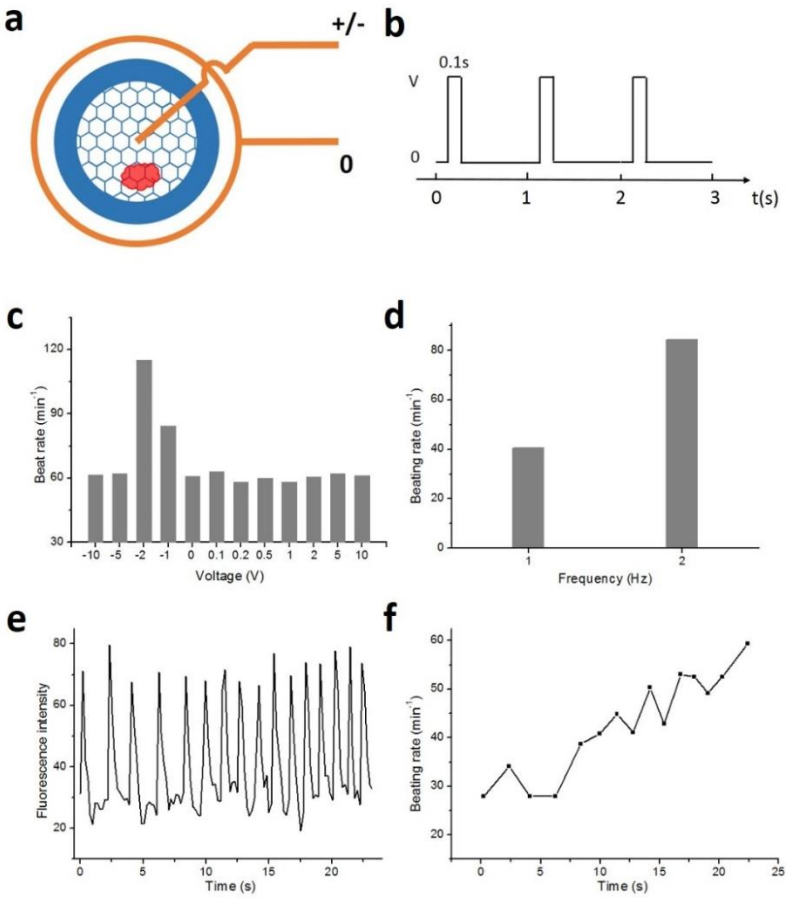


**Fig. 5.22** Electrical stimulation of hiPSCs derived cardiac tissue on PDMS/gelatin nanofiber patch. (a) Illustration of electrical stimulation setup. (b) Illustration of electrical impulse. (c) Beating rates of cardiac tissue stimulated under a series of voltages and 1Hz frequency. (d) Beating rates of cardiac tissue stimulated under voltage of 1V and frequencies of 1 and 2 Hz. (e) Fluorescence intensity of cardiac tissue stimulated under 1V and 0.5Hz. (f) Beating rate change of cardiac tissue during stimulation of 1V and 0.5 Hz.

## 5.3.8 Drug test

Previous drug development are hampered by high failure rates attributed to the reliance on non-human animal models for safety and efficacy testing, which arouses a fundamental problem that non-human animal models cannot adequately represent human biology. So hiPSCs derived cardiomyocytes has great advantages over non-human ones in providing more convincing data in drug development.

In order to analyze the feasibility of hiPSCs derived cardiomyocytes for drug test,

we use two drugs isoproterenol (ISP) and propranolol (PRO) which have known effects on cardiomyocytes functionality to increase and decrease the cardiac contraction rate, respectively. Briefly, cardiomyocytes on PDMS/gelatin nanofibers patch were incubated with fluo-4 for calcium imaging in order to measure the contraction rate. Then Tyrode's salt was added to replace the incubation solution. Cardiomyocytes were incubated with drugs at different concentrations and then were characterized for calcium imaging to obtain the contraction rate. The results are shown in **Fig. 5.23**. Isoproterenol, a beta-agonist, was introduced to the cells with gradually increased concentrations, which leads to a dose-dependent increase of contraction rate. Then the addition of different concentrations of propranolol, a beta-blocker, resulted in a dose-dependent decrease of contraction rate. The above results of cardiac drug tests indicated a good drug reaction and functional performance of the cardiomyocytes generated on PDMS/gelatin nanofiber patch.

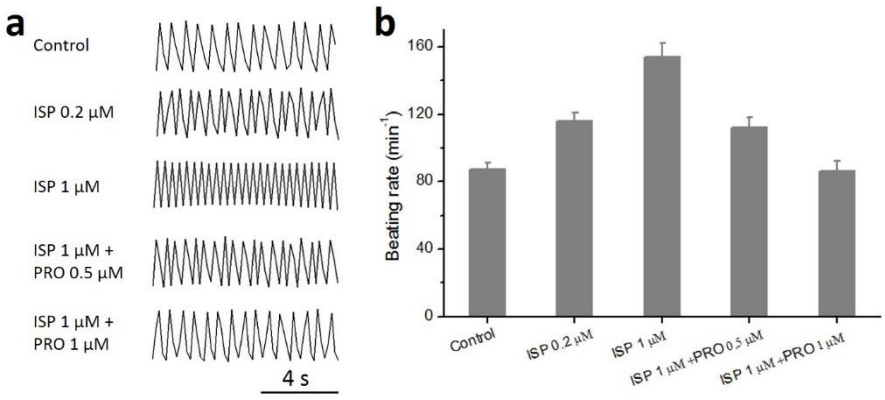


**Fig. 5.23** Drug test of cardiac patch. (a) Fluorescence intensity in calcium imaging showing the effect and dosage dependency of cardiac drug ISP and PRO. (b) Cardiac beating frequency as a function of the concentration of ISP and PRO.

## 5.3.9 Deformation of PDMS frame

The monolayer of gelatin nanofibers is gradually degraded by cells and finally replaced by generated cardiac tissue. The cardiac tissue attaches on the elastic PDMS honeycomb frame and avoidably deforms the underneath PDMS honeycomb frame

during contraction. **Fig. 5.24** shows the deformation of three kinds of PDMS honeycomb frames in one contraction cycle. For PDMS frame with feature size 100 μm, there is nearly no displacement of PDMS honeycomb frame between contraction and relax of cardiac tissue, as is shown by the white arrow in **Fig. 5.24a,d**. For PDMS frame with feature size 50 μm, there is slight displacement of PDMS honeycomb frame in contractile cycle of cardiac tissue (**Fig. 5.24**). For PDMS frame with deformed honeycomb pattern, there is obvious displacement of PDMS honeycomb frame between contraction and relax of cardiac tissue, as is shown by the white arrow in **Fig. 5.24c,f**.

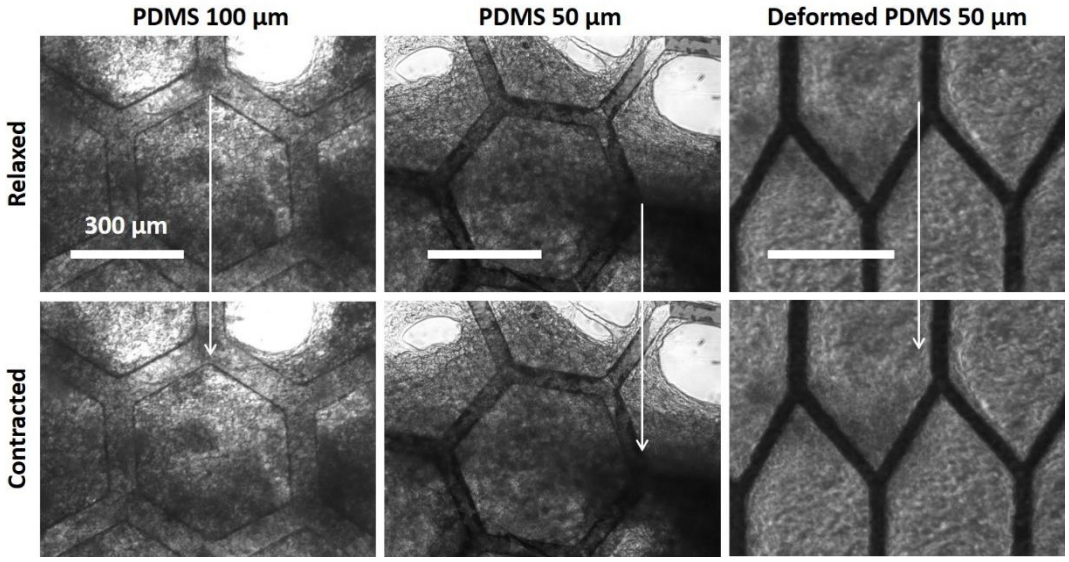


**Fig. 5.24** Deformation of three elastic PDMS frames during cardiac contraction.

We have demonstrated that Young's Modulus of the PDMS frames differs in different directions. We further investigated the effects of the direction-dependent Young's Modulus of PDMS frames exerted on the contraction of cardiac tissue. We have found that on PDMS frames with feature sizes 50 and 100 μm, random direction of contraction of cardiac tissues is observed, while on deformed PDMS frame with feature size 50 μm, the direction of contraction of cardiac tissue is well organized in the direction with smallest Young's Modulus. This phenomenon can be explained as follow: for PDMS frames with feature sizes 50 and 100 μm, the variation of their Young's Modulus is small in all directions, but for deformed PDMS frame, there is sharp disparity of Young's modulus in different directions. So cardiac tissue prefers to contract in the direction with smallest Young's modulus due to its ease to be deformed,

as is shown in **Fig. 5.25**.

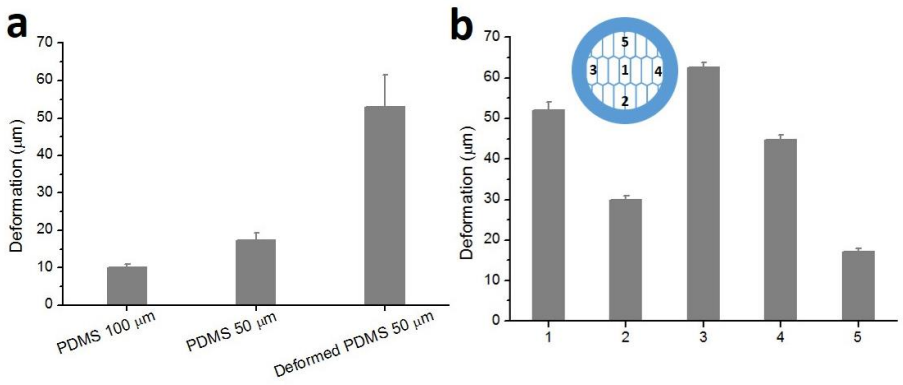


**Fig. 5.25** (a) Deformation amplitude of three elastic PDMS frames during cardiac contraction. (b) Deformation amplitudes of different regions in deformed PDMS frame.

## 5.4 Conclusion

We have demonstrated a method to fabricate soft culture patch made of an elastic frame in PDMS and a monolayer of gelatin nanofibers for cardiac differentiation from hiPSCs. The honeycomb shaped PDMS frame is generated by micro-fabrication methods with precise size. The monolayer of gelatin nanofibers is electrospun on the PDMS frame with ~62% porosity and major pore sizes less than 5 μm. The as-fabricated patch is highly compatible to hiPSCs culture and proliferation. Besides, the immunostaining results show a good maintenance of the pluripotency of hiPSCs on the surface of patch. We have generated cardiac tissue with higher contraction strength and a higher beating homogeneity comparing to the conventional approaches. The immunostaining results of generated cells show higher expression of cardiac specific proteins on the soft gelatin patch than that on glass substrate. Calcium imaging demonstrates a homogeneous contraction of hiPSCs derived cardiac tissues. The electric stimulation and drug test have demonstrated the feasibility and versatility of our cardiac patch for advanced biomedical applications. The engineered elasticity of PDMS frame has a regulatory effect on guiding cardiac contraction.

# Reference


1. R. Lozano, M. Naghavi, K. Foreman, S. Lim, K. Shibuya, V. Aboyans, J. Abraham, T. Adair, R. Aggarwal, and S.Y. Ahn, *Global and regional mortality from 235 causes of death for 20 age groups in 1990 and 2010: a systematic analysis for the Global Burden of Disease Study 2010.* The Lancet, 2013. **380**(9859): p. 2095-2128.
2. K.D. Kochanek, S.L. Murphy, J. Xu, and E. Arias, *Mortality in the united states, 2013*. 2014, US Department of Health and Human Services, Centers for Disease Control and Prevention, National Center for Health Statistics.
3. K.B. Margulies, A.F. Hernandez, M.M. Redfield, M.M. Givertz, G.H. Oliveira, R. Cole, D.L. Mann, D.J. Whellan, M.S. Kiernan, and G.M. Felker, *Effects of liraglutide on clinical stability among patients with advanced heart failure and reduced ejection fraction: a randomized clinical trial.* Jama, 2016. **316**(5): p. 500-508.
4. J. Young and R. Mills, *Clinical Management of Heart Failure. Professional Communications*. 2001, Inc.
5. F.Y. Chen and L.H. Cohn, *The surgical treatment of heart failure. A new frontier: nontransplant surgical alternatives in heart failure.* Cardiology in review, 2002. **10**(6): p. 326-333.
6. C. Martinez, A. Tzur, H. Hrachian, J. Zebede, and G.A. Lamas, *Pacemakers and defibrillators: recent and ongoing studies that impact the elderly.* The American journal of geriatric cardiology, 2006. **15**(2): p. 82-87.
7. J. Narula, N. Haider, R. Virmani, T.G. DiSalvo, F.D. Kolodgie, R.J. Hajjar, U. Schmidt, M.J. Semigran, G.W. Dec, and B.-A. Khaw, *Apoptosis in myocytes in end-stage heart failure.* New England Journal of Medicine, 1996. **335**(16): p. 1182-1189.
8. L. Nordgren and S. Sörensen, *Symptoms experienced in the last six months of life in patients with end-stage heart failure.* European Journal of Cardiovascular Nursing, 2003. **2**(3): p. 213-217.
9. E. Kaba, D.R. Thompson, P. Burnard, D. Edwards, and E. Theodosopoulou, *Somebody else's heart inside me: a descriptive study of psychological problems after a heart transplantation.* Issues in mental health nursing, 2005. **26**(6): p. 611-625.
10. R.W. Evans, D.L. Manninen, L.P. Garrison, and A.M. Maier, *Donor*

*availability as the primary determinant of the future of heart transplantation.* Jama, 1986. **255**(14): p. 1892-1898.

11. G.Y. Koh, M.G. Klug, M.H. Soonpaa, and L.J. Field, *Differentiation and long-term survival of C2C12 myoblast grafts in heart.* Journal of Clinical Investigation, 1993. **92**(3): p. 1548.
12. M.G. Klug, M.H. Soonpaa, G.Y. Koh, and L.J. Field, *Genetically selected cardiomyocytes from differentiating embronic stem cells form stable intracardiac grafts.* Journal of clinical investigation, 1996. **98**(1): p. 216.
13. W. Roell, Z.J. Lu, W. Bloch, S. Siedner, K. Tiemann, Y. Xia, E. Stoecker, M. Fleischmann, H. Bohlen, and R. Stehle, *Cellular cardiomyoplasty improves survival after myocardial injury.* Circulation, 2002. **105**(20): p. 2435-2441.
14. J. Müller-Ehmsen, K.L. Peterson, L. Kedes, P. Whittaker, J.S. Dow, T.I. Long, P.W. Laird, and R.A. Kloner, *Rebuilding a damaged heart.* Circulation, 2002. **105**(14): p. 1720-1726.
15. J. Müller-Ehmsen, P. Whittaker, R.A. Kloner, J.S. Dow, T. Sakoda, T.I. Long, P.W. Laird, and L. Kedes, *Survival and development of neonatal rat cardiomyocytes transplanted into adult myocardium.* Journal of molecular and cellular cardiology, 2002. **34**(2): p. 107-116.
16. J.A. Thomson, J. Itskovitz-Eldor, S.S. Shapiro, M.A. Waknitz, J.J. Swiergiel, V.S. Marshall, and J.M. Jones, *Embryonic stem cell lines derived from human blastocysts.* science, 1998. **282**(5391): p. 1145-1147.
17. H. Jawad, N. Ali, A. Lyon, Q. Chen, S. Harding, and A. Boccaccini, *Myocardial tissue engineering: a review.* Journal of tissue engineering and regenerative medicine, 2007. **1**(5): p. 327-342.
18. P. Zammaretti and M. Jaconi, *Cardiac tissue engineering: regeneration of the wounded heart.* Current opinion in biotechnology, 2004. **15**(5): p. 430-434.
19. K. Takahashi and S. Yamanaka, *Induction of pluripotent stem cells from mouse embryonic and adult fibroblast cultures by defined factors.* cell, 2006. **126**(4): p. 663-676.
20. K. Takahashi, K. Okita, M. Nakagawa, and S. Yamanaka, *Induction of pluripotent stem cells from fibroblast cultures.* Nature protocols, 2007. **2**(12): p. 3081-3089.
21. C. Shi, Q. Li, Y. Zhao, W. Chen, B. Chen, Z. Xiao, H. Lin, L. Nie, D. Wang, and J. Dai, *Stem-cell-capturing collagen scaffold promotes cardiac tissue regeneration.* Biomaterials, 2011. **32**(10): p. 2508-2515.

22. J. Leor, Y. Amsalem, and S. Cohen, *Cells, scaffolds, and molecules for myocardial tissue engineering.* Pharmacology & therapeutics, 2005. **105**(2): p. 151-163.
23. J. Radhakrishnan, U.M. Krishnan, and S. Sethuraman, *Hydrogel based injectable scaffolds for cardiac tissue regeneration.* Biotechnology advances, 2014. **32**(2): p. 449-461.
24. Z. Ma, M. Kotaki, R. Inai, and S. Ramakrishna, *Potential of nanofiber matrix as tissue-engineering scaffolds.* Tissue engineering, 2005. **11**(1-2): p. 101-109.
25. Y. Tang, L. Liu, J. Li, L. Yu, L. Wang, J. Shi, and Y. Chen, *Induction and differentiation of human induced pluripotent stem cells into functional cardiomyocytes on a compartmented monolayer of gelatin nanofibers.* Nanoscale, 2016. **8**(30): p. 14530-14540.
26. P.J. Mackenzie, R.M. Schertzer, and C.M. Isbister, *Comparison of silicone and polypropylene Ahmed glaucoma valves: two-year follow-up.* Canadian Journal of Ophthalmology/Journal Canadien d'Ophtalmologie, 2007. **42**(2): p. 227-232.
27. R. Bellucci, *An introduction to intraocular lenses: material, optics, haptics, design and aberration*, in *Cataract*. 2013, Karger Publishers. p. 38-55.
28. C.-H. Wong, M. Samuel, B.-K. Tan, and C. Song, *Capsular contracture in subglandular breast augmentation with textured versus smooth breast implants: a systematic review.* Plastic and reconstructive surgery, 2006. **118**(5): p. 1224-1236.
29. D. Pugliese, D. Bush, and T. Harrington, *Silicone synovitis: longer term outcome data and review of the literature.* JCR: Journal of Clinical Rheumatology, 2009. **15**(1): p. 8-11.
30. X. Lian, J. Zhang, S.M. Azarin, K. Zhu, L.B. Hazeltine, X. Bao, C. Hsiao, T.J. Kamp, and S.P. Palecek, *Directed cardiomyocyte differentiation from human pluripotent stem cells by modulating Wnt/β-catenin signaling under fully defined conditions.* Nature protocols, 2013. **8**(1): p. 162.

# Chapter 6

# Conclusion and perspective

Tis thesis work aimed at the development of multidimensional scaffolds for improved cell culture and stem cell derived tissue engineering, which can be used for drug assays in pharmaceutical industry, disease model and treatment as well as regenerative medicine. By using different fabrication techniques, functional scaffolds have been obtained and used to demonstrate their high potential in cell processing and clinical applications.

Firstly, we applied a 3D printing technique to produce a lattice type micro-frame in PEGDA and then filled the free-space of the lattice with gelatin gel. After freezing and drying, a hybrid 3D scaffold made of gelatin porous structures and PEDGA backbone was obtained. As expected, the PEGDA/porous gelatin scaffold showed not only robust mechanical strength but also high porosity with cellular pore size. The high porous gelatin scaffold possessed high water holding ability and favorable degradation in physiological conditions. Cell tests demonstrated a high cell compatibility and viability and faster cell proliferation than that on culture dish. The highly porous scaffolds show high support for cell migration due to the interconnected pores. We also prove that the scaffolds can promote the culture and neuronal differentiation of neural progenitor cells, in which the porous gelatin structure is helpful for neuron network formation.

Then, we demonstrated a 2D porous PCL membrane supported by a PEGDA porous honeycomb frame by combined methods of self-organization and microfabrication for improved cell performance. The porous PCL patch was used to mimic the fibrous ECM. The as-fabricated substrate possessed high porosity with uniform pores mainly less than 5 μm, which is suitable for cell seeding and continuous culture. Honeycomb PEGDA frame showed good control of shape and film integrity during self-assembly, and also provided easy handling for routine characterization and application. Cell culture studies demonstrated that cells showed high tendency to attach and spread on the substrates. The high porosity provided more access for cells to uptake nutrients from medium, thus improving cell performance on porous PCL patch like proliferation and gene transfection. IPSCs cultured on the porous PCL patch can keep their pluripotency and showed higher viability and proliferation than those on glass substrates. The porous PCL patch was also demonstrated to improve the cardiac differentiation of iPSCs in terms of cardiac connection, contraction strength and

homogeneity. The porous PCL patch also showed controlled biodegradation, holding great potential for *in vivo* applications.

Finally, we demonstrated a method to fabricate soft culture patch made of an elastic frame in PDMS and a monolayer of gelatin nanofibers for cardiac differentiation from human induced pluripotent stem cells. The honeycomb shaped PDMS frame was generated by micro-fabrication methods. Then, a monolayer of gelatin nanofibers was electrospun on the PDMS frame with ~62% porosity and major pore sizes less than 5 μm. The as-fabricated patch was highly compatible to hiPSCs culture and proliferation. Besides, the immunostaining results showed a good maintenance of the pluripotency of hiPSCs on the surface of patch. As expected, we achieved a cardiac generation with higher contraction strength and a higher beating homogeneity comparing to the conventional approaches. The immunostaining results of generated cells showed higher expression of cardiac specific proteins on the soft gelatin patch than that on glass substrate. Calcium imaging demonstrated a homogeneous contraction of hiPSCs derived cardiac tissues. The electric stimulation and drug test demonstrated the feasibility and versatility of our cardiac patch for advanced applications in pharmaceutics and regenerative medicine. The elasticity of PDMS frame can be engineered to guide cardiac tissue contraction.

Altogether, we have successfully demonstrated several functional scaffolds for advanced studies in cell biology and tissue engineering. Our work has demonstrated the utility of hybrid scaffolds for micro-tissue engineering which could impact the future studies in the fields of tissue engineering, drug screening and regenerative medicine.

This thesis work is limited to proof-of-concepts studies. More systematic investigations are expected for better evaluation on the feasibility and efficacy of the functional scaffolds we proposed for drug development and tissue engineering applications. We believe in the high application potential of these approaches due to the versatility of device form and fabrication and the high compatibility of the protocol to different cell-based assays.

First of all, lithography methods have been developed and used very successfully by semiconductor industry for many years but they are mainly based on photolithography and selective etch of semiconductor and other inorganic materials.

However, these conventional lithography techniques have low compatibility for natural biomaterial processing and it is unexpected to make for large scale applications such as scaffold manufacturing. Instead, nonconventional lithography techniques developed more recently are plausible since they rely essentially on casting and molding of polymer and their resolution and product rate can be pretty high. The problem is that much less efforts have been devoted to the study of high resolution and high biocompatibility pattern replication. In addition, the casting and molding of biopolymers are generally time consuming and material-type dependent. Moreover, the biomedical applications are variable which require different processing protocols but it is often difficult to identify real killer applications so that no big industry would be engaged for a large scale development. The chicken-egg paradox is the *de facto* psychological blocker. The culture patch method was proposed to overcome this difficulty since it can be easily generalized for both large scale manufacturing and large scale applications.

3D printing is promising to produce structures or scaffolds in a flexible way. Although high resolution features could be printed by two-photo-polymerization, its production rate remains pretty low. Other 3D printing techniques still faces low printing resolution and limited printable biomaterials, especially for natural polymers such as proteins and polysaccharides with weak mechanical strength. Besides, key parameters in freeze-drying are not well understood to recover the fibrous structure of ECM proteins like gelatin and collagen. Although electrospinning is very powerful, the uniform deposition of fibers on patch is difficult to achieve. Electrospun fibers vary from batch to batch in fiber diameter, deposition density and fiber mat porosity.

The ideal tissue engineering system allows generated tissues to replace the implanted scaffolds, which needs the scaffolds to be biodegradable in a safe metabolic way with controlled rate. Although gelatin is already a natural biodegrade material, the pure gelatin and most other natural polymers lack enough mechanical strength in physiological conditions. Alternative biodegradable materials replacing PEGDA are highly desired in porous frame fabrication, such as poly(lactic-co-glycolic acid) (PLGA) and other similar polyester synthetic polymers, which currently are difficult to fabricate due to lack of facile techniques.

The elastic materials like PDMS are highly desired to fabricate smart scaffolds

with stiffness gradient or antistrophic Young's Modulus for directed growth and contraction guidance of cardiac tissue. Such kind of smart scaffold can also be engineered to measure the cardiac contraction force.

The tissue generating scaffolds can also be integrated with microfluidics for organ-on-a-chip based disease modeling, drug test, and other biomedical studies, as is shown in **Fig. 6.1a**. An organ-on-a-chip is a microfluidic cell culture device created with chip manufacturing methods that contains continuously perfused chambers inhabited by living cells arranged to simulate tissue- and organ-level physiology. By recapitulating the multicellular architectures, tissue-tissue interfaces, physicochemical microenvironments and vascular perfusion of the body (**Fig. 6.1b**), these devices produce levels of tissue and organ functionality not possible with conventional culture systems. They also enable high-resolution, real-time imaging and *in vitro* analysis of biochemical, genetic and metabolic activities of living cells in a functional tissue and organ context. This technology has great potential to advance the study of tissue development, organ physiology and disease etiology. In the context of drug discovery and development, it should be especially valuable for the study of molecular mechanisms of action, prioritization of lead candidates, toxicity testing and biomarker identification.

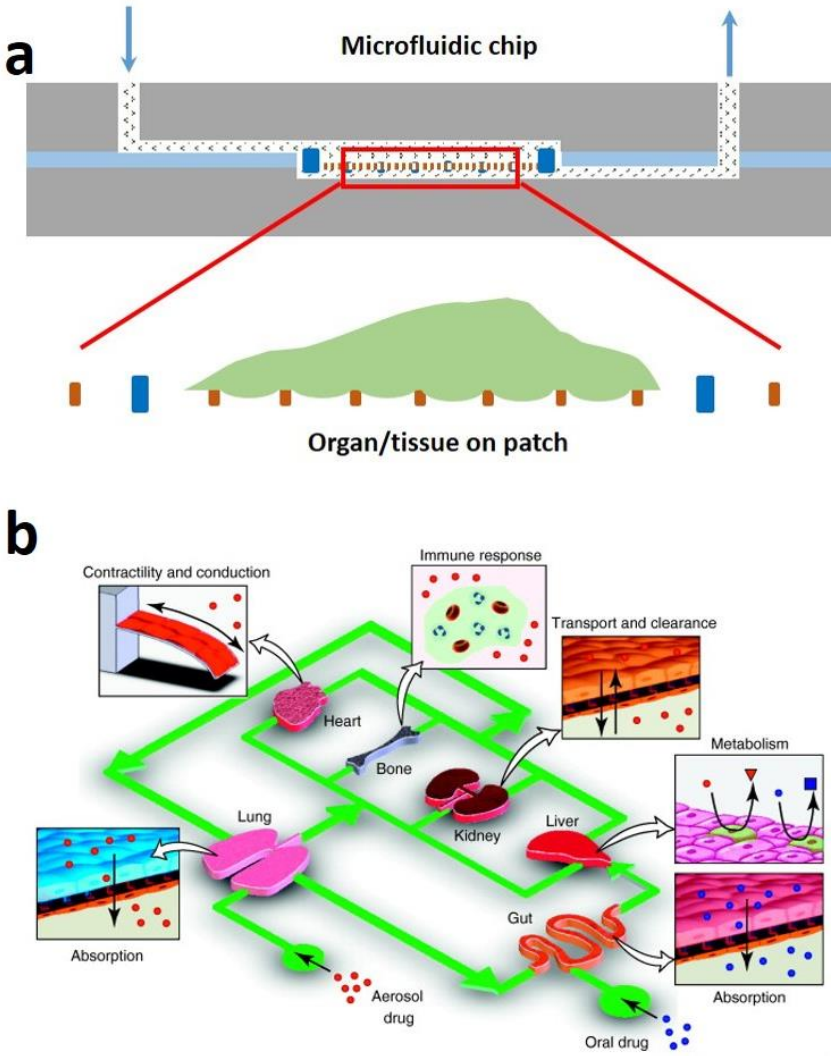


**Fig. 6.1** (a) A scheme of organ/tissue on culture patch integrated in a microfluidic chip for dynamic organ/tissue maintenance. (b) A schematic illustration of human body-on-chip model [1].

# Reference

1. D. Huh, G.A. Hamilton, and D.E. Ingber, *From 3D cell culture to organs-on-chips.* Trends in cell biology, 2011. **21**(12): p. 745-754.

# Appendix A

## Patterned parylene C for cell adhesion, spreading and alignment studies

In this chapter, we will present a study of cell performance on parylene C substrates with different patterns. We will first describe the fabrication of parylene C substrates with different patterns (pillar and stripe). Then we will present the results of cell adhesion and spreading on the above patterned substrates and flat parylene C films. Further we will show the contact guidance effects of parylene C stripes with different pitch sizes on cell alignment growth by cell orientation, nuclear deformation and cell elongation.

## A.1 Introduction

The interaction between cells and extracellular matrix (ECM) is one of the most interesting research topics in cell biology, which deserves a great emphasis of both material and bioengineering communities. Indeed, the ECM can effectively regulate cell adhesion, spreading, migration, proliferation and differentiation [1-3]. For in-vitro studies, the physicochemical properties of culture substrates (composition, stiffness and topography) can be designed to control cell-material interactions [4-12]. For example, topographical features such as grooves, ridges and pillars can be used to elucidate the effect of contact guidance [13, 14] whereas the stiffness of substrates can be modulated to direct stem cell lineage specification [15]. Furthermore, the chemical properties including the surface charge and the wettability can be changed to affect cell adhesion and other cell functions [11, 16].

The great impacts of ECM exerts on cell performance has drawn increasing attention by researchers in tissue engineering, in order to engineer *in vitro* functional substrates for specific objectives. Of particular interest is patterning polymeric biomaterials for cell culture studies [17-19]. Poly-(chloro-p-xylene), also known as parylene C, is a biocompatible and biostable polymer widely used for insulating coating of implantable biomedical devices [20]. The high molecular weight, all carbon backbone, and non-polarity characteristics make parylene C chemically inert and non-biodegradable. Parylene C also has extremely low permeability to moisture and corrosive gases due to uniform and defect-free deposition. In addition, parylene C is able to deposit on different substrates such as metals, glass, Si wafer and plastic [21,

22]. All these merits have strengthened its in-vivo applications. However, the interaction between cells and parylene C has not been well understood yet and recent studies mainly focus on the use of parylene C as peel-off stencils for deposition of biomolecular patterns [21, 23-25]. Only a few studies investigated cell behavior on plasma treated parylene C [19, 26].

In this work, we fabricated parylene C pillar and stripe arrays for cell culture studies. We first deposited parylene C on a lithography patterned mold by chemical vapor deposition. Then, we transferred the mold pattern to a glass slide by peeling-off and bonding, followed by air plasma treatment to make the parylene C pattern hydrophilic. We show that the as-deposited parylene C on a flat substrate does not support cell adhesion but the plasma treated parylene C is readily useful for cell culture. We also show that pillars made of parylene C can improve the adhesion but has little effect on cell spreading. Finally, we show the effect of contact guidance of cells on parylene C stripes with a pitch size dependent performance.

## A.2 Parylene C pattern fabrication

### A.2.1 Fabrication process

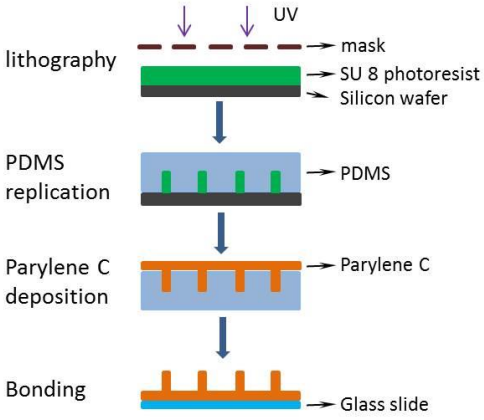


**Fig. A.1** A schematic fabrication flowchart of parylene C patterns including SU 8 photo lithography, PDMS soft lithography, parylene C deposition and glass slide bonding.

Parylene C pattern generation is based on microfabrication methods. The

fabrication process is shown in **Fig. A.1**, which includes three main steps:

### a) PDMS mold fabrication

Micropatterns were designed using L-Edit and generated on a chrome plate by a Micro Pattern Generator (μPG 101, Heidelberg Instruments), followed by resist development, chemical etching in a chrome etchant solution and sonication cleansing in acetone for 5 min . A 7 μm SU-8 photoresist layer was spin-coated on a silicon-wafer, exposed with UV light through the chrome mask and developed, as is shown in **Fig. A.2**. After an air plasma treatment for 2 min, the resist pattern was exposed in Trimethylchlorosilane (TMCS) for 10 min to facilitate mold release. Then, a PDMS pre-polymer (RTV 615 A + B, Momentive Performance Materials Incorporation) at a ratio of 1:10 (B:A) was cast with a typical thickness of 5 mm. After degassing in a vacuum chamber for 30 min, the PDMS pre-polymer was cured at 80℃ for 2 h. The PDMS stamp was then peeled off, treated with air plasma and coated with polyethylene glycol (PEG 2k) to facilitate mold release, as is shown in **Fig. A.3**.

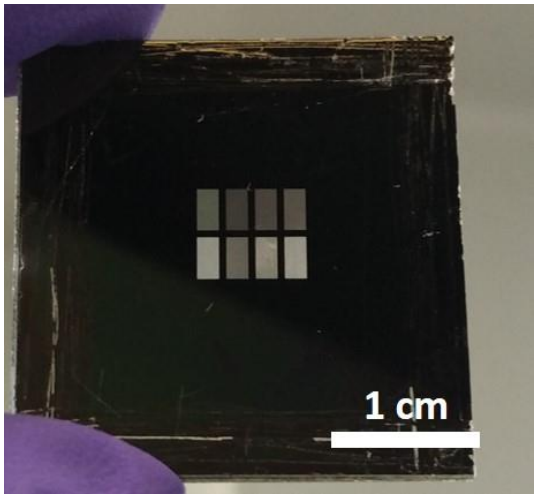


**Fig. A.2** Photograph of SU-8 photoresist master after TMCS treatment.

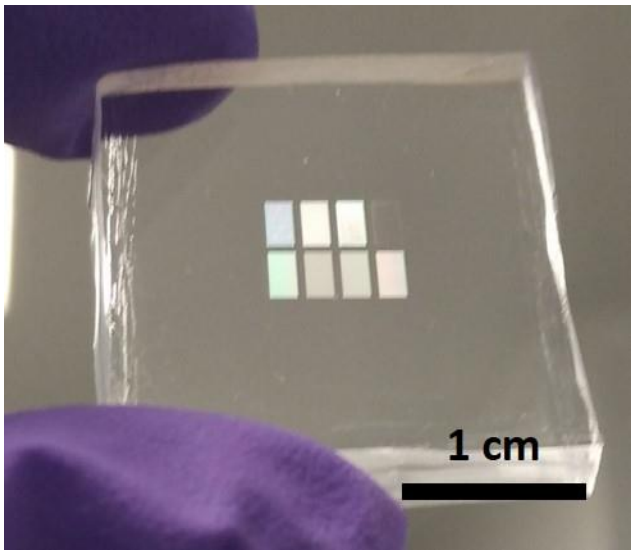


**Fig. A.3** Photograph of PDMS mold after PEG coating.

### b) Parylene C deposition on PDMS mold

By using a Labcoater Parylene Deposition System (Model 2010E, SCS Ltd., UK), 3 μm thick parylene C was deposited on a PDMS mold. Briefly, a cooling system was started and a pyrolysis chamber was preheated. 4.95 g (1.65 g/μm according to manufacturer's guide) of parylene C dimer in an Aluminum boat was transferred to a loading chamber. After sample loading, vacuum system was started. The deposition process started when the system pressure was under critical value. At the beginning of deposition, parylene C dimers were heated, sublimed, and then pyrolized into monomers in the pyrolysis chamber. The active monomers polymerized uniformly on any surface they meet in the deposition chamber to form a transparent parylene C membrane. The deposition process stopped when all parylene C dimers were used up or the pressure was over the critical point.

### c) Glass slide bonding

To transfer the parylene C layer from PDMS to glass, a Norland optical adhesive was dropped on a glass slide and the parylene-coated PDMS layer was pressed against the slide. After UV exposure, the PDMS mold was peeled off, resulting in a substrate patterned with parylene C, as is shown in **Fig. A.4**. After 2 min of oxygen plasma treatment to improve hydrophilicity, the parylene C patterns can be used for cell studies.

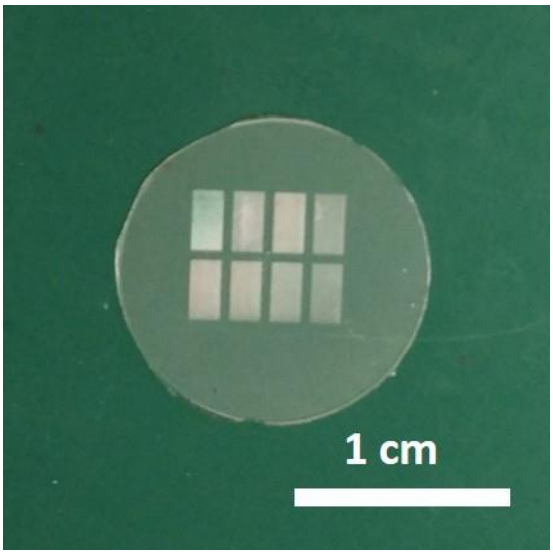


**Fig. A.4** Photograph of parylene C pattern sample after bonding with glass slide (diameter 15 mm).

Studies show that parylene C patterns can be used as peel-off stencils cell culture and cell patterns formation. Such kind of parylene C patterns are mostly fabricated by reactive ion etching (RIE) on flat substrates [23, 25] which is time-consuming and inflexible. Here, parylene C patterning is achieved in an alternative way by pattern replication with PDMS soft lithography. Originally the obtained PDMS mold is highly sticky to deposited parylene C. To facilitate the peel-off and repeated use of the PDMS mold, PEG (MW 2k) coating is introduced which effectively prevents sticking of parylene C to PDMS. Comparing with the RIE-based techniques, our method is more robust, less time-consuming and easier for the fabrication of high parylene C patterns. Four types of parylene C substrates, including plain (pPCm) and plasma treated (ptPCm) parylene C membranes, parylene C micropillars (PCmp) and microstripes (PCms), are studied in this work.

## A.2.2 SEM observation

The fabricated parylene C pattern is examined using a scanning electron microscope (SEM, Hitachi TM3030) with an accelerating voltage of 15 kV. All samples were deposited with a 10 nm thick Au layer by sputtering before SEM observation.

PPCm and ptPCm are flat due to the uniform parylene C deposition (**Fig. A.5a, d**). PCmp are pillar arrays of 7 μm height, 3 μm width and 2 μm pitch size (**Fig. A.5b, e**). PCms are stripes of 7 μm height, 5 μm width and 10 μm pitch size (**Fig. A.5c, f**). These patterns are defined to have sizes and pitch sizes suited for cell adhesion, spreading and migration studies.

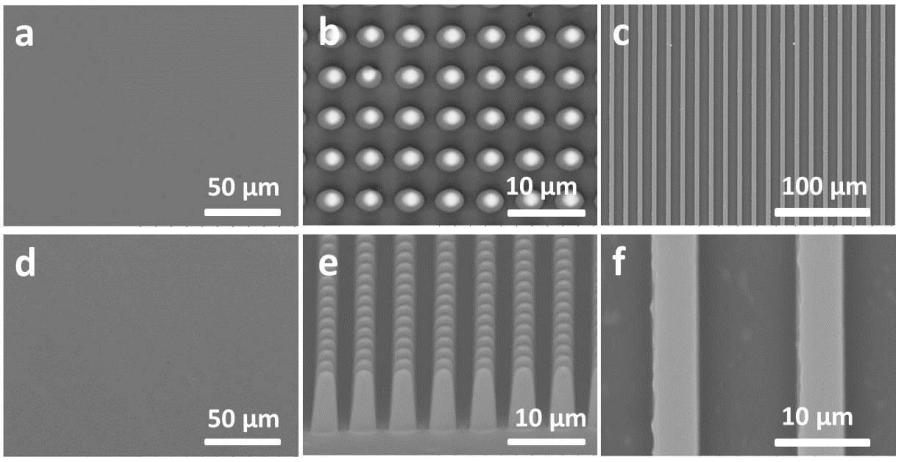


**Fig. A.5** SEM images of parylene C patterns. (a) Plain and (d) plasma treated parylene C films. (b) Top view and (e) front view of parylene C pillar arrays. (c,f) Parylene C stripes.

## A.3 Cell culture studies

NIH 3T3 cells were cultured in Dulbecco's Modified Eagle Medium (DMEM) supplemented with 10% Fetal Bovine Serum (FBS) and 1% penicillin/streptomycin at 37 ℃ with 5% $CO_2$. When cells reach 80~90% confluence, they were dissociated with Trypsin at 37 ℃ for 3 min. After centrifugation at 1000 rpm for 5 min, cells were collected by removing the supernatant medium. At the same time 0.1 μL of cells can be counted with a commercially available hemocytometer. With centrifuge and counting, cells can be resuspended in fresh medium to a specific density for seeding.

### A.3.1 Gelatin coating on parylene C film

Parylene C substrates are tested for ECM protein adsorption. Gelatin, from the

richest protein Collagen in ECM, was used as a model protein. Parylene C film was treated with oxygen plasma against a stripe pattern mask with the same feature size and pitch size being 100 μm. Gelatin was dissolved in DI water and conjugated with a fluorescent dye FITC for 2 h under stirring at room temperature. Then parylene C film was immersed in the above gelatin-FITC solution for 1h at room temperature, washed with PBS three times and characterized under Zeiss Observer Z1 fluorescence microscope.

**Fig. A.6a** shows an alternative bright and dark stripes pattern of gelatin-FITC coated parylene C substrate under fluorescent microscope. Area with bright stripes is treated with plasma while dark area is without plasma treatment. Results show that the plasma treated area is much brighter than that without plasma treatment, with the fluorescence intensity twice higher than that without plasma treatment shown in **Fig. A.6b**.

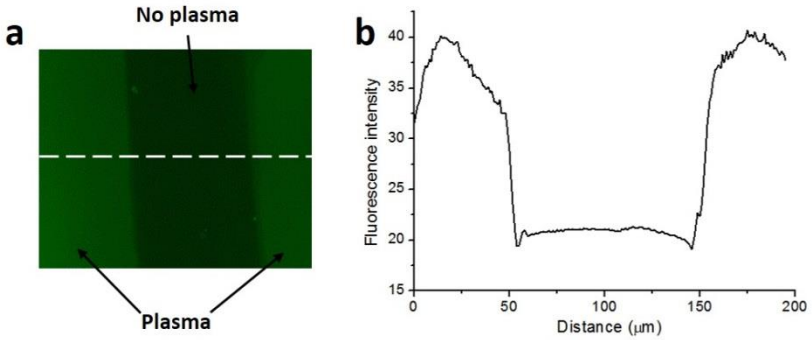


**Fig. A.6** Gelatin-FITC coating on plain and plasma treated parylene C film. (a) Fluorescence image of parylene C film after protein coating. (b) Fluorescence intensity of parylene C film marked by white dots line.

## A.3.2 Cell adhesion and spreading

The fabricated parylene C substrates are used for cell culture. First these substrates were sterilized with 70% ethanol and UV exposure. Then they were washed thoroughly in DPBS to remove remnant ethanol. Cells were seeded at a density $5\times10^4$ cells/mL for each sample. After 2 days culture, cells were fixed with 4% PFA for 15 min, dehydrated gradually in ethanol twice (50%, 60%, 70%, 80%, 90% and 100%, each for 10 min),

and dried in vacuum overnight. Then the cells were sputtered with 10 nm thick Au layer and characterized with SEM (**Fig. A.7**).

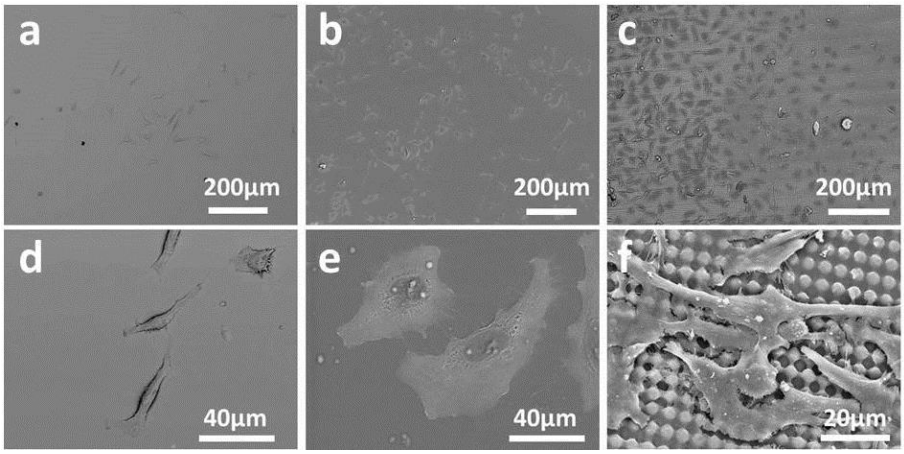


**Fig. A.7** SEM images of Hela cells cultured on (a,d) plain Parylene C films, (b,e) plasma treated parylene C films and (c,f) Parylene C pillar arrays. A, b and c are typical images of Hela cells in wide scope. D,e and f are typical images of individual Hela cells.

On pPCm, only a few cells can be found, which show a great repugnance to spread and look like worms with clear ridges, as they usually do in a tissue culture plate (**Fig. A.7a, d**). On ptPCm, cells show a high tendency to spread (**Fig. A.7b, e**). On PCmp, the cell spreading is less important than that on ptPCm and they tend to stretch more pseudopods to grasp the substrate (**Fig. A.7c, f**). Statistical results show that the average cell size on ptPCm is about 2100 μm2, which is about 6 and 3 times larger than those on pPCm and PCmp, respectively (**Fig. A.8a**). Cell density also depends on the type of the pattern: it is nearly the same on ptPCm and PCmp but about 5 times higher than that on pPCm. The disparities of cell size and cell density on the above substrates can be explained as follows: (1) plasma treatment makes parylene C more hydrophilic which facilitates deposition of ECM proteins of the medium and thus the cell adhesion and spreading; (2) pPCm is hydrophobic which leads to denaturation of the ECM proteins and thus less cell adhesion and spreading [27]; (3) PCmp, although hydrophobic, can provide more anchoring sites for cells to grasp and thus facilitates cell adhesion and spreading, as can be seen from the different number of pseudopods on PCmp and pPCm. As shown in **Fig. A.8b**, ptPCm also supports Hela cell proliferation with a similar rate compared with that in a culture dish (similar doubling time ~ 24 h).

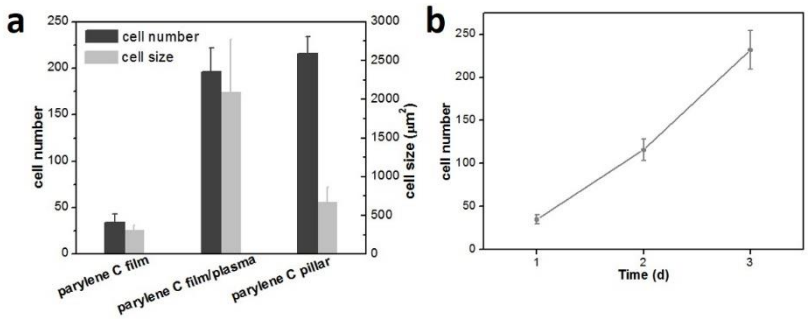


**Fig. A.8** (a) Statistical results of cell number and cell size on plain parylene C film, plasma treated parylene C film and parylene C pillar array. (b) Proliferation of Hela cells cultured on plasma treated parylene C films for 1, 2 and 3 days, respectively.

## A.3.3 Cell alignment

### A.3.3.1 PCms with different pitch sizes

As we know, cells growth can be directed by the structure cues on culture substrates. Here we use PCms to direct cell alignment growth. When cells grow along with a stripe for specific orientation, the neighboring stripes also have a chance to interact with cells, thus change the final cell orientation. We believe pitch size of PCms plays a key role in the interaction of cells and stripes. In order to clarify the effects PCms exerted on cell alignment pattern formation, we set the feature size of PCms to be 5μm with a series of pitch sizes (1, 2, 5, 7, 9, 10, 15 and 19μm). The SEM results of PCms with different pitch sizes are shown in **Fig. A.9**. Considering cell size to be around 20 μm, we believe the number of stripes in PCms interacting with cells will decrease with the increase of pitch size s from 1 to 19 μm.

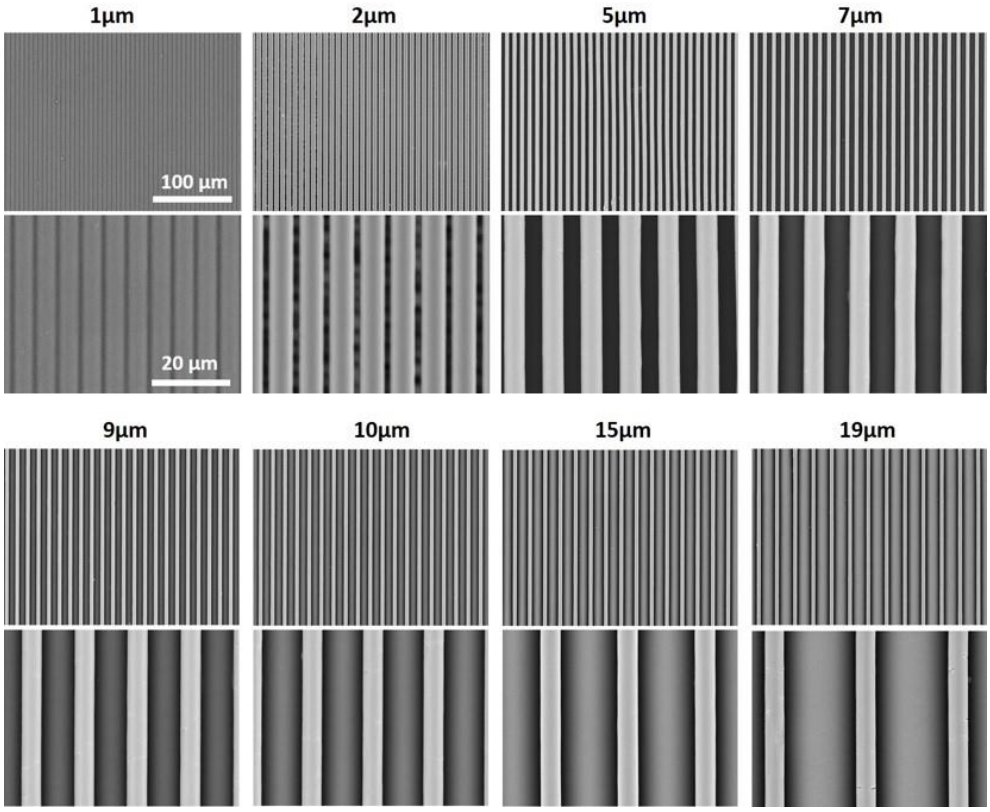


**Fig. A.9** SEM images of PCms with different pitch sizes (1, 2, 5, 7, 9, 10, 15 and 19 μm).

### A.3.3.2 Immunostaining and SEM observation of cells on PCms

The fabricated PCms were treated with oxygen plasma and seeded with NIH 3T3 cells. After cells were cultured for 1 day, cells were fixed with 4% PFA for 15 min, permeabilized with 0.5% Triton X-100 for 30 min, blocked with 1% BSA for 30 min and stained with Phalloidin- FITC and DAPI for fluorescence imaging which was conducted on a Zeiss Observer Z1 fluorescence microscope.

Cellular actin filaments were stained in green, shown in **Fig. A.10**, to investigate the cell orientation. For PCms with 1μm pitch size, cells were spreading on the substrate with random orientation as they usually do in traditional tissue culture plate. Cells can easily spread over several stripes. The failure of cell orientation on such substrate is probably due to the extremely small pitch size which is too small for cells to sense. When the pitch size increases to 2 μm, cells started to elongate and show directed growth orientation. However, in this substrate cells still can spread over neighboring stripes. When the pitch size increases to 5 μm, cells showed obvious elongation and high directed growth orientation with few cells spreading over neighboring stripes.

When the pitch size in the range of 7~10 μm, all the cells were elongated and grew in highly orientated direction guided by stripes, which is probably due to the minimal interaction with neighboring stripes caused by the large pitch size for cells to reach. When the pitch size further increases to 15 and 19 μm, cells continue to show elongated shape with a small portion of cells showing different orientation.

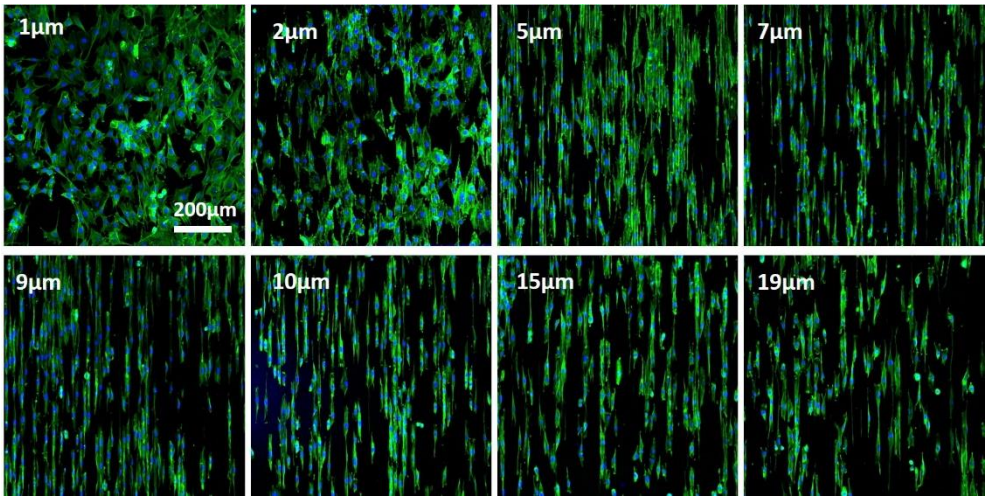


**Fig. A.10** Fluorescence images of NIH 3T3 cells cultured on PCms with different pitch sizes (1, 2, 5, 7, 9, 10, 15 and 19 μm).

After dehydration, cells morphology on PCms was characterized by SEM. The results are shown in **Fig. A.11**. On PCms with 1μm pitch size, cells spread with random orientation over several neighboring stripes. When pitch size increases from 2 μm to 7 μm, cells spread over decreasing number of stripes while showing increasing elongation. When the pitch size increased in the range of 9 to 19 μm, cells dropped into the grooves between two neighboring stripes. For pitch size 9 and 10 μm which is relatively narrow for cells to spread except for one direction, cells can only spread along the this direction, thus showing high consistent orientation. For pitch size 15 and 19 μm which is relatively free for cells to spread in other direction, most cells kept in the same direction with a small portion showing a slight deviated orientation.

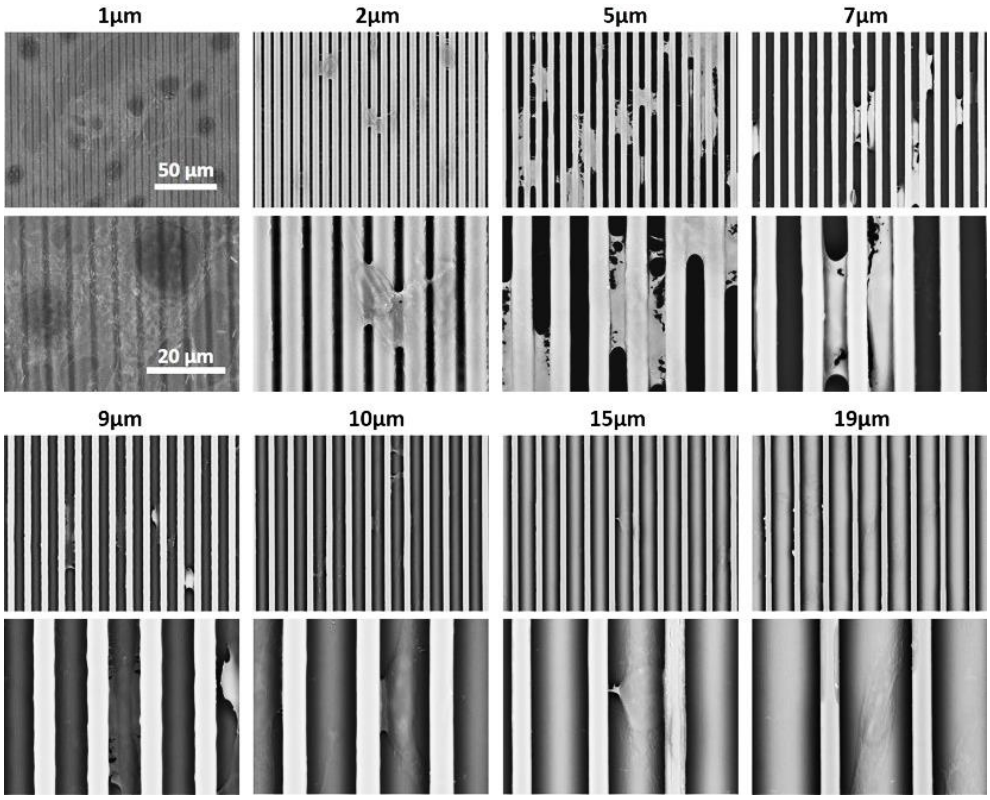


**Fig. A.11** SEM images of NIH 3T3 cells culture on PCms with different pitch sizes (1, 2, 5, 7, 9, 10, 15 and 19 μm).

### A.3.3.3 Cell growth orientation

We then did the statistical studies to quantify cell orientation performance, as is shown in **Fig. A.12**. Cell orientation was measured by its deviation from the direction of PCms defined as orientation angle. For pitch size from 1 μm to 9 μm, the degree of cell orientation increases with increasing cells exhibit low orientation angle which is less than 10 °. For pitch size from 9 μm to 19 μm, the degree of cell orientation decreases with decreasing cells exhibiting low orientation angle which is less than 10 ° and increasing number of cells with high orientation angle. Results shows that pitch sizes 7 μm and 9 μm are the optimal parameters in our PCms for cell orientation.

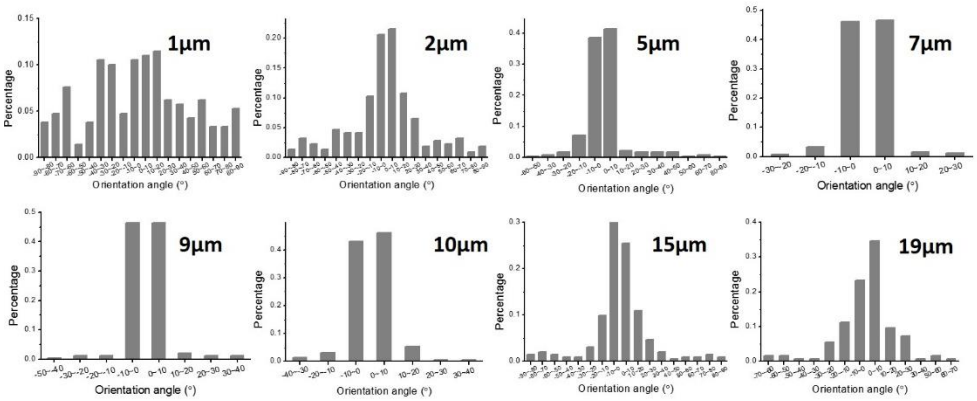


**Fig. A.12** Cell growth orientation on PCms with different pitch sizes (1, 2, 5, 7, 9, 10, 15 and 19 μm) after 2 days incubation.

### A.3.3.4 Nuclear deformation

The degree of cells elongation is measure by both the deformed nuclei aspect ratio and cell elongation length, as is shown in **Fig. A.13**. First we measure the aspect ratio of deformed nuclei. For pitch size from 1 μm to 7 μm, major cells show increasing elongation degree of cell nuclei from 1~1.5, 1.5~2 to 2.5~3. For pitch size from 9 μm to 19 μm, major cells show decreasing elongation degree of cell nuclei from 2~2.5, 1.5~2 to 1~1.5. So pitch size 7 μm is the best in our PCms for cell nuclei deformation.

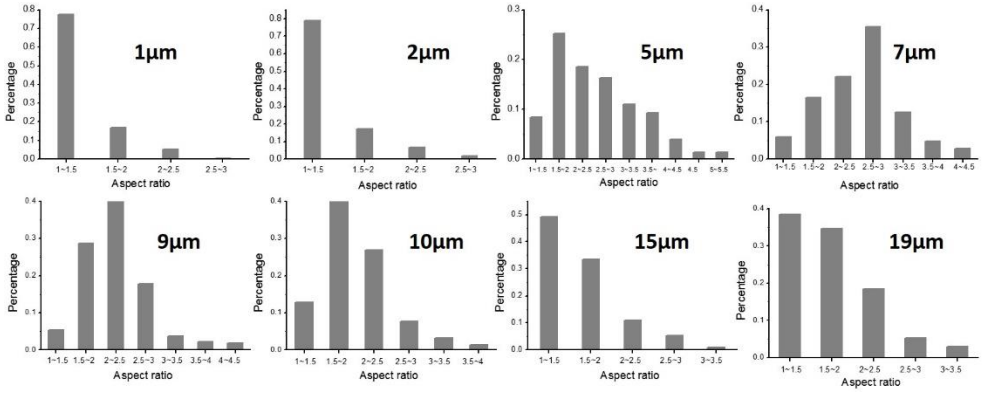


**Fig. A.13** Cell nuclei deformation on PCms with different pitch sizes (1, 2, 5, 7, 9, 10, 15 and 19 μm) after 2 days incubation.

### A.3.3.5 Cell elongation

Then we measured the cell elongation length, as is shown in **Fig. A.14**. For pitch size from 1 μm to 7 μm, major cells show increasing elongation length from 75~100

μm, 100~125 μm to 175~200 μm. For pitch size from 9 μm to 19 μm, major cells show decreasing elongation length from 125~150 μm to 100~125 μm. So pitch size 7 μm is the best in our PCms for cell elongation.

Based on the analysis of cell orientation, cell nuclei deformation and cell elongation, PCms with pitch size 7 μm is the best one for cell alignment study.

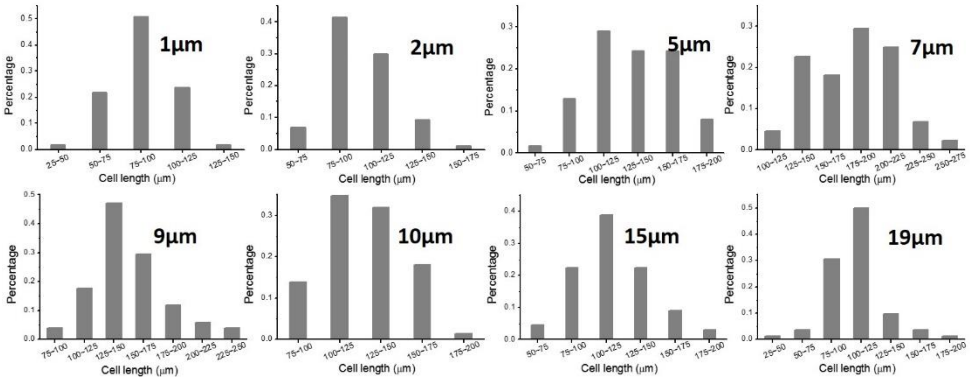


**Fig. A.14** Elongated cell length on PCms with different pitch sizes (1, 2, 5, 7, 9, 10, 15 and 19 μm) after 2 days incubation.

### A.3.2.6 Cell alignment in continuous culture

Then we study whether PCms can will support other cell lines alignment growth and keep cell alignment during long time cell culture. **Fig. A.15** shows the fluorescence images of Hela cells cultured for 1, 2 and 3 days respectively. Typically, cells on day 1 exhibit random cell skeleton stretch on ptPCm (**Fig. A.15a**) but elongated shapes along the stripes on PCms. On days 2 and 3, cells grow keeping the elongated shapes and alignment. **Fig. A.15e–h** show SEM images of the cell morphology after dehydration. Clearly, most cells are elongated along the stripe ridge while stretching toward neighboring stripes and few cells are trapped between stripes. Statistical results show that more than 70% of the cells grow with orientation angles less than 10 °and only ~ 10% of the cells have orientation angles more than 20 °in days 1–3 (**Fig. A.16a**). Finally, the proliferation behavior on PCms is similar to that on ptPCm (**Fig. A.16b**).

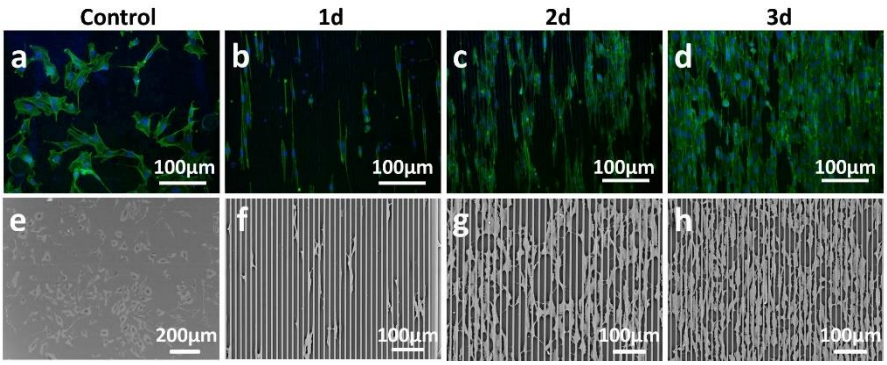


**Fig. A.15** (a-d) Fluorescence images of Hela cells cultured on plasma treated parylene C film and parylene stripe for 1, 2 and 3 days. (e-h) SEM images of Hela cells cultured on plasma treated parylene C film and Parylene C stripe for 1, 2 and 3 days.

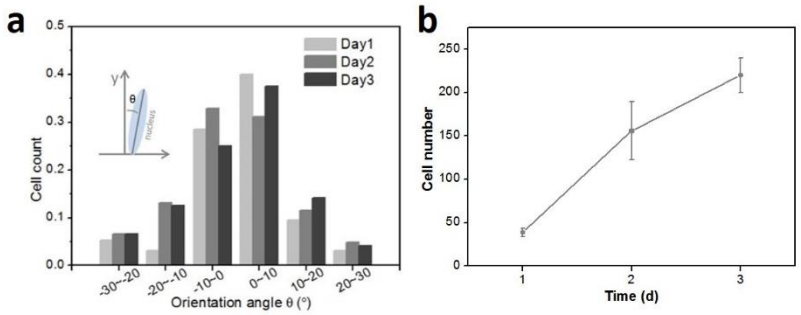


**Fig. A.16** (a) Orientation of cells cultured on parylene C stripe substrates for 1, 2 and 3 days. (b) Proliferation of Hela cells cultured on parylene C stripe substrates for 1, 2 and 3 days, respectively.

## A.4 Conclusion

We have fabricated parylene C patterns by chemical vapor deposition and thin layer transfer techniques. Our results show that the as-deposited parylene C on a flat substrate does not support cell adhesion due to its hydrophobic surface while air plasma treated parylene C is readily useful for cell adhesion and spreading studies. Parylene C pillars without air plasma treatment can improve the adhesion but have little effect on cell spreading. As expected, parylene C stripes have a strong effect of contact guidance. Thus, we demonstrate an easy fabrication of parylene C micro-patterns as well as their usefulness for cell behavior studies, which should be beneficial to improve the

performance of implantable medical devices.

# Reference


1. H.S. Dhowre, S. Rajput, N.A. Russell, and M. Zelzer, *Responsive cell–material interfaces.* Nanomedicine, 2015. **10**(5): p. 849-871.
2. X. Yao, R. Peng, and J. Ding, *Cell–material interactions revealed via material techniques of surface patterning.* Advanced Materials, 2013. **25**(37): p. 5257-5286.
3. W.F. Liu and C.S. Chen, *Engineering biomaterials to control cell function.* Materials Today, 2005. **8**(12): p. 28-35.
4. P.M. Davidson, H. Özçelik, V. Hasirci, G. Reiter, and K. Anselme, *Microstructured Surfaces Cause Severe but Non‐Detrimental Deformation of the Cell Nucleus.* Advanced Materials, 2009. **21**(35): p. 3586-3590.
5. K. Kolind, A. Dolatshahi-Pirouz, J. Lovmand, F.S. Pedersen, M. Foss, and F. Besenbacher, *A combinatorial screening of human fibroblast responses on micro-structured surfaces.* Biomaterials, 2010. **31**(35): p. 9182-9191.
6. Z. Pan, C. Yan, R. Peng, Y. Zhao, Y. He, and J. Ding, *Control of cell nucleus shapes via micropillar patterns.* Biomaterials, 2012. **33**(6): p. 1730-1735.
7. D.E. Discher, P. Janmey, and Y.-l. Wang, *Tissue cells feel and respond to the stiffness of their substrate.* Science, 2005. **310**(5751): p. 1139-1143.
8. J. Fouchard, D. Mitrossilis, and A. Asnacios, *Acto-myosin based response to stiffness and rigidity sensing.* Cell adhesion & migration, 2011. **5**(1): p. 16-19.
9. R.T. Justin and A.J. Engler, *Stiffness gradients mimicking in vivo tissue variation regulate mesenchymal stem cell fate.* PloS one, 2011. **6**(1): p. e15978.
10. B.G. Keselowsky, D.M. Collard, and A.J. García, *Surface chemistry modulates fibronectin conformation and directs integrin binding and specificity to control cell adhesion.* Journal of Biomedical Materials Research Part A, 2003. **66**(2): p. 247-259.
11. K. Webb, V. Hlady, and P.A. Tresco, *Relative importance of surface wettability and charged functional groups on NIH 3T3 fibroblast attachment, spreading, and cytoskeletal organization.* Journal of biomedical materials research, 1998. **41**(3): p. 422.

12. J.T. Smith, J.K. Tomfohr, M.C. Wells, T.P. Beebe, T.B. Kepler, and W.M. Reichert, *Measurement of cell migration on surface-bound fibronectin gradients.* Langmuir, 2004. **20**(19): p. 8279-8286.
13. A. Curtis and C. Wilkinson. *New depths in cell behaviour: reactions of cells to nanotopography*. in *Biochemical Society Symposium*. 1999.
14. K. Kulangara, Y. Yang, J. Yang, and K.W. Leong, *Nanotopography as modulator of human mesenchymal stem cell function.* Biomaterials, 2012. **33**(20): p. 4998-5003.
15. A.J. Engler, S. Sen, H.L. Sweeney, and D.E. Discher, *Matrix elasticity directs stem cell lineage specification.* Cell, 2006. **126**(4): p. 677-689.
16. Y. Arima and H. Iwata, *Effect of wettability and surface functional groups on protein adsorption and cell adhesion using well-defined mixed self-assembled monolayers.* Biomaterials, 2007. **28**(20): p. 3074-3082.
17. L. Nair and C. Laurencin, *Polymers as biomaterials for tissue engineering and controlled drug delivery.* Tissue engineering I, 2006: p. 47-90.
18. F. Khan, M. Tanaka, and S.R. Ahmad, *Fabrication of polymeric biomaterials: a strategy for tissue engineering and medical devices.* Journal of Materials Chemistry B, 2015. **3**(42): p. 8224-8249.
19. M. Gołda, M. Brzychczy-Włoch, M. Faryna, K. Engvall, and A. Kotarba, *Oxygen plasma functionalization of parylene C coating for implants surface: nanotopography and active sites for drug anchoring.* Materials Science and Engineering: C, 2013. **33**(7): p. 4221-4227.
20. S. Kuppusami and R.H. Oskouei, *Parylene coatings in medical devices and implants: a review.* Univ. J. Biomed. Eng, 2015. **3**: p. 9-14.
21. C.P. Tan and H.G. Craighead, *Surface engineering and patterning using parylene for biological applications.* Materials, 2010. **3**(3): p. 1803-1832.
22. H.-w. Lo and Y.-C. Tai, *Parylene-based electret power generators.* Journal of Micromechanics and Microengineering, 2008. **18**(10): p. 104006.
23. B. Ilic and H. Craighead, *Topographical patterning of chemically sensitive biological materials using a polymer-based dry lift off.* Biomedical Microdevices, 2000. **2**(4): p. 317-322.
24. D. Wright, B. Rajalingam, S. Selvarasah, M.R. Dokmeci, and A. Khademhosseini, *Generation of static and dynamic patterned co-cultures using microfabricated parylene-C stencils.* Lab on a Chip, 2007. **7**(10): p. 1272-1279.

25. D. Wright, B. Rajalingam, J.M. Karp, S. Selvarasah, Y. Ling, J. Yeh, R. Langer, M.R. Dokmeci, and A. Khademhosseini, *Reusable, reversibly sealable parylene membranes for cell and protein patterning.* Journal of biomedical materials research Part A, 2008. **85**(2): p. 530-538.

26. T.Y. Chang, V.G. Yadav, S. De Leo, A. Mohedas, B. Rajalingam, C.-L. Chen, S. Selvarasah, M.R. Dokmeci, and A. Khademhosseini, *Cell and protein compatibility of parylene-C surfaces.* Langmuir, 2007. **23**(23): p. 11718-11725.

27. E. Delivopoulos, M.M. Ouberai, P.D. Coffey, M.J. Swann, K.M. Shakesheff, and M.E. Welland, *Serum protein layers on parylene-C and silicon oxide: Effect on cell adhesion.* Colloids and Surfaces B: Biointerfaces, 2015. **126**: p. 169-177.

# Appendix B

# Porous gelatin patch for VEGF loading and controlled release

In Appendix B, we present a study on the fabrication of biodegradable porous gelatin patch. First we describe the fabrication of porous gelatin patch including gelatin honeycomb frame and aligned gelatin nanofibers. Then we present the application of the gelatin nanofibers for delivery of vascular endothelial growth factor (VEGF) including loading and controlled release.

## B.1 Introduction

Tissue engineering has drawn increasing attention and shows great potential in treatment of clinical diseases such as diseases in nervous system and cardiovascular system [1, 2]. In tissue engineering, functional scaffolds play key roles in sustaining culture of stem cells, directing formation of targeted tissues and guiding tissue organization in multidimensions. An ideal scaffold can not only support tissue formation but allow tissue to finally replace the scaffold, resulting in the functional tissue in situ [3]. Thus biocompatible scaffolds with controlled *in vivo* biodegradability are highly demanding.

Natural polymers such as collagen, gelatin, silk fibrin, chitosan, starch, alginate and hyaluronic are biodegradable biomaterials used in tissue engineering [4, 5]. Of all, gelatin, a hydrolyzed product of collagen, is not only biocompatible but also biodegradable with low immunogenicity [6]. Furthermore, gelatin can be obtained from a wide range of natural sources and easily manipulated or surface functionalized. Thus, gelatin has been extensively used in tissue engineering alone or associated with other materials [7].

Growth factors are soluble signaling polypeptides capable of instructing specific cellular responses in a biological environment. The specific cellular response trigged by growth factor signaling can result in a very wide range of cell behavior, including cell survival, and control over migration, differentiation or proliferation of a specific subset of cells [8]. So growth factors play essential roles in tissue engineering in which fabricating biodegradable scaffold decorated with functional growth factors for controlled and sustainable release in physiological conditions is highly beneficial. Vascular endothelial growth factors (VEGF) have been proved to stimulate

angiogenesis during the formation of tissues, which is important to sustain generated tissue or organ by restoring the oxygen supply with blood circulation system [9].

In this thesis, we have develop an aspiration assisted method which is applied not only for the fabrication of PEGDA honeycomb frame shown in **Chapter 4**, but also for the fabrication of porous gelatin honeycomb frame. The fabricated gelatin honeycomb frame shows well defined micro structure. Then aligned nanofiber was deposited on the frame with two parallel collectors. The electrospun gelatin nanofibers can be used as a platform for controlled delivery of VEGF,

## B.2 Fabrication of VEGF loaded porous gelatin patch

### B.2.1 Fabrication of porous gelatin patch

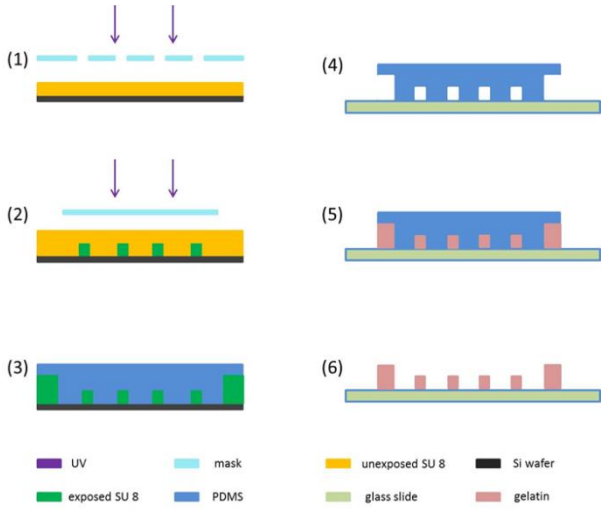


**Fig. B.1** A schematic fabrication flowchart of porous gelatin honeycomb frame

The fabrication of porous gelatin honeycomb frame shares in common with that of porous PEGDA honeycomb frame including the fabrication of PDMS mold and aspiration assisted cavity filling by gelatin solution (**Fig. B.1**). The difference lies in the solidification ways of PEGDA and gelatin. Different from UV crosslinking used for PEGDA, gelatin solution was dried and solidified in vacuum. After totally dried in vacuum for two days, gelatin honeycomb frame was peeled off from the glass substrate.

The electrospinning setup used here is similar to that in Chapter 5 except for the design of collector, as is shown in **Fig. B.2**. In order to obtain aligned nanofiber, two parallel collector made of Si wafer were used. The distance between the collectors is 14 mm which is a little larger than the diameter of gelatin frame (13 mm). The electrospun gelatin nanofiber was cross-linked in ethanol containing 1-Ethyl-3-(3-Dimethylaminopropyl)carbodiimide (EDAC) and N-Hydroxysuccinimide (NHS) for 4h.

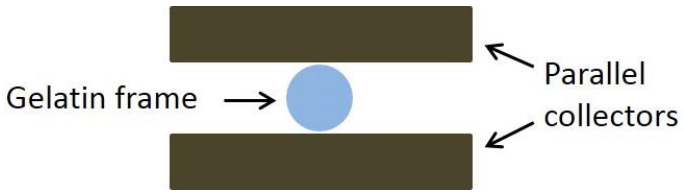


**Fig. B.2** An illustration of collector design for aligned nanofiber fabrication

## B.2.2 VEGF loading on porous gelatin patch

VEGF loading is achieved by taking advantages of its high affinity to heparin, as is shown in **Fig. B.3**. Due to the negative charged heparin, positive charged chitosan is used to coat on gelatin nanofiber to increase the conjugation of heparin. Briefly, 1mg of heparin sodium was dissolved in 1 ml of DI $H_2O$ to make 1mg/mL of heparin solution. Then gelatin nanofiber patch coated with chitosan was immersed in the heparin solution for 30 min. EDAC and NHS were added to the above solution every 30 min for three times. Then the patch was rinsed with DI $H_2O$ three times. With similar process, we set a control by only immersing patch in heparin solution without addition of chitosan, EDAC and NHS. Toluidine blue is used to quantify heparin on patch, resulting in purple complex of heparin and Toluidine blue. VEGF loading on the patch is conducted as follows: human recombinant VEGF165 was dissolved in PBS to make 1μg/mL of VEGF solution. The heparin conjugated patch was immersed in the VEGF solution for 4h and rinsed with DI $H_2O$ for three times.

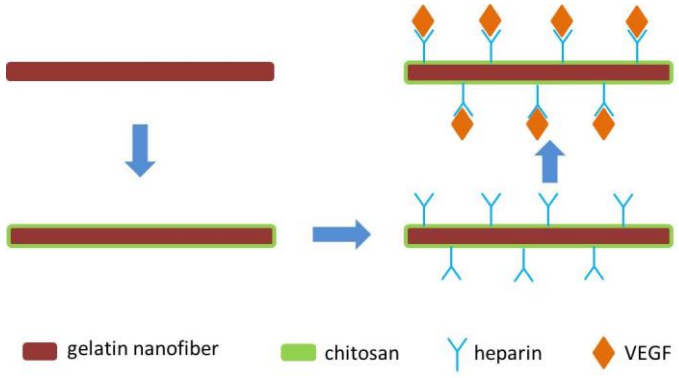


**Fig. B.3** An illustration of VEGF loading on gelatin nanofiber.

VEGF release from gelatin nanofiber patch is conducted as follows: VEGF loaded patch was placed in 24-well plate with 200 μL of PBS in cell culture incubator. The PBS solution in each well was collected every other day and 200 μL of fresh PBS was added, which lasted 16 days. The amount of released VEGF in collected PBS solution was measured with a sandwich Enzyme-Linked Immunosorbent Assay (ELISA) using a commercial kit.

## B.3 Results

### B.3.1 Porous gelatin patch

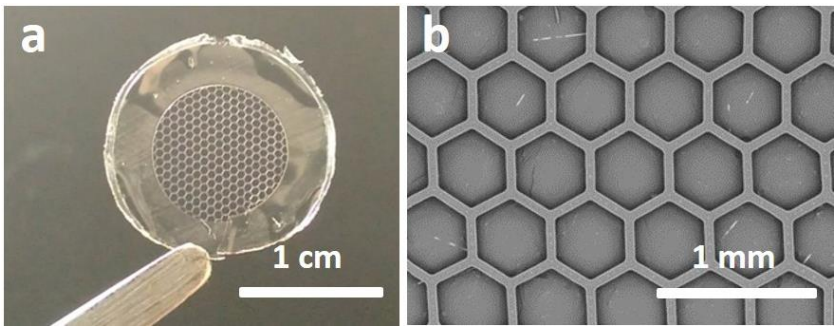


**Fig. B.4** (a) Photograph and (b) SEM image of porous gelatin honeycomb frame.

**Fig. B.4a** shows a newly made porous gelatin honeycomb frame which is transparent and has well defined honeycomb structure. **Fig. B.4b** shows the SEM image of porous gelatin honeycomb frame with a feature size and pitch size being 50 μm and 400 μm, respectively.

**Fig. B.5a,b** show the electrospun gelatin nanofibers deposited on porous gelatin honeycomb frame. Most of gelatin nanofibers deposited in the same direction with narrow deviation range while a small portion of nanofibers shows random deposition on the frame. After being cross-linked by EDAC and NHS, gelatin nanofibers still keep their alignment (**Fig. B.5c**).

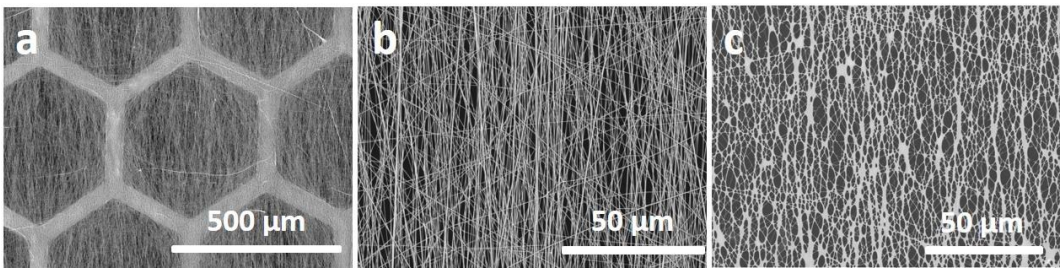


**Fig. B.5** SEM images of gelatin nanofibers on gelatin honeycomb patch (a) and (b) before crosslinking and (c) after crosslinking.

## B.3.2 VEGF loading and release

We then use the cross-linked porous gelatin patch for VEGF delivery. First a polysaccharide heparin which possesses high affinity to VEGF was conjugated with gelatin nanofiber. The amount of heparin on patch was measured by Toluidine blue staining, as is shown in **Fig. B.6**. Quantified assay shows that the amount of heparin on patch with EDAC and NHS is about 2.4±0.85 μg per patch while only 0.1±0.01 μg per patch was detected on control. The results show that heparin shows low affinity to gelatin nanofibers and that chitosan/EDAC/NHS method can obtaining large amounts of heparin conjugated with gelatin nanofibers.

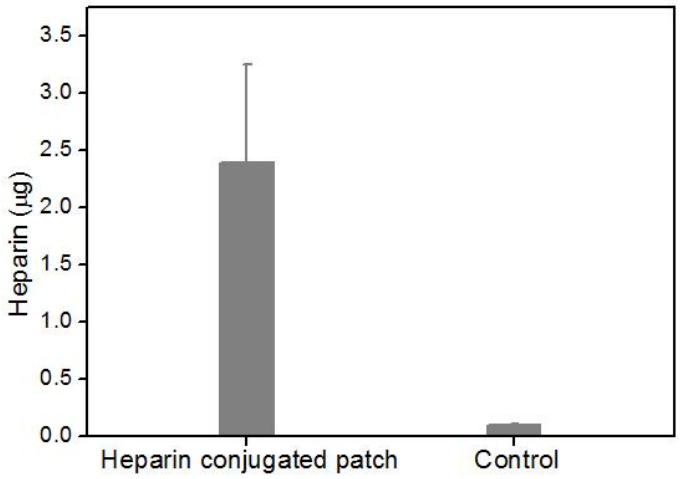


**Fig. B.6** The amount of heparin on patch measured by Toluidine blue staining.

After all samples being collected, the amount of VEGF release from porous gelatin patch was detected with ELISA. **Fig. B.7** shows the release profile of VEGF loaded on porous gelatin patch for 16 days. At the first two days, the average release rate is about 60 ng per day. The release rate decreased slowly with the final release rate being ~14 ng per day. The accumulative release of VEGF after 16 days is about 400 ng. The results show that our strategy for VEGF delivery exhibits sustainable release.

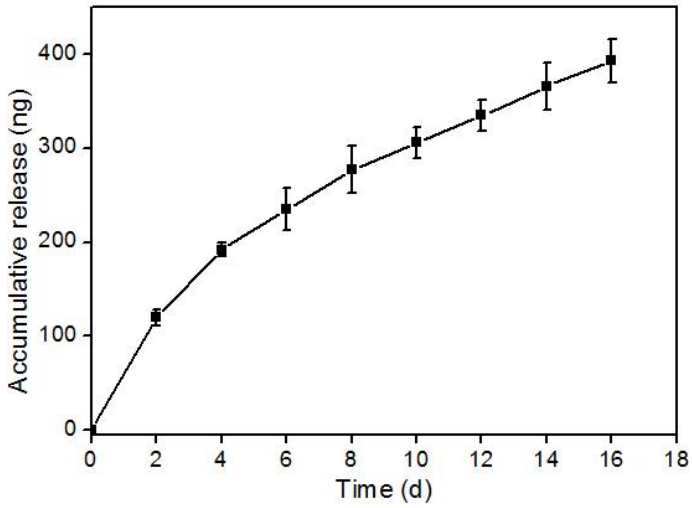


**Fig. B.7** Accumulative release of VEGF loaded on porous gelatin patch.

## B.4 Conclusion

In this work, we have fabricated a biodegradable porous gelatin patch with aligned gelatin nanofibers for VEGF loading and controlled and sustainable release. The fabricated gelatin honeycomb frame well defined micropattern with feature size and pitch size being 50 μm and 400 μm. The electrospun nanofibers show high alignment even after crosslinking. The amount of heparin loaded on crosslinked gelatin nanofibers can be largely increased with chitosan/EDAC/NHS method and thus increases the amount of VEGF loaded on the patch. The VEGF loaded exhibits controlled and sustainable release under cell culture conditions.

# Reference


1. R.Y. Kannan, H.J. Salacinski, K. Sales, P. Butler, and A.M. Seifalian, *The roles of tissue engineering and vascularisation in the development of micro-vascular networks: a review.* Biomaterials, 2005. **26**(14): p. 1857-1875.
2. S.N. Bhatia, G.H. Underhill, K.S. Zaret, and I.J. Fox, *Cell and tissue engineering for liver disease.* Science translational medicine, 2014. **6**(245): p. 245sr2-245sr2.
3. M.N. Collins and C. Birkinshaw, *Hyaluronic acid based scaffolds for tissue engineering—A review.* Carbohydrate polymers, 2013. **92**(2): p. 1262-1279.
4. J.M. Dang and K.W. Leong, *Natural polymers for gene delivery and tissue engineering.* Advanced drug delivery reviews, 2006. **58**(4): p. 487-499.
5. W. Zhao, X. Jin, Y. Cong, Y. Liu, and J. Fu, *Degradable natural polymer hydrogels for articular cartilage tissue engineering.* Journal of Chemical Technology and Biotechnology, 2013. **88**(3): p. 327-339.
6. K. Su and C. Wang, *Recent advances in the use of gelatin in biomedical research.* Biotechnology letters, 2015. **37**(11): p. 2139-2145.
7. H.-W. Kang, Y. Tabata, and Y. Ikada, *Fabrication of porous gelatin scaffolds for tissue engineering.* Biomaterials, 1999. **20**(14): p. 1339-1344.
8. J.E. Raber-Durlacher, I. von Bültzingslöwen, R.M. Logan, J. Bowen, A.R. Al-Azri, H. Everaus, E. Gerber, J.G. Gomez, B.G. Pettersson, and Y. Soga, *Systematic review of cytokines and growth factors for the management of oral mucositis in cancer patients.* Supportive Care in Cancer, 2013. **21**(1): p. 343-355.
9. S. Moens, J. Goveia, P.C. Stapor, A.R. Cantelmo, and P. Carmeliet, *The multifaceted activity of VEGF in angiogenesis–Implications for therapy responses.* Cytokine & growth factor reviews, 2014. **25**(4): p. 473-482.

# Appendix C

## French summary

# C.1 Introduction

L'ingénierie tissulaire a reçu une attention croissante au cours des dernières décennies en raison de ses avantages supérieurs dans le traitement des blessures tissulaires sévères par traitement conventionnel. L'objectif de l'ingénierie tissulaire est d'assembler des structures fonctionnelles qui rétablissent, maintiennent ou améliorent les tissus endommagés ou des organes entiers. Avec l'aide de l'ingénierie tissulaire, le corps peut utiliser ses propres systèmes pour recréer des cellules et reconstruire les tissus et les organes, le but de toute médecine régénératrice. Les méthodes d'ingénierie tissulaire offrent un avenir prometteur pour le traitement des lésions sévères des tissus, en particulier dans les systèmes cardiovasculaire et nerveux, car ils manquent de la capacité de s'auto-réparer. Dans la pratique de l'ingénierie tissulaire, les scaffolds biomatériaux jouent un rôle clef dans l'organisation de molécules biologiquement actives, en manipulant le comportement des cellules et en guidant la formation des tissus. À cette fin, de nombreux efforts ont été faits pour fabriquer des scaffolds optimaux pour la fabrication de tissus, en se concentrant sur le choix des matériaux, les qualités mécaniques, l'architecture 3D et les effets biologiques des scaffolds.

Nous nous intéressons particulièrement à la fabrication de scaffolds pour l'ingénierie tissulaire dans le but de maîtriser le microenvironnement cellulaire d'un tissu, ce qui implique l'organisation de la matrice extracellulaire (ECM), la gestion des facteurs solubles et l'organisation des contacts cellulaires. En effet, le comportement d'une cellule est déterminé non seulement par ses gènes et ses molécules solubles externes biologiquement actives, mais aussi par le microenvironnement viral de la cellule. L'ECM, par exemple, fournit un support structurel et biochimique aux cellules, ce qui est essentiel pour l'adhésion cellulaire, la prolifération, la migration et la différenciation. En raison de la complexité de l'ECM et de l'interaction cellule-ECM, une compréhension approfondie du rôle du microenvironnement cellulaire sur le comportement des cellules est importante pour la culture des tissus fonctionnels.

Le besoin de scaffolds fonctionnels dans l'ingénierie tissulaire est survenu lorsque l'on a réalisé l'importance du microenvironnement dans le contrôle du comportement des cellules. Traditionnellement, après avoir été isolées du tissu corporel, les cellules ne sont plus cultivées dans un environnement naturel, mais dans un milieu artificiel (in

vitro) sur une plaque de culture tissulaire. Les cellules sont forcées à adhérer sur un support bidimensionnel où à la fois la diffusion basale et, la communication cellule-cellule sont moins efficaces. En outre, la rigidité de la surface, le caractère inerte et la haute résistance mécanique des substrats sont très différents des compartiments *in vivo*. Puisque les cellules sont sensibles aux environnements de culture qui, en retour, ont de forts effets sur le comportement des cellules, la grande disparité entre les environnements de culture *in vitro* et *in vivo* entraînera inévitablement une incohérence au niveau du comportement et des états des cellules. Ainsi donc, la fabrication de scaffolds fonctionnels imitant le microenvironnement extracellulaire est très exigeante.

Les premières pratiques d'ingénierie tissulaire ont encore souffert de plusieurs problèmes, notamment les ressources cellulaires limitées et les inévitables rejets immunitaires. Ce dilemme a été dépassé par l'apparition de cellules souches telles que des cellules embryonnaires et des cellules pluripotentes induites. Les cellules souches sont des cellules indifférenciées qui conservent la capacité de se différencier en lignées cellulaires multiples. Premièrement, elles peuvent s'auto-répliquer tout au long de la vie, donc un nombre illimité de cellules souches de propriétés similaires peuvent être produites in vitro. Deuxièmement, les cellules souches sont clonogènes, ce qui signifie que chaque cellule peut générer une colonie dans laquelle toutes les cellules sont dérivées de cette cellule unique et, ont donc une constitution génétique identique. Troisièmement, elles possèdent la capacité de se différencier en divers types de cellules spécialisées. Pour toutes ces raisons, la thérapie à base de cellules souches a fait l'objet de recherches intensives au cours de la dernière décennie. En somme, les iPSCs humaines ont attiré une attention croissante en raison de leurs avantages supérieurs. En effet, les iPSC peuvent facilement être obtenues à partir d'une la cellule somatique d'un patient par un processus de reprogrammation. Les iPSCs spécifiques du patient permettront alors d'effectuer des tests médicamenteux ciblés, ainsi qu'une transplantation tissulaire avec un risque de rejet immunitaire minimal.

L'objectif de ce travail est de développer une méthode de réalisation de scaffolds multidimensionnels pour la culture cellulaire et l'ingénierie tissulaire. Nous avons d'abord appliqué une technique d'impression 3D pour produire un scaffold en PEGDA et, ensuite rempli l'espace libre du scaffold avec du gel de gélatine. Après la congélation et le séchage, un scaffold hybride en PEGDA avec des structures fines de gélatine a été

obtenu, qui a été ensuite validé pour la culture et la différenciation de cellules progénitrices neuronales. Pour l'intégrer plus facilement dans un dispositif microfluidique, nous avons également conçu un scaffold 2D sous forme d'une couche mince de nid d'abeilles de PEGDA rempli de structures poreuses auto-assemblées en PCL. Ce scaffold 2D a été utilisé pour la culture cellulaire et la transfection des gènes, montrant des avantages par rapport aux méthodes classiques en termes d'absorption des nutriments et des facteurs solubles. Enfin, nous avons fabriqué un scaffold mou constitué d'une couche mince de nid d'abeilles en élastomère de PDMS et d'une monocouche de nanofibres de gélatine, afin de faciliter la différenciation cardiaque à partir des cellules souches pluripotentes humaines. Comme prévu, nous avons généré des cellules cardiaques ayant une contraction plus forte et des battements plus homogènes que lors des approches classiques. Finalement, nous avons démontré l'utilité des scaffolds hybrides pour l'ingénierie micro-tissulaire, lesquels pourraient avoir un impact sur les recherches futures dans le domaine de l'ingénierie tissulaire, du criblage des médicaments et de la médecine régénératrice.

## C.2 Microstructures en PEGDA par impression 3D pour l'intégration de la gélatine poreuse, la culture cellulaire et la différenciation neurale

### C.2.1 Introduction

L'impression tridimensionnelle (3D) est une technique avec un potentiel d'application élevé dans de nombreux domaines tels que l'automobile, l'avion, l'alimentation et la santé. Entre autres, l'impression 3D facilite la fabrication de scaffolds qui peut être utilisé dans l'ingénierie tissulaire et la médecine régénératrice. Les limitations technologiques, cependant, sont encore à venir pour l'impression directe de tissus et d'organes complexes. L'accent actuel est donc mis sur la fabrication de scaffolds 3D biocompatibles avec une géométrie et des fonctions bien définies. À cet égard, les efforts de recherche visent à trouver des biomatériaux imprimables à haute

résolution, ainsi qu'une fonctionnalisation travaillée pour une culture cellulaire améliorée et la reformation de tissus, voire d'organes.

Les biomatériaux couramment utilisés en ingénierie tissulaire sont des polymères synthétiques. Par exemple, le polyéthylène glycol (PEG), non toxique et non immunogène, a de larges applications allant de la fabrication industrielle à la médecine. La rigidité du PEGDA réticulé est excellente, mais les cellules ne peuvent pas y adhérer, se remodeler ou proliférer directement sur un scaffold en PEG en raison de la nature inertielle du PEG. Des polymères naturels tels que le collagène, la gélatine, la fibrine de soie, le chitosane, l'amidon, l'alginate et l'hyaluronique peuvent également être utilisés pour l'ingénierie tissulaire. La gélatine, qui est un produit hydrolysé du collagène, n'est pas seulement biocompatible, mais aussi biodégradable avec une faible immunogénicité. En outre, la gélatine peut être obtenue à partir d'une large gamme de sources naturelles et facilement manipulée ou fonctionnalisée en surface. Ainsi, la gélatine a été largement utilisée dans l'ingénierie tissulaire, seule ou associée à d'autres matériaux. Grâce au procédé de lyophilisation ou la «congélation par séchage», on peut fabriquer un scaffold de gélatine avec une taille de pore contrôlée, ce qui convient à l'attachement, à la prolifération et à la différenciation des cellules.

Ici, nous détaillons la fabrication de scaffolds de PEGDA imitant les matrices extracellulaires par l'impression 3D, avec des microstructures de gélatine poreuse intégrées par des techniques de congélation-séchage pour éviter la résolution indésirable de l'impression 3D et la mauvaise résistance mécanique des scaffolds de gélatine pure. Le scaffold en PEGDA a été conçu et imprimé par une imprimante 3D avec une forme régulière et des pores interconnectés où la gélatine en éponge est remplie pour réduire la taille des pores et augmenter la surface active pour la fixation des cellules. Nos résultats montrent que le scaffold en PEGDA imprimé est fort et résiste aux contraintes mécaniques, tandis que les structures de gélatine poreuse, soutenues par le scaffold en PEGDA, ont une propriété de gonflement et une dégradabilité inchangées après intégration. Nos résultats montrent également que le scaffold en PEGDA / gélatine est excellent pour l'attachement, la prolifération et la migration des fibroblastes NIH 3T3 et la différenciation des cellules progénitrices neuronales (NPC) en neurones.

## C.2.2 Fabrication du scaffold de PEGDA/gélatine poreux

La microstructure 3D du scaffold de diacrylate de polyéthylène glycol (PEGDA) a été obtenue à l'aide de l'imprimante 3D ProJet 1200 et d'une solution verte de PEGDA du même fabricant. La figure 1a montre le cadre en nid d'abeilles PEGDA imprimé en 3D. Le cadre en nid d'abeilles PEGDA a été recouvert d'une mince couche d'or par pulvérisation pour l'observation par MEB, comme le montre la Fig. 1b. Les tailles caractéristiques du motif et du pas en PEGDA fabriqué sont respectivement de 1200 et 200 µm. L'épaisseur est estimée à 200 µm, comme illustré par la Fig. 1c. Les résultats ci-dessus révèlent la bonne fidélité de l'imprimante 3D par rapport au modèle de conception.

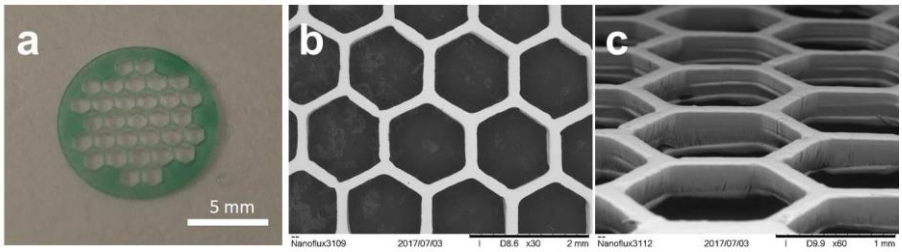


Figure 1 (a) Photographie, (b) et (c) images MEB du cadre en PEGDA.

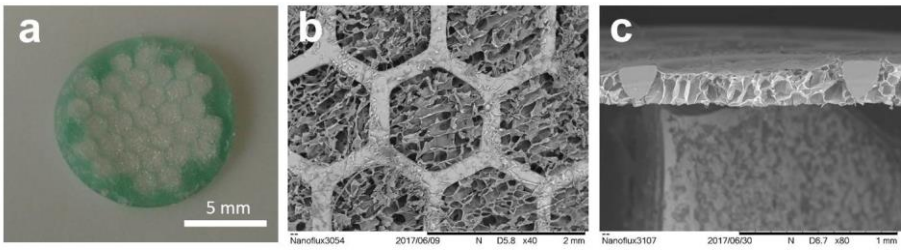


Figure 2 (a) Photographie, (b) et (c) images MEB du scaffold en PEGDA/ gélatine poreux.

Le cadre PEGDA imprimé en 3D est utilisé comme squelette pour soutenir la formation de structure poreuse de gélatine à l'intérieur. Le cadre PEGDA 3D a été immergé dans une solution de gélatine qui a été congelée à -20C °pendant la nuit et séchée sous vide pendant 24h à température ambiante. La gélatine poreuse, ainsi que le cadre PEGDA sont représentés dans la Fig. 2a. La morphologie de la gélatine poreuse a été caractérisée avec la MEB, comme le montre la Fig. 2b, c. Le scaffold de PEGDA

/ gélatine présente des microstructures de gélatine en éponge qui sont intégrées dans le cadre PEGDA, montrant des tailles de pores comprises entre 20 µm et 200 µm. L'épaisseur de la gélatine poreuse est cohérente avec celle du cadre PEGDA. Cette structure hautement poreuse facilitera la diffusion des nutriments et des produits métaboliques. Elle fournira aussi un excellent micro-environnement 3D pour les cellules.

## C.2.3 Scaffold de PEGDA/gélatine poreux pour la culture cellulaire

La dilatation du scaffold est illustrée à la Fig. 3a. Ce scaffold peut retenir environ 9 fois son poids à sec au bout d'une journée et, tend à saturer après 7 jours, atteignant ainsi une estimation de 13 fois son poids à sec. La capacité de retenue d'eau élevée offre suffisamment d'espace pour la diffusion des nutriments et des produits métaboliques, ainsi que pour la croissance, la migration, l'interaction et la différenciation cellulaire. Après 10, 20 et 30 jours d'incubation, les scaffolds ont été rincés avec du PBS, lyophilisés pendant la nuit et pesés, comme le montre la Fig. 3b. La gélatine a été dégradée, pesant environ 45% du poids initial après 30 jours.

La toxicité *in vitro* du scaffold en PEGDA / gélatine a été testée par dosage WST. À titre de comparaison, une plaque de culture tissulaire traditionnelle (TCP) a été utilisée comme contrôle (viabilité cellulaire à 100%) et, un scaffold à base de gélatine pure a été utilisé comme autre contrôle. Les résultats ont été montrés à la Fig. 3c. Par rapport au TCP et au scaffold de gélatine pure, celui en PEGDA / gélatine présente une toxicité négligeable envers les cellules NIH 3T3, ce qui indique sa bonne biocompatibilité.

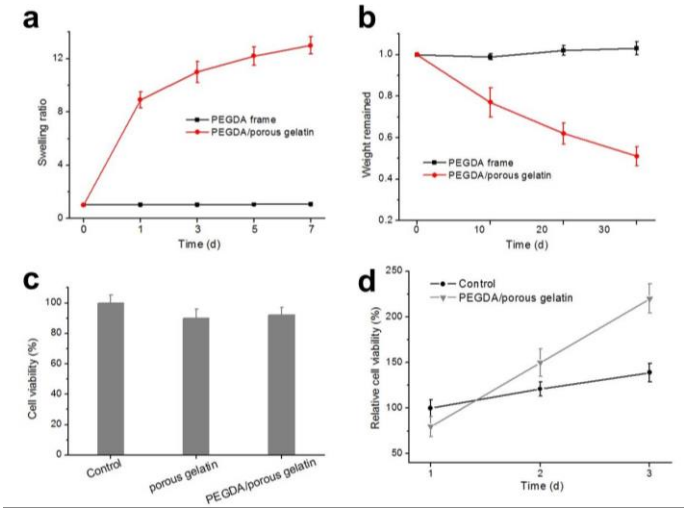


Figure 3 (a) Gonflement et (b) dégradabilité de le scaffold. (c) Viabilité et (d) prolifération des cellules sur le scaffold.

La prolifération des cellules NIH 3T3 sur le scaffold de PEGDA/gélatine poreux a ensuite été étudiée. La prolifération des cellules a été déterminée par un dosage WST, comme le montre la Fig. 3d. Une TCP a été utilisée comme un contrôle. La viabilité cellulaire sur le scaffold de PEGDA/gélatine poreux est de 11%, 52% et 85%, respectivement sur le 1er, 2e et 3e, respectivement. Par rapport au TCP, les cellules présentent une prolifération beaucoup plus élevée sur le scaffold de PEGDA/gélatine poreux.

Les scaffolds poreux idéaux doivent posséder des pores interconnectés et permettre une migration cellulaire efficace. La migration cellulaire a été mesurée en étudiant la répartition des cellules dans les scaffolds en termes de profondeur. Avec une technique d'immunomarquage, les scaffolds de cellules ont été observés sous microscope confocal avec un mode de Z-stack. Les résultats sont montrés à la Fig. 4. Après un jour d'incubation, la profondeur de pénétration des cellules à l'intérieur du scaffold était estimée à 50 µm. Après l'incubation de 2 et 3 jours, la profondeur de perméation augmente jusqu'à environ 120 et 190 µm respectivement. Cette augmentation de la profondeur de pénétration est causée par la migration des cellules à l'intérieur des scaffolds poreux. Les résultats révèlent que le scaffold hautement poreux possède des pores interconnectés, offrant une bonne plate-forme pour la migration cellulaire.

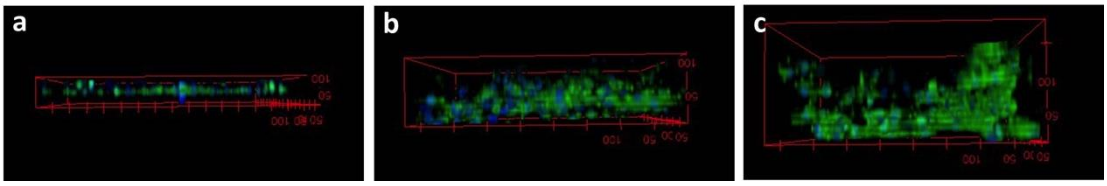


Figure 4 Immunomarquage de la F-actine des cellules dans le scaffold.

## C.2.4 Scaffold de PEGDA/gélatine poreux pour la différenciation neuronale

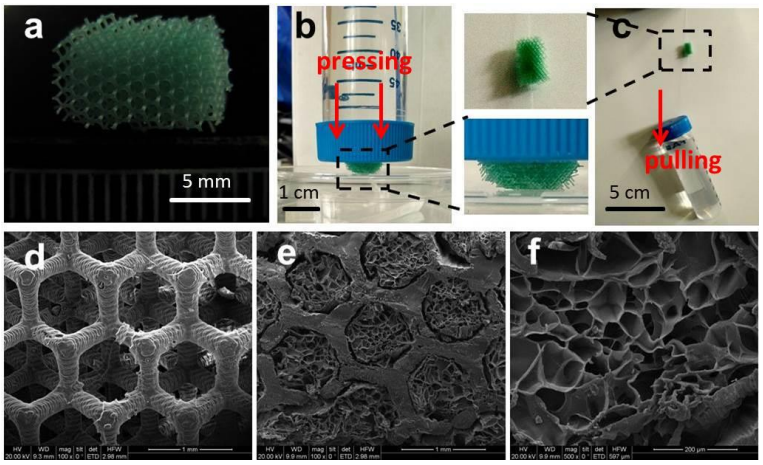


Figure 5 (a) Photograpgie du cadre PEGDA. (b) et (c) Test de résistance mécanique sur le scaffold. Images SEM de (d) cadre PEGDA, (e) et (f) scaffold de PEGDA/ gélatine poreux.

Nous avons également fabriqué un scaffold 3D poreux en PEGDA par impression 3D. La structure 3D a été produite en 8 min pour un scaffold de $1 \times 0{,}5 \times 0{,}25$ cm$^3$ de taille. Par la suite, le scaffold a été lavé dans de l'isopropanol et cuit a posteriori avec des rayons UV. Le cadre en PEGDA ainsi fabriqué est montré dans la Fig. 5a. Comme prévu, ce scaffold en treillis est assez solide pour garder sa forme, mais est quelque peu élastique sous l'action de forces externes (figure 5b, c).

La figue 5d montre une image par microscopie électronique à balayage (MEB) du réseau de scaffold ainsi fabriqué. De même, le cadre en PEGDA a été utilisé pour l'intégration de gélatine poreuse. La section transversale de la scaffold a été caractérisée par MEB, illustrée à la Fig. 5e, f. Le scaffold de PEGDA / gélatine poreux a des

microstructures de gélatine-éponge qui sont intégrées dans le cadre PEGDA. Cette microstructure en éponge a une porosité élevée avec des tailles de pores comprises entre 20 µm et 100 µm. Cette structure hautement poreuse facilitera la diffusion des nutriments et des produits métaboliques et fournira un excellent micro-environnement 3D pour les cellules.

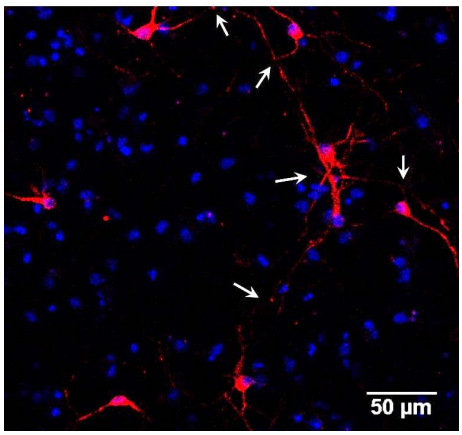


Figure 6 Image en fluorescence des neurones immuno-marqués pour MAP-2 (rouge) après une différenciation de 7 jours.

La figure 6 montre les images représentatives des neurones après immuno-marquage MAP-2, après une différenciation de 7 jours. Comme on peut le voir, chaque neurone a un corps cellulaire sphérique avec plusieurs filaments cellulaires minces s'étalant sur des dizaines ou des centaines de microns. Ces filaments ont tendance à se connecter entre eux (ce qui est montré par des flèches blanches) pour former un grand réseau de neurones, probablement en 3D. Une telle architecture hiérarchisée en 3D devrait favoriser la formation du réseau neuronal et leurs activités d'impulsion, fournissant ainsi un choix alternatif de scaffold pour la réparation des systèmes nerveux blessés.

## C.3 Patch poreux en PCL par auto-assemblage pour améliorer la performance cellulaire et la différenciation cardiaque dérivée d'iPSCs

## C.3.1 Introduction

La matrice extracellulaire (ECM) joue un rôle important, non seulement en reliant les cellules ensemble, mais aussi en influençant leur survie, leur développement, leur forme, leur polarité, leur migration et leur comportement de prolifération. L'ingénierie *in vitro* de substrats de culture cellulaire avancés qui imitent de près l'ECM *in vivo* a longtemps été un problème difficile. Divers substrats ont été proposés pour améliorer la culture cellulaire *in vitro* comme le tapis de fibres et le film polymère. Cependant, ces substrats manquent d'une structure 3D et d'une diffusion efficace de cellules et de nutriments.

Inspirés par la structure des protéines fibreuses dans l'ECM, certains substrats attirent de plus en plus d'attention au cours de la dernière décennie, en utilisant la technique d'électrospinning pour reproduire cette structure fibreuse. Cependant, ces substrats de nanofibres sont minces et fragiles, de sorte qu'ils sont habituellement dotés de supports tels que des lames de verre ou des plaques métalliques qui sont imperméables à l'eau et gâtent les mérites des nanofibres. Les polymères synthétiques biodégradables tels que le PCL et le PLGA ont montré un potentiel croissant dans la fabrication de scaffolds tissulaires, en raison de leur haute résistance mécanique, de leur fabrication facile et de leur biodégradabilité contrôlable. Cependant, ce procédé d'électrospinning de nanofibres est limité par le nombre de solvants qu'on peut utiliser, en particulier pour l'électrospinning de polymères mixtes. En outre, pour l'électrospinning de polymères synthétiques, la formation des nanofibre est très sensible aux paramètres ambiants environnants comme la température, l'humidité et le flux d'air.

L'auto-assemblage de polymères est une méthode nouvelle pour fabriquer des substrats avec des structures ordonnées spécifiques. En profitant des interactions non covalentes, l'auto-assemblage part d'un système désordonné de polymères pré-existants pour former une structure organisée de particules, de films ou en 3D, avec des étapes de fabrication faciles. Ces structures sont cependant difficiles à manipuler, notamment pour des structures minces auto-assemblées comme des films. De plus, une certaine déformation est difficile à éviter lors de la formation de la structure 3D.

Ici, nous avons développé une nouvelle méthode qui combine l'auto-assemblage

de polymères avec la microfabrication, afin de fabriquer un cadre de nid d'abeilles poreux en PEGDA ayant avec une résistance mécanique élevée, sur laquelle une couche mince de PCL poreux est déposée par auto-assemblage. Le cadre de PEGDA agit non seulement comme un support facile à manipuler, mais également comme un garant de la structure afin d'assurer une plus grande intégrité et une porosité uniforme. Le plasma d'oxygène peut être utilisé pour améliorer l'adhérence cellulaire du patch en PCL poreux. Les tests de culture cellulaire ont démontré une amélioration des performances cellulaires telles que la prolifération, l'absorption cellulaire des nutriments et la transfection de gènes sur ce type de substrat. Nous avons également étudié son application pour la culture et la différenciation cardiaque des iPSC. Enfin, nous avons également étudié la biodégradation du patch poreux PCL.

## C.3.2 Fabrication du patch poreux en PCL

La procédure de fabrication du cadre de nid d'abeilles en PEGDA est illustrée à la Fig. 7, qui comprend deux étapes principales: la fabrication de moules en PDMS et la production du châssis de PEGDA.

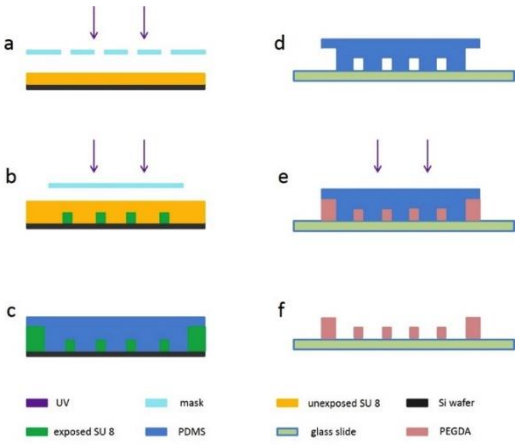


Figure 7 Un diagramme de fabrication schématique du cadre en nid d'abeilles PEGDA.

Le moule en PDMS est fabriqué par lithographie UV et lithographie molle. Le processus a commencé avec la production d'un masque de Cr suivi d'une photolithographie de SU8 pour fabriquer le moule principal. Ensuite, le motif du moule principal a été transféré par tampon sur du PDMS en utilisant une lithographie molle.

Le cadre de nid d'abeilles en PEGDA a été fabriqué avec une technique de moulage aidée par l'aspiration du PDMS. En bref, le moule de PDMS a été attaché motif vers le bas sur une lame de verre propre. Ensuite, l'assemblage de verre-PDMS a été transféré dans une chambre à vide durant 15 minutes de dégazage. Parallèlement, une solution de prépolymère PEGDA a été préparée et utilisée pour remplir la cavité de verre-PDMS grâce à l'aspiration produite par le passage sous vide du moule de PDMS. L'ensemble de l'assemblage a ensuite été exposé avec des rayons UV (365 nm de longueur d'onde) à 12 mJ / s pendant 40 s. Le réseau de PEGDA s'est solidifié, a été décollé de la lame de verre et été rincé avec l'isopropanol (IPA) pour une utilisation prête à l'emploi. L'image MEB illustre à la Fig. 9a la taille de pore moyenne de 3 µm et la porosité de 57%.

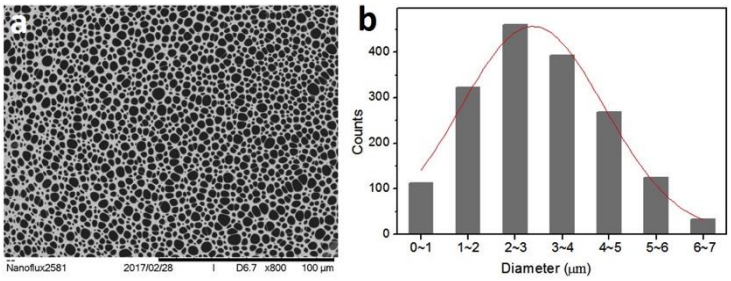


Figure 9 (a) Image SEM et (b) distribution de la taille des pores d'un patch PCL poreux typique.

## C.3.3 Patch PCL poreux pour culture cellulaire

Un isothiocyanate de fluorescéine à colorant fluorescent (FITC) a été conjugué au PLL pour suivre et quantifier le PLL à l'intérieur des cellules. Comme le montre la Fig. 10, pour chaque substrat, l'intensité de fluorescence devient plus forte lorsqu'on augmente le temps d'incubation.

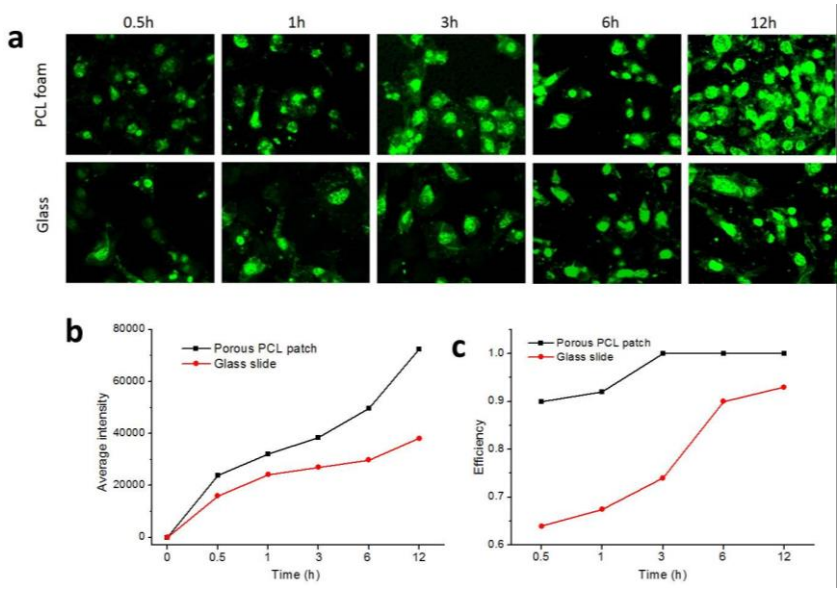


Figure 10 (a) Images de fluorescence, (b) évolution de l'intensité de fluorescence moyenne et (c) évolution de l'efficacité de l'absorption cellulaire de cellules NIH 3T3 sur un patch de PCL poreux et une lamelle de verre après incubation avec PLL-FITC pour 0,5, 1, 3, 6 et 12h.

Pour une incubation de 0,5, 1, 3, 6 et 12h, l'intensité moyenne de fluorescence pour une cellule unique sur le patch de PCL poreux sont 1,48, 1,34, 1,43, 1,67 et 1,89 fois supérieures à celles du contrôle ; la lame de verre. Avec l'augmentation du temps d'incubation (1, 3, 6 et 12h), les rendements atteignent respectivement 67%, 74%, 90% et 93%, tandis que sur un patch en PCL poreux, l'efficacité atteint jusqu'à 90% après une incubation de 0,5 heure. Après 3 heures d'incubation, l'efficacité atteint 100% et se conserve jusqu'à 12 heures d'incubation. Ces résultats indiquent donc que le patch de PCL poreux peut faciliter l'absorption cellulaire de molécules du milieu de culture.

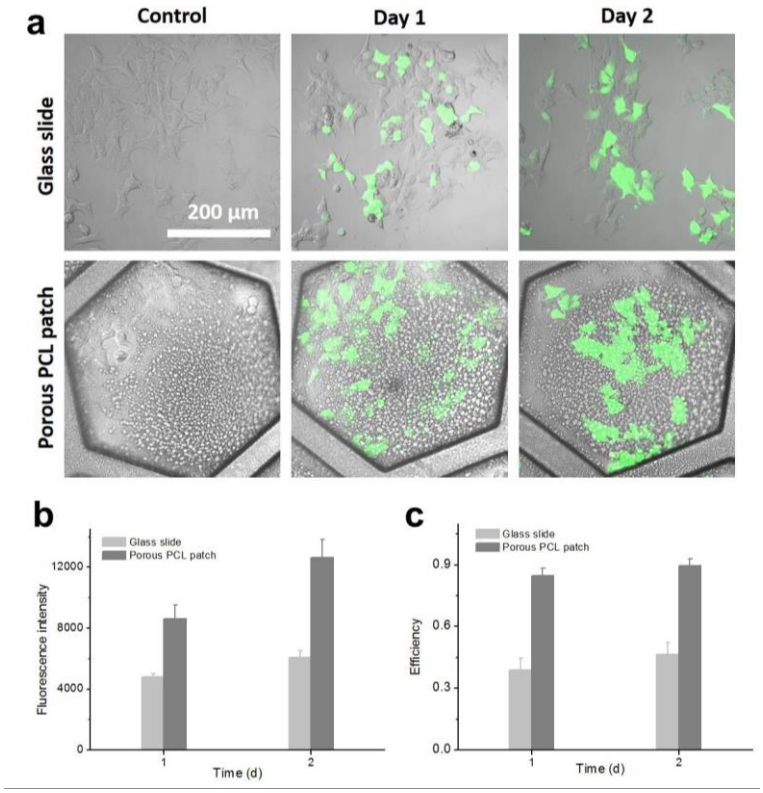


Figure 11 (a) Des images de fluorescence, (b) une intensité moyenne de fluorescence et (c) l'efficacité de la transfection des gènes sur un patch PCL poreux et une lamelle de verre avec un et deux jours d'incubation après transfection du gène.

Nous avons étudié davantage la transfection des gènes, qui dépend fortement de la performance de l'absorption cellulaire sur le patch. Les résultats sont présentés à la Fig. 11. Sur la lamelle de verre, seule une partie des cellules a exprimé les protéines fluorescentes après 1 et 2 jours de culture. Cependant, sur un patch de PCL poreux, presque toutes les cellules ont exprimé les protéines fluorescentes, avec une intensité de fluorescence beaucoup plus forte que celle des lamelles en verre au jour 1 et jour 2. Les résultats statistiques montrent que l'intensité sur le patch de PCL poreux est environ 1,8 et 2,1 fois plus important que sur la lamelle de verre 1 et 2 jours après la transfection. Sur la lamelle de verre, le pourcentage de cellules exprimant des protéines fluorescentes est de 39%, avec une légère augmentation à 46% au deuxième jour. Pour le patch de PCL poreux, le pourcentage atteint 86% en un jour et une légère augmentation à 91% au jour 2. Les résultats indiquent que le patch poreux de PCL possède un grand potentiel pour une transfection génétique hautement efficace par rapport aux méthodes

traditionnelles en plaques de culture.

## C.3.4 Patch de PCL poreux pour la différenciation cardiaque

Nous avons d'abord évalué la pluripotence de la monocouche d'iPSCs et des EB (embryoid bodies) générés sur notre patch PCL poreux. Les marqueurs des cellules souches pluripotentes SOX2 et TRA-1-60 sont utilisés pour marquer les iPSCs. Les résultats sont présentés à la Fig. 12a. L'immunofluorescence a montré un schéma de coloration typique de type hiPSC à la fois sur les monocouches et les EB d'iPSCs, ce qui révèle que l'expression de ces marqueurs est maintenue sur le patch. Ces résultats confirment que la formation de monocouches et d'EB sur un patch de PCL poreux n'affecte pas la pluripotence des iPSC.

La différenciation des cardiomyocytes a été effectuée selon le protocole GiWi en modulant la signalisation de Wnt avec de petites molécules. Durant la différenciation, les EB ont commencé à se connecter entre eux pour former une couche épaisse de cellules. Avec le même protocole, les hiPSCs cultivés sur lamelle de verre ont été différenciés en cardiomyocytes en même temps que le contrôle.

Les résultats de marquage par immunofluorescence sont présentés à la Fig. 12b. TnnT2, une protéine hautement spécifique des cardiomyocytes, est exprimée positivement pour les cellules différenciées sur un patch PCL poreux, tandis que sur la lamelle de verre, l'expression de TnnT2 se révèle extrêmement faible, ce qui indique un état cellulaire cardiaque plus mature sur un patch PCL poreux. On observe une expression croissante de Myosine sur le patch de PCL poreux par rapport aux cellules sur la lamelle de verre. Des sarcomères striés (positifs à l'α-actinine) peuvent être observés pour les cellules différenciées sur un patch de PCL poreux tandis que, sur la lamelle de verre 2D, l'expression de l'α-actinine est relativement faible. La connexin43, présente dans les jonctions communiquantes et qui joue un rôle important dans la coordination de la contraction des cellules, s'est avérée plus positive sur le patch de PCL poreux que sur la lamelle de verre.

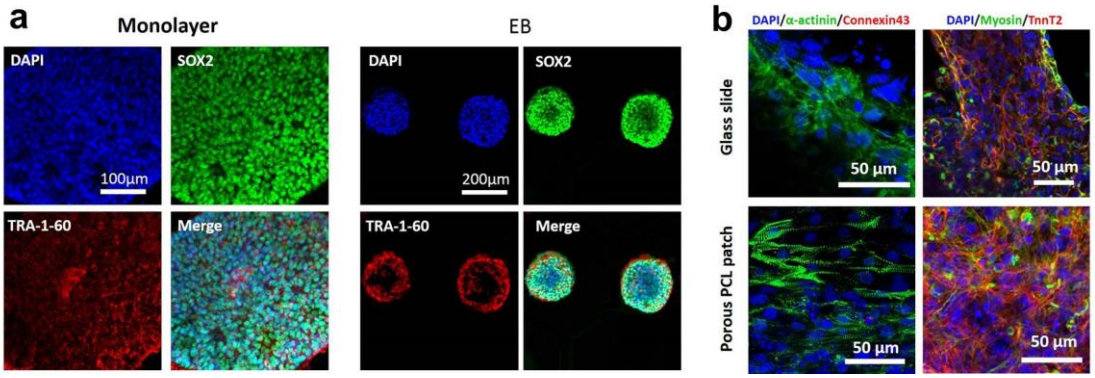


Figure 12 (a) Images d'immunofluorescence des marqueurs de pluripotence des iPSCs en monocouche et des EB sur patch poreux de PCL. (b) Image d'immunofluorescence des marqueurs de cardiomyocytes dérivés d'hiPSCs sur patch de PCL poreux v.s. lamelles de verre.

## C.4 Nanofibres de gélatine en monocouche sur cadre de PDMS pour la différenciation cardiaque

### C.4.1 Introduction

Les maladies cardiaques sont la principale cause de décès et d'invalidité dans le monde, comptant pour près de 30% de la mortalité humaine. Une blessure du cœur est permanente car, après une perte ou une destruction massive de cellules, le tissu cardiaque n'a pas de capacité régénératrice intrinsèque assez importante pour remplacer les cellules perdues ou détruites. Les traitements actuels ne peuvent donc pas contrôler de manière adéquate la progression de la maladie jusqu'au stade final.

Les premières études effectuées dans le domaine ont porté sur une stratégie intrigante: l'utilisation de la transplantation cellulaire. Cependant, l'obtention d'une population cellulaire suffisante ayant une incompatibilité immunitaire minimale est toujours un obstacle énorme pour les chercheurs. Ainsi, une stratégie plus ambitieuse consiste à générer des tissus cardiaques ex vivo à partir de la différenciation des cellules souches et à transplanter ce tissu cardiaque sur la zone ciblée dans l'espoir d'une amélioration. Cette thérapie à base de cellules souches pour la régénération des tissus cardiaques a fait l'objet d'une recherche intensive au cours de la dernière décennie. Les iPSCs humaines ont suscité une attention croissante en raison de leurs avantages

supérieurs, tels que leur simple obtention à partir de la cellule somatique du patient par un processus de reprogrammation, ce qui permet le développement d'une médecine ciblée et une implantation tissulaire dérivée d'iPSCs avec un risque de rejet immunitaire minimal.

Les travaux antérieurs ont principalement été menés avec des iPSCs cultivés dans des boîtes de Petri, lesquelles sont totalement différentes de l'ECM *in vivo*. Une attention croissante a été accordée à une nouvelle stratégie d'ingénierie tissulaire qui consiste à cultiver des cellules souches sur des scaffolds modifiés afin d'améliorer la culture des cellules souches et la performance de la différenciation cardiaque. Cependant, les scaffolds ci-dessus ne sont pas encore assez proches de l'ECM *in vivo* au niveau de certaines de leurs aspects tels que la rigidité du substrat, l'organisation structurelle, la pénétration des cellules et des nutriments, et les échanges intercellulaires.

Le polydiméthylsiloxane (PDMS) est un polymère synthétique flexible et élastique. Le PDMS est très flexible et peut être conçu dans différentes structures, géométries et modèles en 2D et 3D. Le PDMS a été largement utilisé dans le domaine biomédical. Dans ce travail, nous avons fabriqué un cadre de nid d'abeilles poreux de PDMS avec une élasticité réglable, sur lequel une couche poreuse de nanofibres de gélatine a été déposée par electrospinning, pour une l'amélioration des cultures cellulaires. Avec cette méthode, nous avons également fabriqué des cadres de PDMS avec diverses propriétés élastiques. Les qualités élastiques de ces cadres PDMS ont été étudiées. Le patch de nanofibres de gélatine ainsi fabriqué a été utilisé pour la culture des iPSCs et la différenciation cardiaque. Nous avons ensuite procédé à de l'immunomarquage, à de l'imagerie au calcium et à des tests médicamenteux sur les tissus cardiaques générés, afin de montrer les performances accrues du patch de nanofibres de gélatine par rapport au groupe témoin sur lamelle de verre. Enfin, nous avons également observé une déformation élastique du PDMS pendant la contraction cardiaque, ce qui montre le grand potentiel du substrat pour diriger la différenciation cardiaque ainsi que l'organisation du tissu cardiaque.

## C.4.2 Fabrication d'un patch de PDMS / nanofibres de gélatine

La procédure de fabrication du cadre en nid d'abeilles PDMS est illustrée à la Fig.

13, qui comprend trois étapes principales: la fabrication principale du moule en SU8, la fabrication du réseau de nid d'abeilles en PDMS et le montage de l'anneau de silicone.

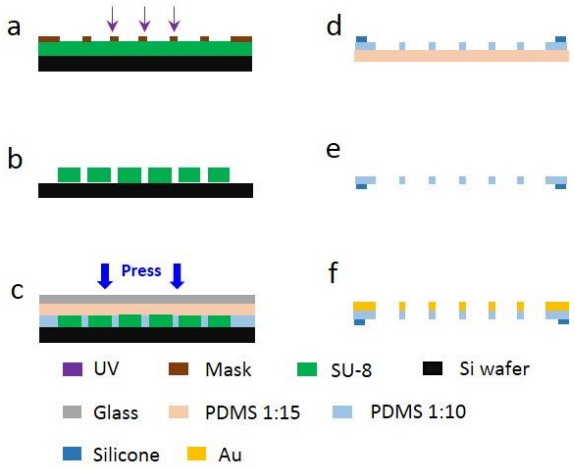


Figure 13 Organigramme schématique de la fabrication du cadre de nid d'abeilles en PDMS.

Avec le processus ci-dessus, le cadre de nid d'abeilles en PDMS peut ainsi être réalisé(figure 14), réalisation qui a été caractérisée par MEB. Le cadre de nid d'abeilles en PDMS ainsi fabriqué présente un réseau hexagonal régulier et uniforme sans défaut. La taille caractéristique et la taille des pas sont respectivement de 400 et 100 µm. La Fig.14c est une image obtenue avec un support d'échantillon incliné, qui montre l'épaisseur de la trame PDMS estimée à 52 µm.

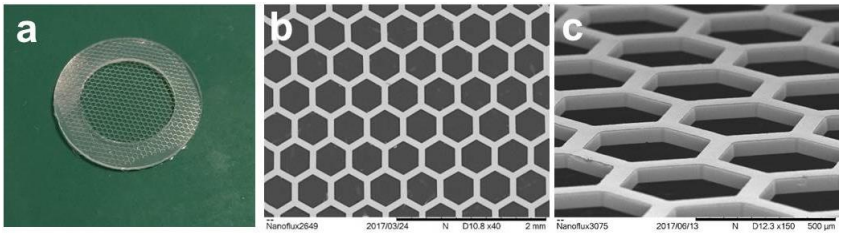


Figure 14 (a) Photographie, (b) et (c) images SEM du cadre PDMS.

La monocouche de nanofibres de gélatine a été déposée sur le cadre en nid d'abeilles PDMS en utilisant l'électrospinning. La morphologie des fibres observée par MEB est représentée par la Fig. 15 avec une grande uniformité. La distribution du diamètre des fibres est représentée sur la figure 15d avec une grande majorité comprise entre 0,35 et 0,5 µm. Après 5 minutes d'electrospinning, la taille des pores de la couche

de nanofibres est principalement inférieure à 6 µm, qui convient à l'ensemencement et à la culture cellulaire.

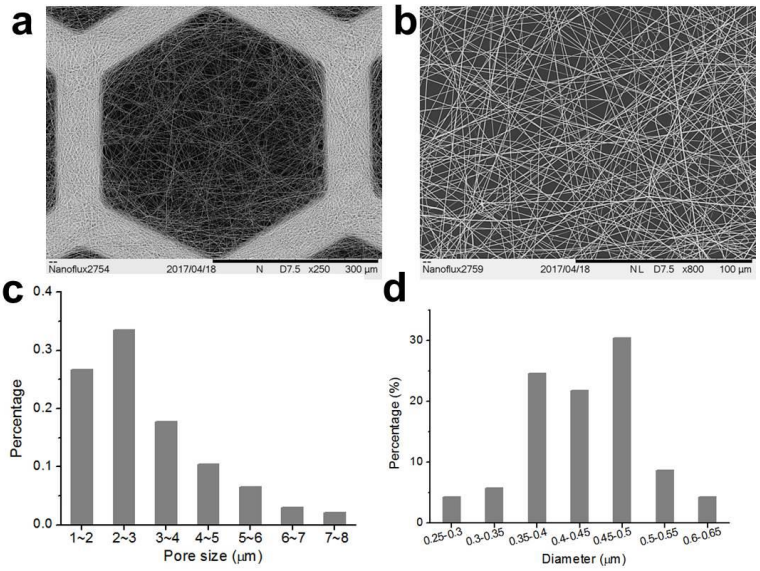


Figure 15 (a) et (b) images MEB des nanofibres de gélatine sur le cadre PDMS. (C) Taille des pore et (d) distribution du diamètre des nanofibres de gélatine.

## C.4.3 Le patch de PDMS/nanofibres de gélatine pour la différenciation cardiaque

Nous avons d'abord évalué la pluripotence de la monocouche d'iPSC et des EB générés sur notre patch de PDMS/nanofibres de gélatine. Les marqueurs des cellules souches pluripotentes SOX2 et TRA-1-60 sont utilisés pour caractériser les iPSCs. Les résultats sont présentés à la Fig. 16a, b. L'immunofluorescence a montré une situation de coloration typique des hiPSCs à la fois sur monocouche et sur les EB, ce qui révèle que l'expression de ces marqueurs a été maintenue. Les résultats confirment que la formation de la monocouche et des EB sur le patch de PDMS/nanofibres de gélatine n'affecte pas la pluripotence des iPSCs.

La différenciation des cardiomyocytes a été effectuée selon le protocole GiWi en modulant la signalisation Wnt avec de petites molécules. Au cours de la différenciation, les iPSCs ont commencé à se connecter entre elles pour former une couche épaisse de cellules. Avec le même protocole, les hiPSC cultivés sur lamelle de verre ont été différenciées en cardiomyocytes en même temps que le contrôle.

Les résultats du marquage par immunofluorescence sont présentés sur la Fig. 16c. TnnT2, une protéine hautement cardiomyocytaire spécifique, est positive pour les cellules différenciées sur le patch de PDMS/nanofibres de gélatine, tandis que sur la lamelle de verre, l'expression de TnnT2 est extrêmement faible, ce qui indique un état cellulaire cardiaque plus mature sur le patch de PDMS/nanofibres de gélatine. Une expression croissante de Myosine sur le patch de PDMS/nanofibres de gélatine est observée par rapport aux cellules sur la lamelle de verre. Les sarcomères striés (α-actinine positive) peuvent être observés pour les cellules différenciées sur le patch de PDMS nanofibres de gélatine tandis que sur lamelle de verre 2D, l'expression de l'α-actinine est faible. Connexin43,un marqueur spécifique des jonctions communiquantes qui joue un rôle important dans la coordination de la contraction des cellules, s'est avéré plus positif sur le patch de PDMS/nanofibres de gélatine que sur la lamelle de verre.

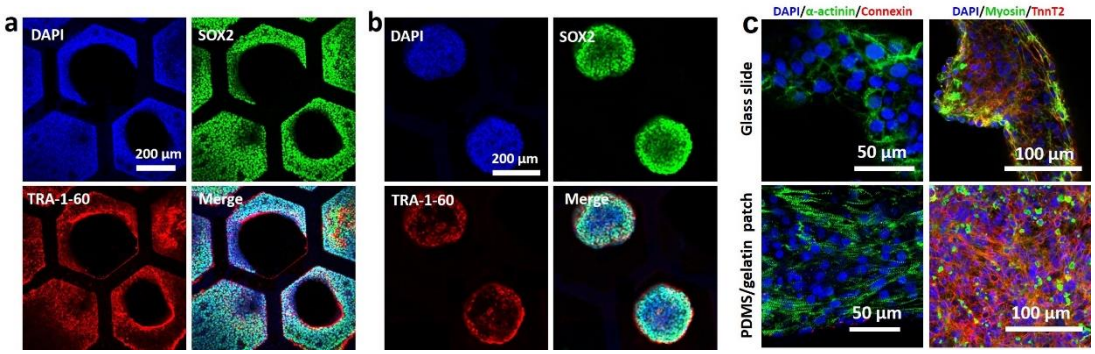


Figure 16 (a) and (b) Images d'immunofluorescence des marquers de pluripotence des iPSCs en monocouche et EB sur le patch de PDMS/ nanofibres de gélatine. (c) Images d'immunofluorescence cardiomyocytes dérivées d'hiPSCs sur le patch de PDMS/ nanofibres de gélatine et lamelles de verre.

Afin d'analyser l'utilisation des cardiomyocytes dérivés d'iPSCs humains pour des tests médicamenteux, nous avons testé deux médicaments : l'isoproterenol (ISP) et le propranolol (PRO), qui ont des effets connus sur la fonctionnalité des cardiomyocytes. L'ISP augmente et et le PRO diminue le taux de contraction cardiaque. En bref, les cardiomyocytes sur le patch de PDMS/nanofibres de gélatine ont été incubés avec fluo-4 pour une imagerie au calcium afin de mesurer le taux de contraction. Les résultats sont présentés sur la Fig. 17. L'isoprotérénol, un bêta-antagoniste, a été introduit dans

les cellules avec des concentrations progressivement augmentées, ce qui conduit à une augmentation du taux de contraction dépendante de la dose. Ensuite, l'addition de différentes concentrations de propranolol, un bêta-bloquant, a entraîné une diminution du taux de contraction dépendante de la dose. Les résultats ci-dessus des tests de ces médicaments cardiaques ont indiqué une bonne réaction médicamenteuse et une performance fonctionnelle des cardiomyocytes ainsi générés sur le patch de PDMS/nanofibres de gélatine.

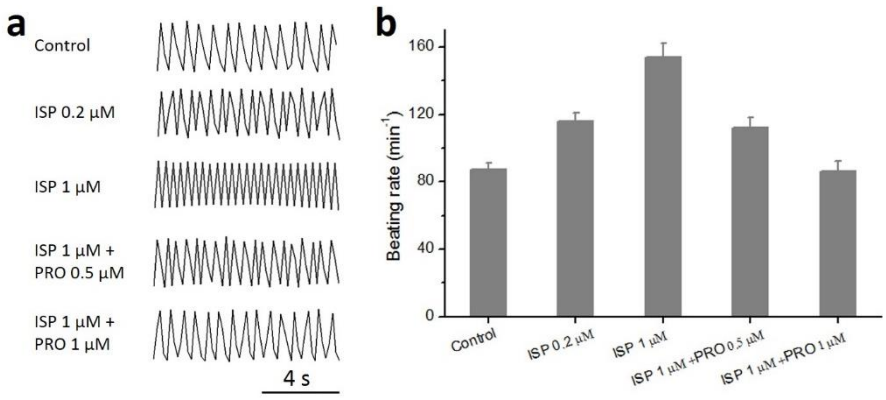


Figure 17 (a) Intensité de fluorescence dans l'imagerie de calcium montrant l'effet et la dépendance à la dose de médicament cardiaque ISP et PRO. (B) Fréquence du battement cardiaque en fonction de la concentration d'ISP et de PRO.

## C.5 Conclusion et perspective

Ce travail de thèse visait le développement de scaffolds multidimensionnels pour l'amélioration de la culture cellulaire et des applications d'ingénierie tissulaire avec des cellules souches, afin de les utiliser pour des tests cliniques et pour des implantations dans des sujets malades. Avec diverses techniques de fabrication, nous avons utilisé des scaffolds fonctionnels et nous avons démontré leur potentiel élevé pour les études cellulaires et autres applications cliniques.

Tout d'abord, nous avons utilisé une technique d'impression 3D pour produire un cadre conçu en PEGDA, et puis rempli les espaces libres du cadre avec un gel de gélatine afin d'obtenir une culture cellulaire améliorée et une différenciation neuronale optimale. Ensuite, nous avons fabriqué un substrat de film de PCL poreux en couche

mince soutenu par un cadre en nid d'abeilles poreux en PEGDA par des méthodes combinées d'auto-assemblage et de microfabrication, pour améliorer la performance cellulaire et la différenciation cardiaque. Enfin, nous avons démontré que l'utilisation d'un patch souple fait d'un cadre élastique de PDMS et d'une monocouche de nanofibres de gélatine, peut faciliter la différenciation cardiaque à partir de cellules pluripotentes induites humaines. Ainsi, dans cette thèse nous avons réalisé avec succès plusieurs scaffolds fonctionnels pour des applications avancées en biologie cellulaire et en génie tissulaire. Notre travail a démontré l'utilité des scaffolds hybrides pour l'ingénierie des micro-tissus qui pourraient avoir un impact sur les études futures dans les domaines de l'ingénierie tissulaire, du ciblage de médicaments et de la médecine régénératrice

Ce travail de thèse se limite à l'étude de la preuve-de-concept. Des études plus systématiques sont encore nécessaires pour une meilleure évaluation de la faisabilité et l'efficacité de ces scaffolds fonctionnels dans les applications d'ingénierie tissulaire. Elles comprennent le développement de nouvelles méthodes, la préparation de matériaux biodégradables et intelligents, ainsi que l'intégration dans des puces microfluidiques pour des applications type organe-sur-puce. Quoi qu'il en soit, nous croyons au potentiel d'application élevé de nos approches de génie tissulaire dans le futur, la médecine régénératrice et d'autres domaines biomédicaux.

# List of Abbreviations

| | |
|---|---|
| 2D | Two dimensional |
| 3D | Three dimensional |
| ABS | Acrylonitrile butadiene styrene |
| ATP | Adenosine triphosphate |
| BMCs | Bone marrow cells |
| BSA | Bovine serum albumin |
| CAD | Computer aided design |
| CAM | Calcein AM |
| CNS | Central nervous system |
| CVD | Chemical vapor deposition |
| DAPI | 4',6-diamidino-2-phenylindole |
| DI | Deionized |
| DMEM | Dulbecco’s modified eagle medium |
| DMSO | Dimethyl sulfoxide |
| DNA | Deoxyribonucleic acid |
| Dox | Doxorubicin |
| DPBS | Dulbecco’s phosphate buffer saline |
| EBs | Embryonic bodies |
| ECM | Extracellular matrix |
| EDTA | Ethylenediaminetetraacetic acid |
| EGF | Epidermal growth factor |
| EGFR | Epidermal growth factor receptor |
| ESCs | Embryonic stem cells |
| FBS | Fetal bovine serum |
| FDA | Food and drug administration |
| FGFs | Fibroblast growth factors |

| | |
|---|---|
| FITC | Fluorescein isothiocyanate |
| GELMA | Gelatin methacrylate |
| GSK3 | Glycogen synthase kinase 3 |
| HA | Hydroxyapatite |
| iPSCs | induced pluripotent stem cells |
| ISP | Isoproterenol |
| LOM | Laminated object manufacturing |
| MAP-2 | Microtubule-associated protein 2 |
| MEMS | Microelectromechanical systems |
| mRNA | Message deoxyribonucleic acid |
| MSCs | Mesenchymal stem cells |
| MTT | 3-(4,5-dimethylthiazol-2-yl)-2,5-diphenyltetrazolium bromide |
| MW | Molecular weight |
| NPCs | Neural progenitor cells |
| NSCs | Neural stem cells |
| PBS | Phosphate buffer saline |
| PLA | Poly-lactic acid |
| PNS | Peripheral nervous system |
| PCL | Polycaprolactone |
| PDMS | Polydimethylsiloxane |
| PEDGA | Poly(ethylene glycol) dimethacrylates |
| PEO | Poly(ethylene oxide) |
| PFA | Paraformaldehyde |
| PMPC | Poly(2-methacryloyloxyethyl phosphorylcholine) |
| PGA | Poly-glycolic acid |
| PLGA | Poly lactic-co-glycolide |
| PVA | Poly vinyl alcohol |
| RIE | Reactive ion etching |
| RGD | Arg-Gly-Asp tripeptide |
| ROCK | Rho-associated protein kinase |

| | |
|---|---|
| RPMI | Roswell Park Memorial Institute |
| SCI | Spinal cord injury |
| SEM | Scanning electron microscope |
| SLA | Stereo-lithography |
| SLS | Selective laser sintering |
| TCP | Tissue culture plate |
| THF | Tetrahydrofuran |
| TMCS | Trimethylchlorosilane |
| WST | Water soluble tetrazolium |
| VEGF | Vascular endothelial growth factor |
| μPG | Micro pattern generator |

# List of publications

1. **Xiaolong Tu**, Jin Wei, Bin Wang, Yadong Tang, Jian Shi, Yong Chen. Patterned Parylene C for cell adhesion, spreading and alignment studies. *Microelectronic Engineering.* 2017, 175, 56-60.
2. **Xiaolong Tu**, Lina Wang, Jin Wei, Bin Wang, Yadong Tang, Jian Shi, Zhijun Zhang, Yong Chen. 3D Printed PEGDA microstructures for gelatin scaffold integration and neuron differentiation. *Microelectronic Engineering.* 2016, 158, 30-34.
3. **Xiaolong Tu**, Li Wang, Yong Chen. PEGDA frame assisted self-assembly of porous PCL patch for high efficient gene transfection. In preparation.
4. **Xiaolong Tu**, Li Wang, Bin Wang, Yong Chen. Porous PDMS frame with anisotropic elasticity regulates unidirectional contraction of human iPSCs derived cardiac tissue. In preparation.
5. Bin Wang, Jian Shi, Jin Wei, Li Wang, **Xiaolong Tu**, Yadong Tang, Yong Chen. Fabrication of elastomer pillar arrays with height gradient for cell culture studies. *Microelectronic Engineering.* 2017, 175, 50-55.
6. Yadong Tang, Li Liu, Junjun Li, Leqian Yu, Francesco Paolo Ulloa Severino, Li Wang, Jian Shi, **Xiaolong Tu**, Vincent Torre, Yong Chen. Effective motor neuron differentiation of human induced pluripotent stem cells on a patch made of crosslinked monolayer gelatin nanofibers. *Journal of Materials Chemistry B.*2016, 4, 3305-3312.
7. Jin Wei, Jian Shi, Bin Wang, Yadong Tang, **Xiaolong Tu**, Emmanuel Roy, Benoit Ladoux, Yong Chen. Fabrication of adjacent micropillar arrays with different heights for cell studies. *Microelectronic Engineering.* 2016, 158, 22-25.

## Résumé

L'objectif de ce travail est de développer une méthode d'ingénierie de scaffolds multidimensionnels pour la culture cellulaire et l'ingénierie tissulaire. Nous avons d'abord appliqué une technique d'impression 3D pour produire un scaffold en PEGDA et ensuite rempli l'espace libre du scaffold avec du gel de gélatine. Après la congélation et le séchage, un scaffold hybride en PEGDA avec des structures fine de gélatine a été obtenu, qui a été ensuite valisé par la culture et la différenciation des cellules progénitrices neuronales. Pour intégrer plus facilement dans un dispositif microfluidique, nous avons également conçu un scaffold 2D sous forme d'une couche mince de nid d'abeilles de PEGDA rempli des structures poreuses auto-assemblée de PCL. Ce scaffold 2D a été utilisé pour la culture cellulaire et la transfection des gènes, montrant des avantages par rapport aux méthodes classiques en termes d'absorption des nutriments et des facteurs solubles. Enfin, nous avons fabriqué un scaffold mous constitué d'une couche mince de nid d'abeilles en élastomère de PDMS et d'une monocouche de nanofibres de gélatine pour faciliter la différenciation cardiaque à partir des cellules souches pluripotentes humaine. Comme prévu, nous avons réalisé une génération cardiaque avec une contraction plus forte et une homogénéité de battement plus élevée par rapport aux approches classiques. Tous ensemble, nous avons démontré l'utilité des scaffolds hybrides pour l'ingénierie micro-tissulaire qui pourraient avoir un impact sur les études futures dans les domaines de l'ingénierie tissulaire, du criblage des médicaments et de la médecine régénératrice.



## Mots Clés

Biomatériaux, micro-ingénierie, cellules souches, ingénierie tissulaire



## Abstract

The objective of this work is to develop a method of engineering multi-dimensional scaffolds for cell culture and tissue formation. We firstly applied a 3D printing technique to produce the designed frame in PEGDA and then filled the free-space of the frame with a gelatin gel. After freezing and drying, a hybrid 3D scaffold made of gelatin porous structures and PEDGA backbone was obtained, which supported culture and differentiation of neural progenitor cells. To more easily integrate into a microfluidic device, we also designed a 2D scaffold in form of a thin layer of honeycomb frame of PEGDA and self-assembled porous structure of PCL. Such as a patch form scaffold could be used for cell culture and gene transfection, showing advantages over the conventional methods in terms of nutrients and soluble factors uptake. Finally, we fabricated a soft patch made of an elastic frame in PDMS and a monolayer of gelatin nanofibers to facilitate cardiac differentiation from human induced pluripotent stem cells. As expected, we achieved a cardiac generation with higher contraction strength and a higher beating homogeneity comparing to the conventional approaches. All together, we demonstrated the utility of hybrid scaffolds for micro-tissue engineering which could impact the future studies in the fields of tissue engineering, drug screening and regenerative medicine.



## Keywords

Biomaterials, micro-engineering, stem cells, tissue engineering.